

FULL SCALE TURBOFAN DUCT BURNER TEST PROGRAM

by
C. J. Clapp

GPO PRICE \$ _____

CFSTI PRICE(S) \$ _____

Hard copy (HC) 3.00

Microfiche (MF) .65

ff 653 July 65

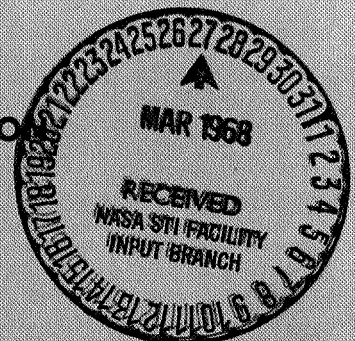


FACILITY FORM 602	<u>N68-19070</u>	
	(ACCESSION NUMBER)	(THRU)
	<u>260</u>	<u>1</u>
	(PAGES)	(CODE)
<u>CR-54637</u>		<u>28</u>
(NASA CR OR TMX OR AD NUMBER)		(CATEGORY)

Prepared for

NATIONAL AERONAUTICS AND SPACE ADMINISTRATION

Contract NAS3-7907



Pratt & Whitney Aircraft
FLORIDA RESEARCH AND DEVELOPMENT CENTER
BOX 2691, WEST PALM BEACH, FLORIDA 33402

DIVISION OF UNITED AIRCRAFT CORPORATION
**U
A®**

NOTICE

This report was prepared as an account of Government sponsored work. Neither the United States, nor the National Aeronautics and Space Administration (NASA), nor any person acting on behalf of NASA:

- A.) Makes any warranty or representation, expressed or implied, with respect to the accuracy, completeness, or usefulness of the information contained in this report, or that the use of any information, apparatus, method, or process disclosed in this report may not infringe privately owned rights; or
- B.) Assumes any liabilities with respect to the use of, or for damages resulting from the use of any information, apparatus, method or process disclosed in this report.

As used above, "person acting on behalf of NASA" includes any employee or contractor of NASA, or employee of such contractor, to the extent that such employee or contractor of NASA, or employee of such contractor prepares, disseminates, or provides access to, any information pursuant to his employment or contract with NASA, or his employment with such contractor.

Requests for copies of this report should be referred to

National Aeronautics and Space Administration
Office of Scientific and Technical Information
Attention: AFSS-A
Washington, D.C. 20546

FINAL REPORT

FULL SCALE TURBOFAN DUCT BURNER

TEST PROGRAM

by
C. J. Clapp

Prepared for
NATIONAL AERONAUTICS AND SPACE ADMINISTRATION

18 March 1968

Contract NAS3-7907

Technical Management
NASA Lewis Research Center
Cleveland, Ohio
Air Breathing Engines Division

Robert Branstetter

Pratt & Whitney Aircraft DIVISION OF UNITED AIRCRAFT CORPORATION
FLORIDA RESEARCH AND DEVELOPMENT CENTER
BOX 2691, WEST PALM BEACH, FLORIDA 33402



FOREWORD

This summary report was prepared by the Pratt & Whitney Aircraft Division of United Aircraft Corporation under Contract NAS3-7907.

The contract was administered by the Air-Breathing Engine Procurement Section of the National Aeronautics and Space Administration, Cleveland, Ohio.

The report summarizes technical effort that was conducted during the period of 29 June 1965 through 30 June 1967.

ABSTRACT

The objective of the effort described in this report was to investigate the performance and structural durability of a full-scale turbofan duct burner using ASTM A-1 type fuel and operating at conditions typical of advanced supersonic aircraft.

A full-scale duct burner of the ram-induction type having an outer casing diameter of 67.7 inches and an inner casing diameter of 47 inches was tested. The burner inlet and outlet flow passages had the size and shape of a Pratt & Whitney Aircraft advanced turbofan engine design rated for 600 lb/sec at sea level static conditions.

Good structural durability of the final ram-induction burner design was demonstrated.

Performance data were obtained for a range of operating conditions including climb and simulated Mach 2.7 at an altitude of 70,000 ft. The final configuration tested had an isothermal total pressure loss of 5% and achieved combustion efficiencies greater than 90% over the range of conditions tested.

The occurrence of combustion instability at some test points prevented covering the entire operating range with a single configuration and fuel flow mode.

CONTENTS

SECTION		PAGE
I	INTRODUCTION AND SUMMARY.	I-1
	A. Introduction.	I-1
	B. Summary	I-2
II	APPARATUS	II-1
	A. Test Rig.	II-1
	B. Facility.	II-14
	C. Instrumentation	II-15
	D. Data Recording System	II-22
III	DIFFUSER, DUCT BURNER, AND FUEL INJECTOR DESIGN . .	III-1
	A. Diffuser Design	III-1
	B. Duct Burner Design.	III-3
	C. Fuel Injector Design.	III-10
IV	COOLING LINER DESIGN.	IV-1
	A. Outer Cooling Liner	IV-1
	B. Inner Cooling Liner	IV-28
V	PERFORMANCE CALCULATION PROCEDURE	V-1
	A. Performance Calculation Procedure for Duct Burner Rig Data	V-1
	B. Nomenclature.	V-7
VI	TEST MODIFICATIONS.	VI-1
VII	PERFORMANCE AND DURABILITY DISCUSSION	VII-1
	A. Exit Nozzle Calibration	VII-1
	B. Diffuser Performance.	VII-2
	C. Cooling Liners.	VII-5
	D. Duct Burner	VII-11
VIII	COMBUSTION INSTABILITY.	VIII-1
IX	CONCLUSIONS	IX-1
	APPENDIX A - Additional Calculations for Outer Cooling Liner.	A-1
	APPENDIX B - Damping Liner Design and Bench Tests.	B-1

CONTENTS (Continued)

SECTION	PAGE
APPENDIX C - References	C-1
APPENDIX D - Test Chronology	D-1
APPENDIX E - Fuel System	E-1
APPENDIX F - Distribution List	F-1

SECTION I INTRODUCTION AND SUMMARY

A. INTRODUCTION

This summary report for the Full-Scale Turbofan Duct Burner Test Program, Contract NAS3-7907, covers the entire program from 29 June 1965 through 30 June 1967. The purpose of this program was to design, fabricate, and test a full-scale annular duct burner sized for an advanced Pratt & Whitney Aircraft turbofan engine with an airflow of 600 lb/sec at sea level static conditions. The test phase of the program was conducted in the NASA Lewis Research Center, Engine Research Building, Test Cell SW-24.

The overall objective of this investigation was to obtain a better understanding of the merits and problems associated with large annular combustors for duct burning applications. This type of combustor has not been subjected to the exhaustive developmental effort expended on primary combustor and afterburner.

A duct burner may be likened in some ways to a ramjet combustor in that both operate over a similar range of fuel-air ratios and inlet airflow parameters. However, for a commercial engine application, the duct burner must possess very high performance and long life. For this project, the duct burner was designed to attain 95% combustion efficiency, a maximum isothermal total pressure loss of 5% at a duct reference Mach number of 0.150, and a minimum life of 600 hr. The program was to include limited development testing followed by cyclic endurance testing. The duct burner was designed for testing with commercial fuel of the ASTM A-1 type.

A ram-induction type of duct burner was selected because previous segment rig tests had demonstrated that this type of burner had a potential to produce the required performance over a wide operating range.

Several problem areas resulted in changing the original objectives and test conditions. The occurrence of combustion instability caused the objective to be changed to a development program involving both the duct burner and the facility. Facility problems placed limitations upon the test operating conditions.

Development testing was subsequently conducted at the following test conditions:

	Condition A "Transonic Climb"	Condition B "Transonic Climb"	Condition C "Cruise"
Inlet Total Pressure, psia	10	15	30
Inlet Total Temperature, °F	200	285	550
Duct Reference Mach Number	0.139	0.144	0.175
Fuel/Air Ratio	0.05	0.05	0.016-0.05

Test Condition A simulated an abnormal flight condition at which the lowest anticipated duct burner pressure level is encountered. Test Condition B simulated a normal transonic climb flight condition, and Condition C simulated a cruise (near 0.02 fuel/air ratio) or cruise-approach flight condition (near 0.05 fuel/air ratio).

Detailed discussions of the program can be found in the following sections:

- Section II - General description of apparatus
- Section III - Design procedure of the ram-induction burner
- Section IV - Heat transfer and acoustical design of the cooling liners
- Section V - Performance calculation procedure
- Section VI - Test modifications
- Section VII - Performance results, including modifications made to improve hardware durability
- Section VIII - Combustion instability, including modifications made to the facility as well as the test hardware to combat combustion instability and inlet plenum noise

B. SUMMARY

A full-scale duct burner of the ram-induction type was designed, built, and subjected to development testing at simulated flight conditions of a supersonic transport aircraft. The diffuser exhibited excellent pressure recovery. A ram-induction duct burner configuration was developed that met the maximum isothermal total pressure loss of 5% and achieved combustion efficiencies greater than 90% at test conditions

simulating transonic climb, cruise-approach, and cruise flight conditions as shown in figure I-1. Combustion instability, however, limited the duct burner to rather narrow and restricted operating ranges as the fuel/air ratio was varied. Also, the rig was subjected to noise from the facility air supply. Twelve changes were incorporated into the facility and the rig, whereas the duct burner was modified 10 times in an attempt to reduce facility noise and eliminate combustion instability. Although some modifications gave improvements, no change was completely effective. Only one duct burner modification was employed specifically to improve combustion efficiency. The elimination of combustion instability became the major effort of the test program.

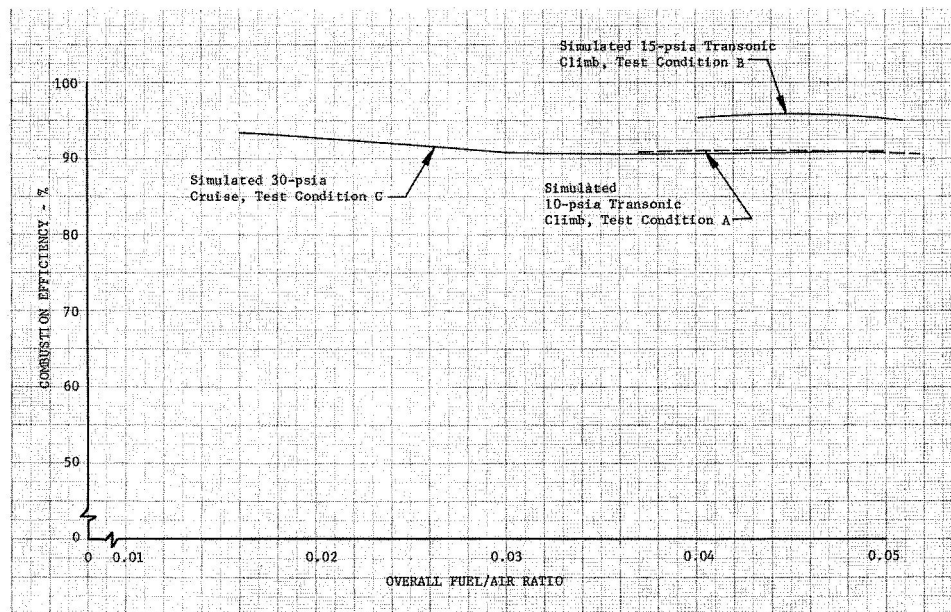


Figure I-1. Combustion Efficiency Achieved
With Ram-Induction Duct Burner

DF 58513

The first test burner failed due to (1) severe operating conditions during nonburning calibrations, (2) overheating during combustion tests because of insufficient firewall cooling, and (3) extreme pressure oscillations when combustion instability occurred. Half the burner was replaced with new parts and modifications were made to improve firewall cooling. The entire burner subsequently endured the remainder of the program while remaining in excellent structural condition. During the program, 97.2 hours of combustion testing were accumulated.

SECTION II APPARATUS

This general description of apparatus includes a cursory description of test hardware.

Design details of major components are contained in Sections III and IV. Numerous minor hardware alterations made during the course of the test program are described in the results (Sections VII and VIII).

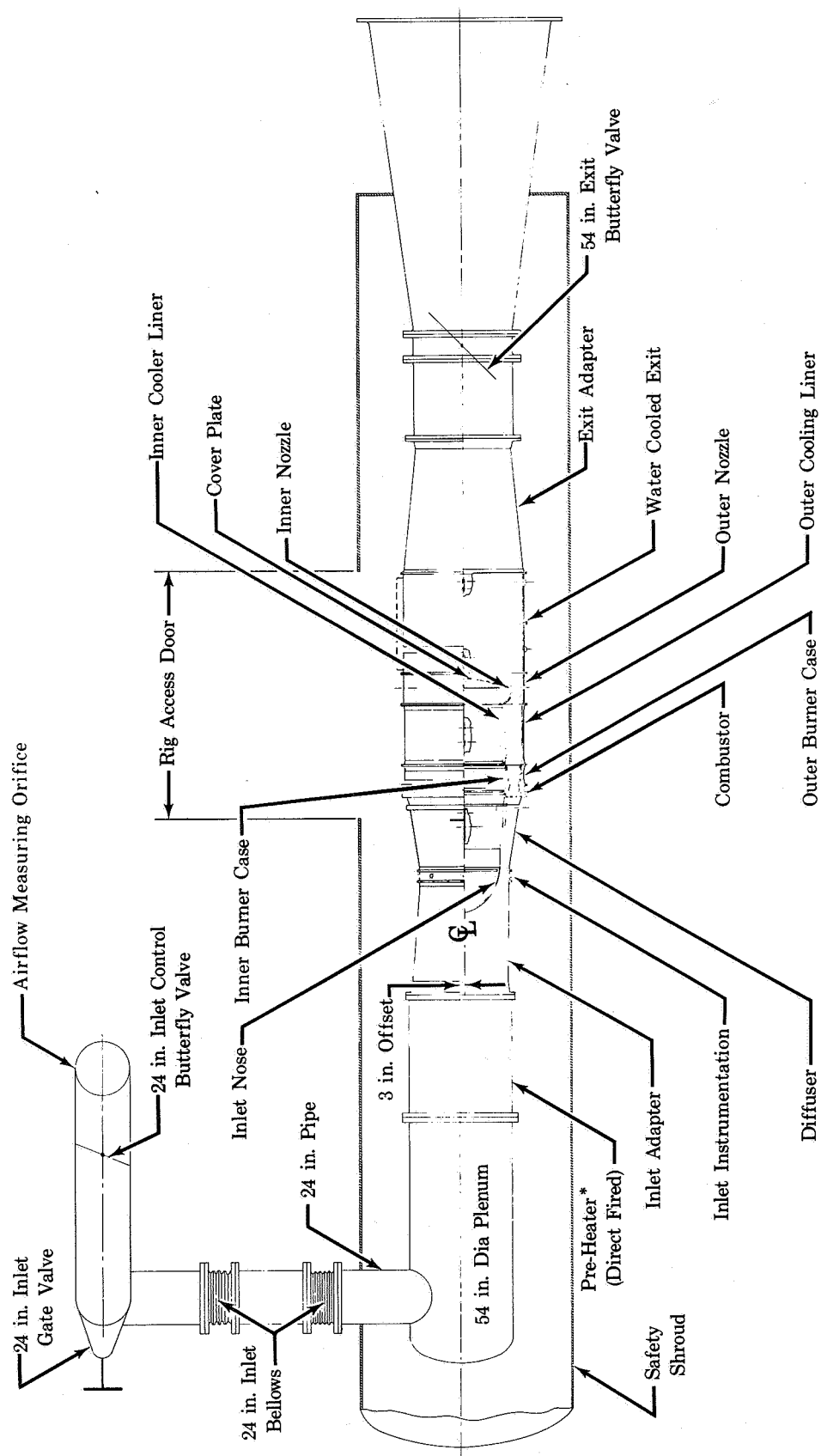
A. TEST RIG

Design of the rig hardware was initiated on 29 June 1965. Figure II-1 shows the rig installed in Test Cell SW-24 at the Lewis Research Center. Photographs of the rig installation in the test facility are shown in figures II-2 and II-3.

The inlet duct adapter was designed with a 3-in. offset between the inlet and exit centerlines to accommodate the 3-in. offset between the NASA facility inlet ducting and the exit ducting.

The inlet instrumentation section (figure II-4) was a precision-machined ring providing the desired inlet instrumentation area. The section was an annulus used to determine diffuser inlet operating conditions and also as an accurate, redundant airflow measuring device. The inlet nose cone, also held to close tolerances, formed the ID wall of this section. The hemispherical nose cone provided an inlet bell-mouth.

Instrumentation was also located at the diffuser exit (inlet to burner) for setting the burner inlet airflow condition. Eight struts were provided to support the duct burner dome assembly at the diffuser exit (figure II-5). A bleed air passage was provided halfway along the diffuser ID wall for inner liner cooling air. At the inlet of the bleed passage, static and total pressure instrumentation were provided to determine cooling airflow rate. The diffuser case had 40 external pads for mounting the Zone-1 fuel nozzles. Four main structural struts in the diffuser inlet supported the centerbody and supplied cooling water for the inner exit nozzle and the cover plate. These struts also provided a path for pressure and temperature instrumentation leads and Zone 2 ID fuel lines.



*Used Only as a Flow Distribution Device

FD 14326G

Figure II-1. Duct Burner Rig Installation in Test Facility

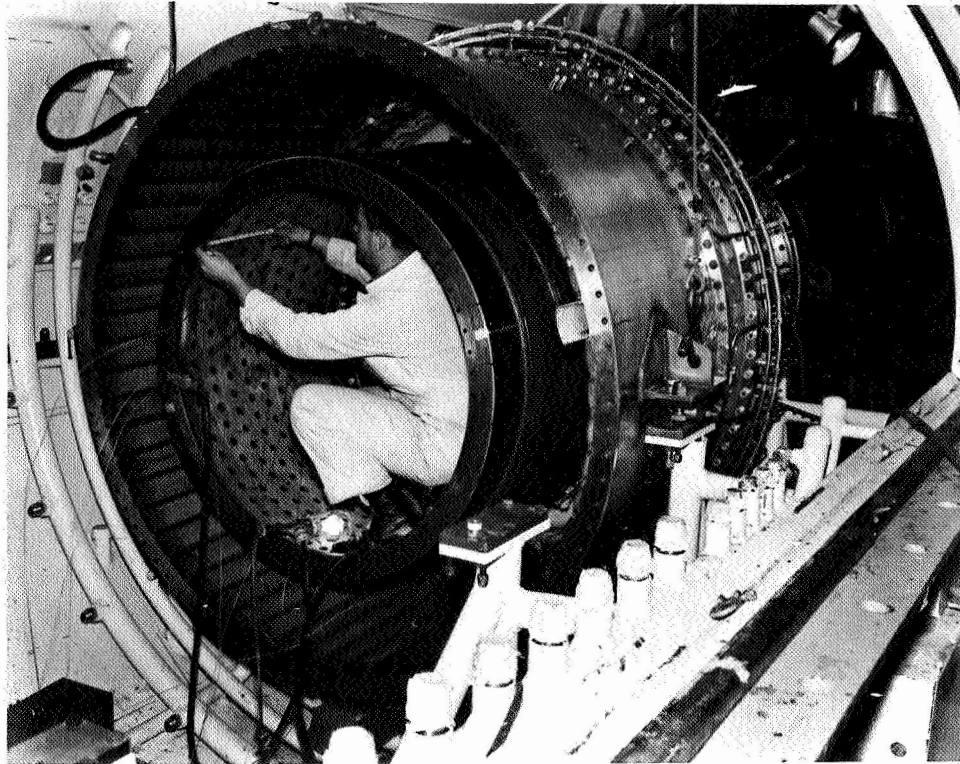


Figure II-2. Duct Burner Rig Installation in
Test Facility, Exit Nozzle Removed

FE 59721

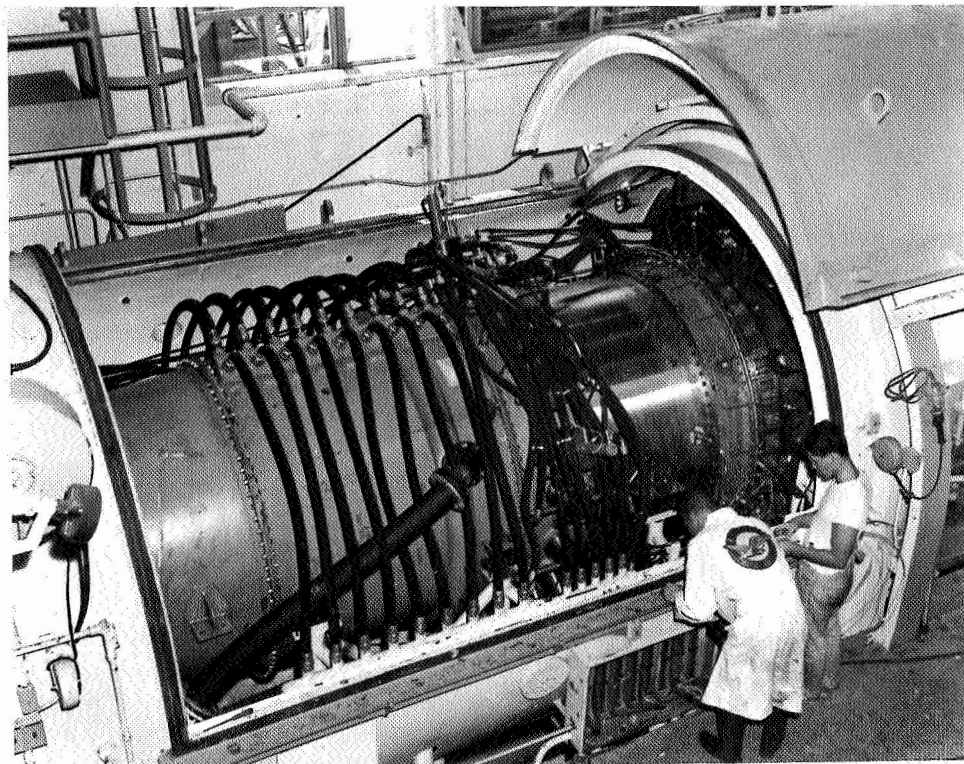


Figure II-3. Duct Burner Rig Installation in
Test Facility, Rig Access Door Open

FE 59720

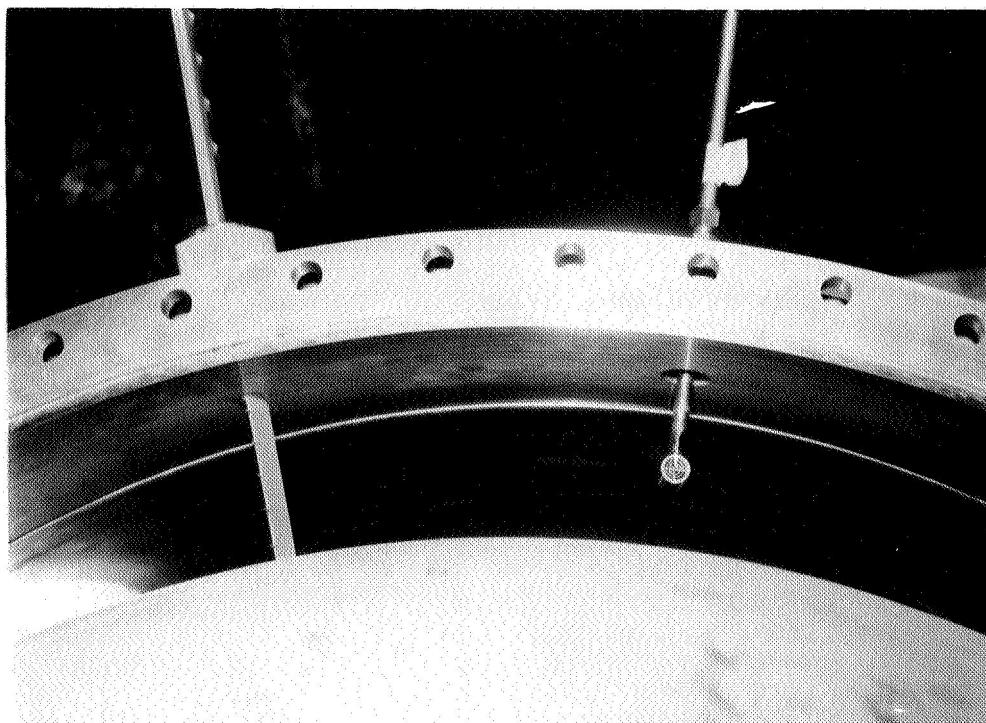


Figure II-4. Inlet Instrumentation Section,
Looking Downstream

FE 57535

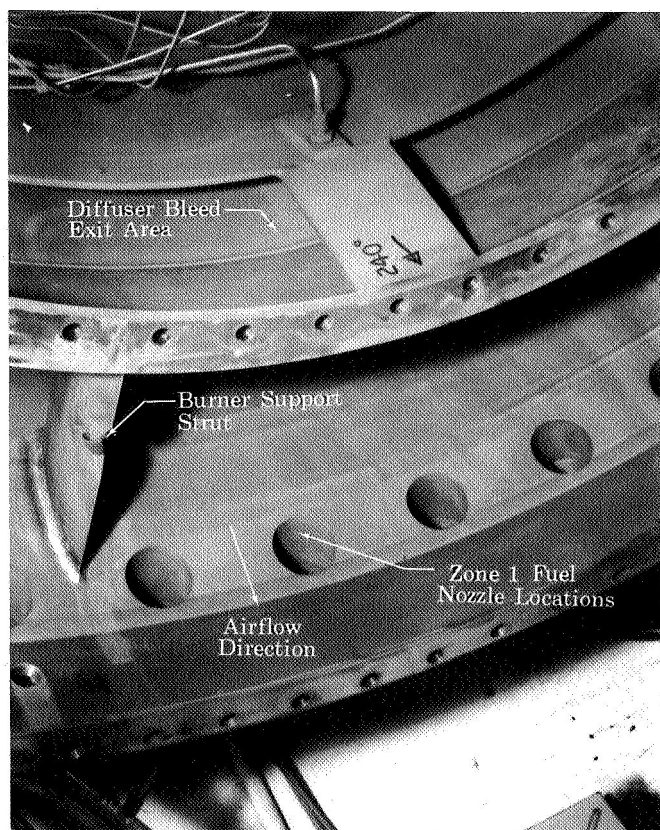


Figure II-5. Diffuser Exit, Looking Upstream

FD 22327

The ram-induction combustor (figures II-6 through II-8) was designed as two basic assemblies: the dome and primary liner assembly and the secondary liner assembly. The dome and primary liner assembly (figure II-9) included the primary liner, the No. 1 and No. 2 scoops, the firewall and circular-shaped air swirlers and the snout. This assembly was fastened to the exit diffuser struts by 8 pins. The secondary ID and OD liner assemblies consisted of the liners and the No. 3 scoops. The secondary liners were bolted to the inner and outer burner cases. The secondary liners supported the aft end of the primary burner liner by support tabs. The ID and OD vortex generators and Zone-2 fuel spraybars were attached to the inner and outer burner cases. The vortex generators are shown in figure II-10; turbulators, used later in the development program are included in the figure. The primary liner accepted two spark igniters located 180 deg apart. Ignition was provided by two surface-discharge spark igniters with 20-joule exciters.

The outer cooling liner (figure II-11) consisted of 60 one-piece convoluted segments (figure II-12) installed in liner tracks (figure II-13) welded to the outer liner case. To increase the effectiveness of the cooling air under the convectively cooled liner segments, ramps were installed as shown in figures II-13 and II-14. The acoustical liners used later in the development program are shown in figure II-15.

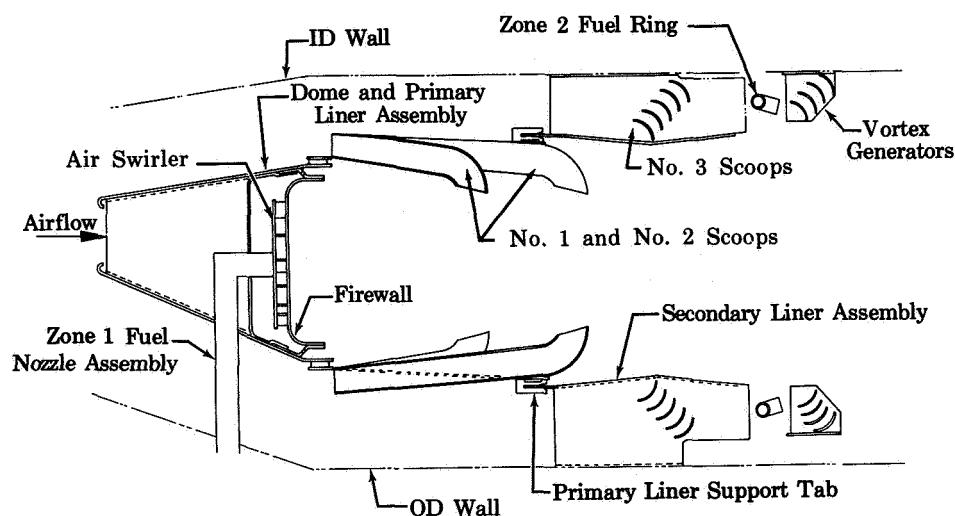


Figure II-6. Schematic of Full Annular Turbofan Duct Burner FD 13591C

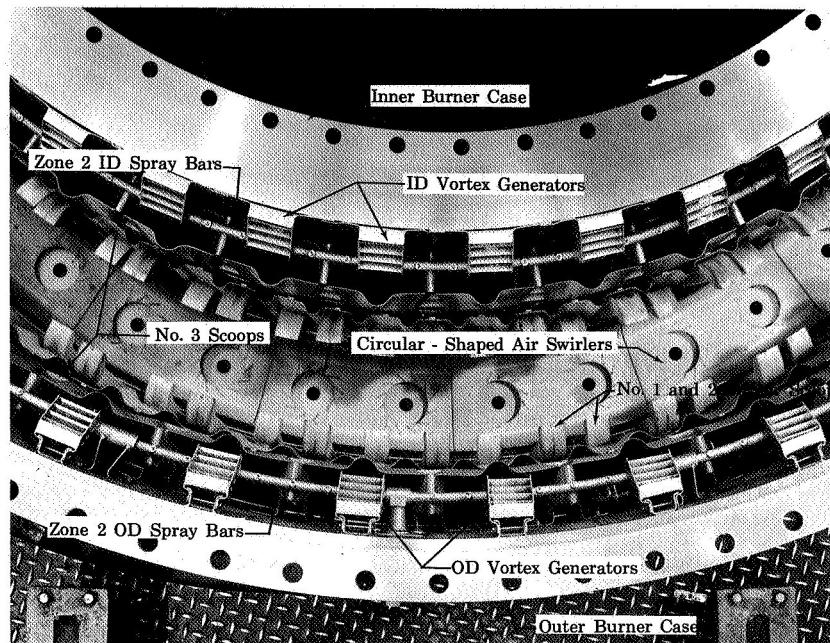


Figure II-7. Ram-Induction Burner, Looking Upstream FD 22344

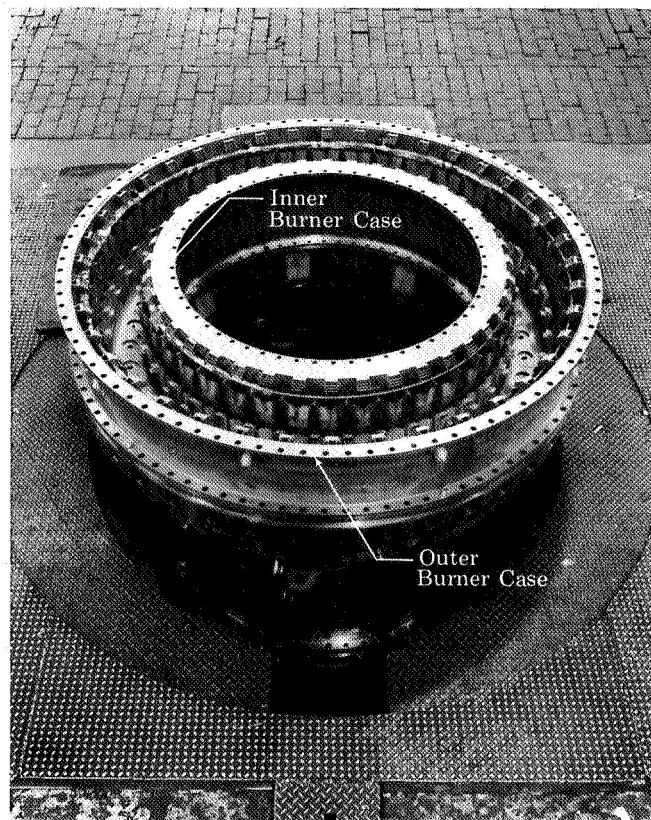


Figure II-8. Assembled Burner Section

FD 22328

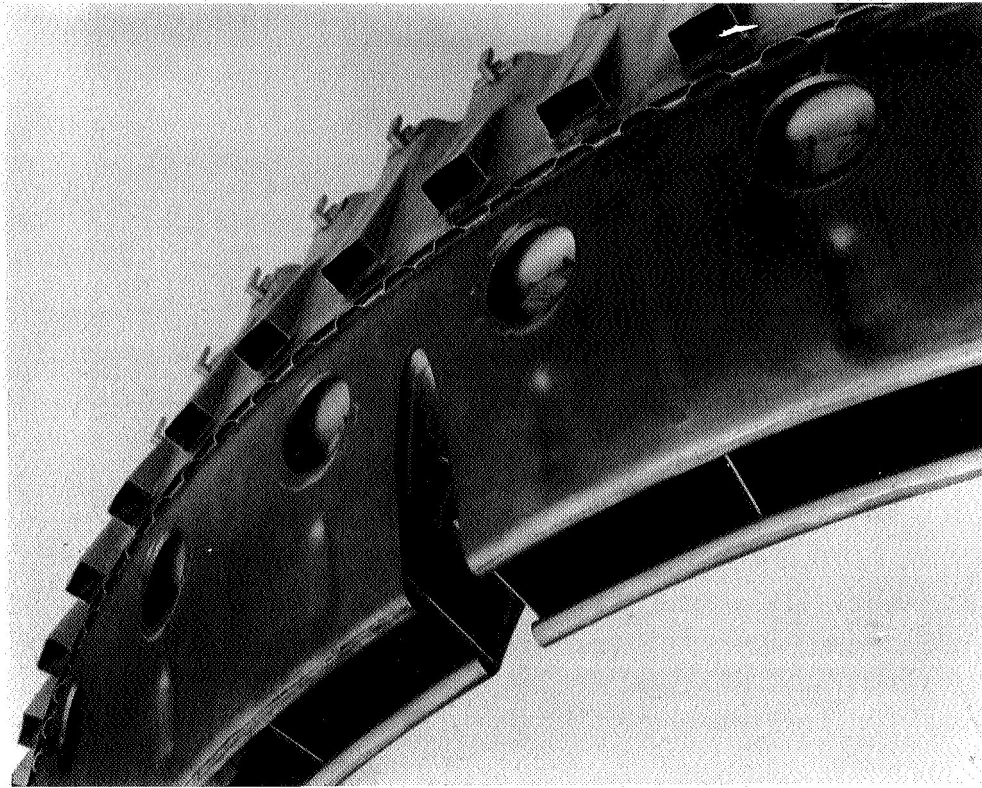


Figure II-9. Dome and Primary Liner Assembly

FE 57542

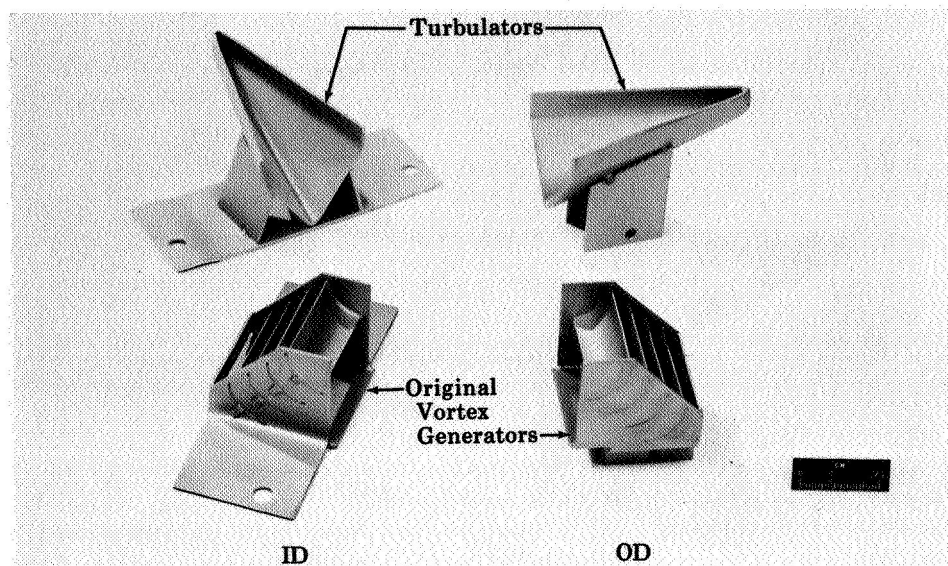


Figure II-10. Vortex Generators

FD 20601A

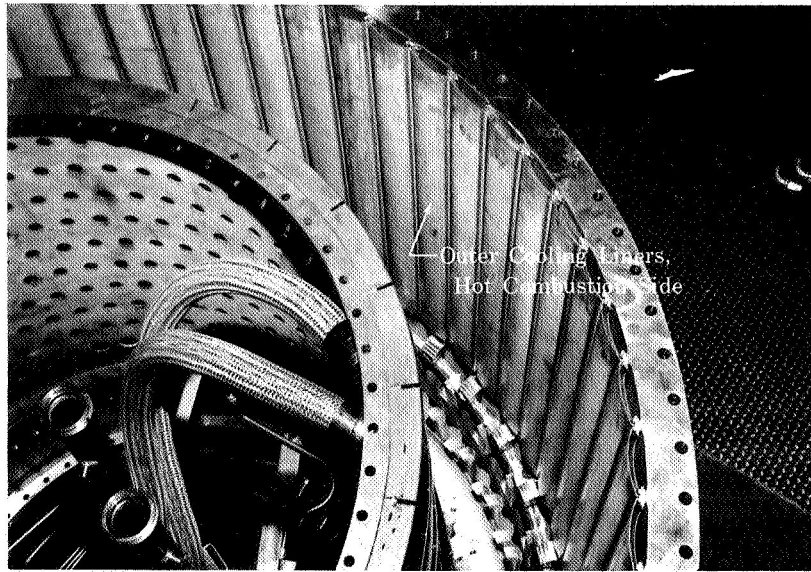


Figure II-11. Assembly of Outer Cooling Liners

FD 22329

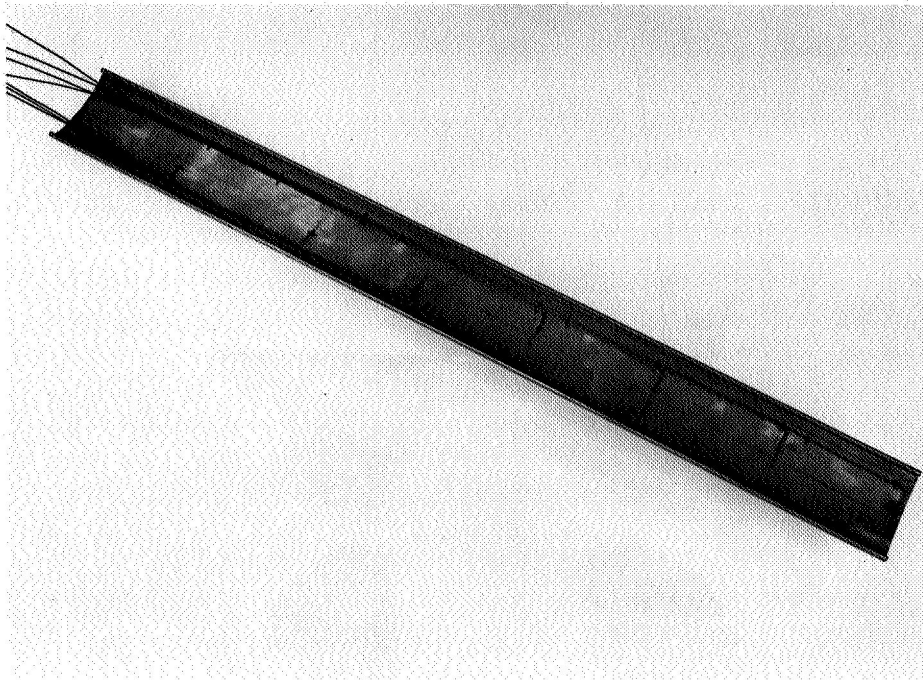


Figure II-12. Outer Cooling Liner Segment

FE 57718

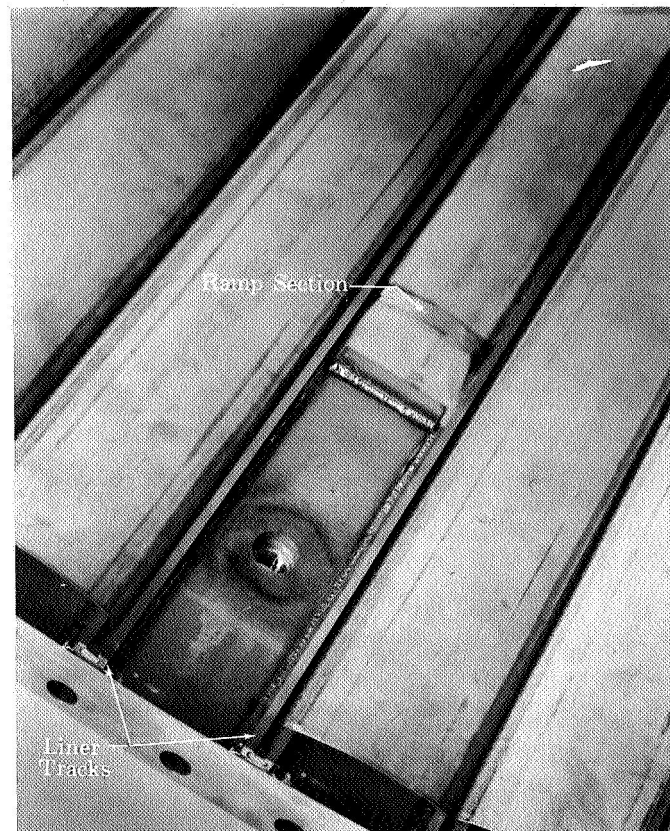


Figure II-13. Outer Cooling Liner

FD 22330

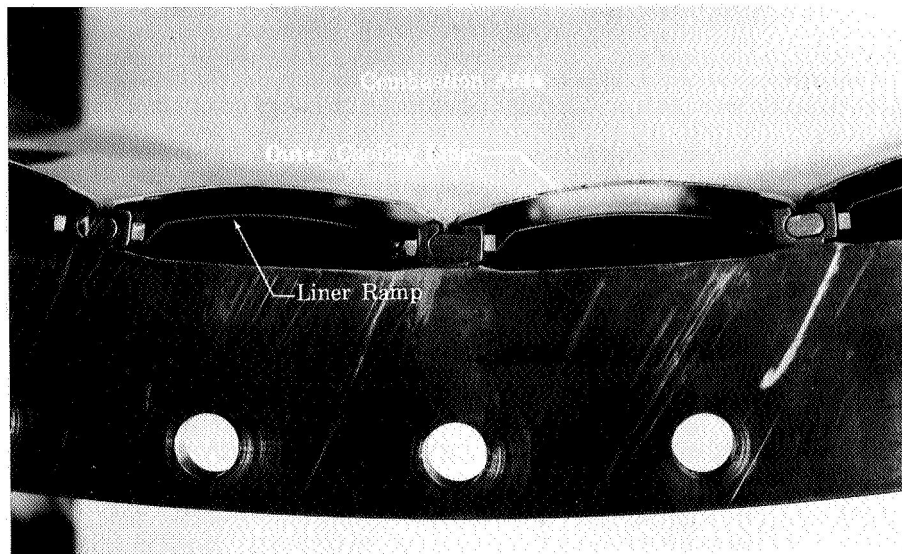


Figure II-14. Outer Cooling Liner as Viewed
Looking Upstream

FD 22331

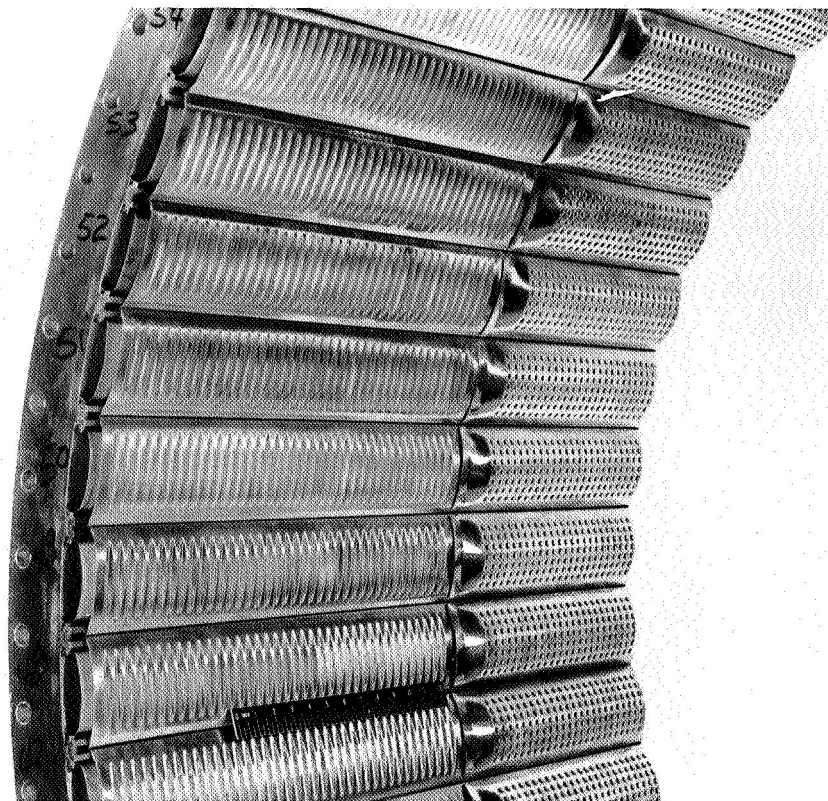


Figure II-15. Revised Outer Cooling Liners
With Acoustic Damping

FE 71984

The inner cooling liner was film-cooled with three cooling louvers and a bypass louver (figures II-16 and II-17). Total and static pressure instrumentation were provided at the bypass louver to determine the diffuser bleed bypass airflow. The inner liner case was a perforated cylinder used as a structural member for attaching the inner nozzle and cover plate. The inner liner was attached to the front of the inner liner case by a rotating locking device. The aft end of the liner was rigidly held between the inner liner case and the inner nozzle, allowing the remainder of the cooling liner to thermally expand upstream. During the test program, the inner cooling liner was modified to include acoustical boxes, as shown in figure II-18.

The exit nozzle section (figures II-19 and II-20) consisted of a converging annulus with movable radial plugs for varying the flow area. This design was adapted from a similar nozzle used in duct burner segment rig tests. Of the 20 cylindrical plugs with spherical ends, 18 could be positioned either fully into the annulus or retracted to leave only the

spherical end protruding into the annulus. The remaining 2 plugs were hydraulically actuated from the control cell and used to trim a test point, allowing a 0 to 5.5% change in the nozzle flow area. This design provided a high degree of precision and repeatability.

The exit nozzle assembly was designed to accept two inner nozzles; the use of two inner nozzles made the determination of the flow area over its entire range more accurate. The inner nozzle assembly was selected to be changeable because it was simpler in design than the outer nozzle, which had the nozzle plugs and pressure probes installed through the nozzle case.

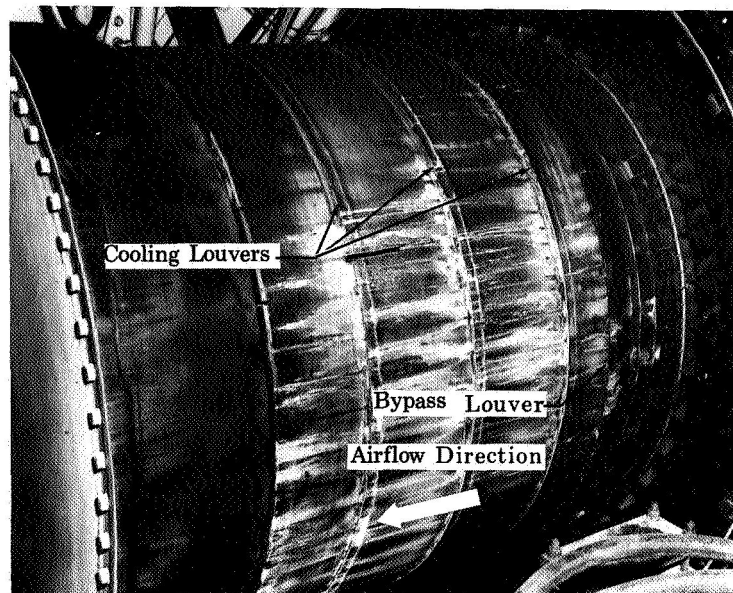


Figure II-16. Inner Cooling Liner, As Viewed
From Hot Combustion Side

FD 22332

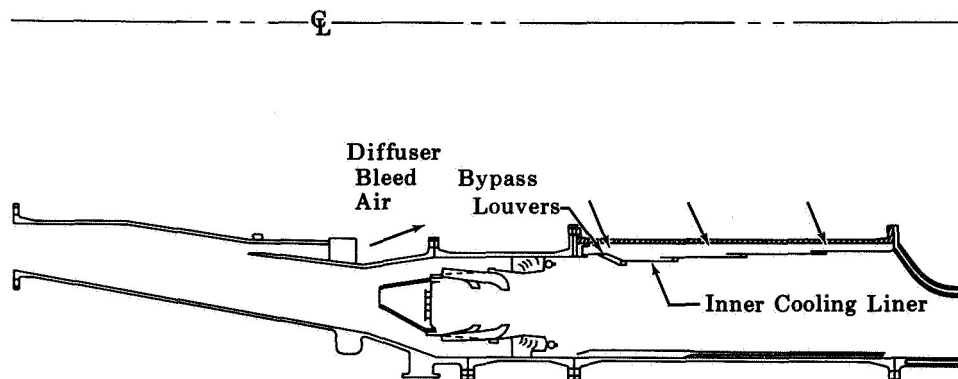


Figure II-17. Inner Cooling Liner

FD 19352C

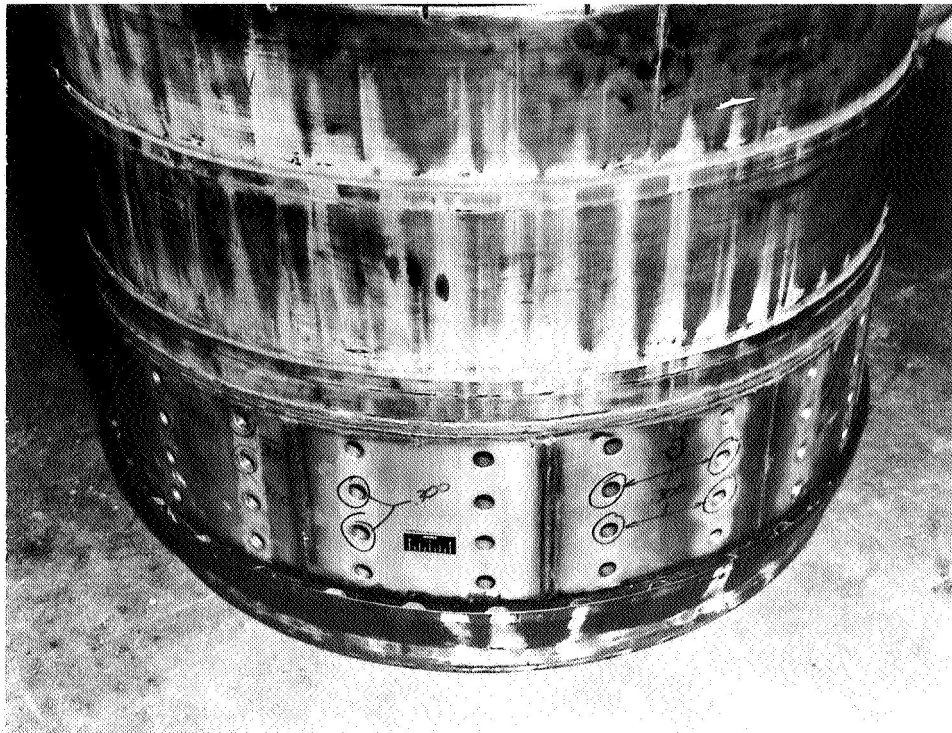


Figure II-18. Inner Cooling Liner With Damping

FE 67931

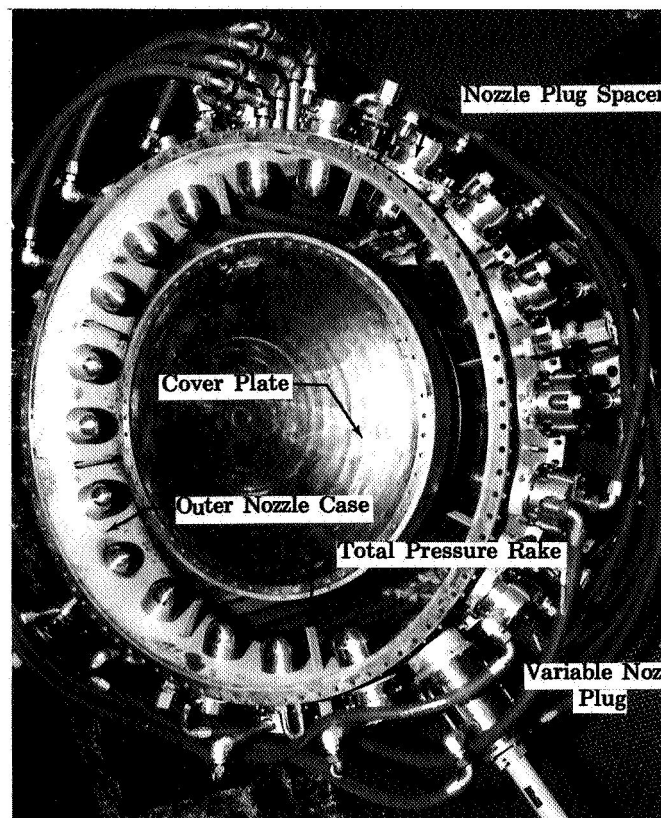


Figure II-19. Rig Exit Nozzle Section

FD 22333

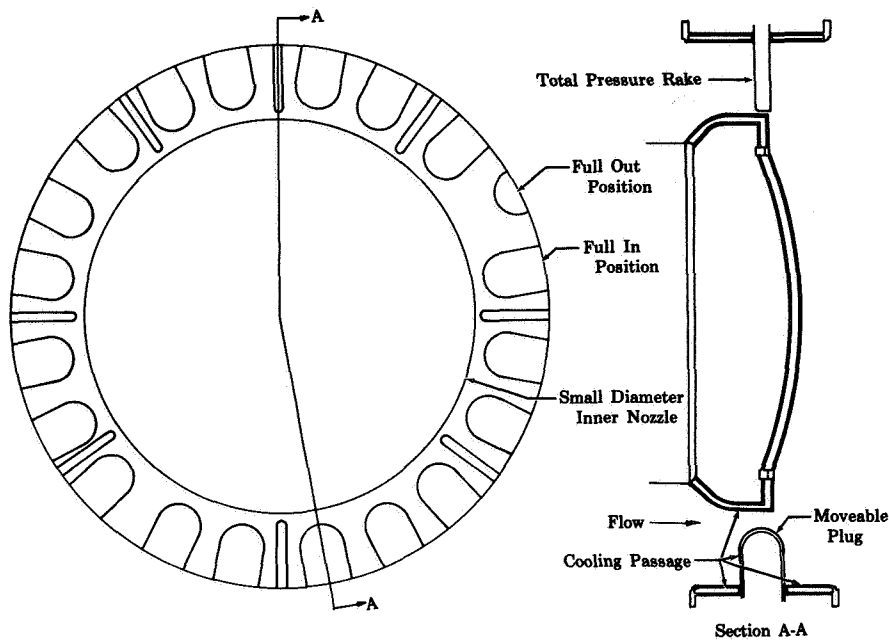


Figure II-20. Schematic of Exit Nozzle Assembly FD 14337A

The required exit flow areas, and the effect of varying combustion efficiency and burner pressure loss, for Conditions 1 through 4 (listed in table II-1) are shown in figure II-21. The maximum required area for each condition occurred at maximum combustion efficiency and maximum burner pressure loss. As shown in figure II-21, deviations from a design point could be made because a sufficient margin for varying the nozzle throat area was provided. Conditions 1 and 2 (which were the alternate endurance points) could be tested using the small diameter inner nozzle. For maximum versatility, both inner nozzles were designed to overlap at Condition 2.

The inner nozzle, outer nozzle, and nozzle plugs were water-cooled and are shown in figure II-20. The nozzle plugs were cooled in groups of 5 plugs in a series. The cooling water then passed into the outer nozzle case for cooling. Total and static pressure instrumentation were also provided through the outer nozzle case.

The water-cooled exit duct (figure II-1) was provided with fog nozzles to water quench the combustion gases.

Table II-1. Duct Burner Design Conditions
(Used To Size the Exhaust Nozzle)

	Condition 1	Condition 2	Condition 3	Condition 4
Duct Airflow, lb/sec	90.8	309	309	309
Duct Inlet Temperature, °F	200	633	633	633
Duct Inlet Total Pressure, psia	10	35	35	35
Duct Ref Mach No.	0.138	0.175	0.175	0.175
Fuel/Air Ratio	0.050	0.020	0.050	0.005

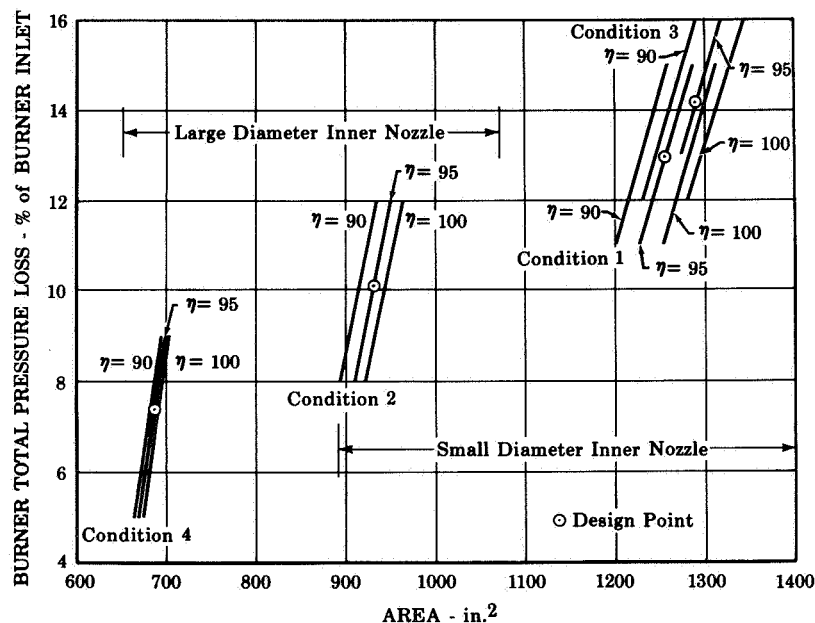


Figure II-21. Exhaust Nozzle Area

FD 14338C

The exit duct adapter provided a transition between the rig and the NASA facility exhaust duct.

B. FACILITY

The facility provided metered combustion air at temperatures up to 600°F. The air was heated in a natural gas-fired, tube-type heat exchanger. The combustion airflow rate was measured by sharp-edged orifices. After water quenching, the exhaust gases were discharged through a 54-inch diameter butterfly valve and into an altitude exhaust system. See figure II-1. When the exhaust nozzle was not choked, the butterfly valve was used to maintain a constant burner pressure.

System capacity was limited at Condition C when operating at 0.05 fuel-air ratio. The condition could not be maintained in warm weather because the required amount of cooling water could not be extracted at a sufficient rate from the facility exhaust system. Also, the facility butterfly valve at the rig exit was small and caused a reduction in rig exit vacuum capability. Hence, careful tailoring of the quench-water flow rate was required in order to choke the exit nozzle.

For this investigation, the direct fired preheater shown in figure II-1 was used as a flow distribution device rather than an air heater. A variety of flow distribution devices were used during the course of the program. These devices are described in Section VIII.

The required fuel system was designed, fabricated, and installed at the NASA Lewis Research Center as one of the program requirements. The fuel system was actually three independent systems and a detailed description is given in Appendix E.

C. INSTRUMENTATION

The rig was designed to provide pressure and temperature instrumentation in the planes shown in figure II-22. The diffuser inlet instrumentation at Plane 2 consisted of eight total pressure rakes, eight static pressure taps, and eight total temperature probes spaced circumferentially, as shown in figure II-23. A typical total pressure rake and a total temperature probe are shown in figure II-24. At the bleed lip, Plane 3, the diffuser bleed airflow was determined with sets of pressure pickups located 180 degrees apart circumferentially. Each set consisted of a total pressure probe and a static pressure tap. The burner inlet instrumentation at Plane 4 consisted of eight total pressure rakes, sixteen static pressure taps (eight on the OD and eight on the ID), and eight total temperature probes spaced circumferentially as shown in figure II-25. Two 1/4-in. diameter immersion thermocouples, spaced 180 degrees apart circumferentially, were inserted through the secondary liner of the burner into the hot combustion gases to detect a burner ignition or blowout. The burner exit instrumentation at Plane 5 included eight water-cooled total pressure rakes and eight static pressure taps (figure II-26).

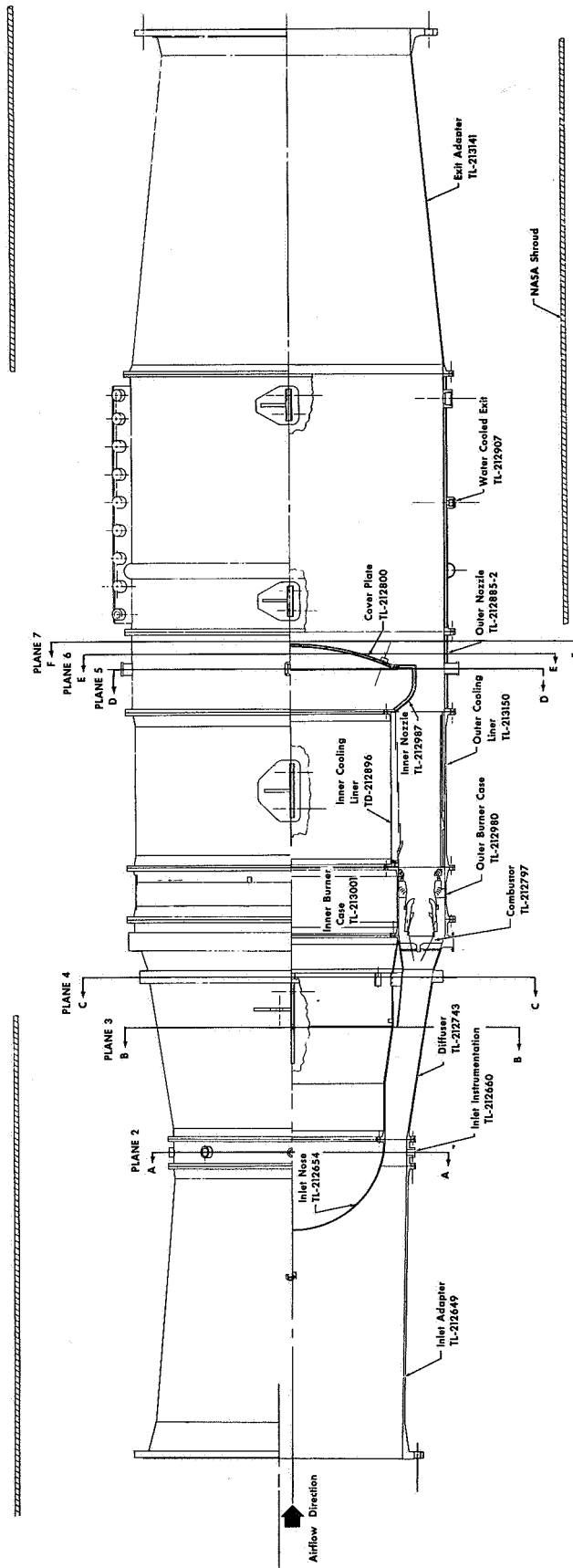


Figure II-22. Rig Instrumentation Planes

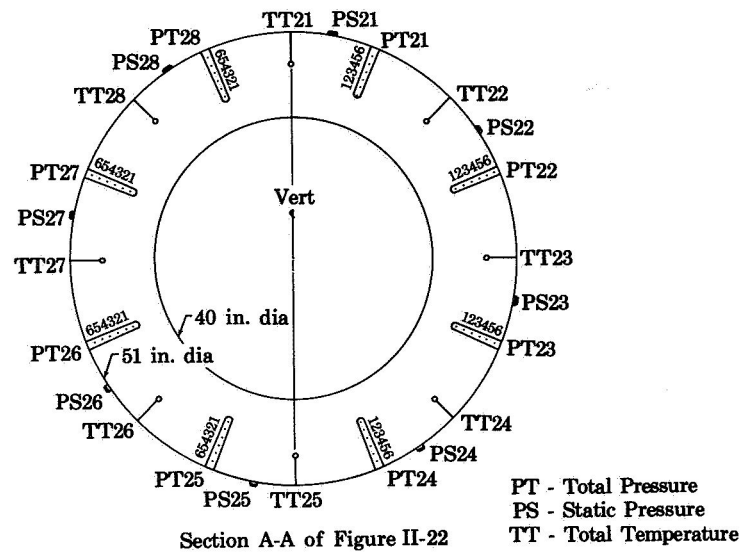


Figure II-23. Diffuser Inlet (Plane 2) Instrument FD 22335

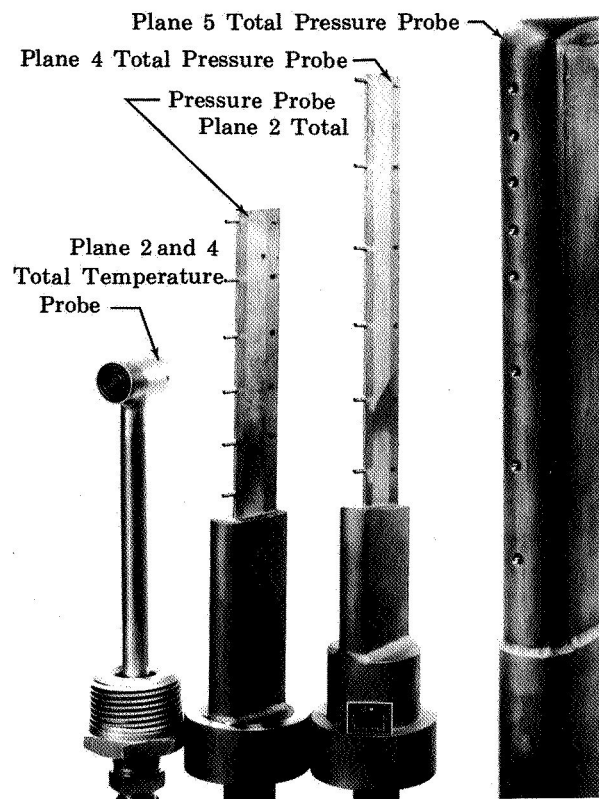


Figure II-24. Rig Instrumentation

FD 22336

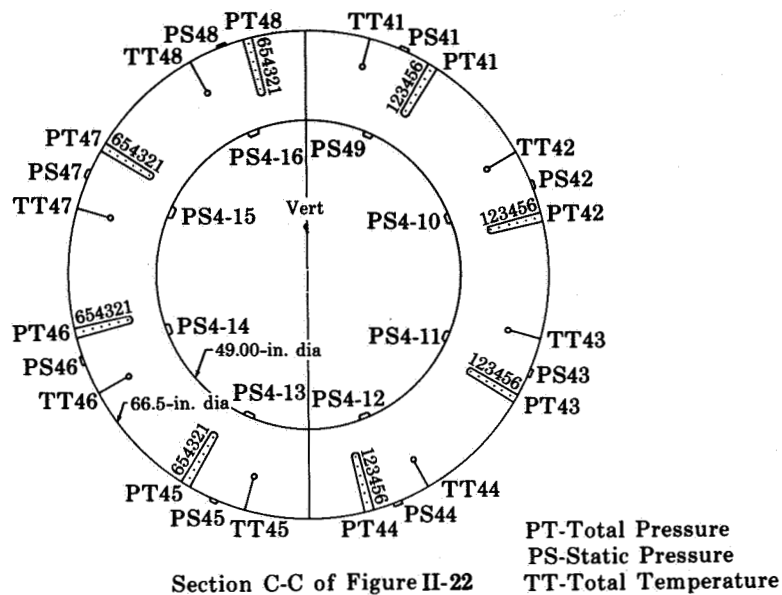


Figure II-25. Burner Inlet (Plane 4)
Instrumentation Locations

FD 22337

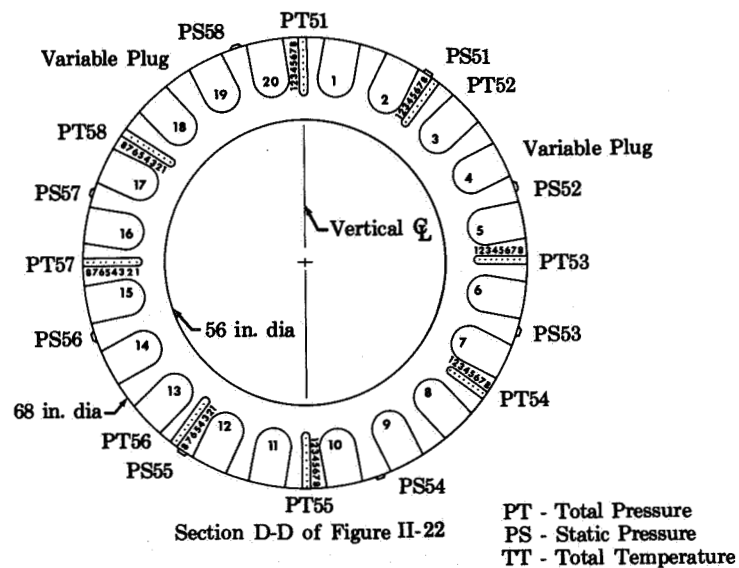
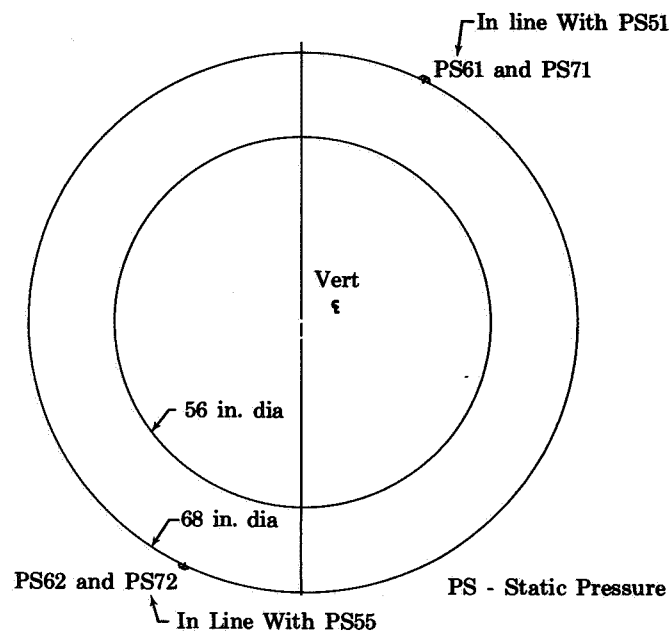


Figure II-26. Exit Nozzle (Plane 5)
Instrumentation Locations

FD 22338

Instrumentation Planes 6 and 7 consisted of two static pressure taps at each plane spaced 180 degrees apart circumferentially (figure II-27). This instrumentation was provided to determine if supersonic flow had occurred aft of Plane 5, indicating whether the exit nozzle was choked or not.



Section E-E and F-F of Figure II-22

Figure II-27. Downstream Nozzle (Planes 6 and 7) FD 22339
Instrumentation Locations

The inner cooling liner was instrumented with chromel-alumel skin thermocouples spaced axially at top and bottom dead center, as shown in figure II-28. Total and static pressure instrumentation were installed in the bypass louver in two circumferential locations to determine the bypass flow. The cooling airflow was obtained by subtracting the bypass flow from the bleed flow.

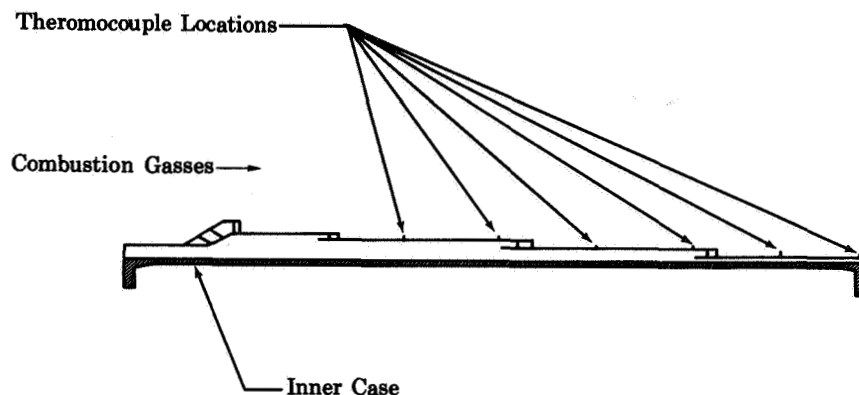


Figure II-28. Inner Cooling Liner Thermocouple Locations FD 22341

Two of the outer cooling liner segments were instrumented with chromel-alumel skin thermocouples, as shown in figure II-12. Outer liner cooling airflow was determined in two circumferential locations with total and static pressure pickups, as shown in figure II-29.

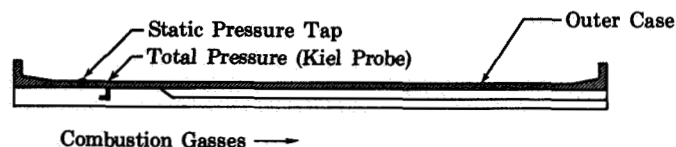


Figure II-29. Outer Cooling Liner Instrumentation FD 22340

Water-cooled radial traversing temperature and pressure probes (figure 30) could be installed in the exit nozzle at locations occupied by the eight-point total pressure rakes. The thermocouples were of the aspirating type and capable of measuring temperatures as high as 3600°F. Two probe assemblies were built.

Bosses were provided in two circumferential locations for dynamic pressure sensors, which were installed through the outer liner to detect burner pressure oscillations, as shown in figure II-31.

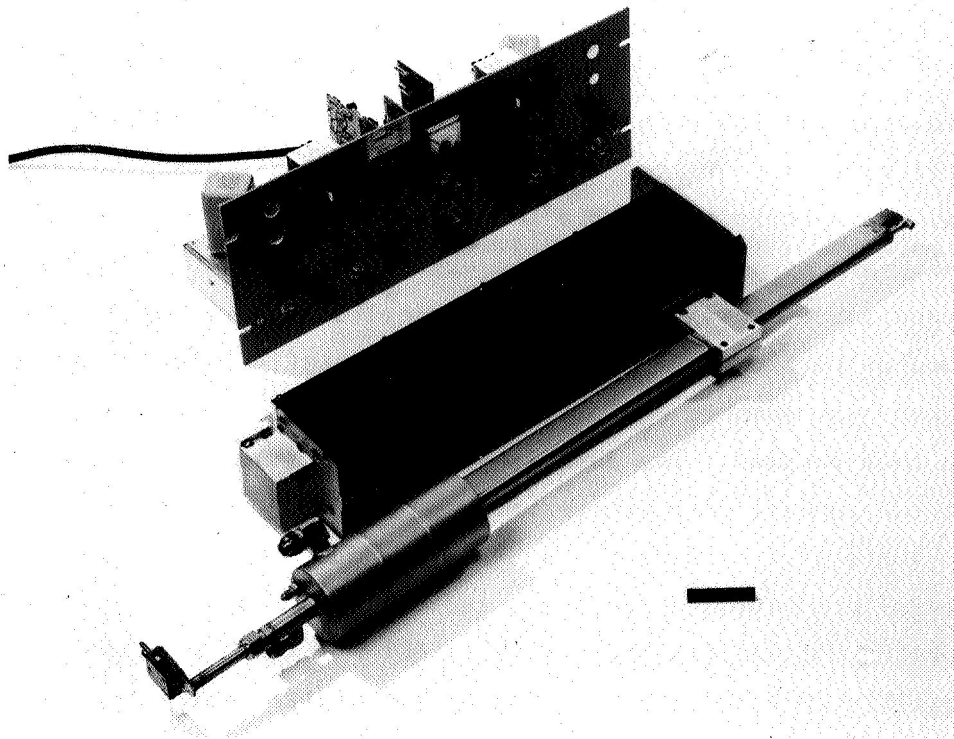


Figure II-30. High-Temperature Traversing Gear FE 65241

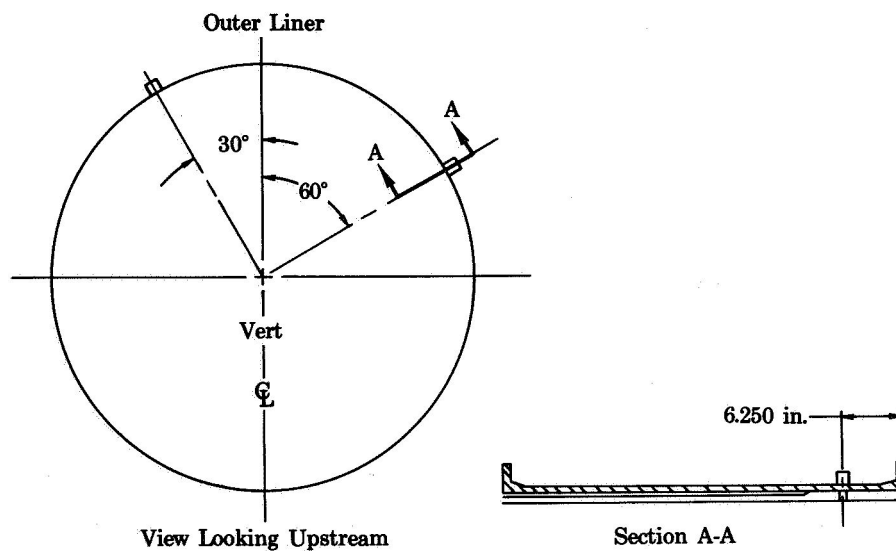


Figure II-31. Dynamic Pressure Sensor Location
on Outer Cooling Liners FD 22342

D. DATA RECORDING SYSTEM

Rig instrumentation data were automatically recorded by the NASA CADDE automatic data recording system. This system automatically records up to 300 pressures and 100 voltages in 30 sec to a quoted accuracy of $\pm 0.15\%$ or better of full-scale range. All information is digitized, encoded, and recorded on magnetic tape for automatic insertion into a high-speed digital computer. The computer accepts the encoded data produced by the recording system and automatically calibrates it, calculates averages, forms ratios, and computes terminal calculations, such as airflow, fuel flow, fuel/air ratio, and Mach numbers. Figure II-32 is a block diagram of the system as used in this program. The SW-24 test facility is connected to the CADDE area of the central data processing room by means of a telephone-type cable. Voltages from sensors (such as thermocouples, potentiometers, and flowmeters) are measured and converted to digital form, one at a time, by an automatic voltage digitizer (AVD). All pressures are taken from the test facility through copper tubing to the digital automatic multiple pressure recorder (DAMPR) system and are transformed into electrical signals. The outputs of the AVD and DAMPR are fed into the temporary storage and sequence control block and are held temporarily to arrange them in proper order. Identification, word numbering, and editing and control instructions are added automatically and the data are fed out in a prescribed sequence according to a predetermined program. The output is fed to the tape handler and recorded at a rate of 20 words per second for all data, except AVD, which may be recorded at different rates depending on the individual digitizer employed.

Recorded data can be sent back to the test cell control room by means of a flexowriter and a facsimile plotter. The raw information permits rough calculations to be made during the testing. The facsimile plotter displays the data for all recorded parameters in a form similar to a calibrated bar graph, which permits easy comparison of proportional numerical values (much like a manometer board). The flexowriter plots 15 data words per second, as compared with one word per second for a typewritten copy.

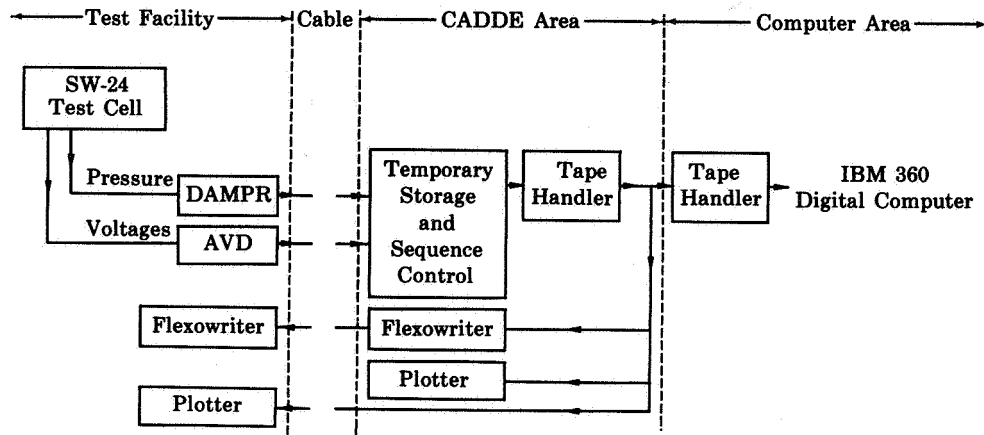


Figure II-32. NASA Data Recording System

FD 22343

SECTION III DIFFUSER, DUCT BURNER, AND FUEL INJECTOR DESIGN

A. DIFFUSER DESIGN

In accordance with the contract requirement, the diffuser was sized for the Pratt & Whitney Aircraft STF-219 turbofan engine, design-rated for 600 lb/sec airflow at sea level static conditions (340 lb/sec duct airflow).

Except for minor contour modifications made to simplify manufacturing, the diffuser configuration and dimensions were taken from the engine design. To reduce construction cost, only four wide diffuser struts were used in the rig instead of four wide and four narrow struts as in the STF-219 engine.

Figure III-1 shows the variation of flow area with length for the rig. A conservative diffuser, having the overall area ratio (duct burner reference area/diffuser inlet area) equal to 2.77, would have been approximately twice the length of the diffuser shown. For this reason, the diffuser and burner designs were integrated so that, instead of diffusing the air to a low velocity and then accelerating it, the air was diffused to the approximate velocity at which it flowed around the burner.

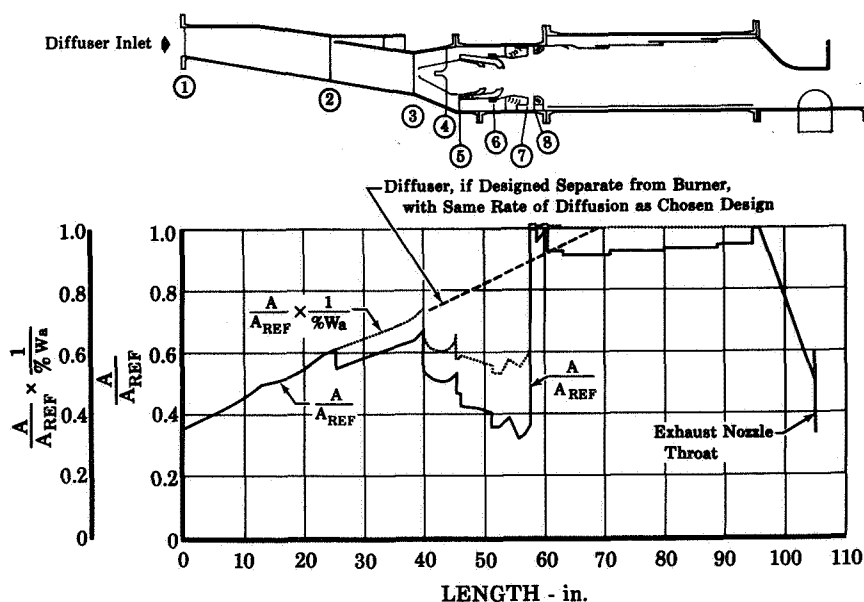


Figure III-1. Flow Area vs Length

FD 13593A

The diffuser length and effective diffusion angle were chosen to satisfy the following requirements:

1. The rate of diffusion was kept low enough to avoid flow separation. Flow separation might cause vibration and non-uniform airflow in the burner; this would, in turn, reduce combustion efficiency. Also, a nonseparating diffuser would generally have high efficiency.
2. The turning angles at the fan discharge and burner inlet, which are at different radii, were minimized. Excessive turning angles create local static pressure variations that cause flow separation.
3. Sufficient space was provided around the inside and outside of the diffuser for the installation of the required engine accessories and equipment.

Figure III-2 shows the separation experience of a series of actual engine diffusers. Compared to these diffusers, the STF-219 engine diffuser was chosen quite conservatively. A conservative design was desirable because of the turns required in the diffuser and because the expected fan discharge airflow would have a large radial velocity variation, with relatively low velocities at the inner diameter.

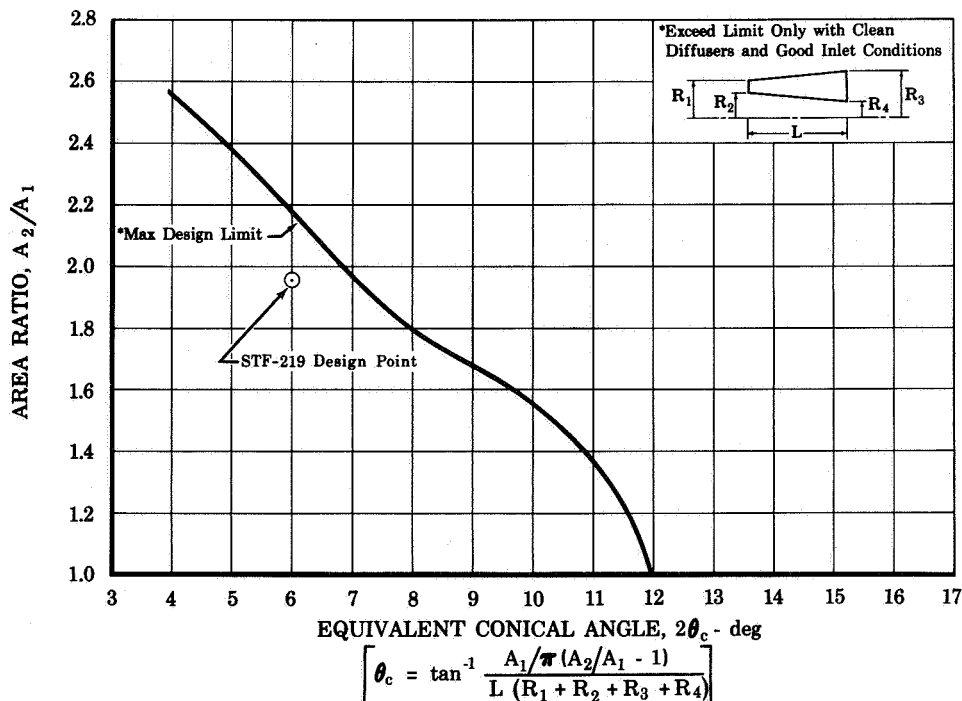


Figure III-2. Diffuser Design Limits

FD 13590A

At Station 2 of figure III-1, approximately 10% of the airflow was bled from the diffuser inner diameter. On the STF-219 engine this flow was diverted for three reasons:

1. To provide approximately 5% of the total airflow to cool the inner cooling liner.
2. To bypass a small additional amount of air (5%) around the burner, using the available space between the engine gas generator and the duct burner. Bleeding allowed the burner radial dimensions to be increased somewhat providing higher burner relative volume with increased burner stability at no additional pressure loss.
3. To remove low velocity airflow from the inner diameter of the diffuser before the turn in the ducting was encountered, minimizing the possibility of flow separation at this turn.

A slight acceleration of the flow was maintained from Station 3 to Station 5 (figure III-1) through the turns and around the sides of the burner dome to improve the flow stability.

B. DUCT BURNER DESIGN

1. Design Criteria

The specific design goals of the duct burner were:

- Minimum combustion efficiency of 95%
- Maximum isothermal total pressure loss of 5% at a duct reference Mach number of 0.15
- Minimum burner life capability of 600 hours
- Smooth, stable operation at all desired operating conditions
- Reasonable simplicity and other characteristics suitable for application to a supersonic transport.

Figure III-3 shows a schematic of a ram-induction duct burner. The ram-induction hardware was positioned in the duct so that it occupied approximately two thirds of the duct cross-sectional area. The burner was fitted with ram air scoops, which turned the air into the combustion zone through efficient, wide-radius turning vanes or scoops. Approximately

30 to 50% of the airflow passed through the dome and liners; the remainder convectively cooled the walls and was burned with fuel further downstream in the tailpipe, as shown in figure III-3. Air entered the burner dome and passed through circular air swirlers located concentrically around each Zone-1 fuel nozzle.

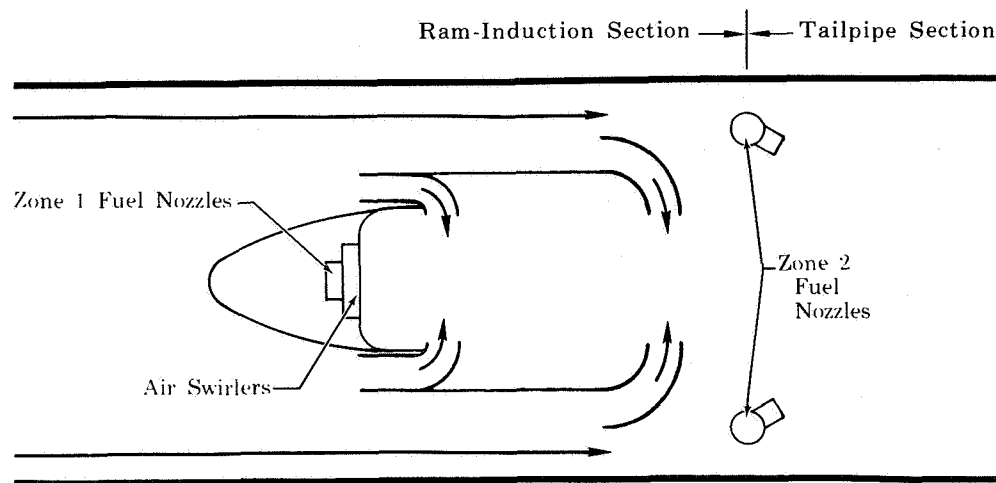
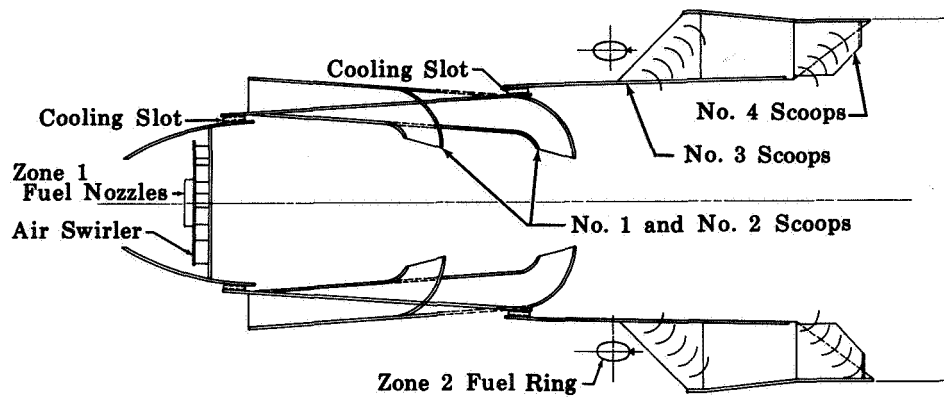


Figure III-3. Typical Ram Induction
Duct Burner

FD 11544B

At low fuel/air ratios, the necessary fuel for combustion was supplied by the Zone-1 fuel nozzles. The efficiently burned gases mixed with the bypass air in the tailpipe; mixing devices immediately downstream of the Zone-2 fuel nozzles ensured a more uniform combustion gas exit temperature profile. At high fuel/air ratios, the additional fuel required was supplied by the Zone-2 fuel nozzles and injected into the bypass air. Combustion took place when the mixture came into contact with the hot, burned Zone-1 gases.

Several segment ram-induction burners had been tested by Pratt & Whitney Aircraft at conditions very similar to those listed in table II-1. The configuration showing the best stability and potential to meet the program requirements was the Model "H" (P&WA designation) burner shown in figure III-4. This model operated with high efficiencies over a fuel/air ratio range of 0.001 to 0.062 at inlet conditions down to 9 psia, 200°F, and a duct reference Mach number of 0.15. It had a low isothermal pressure loss of 4.49 percent.



No. 1 and No. 4 Scoops Are In-Line
No. 2 and No. 3 Scoops Are In-Line

Figure III-4. Schematic of Ram-Induction Duct
Burner, Model "H"

FD 13589A

For the present program, modifications were made to the Model "H" ram-induction burner design to further improve its burning range and efficiency. The most significant changes made were to (1) increase the airflow into the Zone-1 burning region, (2) increase the internal burner volume, and (3) increase the Zone-1 fuel nozzle spacing. These items are discussed in more detail in the following paragraphs.

From segment burner tests, it was found that increasing the Zone-1 fuel flow generally resulted in higher overall burner efficiencies. This was because the high degree of turbulence within the ram-induction section promoted more efficient mixing of the fuel and air. However, the Zone-1 fuel flow could not be arbitrarily increased because the mixture within this section would have become too rich to sustain a flame. The Zone-1 fuel flow could be increased, however, by allowing more air to enter the ram-induction section. Ideally, it was desirable to allow all the air to enter this section; however, the isothermal pressure loss would have been too high. Consequently, the first major modification to the Model "H" burner design was to increase the open areas of the scoops, cooling slots, etc.

To provide operation with this increased airflow over the wide range of test conditions encountered, the internal burner volume was increased. Test results from ram-induction burners indicated a definite relationship

between burning range and the ratio of burner airflow to internal burner volume. This relationship could be expressed as:

$$\frac{\text{Minimum Blowout Pressure at a Given Fuel/Air Ratio}}{\text{Volume}} = \frac{\text{Airflow}}{\text{Volume}} \times K$$

where K was an experimentally determined constant. The ratio of airflow to volume was kept approximately the same as that of the Model "H" ram-induction burner.

The increased internal burner volume was provided by bypassing approximately 10% of the fan discharge airflow through the diffuser bleed and around the inner annulus casing, as previously discussed. Furthermore, because the Model "H" burner had a pressure loss of 4.4% and the target value for the full annular duct burner was 5%, the local area per unit flow at the burner exit (Station 8 of figure III-1) was decreased by the factor $\sqrt{4.4/5}$. This was reasonable because the isothermal pressure loss is very nearly proportional to this factor (the local velocity head).

The final major design modification was to increase the Zone-1 fuel nozzle circumferential spacing to 4.5 inches. This spacing was chosen to obtain high performance while minimizing cost, complexity, and weight, and was wider than the 3.5-inch spacing used in the Model "H" burner. However, the ratio of nozzle spacing to burner dome height was similar for the two burners because of the greater dome height of the full annular duct burner. The nozzle circumferential spacing did not exceed the dome height, a commonly used nozzle spacing criterion. Tests had been made with 3.5- and 7-inch nozzle spacings in another ram induction burner having a 3.125-inch dome height. With the 7-inch spacing, the low pressure rich and lean blowout limits were poorer than those with the 3.5-inch nozzle spacing. However, because the efficiencies were not significantly different, the 4.5-inch spacing was considered fully satisfactory.

2. Design Procedure

As previously stated, the area of the burner openings of the Model "H" burner was increased to provide a higher airflow into the combustion zone. The major changes were made to the No. 1 and 2 cooling slots and the No. 1 and 2 scoops, because of the increased burner durability and efficiency that would result.

The increase in the cooling slot flows was necessary to ensure durability of the burner during tests of long duration. In addition to this increased flow, cooling holes were incorporated into the burner dome firewall to reduce thermal stresses.

The No. 1 and 2 scoops were made wider than those in the Model "H" burner to improve the Zone-1 rich blowout limit. At this limit, the burner front is excessively rich; thus the flame front moves downstream where there is little or no recirculation to hold the flame. Recirculation behind the scoops should aid in holding the flame.

Diffusers were added to the No. 1 and 2 scoops because the annulus velocity was greater than the corresponding scoop velocity in the Model "H" burner. If the diffusers had not been provided, the local annulus velocity would have been higher and the scoop air pressure loss would have been increased. Diffusion also took place in the annulus upstream of the No. 3 scoops.

The number of scoops per Zone-1 fuel nozzle was maintained the same as that in the Model "H" burner. However, the spacing was increased from 3.5 to 4.5 inches, which was consistent with the increased fuel nozzle spacing.

The design calculations for the full annular duct burner were based on the following assumptions:

1. The total pressure around the burner (i.e., in the annular bypass stream) remained constant.
2. The Mach number of the combustion gases leaving Station 8 (figure III-1) was very low (less than half the reference Mach number and less than 30% of the bypass Mach number). Consequently, the internal static pressure variations were negligible (about 10% of the bypass velocity head).
3. The total temperature of the bypass streams remained constant.
4. Frictional losses were negligible.

Using these assumptions and the design criteria previously discussed, a series of trial-and-error calculations was made to determine the radial

position of the burner within the duct and the airflows through and around the burner. The resulting airflow schedule is shown in figure III-5. Pertinent dimensions are included.

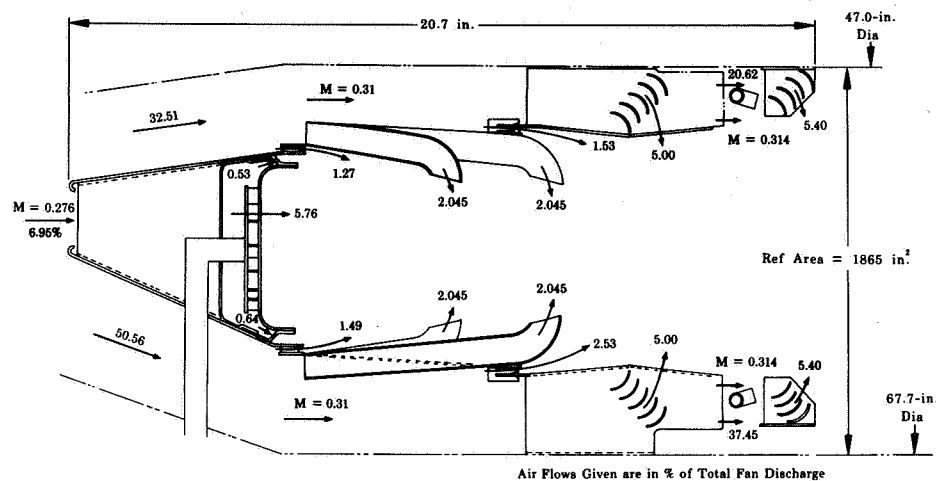


Figure III-5. Airflow Splits for Full
Annular Turbofan Duct Burner

FD 13592A

The total effective flow area (AC_d) of the burner openings and burner bypass areas was calculated as follows. The total effective flow area of the Model "H" ram induction burner was 61.6% of the reference area. Assuming a 5% pressure loss for the full annular burner and that the loss was proportional to the velocity head, the allowable AC_d for the full annular duct burner was then

$$AC_d \text{ total} = AC_{dH \text{ burner}} \times \sqrt{\frac{4.4}{5}}$$

$$AC_d \text{ total} = 61.6 \sqrt{\frac{4.4}{5}} = 58\% \text{ of the duct reference area}$$

Since 90% of the total flow was to pass through and around the burner (10% was diffuser bleed), the total effective flow area for the burner and bypass area was

$$58 \times 0.9 = 52.2\% \text{ of the duct reference area}$$

A comparison of the resulting individual effective flow areas with those of the Model "H" burner is given in table III-2.

As indicated in the flow schedule (figure III-5), 32% of the fan discharge airflow would pass through the burner openings. The corresponding value for the Model "H" burner was 25%. This increased airflow would not only result in higher efficiencies but would also increase the Zone-1 rich blowout limit. This is illustrated by the following example.

At 9 psia, the Model "H" burner had an overall rich blowout fuel/air ratio of 0.014 with only Zone-1 fuel being injected into the burner. Since 25% of the total airflow went into this burner, the local (i.e., within the burner) fuel/air ratio was $0.014 \times \frac{100}{25} = 0.056$. For this local fuel/air ratio to exist in the full annular duct burner, the overall fuel/air ratio would be $0.056 (0.32) = 0.018$. Thus, the burning range of the burner designed for this program was improved over that of the Model "H" ram-induction burner.

Table III-2. Comparison of Model "H" Ram Induction Burner and Full Annular Turbofan Duct Burner

Item	Model "H" Burner	Full Annular Duct Burner	
	$AC_d/A_{ref} - \%$	$AC_d/A_{ref} - \%$	C_d
Swirler	3.08	3.35	0.80
Firewall Cooling Holes			
ID	0	0.31	0.60
OD	0	0.37	0.60
No. 1 Cooling Slots			
ID	0.63	0.74	0.75
OD	0.63	0.87	0.75
No. 1 and 2 Scoops	4.11	4.76	0.71
No. 2 Cooling Slots			
ID	0.63	0.89	0.75
OD	0.63	1.47	0.75
No. 3 Scoops	5.84	5.84	0.80
No. 3 Scoop Bypass	46.00	33.8	0.94
Total	61.55	52.4	
No. 4 Scoops (Vortex Generators)	6.28	6.28	0.80

C. FUEL INJECTOR DESIGN

A two-zone fuel injection system, similar to that used on the Model "H" as well as previous ram-induction burners, was chosen for the full-scale annular duct burner. Zone-1 was located at the upstream portion of the burner and was used from zero to an intermediate fuel/air ratio. Zone-2 was located in the bypass airstream and was used to supplement Zone-1 when high fuel/air ratios were required. With existing designs, one-zone operation did not provide combustion over the extremely wide range of operating conditions and fuel/air ratios required. The Model "H" burner was capable of the full operating range with two zones. All other configurations tested at the date of design had required a third zone (which injected fuel into the third or fourth row of scoops at the minimum pressure and temperature conditions).

Zone-1 was required to operate over a fuel flow range from approximately 30,000 lb/hr at simulated cruise (Zone 1 at 0.035 fuel/air ratio) to about 1600 lb/hr (Zone 1 at as low as a 0.005 fuel/air ratio). This represented a "turndown ratio" of 24.4 to 1. In addition, it was obviously desirable to operate the burner at lower fuel/air ratios at simulated transonic climb, if only for ignition. Since good atomization was required at both low and high pressures, a two-stage (dual-orifice) fuel nozzle system was chosen. This arrangement was the same type as that used in most Pratt & Whitney Aircraft engine primary combustors. The two stages of the fuel nozzle were concentric. The inner stage (or primary orifice) provided a high velocity flow at all test conditions. For small values of secondary flow the high velocity primary stream effectively "pumped" the low velocity secondary stream into the combustion zone at low fuel flow rates. Thus, good atomization was obtained over the 24.4 to 1 "turndown ratio." The fuel flow schedule is shown in figure III-6. In this rig, the two stages were separately manifolded and separately controlled and metered, using two of the three fuel supply systems provided.

The Zone-2 fuel nozzles were located downstream of, and were laterally displaced with respect to, the No. 3 scoops. The location chosen for Zone-2 also allowed removal of the fuel nozzles for inspection or repair without removal of the burner.

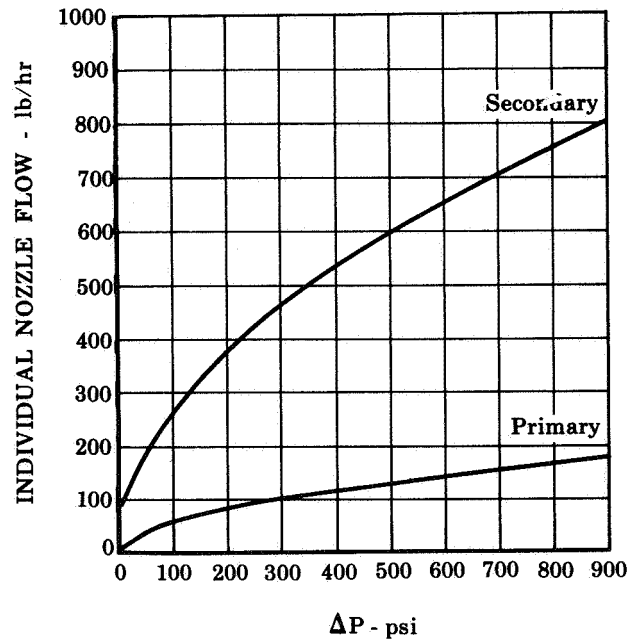


Figure III-6. Zone-1 Flow Schedule

FD 13583A

The Zone-2 fuel nozzles were sized to allow a fuel/air ratio of 0.04 at the simulated cruise condition for experimental purposes, although the program goals could be achieved with a fuel flow corresponding to a fuel/air ratio of 0.03. The minimum fuel flow was established by a fuel/air ratio of 0.01 at the transonic climb condition. The maximum and minimum total flows were 44,500 lb/hr and 3270 lb/hr, respectively, giving a turndown ratio of 13.6 to 1. The Zone-2 fuel injector was mounted in the high velocity bypass air, which aided atomization. Alternative low flow Zone-2 injectors were supplied with the rig for testing. Zone-2 fuel flow was controlled and metered by the third fuel supply system provided. Figure III-7 shows the Zone-2 fuel flow schedule. Simple, swirler-type spray nozzles, mounted on two concentric rings, were chosen. The outer ring consisted of 10 segments with a total of 140 nozzles. The inner ring had four segments with 112 nozzles. The nozzle spacing was approximately 1.4 inches. The factors involved in the design of the Zone-2 fuel rings were:

1. The number of nozzles on the outer ring should be divisible by 10, so that all spray ring segments could be identical. For the same reason, the number of inner ring nozzles should be divisible by four.

2. Fuel flow to the inner ring should be about 78% of the flow to the outer ring because bypass air at the inner ring was 78% of that at the outer ring and the fuel/air ratios at the inner and outer rings should be equal. If identical nozzles were used, the number of nozzles on the inner ring should thus be 78% of the number on the outer ring.

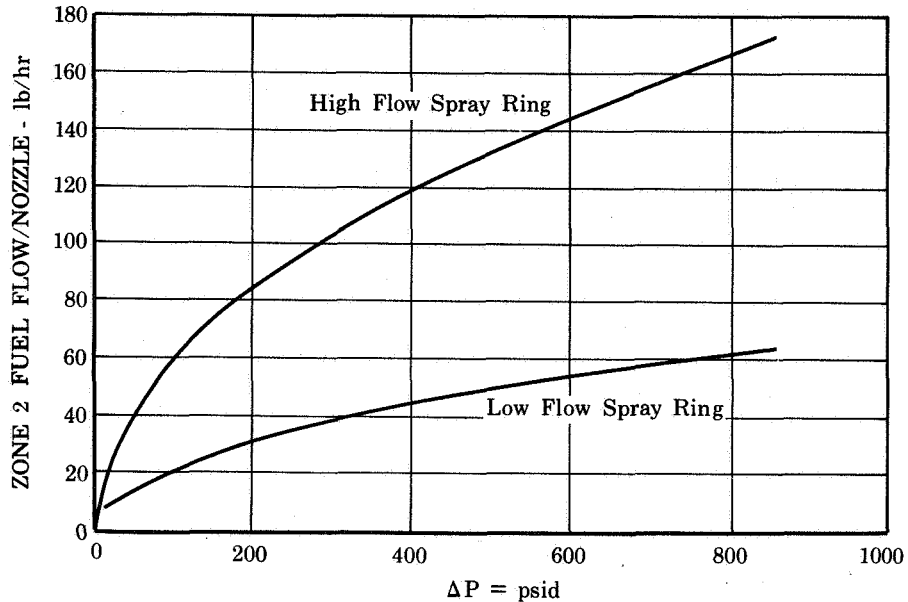


Figure III-7. Zone 2 Fuel Flow Schedule

FD 13582

The "combustion" air at the outer ring was taken to be the outer annular bypass airflow, less 5% for liner cooling air. The "combustion" air at the inner ring was taken to be the inner annular bypass airflow plus one-half of the diffuser bleed air; this bleed air, which was 5% of the total airflow, re-entered the duct just downstream of the vortex generator. The fuel nozzles were aimed 15 degrees inward from the walls to minimize the possibility of fuel from the outer ring entering the cooling air passage and fuel from the inner ring impinging on the inner duct wall. In cold airstreams, such as those at 200°F, impingement of fuel onto cold combustor walls was avoided because it often causes rough operation and reduced combustion efficiency.

SECTION IV
COOLING LINER DESIGN

A. OUTER COOLING LINER

1. Heat Transfer Analysis of Original Liner

(a) General

The outer cooling liner was designed as 60 individual convoluted segments that attached to the outer case as shown in figure II-11. The pressure loading was radially inward and the individual segments were then subjected to hoop loading. This was superior to a single cylindrical liner that would be subjected to a collapsing load due to pressure differentials and would be far more difficult to design, especially with the large diameters involved. A large cylinder would also pose difficulties in maintaining uniform circumferential spacing from the outer casing as it began to expand thermally. The chosen design eliminated this potential problem. The design was further advantageous because individual liner segments could be replaced as required, reducing the replacement cost.

A heat transfer analysis was made to provide an air-cooled liner that would operate in the severe duct burner environment described in the following paragraphs. (Refer to figure IV-1.)

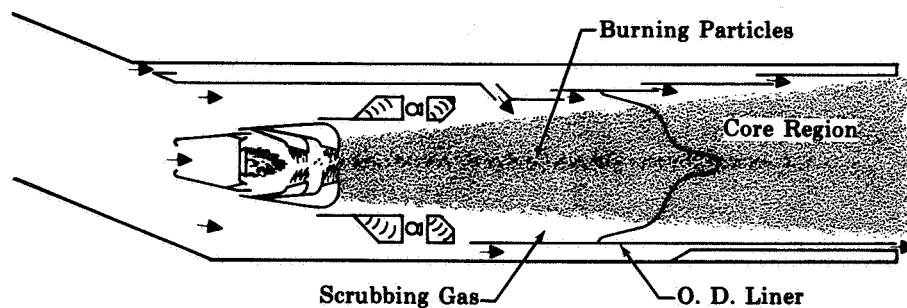


Figure IV-1. Duct Burner Environmental
Conditions

FD 13560A

It was assumed that a hot flame core in the burner contained many localized regions of fuel and air burning at a near-stoichiometric temperature. These particles could burn along most of the duct length and, for illustrative purposes, were shown concentrated in a narrow

strip near the center of the core region. As shown, bypass air flowed past the burner and was injected with fuel from the Zone-2 fuel nozzle ring. This fuel-enriched air passed over the combustion side of the liner and was referred to as "scrubbing gas".

The average core temperature increased in the axial direction because of convective effects and because the combustion process was rate-limited. Similarly, the scrubbing gas axial temperature profile increased with length. The scrubbing gas, which was turbulently mixed with the core gas stream, reached a point of spontaneous ignition, and heat was progressively released as the gas flowed through the duct. The outer liner airflow was supplied from the burner bypass airflow as shown in figure IV-1.

The heat input to a wall element was a combination of forced convection from the scrubbing gas and radiation from the burned products. In the forward section of the liner, the scrubbing gas actually cooled the liner. Heat was normally rejected by forced convection to the coolant air and by radiation to the outer casing.

Because of the multiple zones of burning and different degrees of turbulence within each zone, it was probable that both luminous and non-luminous radiations existed. The luminous radiation, which was caused by a dense concentration of carbon particles in the fuel-rich zones (near the spray nozzle), gave rise to large values of emissivity and was a strong function of pressure level. The nonluminous radiation was caused primarily by CO_2 and H_2O present in the combustion products.

The following general assumptions were made:

1. Both the gas and coolant flows were one-dimensional and steady.
2. The combustion gas properties were the same as those of air.
3. The combustion gas temperature, pressure, velocity, and flow distribution were known (from other independent calculations).
4. Cooling air inlet conditions were known.
5. The combustion products flowing in the duct were nonluminous radiating gases.

6. The emissivity and absorptivity were caused by CO_2 and H_2O present in the products of combustion. They were evaluated at the average gas stream temperature.
7. The radiating gas temperature was equal to that temperature corresponding to the overall fuel/air ratio ($F/A = 0.05$, $T_{gr} = 3890^\circ\text{R}$).
8. The heat balance equation could be written for a local point on the outer diameter liner wall with one-dimensional heat flow.
9. Radiant heat transfer between the outer and inner liners was negligible because of the presence of the absorbing gas separating them.
10. The thermal resistance of the liner wall material was negligible compared to the film resistances.
11. The outer casing wall temperature was approximately equal to the coolant temperature.

Assumptions 5 and 8 warrant further comment. The products of combustion were assumed to be nonluminous because very little free carbon was present. This was the result of the high heat release and intense turbulence level associated with the duct burner design. Previous experience had shown that the assumption of nonluminous radiation adequately accounted for all the radiant heat load over the range of pressures tested. Further evidence of the validity of assuming a nonluminous gas was found in Reference 1.* Assumption 8 placed the gas radiation on the same one-dimensional basis as the convective heat transfer so that calculations could be based on the temperature difference at each station instead of on some integrated mean difference over a finite length of the duct burner. This technique, although a gross approximation of the actual phenomenon, gave good average results, as indicated in References 1 and 2. Other minor assumptions were made during the analysis as required.

*References are given in Appendix C.

(b) General Equations Used in Calculations

The following discussion presents the pertinent equations used in computing wall temperature, coolant temperature rise, and coolant flow rate. Nomenclature is presented at the end of the heat transfer analysis of the outer cooling liner. With the aid of figure IV-2 and assumption 10, the following heat balance equation was written concerning a general point on the wall:

$$q_{r,g_{net}} + q_{c,g} = q_{c,c} + q_{r,w_{net}} \quad (1)$$

where,

$$q_{r,g_{net}} = \sigma \left(\frac{1 + \epsilon_w}{2} \right) \left[\epsilon_g T_{gr}^4 - \alpha_g T_w^4 \right] \quad (2)$$

$$q_{c,g} = h_g (T_{gs} - T_w) \quad (3)$$

$$q_{c,c} = h_c (T_w - T_c) \quad (4)$$

$$q_{r,w_{net}} = \sigma F_{ws} \left[T_w^4 - T_c^4 \right] \quad (5)$$

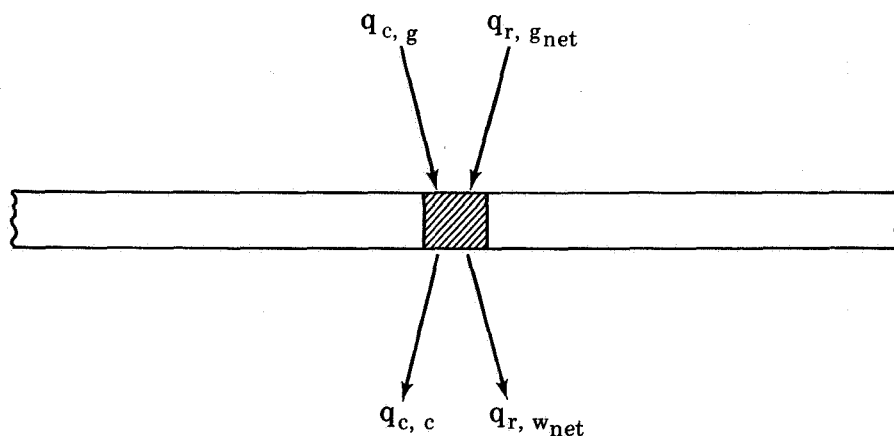


Figure IV-2. Energy Balance for Wall Element

FD 13548

Equation (2) described the radiative heat exchange per unit area between the combustion gas and liner wall. The term $\frac{1}{2} (1 + \epsilon_w)$ approximately accounted for a nonblack enclosure when $\epsilon_w > 0.7$. The emissivity and absorptivity were calculated following methods given in Reference 3. The gas-side convective heat transfer coefficient was derived from the Colburn analogy for a turbulent boundary layer over a flat plate with zero pressure gradient. Laminar starting length was not considered because of the very turbulent free stream conditions induced by the burner, vortex generators, and spraybar. Thus, the final form of the equation for the gas-side heat transfer coefficient, which is derived in Appendix A, was:

$$h_g = 0.0288 \left(\frac{W_g}{A_g} \frac{T_{gs}}{T_{gf}} \right)^{0.8} \frac{f(T_{gf})}{(x - \ell)^{0.2}} \quad (6)$$

where,

$$f(T_{gf}) = \left[\frac{k(P_r)^{1/3}}{(\mu)^{0.8}} \right]_{T = T_{gf}} \quad (7)$$

$$T_{gf} = \frac{T_{gs} + T_w}{2} \quad (8)$$

The coolant heat transfer coefficient was the common Dittus-Boelter Equation for turbulent pipe flow, modified to account for laminar starting length for a sharp-edge entry, as mentioned in Reference 3 (pp 221-226)

$$h_c = 0.023 \left[1 + \left(\frac{D_{HC}}{x - \ell} \right)^{0.7} \right] \left(\frac{W_c}{A_c} \frac{T_c}{T_{cf}} \right)^{0.8} \frac{f(T_{cf})}{(D_{HC})^{0.2}} \quad (9)$$

where,

$$f(T_{cf}) = \left[\frac{k(P_r)^{1/3}}{(\mu)^{0.8}} \right]_{T = T_{cf}} \quad (10)$$

$$T_{cf} = \frac{T_c + T_w}{2} \quad (11)$$

The gray body shape factor, F_{ws} , was for the case of radiation between two parallel plates (end effects neglected). This situation was approximated in the duct burner liner passages.

$$F_{ws} = \frac{1}{1/\epsilon_w + 1/\epsilon_u - 1} \quad (12)$$

The coolant temperature rise was computed by writing the first law of thermodynamics for the control volume shown in figure IV-3. The viscous shear stress at the wall, which gave rise to a work term, was neglected because the coolant pressure loss was known to be small. Therefore,

$$i_{c2} = i_{c1} + \frac{Q}{W_c} \quad (13)$$

where,

$$Q = A \left(\frac{q_1 + q_2}{2} \right) \left(\frac{1}{3600} \right) \quad (14)$$

$$q = q_{c,g} + q_{r,g_{net}} \quad (15)$$

The term i_c referred to the enthalpy per pound of coolant and was known at Station 1. After following an iterative procedure, the enthalpy at Station 2 was determined. The coolant temperature was then obtained from air data, $T_c = f(i_c, p)$.

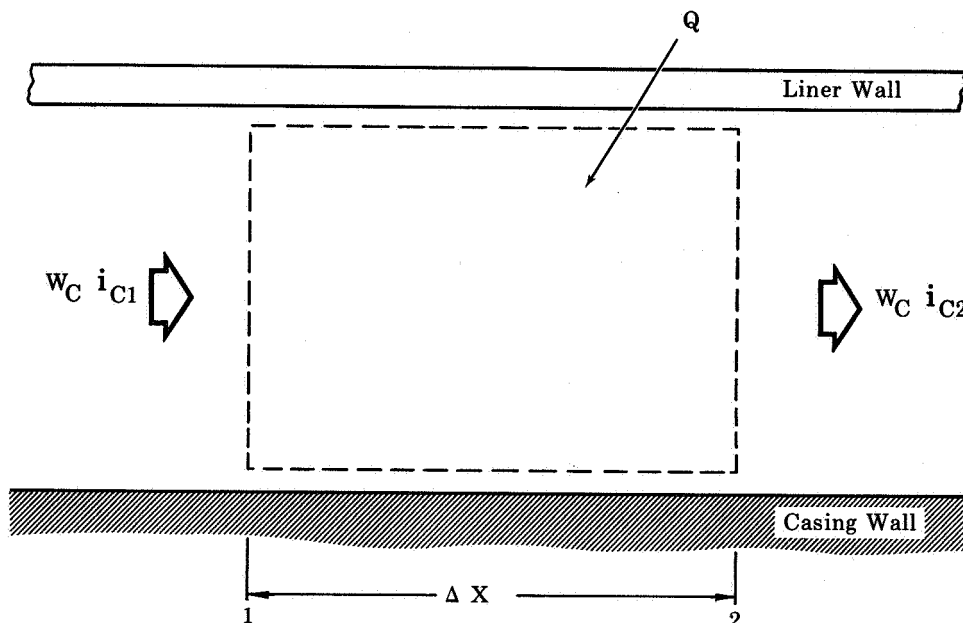


Figure IV-3. Coolant Control Volume Showing Energy Balance

FD 13558

The heat balance equation was then written as follows:

$$\sigma \left(\frac{1 + \epsilon_w}{2} \right) \left[\epsilon_g T_{gr}^4 - \alpha_g T_w^4 \right] + h_g (T_{gs} - T_w) \\ = h_c (T_w - T_c) + \sigma F_{ws} \left[T_w^4 - T_c^4 \right] \quad (16)$$

The following quantities were either known or readily calculable: ϵ_w , α_g , ϵ_g , h_g , h_c , F_{ws} , T_{gr} , and T_{gs} . The coolant and liner wall energy equations, (13) and (16), were solved simultaneously to yield the liner wall temperature (T_w) and coolant temperature (T_c). An IBM 1620 computer program was written to perform the required computations.

(c) Preliminary Calculations

Many preliminary calculations were performed before solving equation (16); the most important were the geometry and coolant flow rate calculations. The geometry equations are presented in Appendix A. These equations gave the coolant flow area, the hydraulic diameter, the perimeter exposed to the heat transfer, and the gas-side flow area. The flow rate was determined by iterative calculations using the static pressure impressed upon the liner entrance by the gas stream and several specified flow rates. The values were processed through an IBM 1620 computer program that calculated the pressure drop in a duct under the influence of friction, area change, and heat transfer. The liner exit static pressure and flow rate were then plotted; the value of flow rate corresponding to the impressed exit pressure gave the desired result. The following equations were used to calculate the static pressure at a given station and are derived in Appendix A:

$$P_{c2} = P_{c1} + \left(\frac{dp_c}{dx} \right) \Delta x \quad (17)$$

$$\frac{dp_c}{dx} = \frac{-4f_m (VH)_m}{D_{HC_m}} - \frac{G_c}{g_c} \left(\frac{V_2 - V_1}{\Delta x} \right) \quad (18)$$

Equations (17) and (18) required values for the geometric variables A_c and D_{HC} plus a temperature profile, which were obtained from the coolant energy balance. This involved two or three trial-and-error calculations. The procedure that was used in the pressure loss program

was one of applying equations (17) and (18) in a stepwise manner. Figure IV-4 illustrates the logic used.

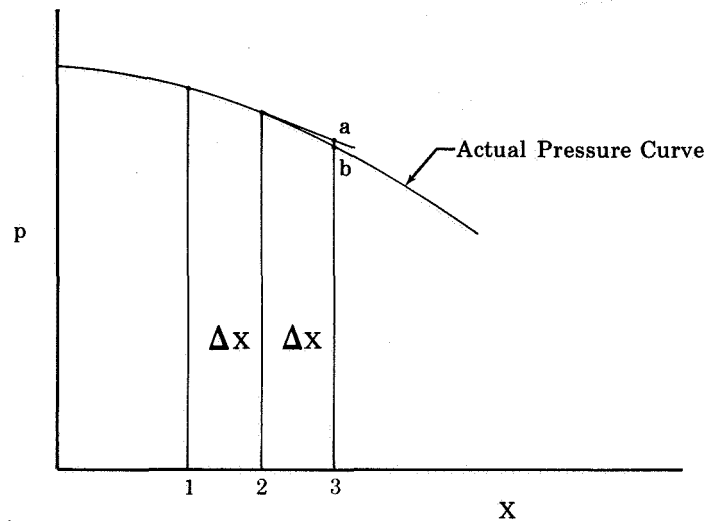


Figure IV-4. Logic Used in Determining Pressure Loss

FD 13547

After calculations at Stations 1 and 2 had been performed, a pressure gradient was calculated and extended to Station 3. A value of pressure (point a) was obtained and then processed through the set of equations until a new gradient was calculated between Stations 2 and 3. The new gradient then yielded a more accurate answer. The computations were repeated until point b was approached to within a specified tolerance. The procedure was applied to all stations.

The following paragraphs present the heat transfer calculations performed on the outer diameter liner design. With reference to figure IV-5, a list of all known quantities are summarized.

$$\begin{aligned}
 N &= 60 \\
 l &= 15.85 \text{ in.} \\
 L &= 34 \text{ in.} \\
 L_s &= 9.28 \text{ in.} \\
 D_i &= 47.7, 47.6, 46.75, 45.85, 44.85 \text{ in.} \\
 D_o &= 67.7 \text{ in.} \\
 t_p &= 0.031 \text{ in.} \\
 \delta &= 0.439 \text{ in.} \\
 h &= 0.77 \text{ in.} \\
 A_{\text{BLK},1} &= 0.1552 \text{ in.}^2/\text{convolution}
 \end{aligned}$$

$$\begin{aligned}
 A_{\text{BLK},2} &= 1.150 \text{ in.}^2/\text{convolution} \\
 \epsilon_w &= 0.72 \\
 F_{ws} &= 0.518 \\
 W_{\text{Total}} &= 309 \text{ lb/sec} \\
 P_o &= 34.1 \text{ psia} \\
 T_o &= 1093^\circ\text{R} \\
 F/A &= 0.050 \text{ (overall)}
 \end{aligned}$$

Total pressure loss from reference section to nozzle,

$$\Delta P/P_o = 0.1417$$

Burner isothermal total pressure loss;

$$\Delta P/P_o = 0.0664$$

The duct burner average temperature profile (figure IV-6) was generated in the following manner. Three points were known and are shown in figure IV-7.

Complete combustion was assumed to occur within the burner from point A to point B. The slight decrease in temperature from point B to point C was the result of the quenching effect of the Zone-2 fuel spray and burner bypass air. The temperature rise curve from point C to point D was important to this analysis. It was assumed that the maximum temperature reached at the nozzle exit plane corresponded to a fuel/air ratio of 0.05. The curve connecting points C and D was calculated from:

$$\frac{T_{gx} - T_{go}}{T_{g1} - T_{go}} = \sin \frac{\pi x}{2 L} \quad (19)$$

where

$$\begin{aligned}
 T_{gx} &= \text{gas bulk temperature at general station} \\
 T_{go} &= 2620^\circ\text{R} \\
 T_{g1} &= 3890^\circ\text{R} \\
 L &= 60 - 16 = 44 \text{ in.}
 \end{aligned}$$

Equation (19) can be found in Reference 2. To apply the relationship, the duct burner heat release was assumed to follow the same physical processes as an afterburner.

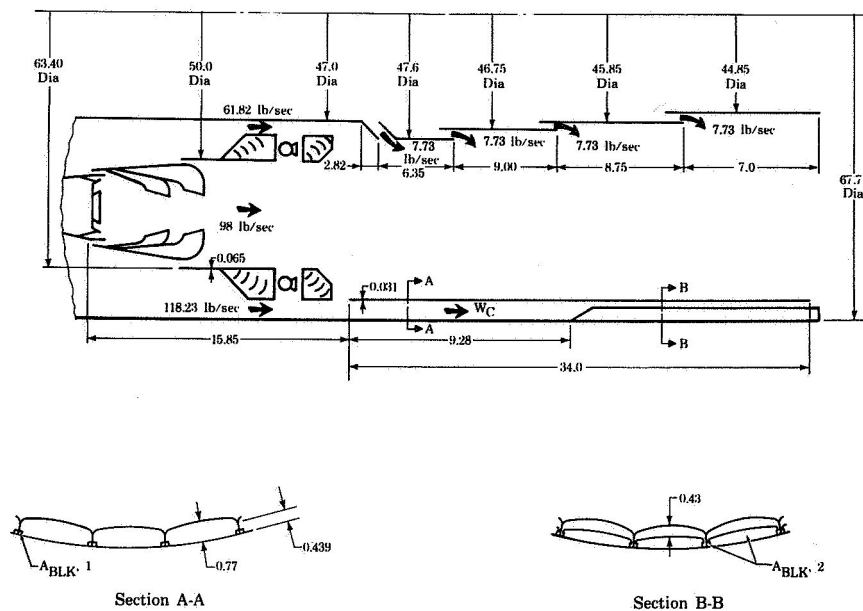


Figure IV-5. Duct Burner Dimensions and Airflow Distribution

FD 13529

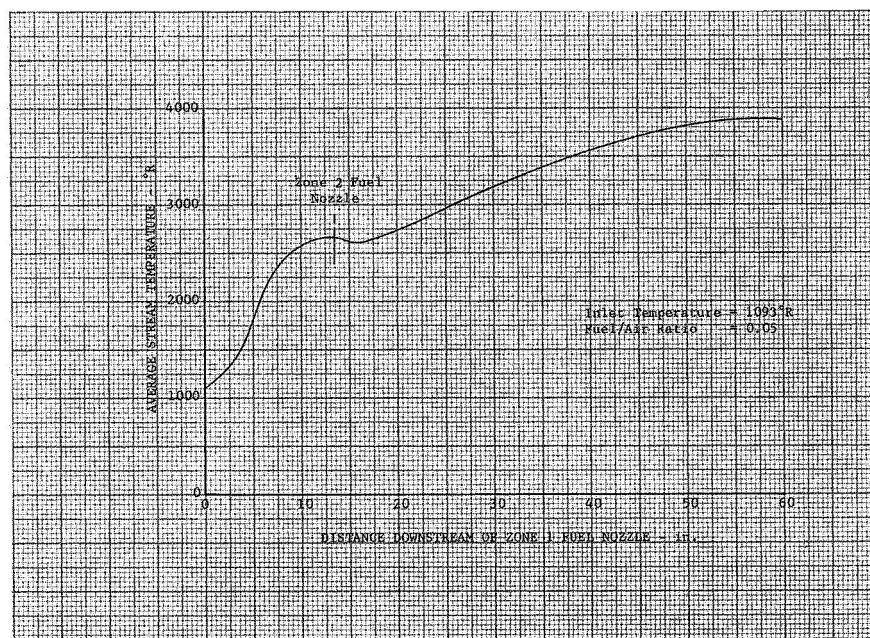


Figure IV-6. Duct Burner Axial Temperature

DF 42359

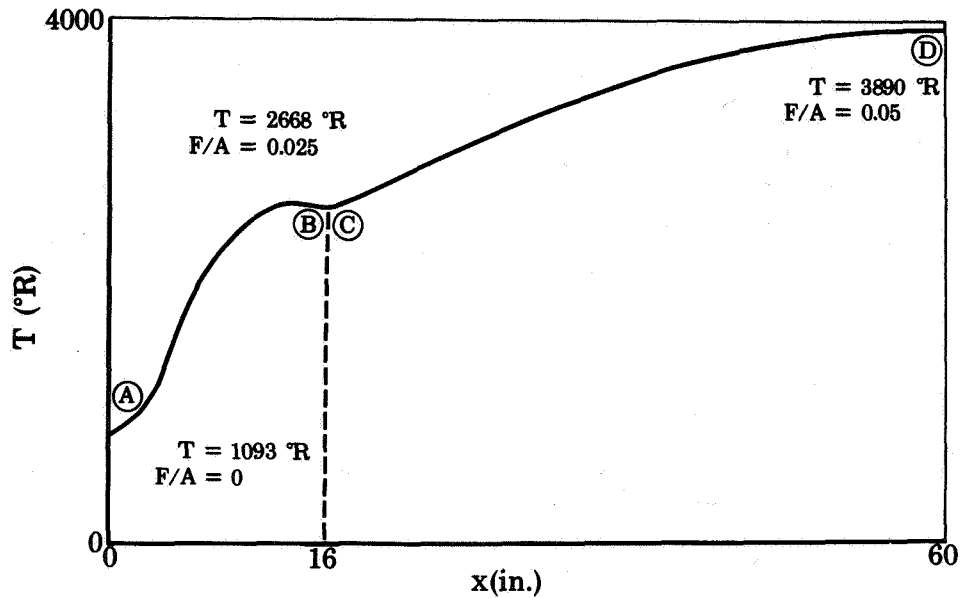


Figure IV-7. Known Temperature Points

FD 22559

The airflow distribution is shown in figure IV-5. The symbol $A_{\text{BLK},1}$ referred to the liner coolant flow area blocked by the fasteners and the symbol $A_{\text{BLK},2}$ to the area blocked by the fasteners plus the filler strip. As mentioned previously, the pressure drop across the liner passage was caused by the external flow. Once the pressure drop was calculated along with the geometry, the coolant airflow rate was determined. These calculations are as follows.

In calculating the liner entrance static pressures, the following quantities were used. (Refer to figure IV-8.)

$$\begin{aligned}
 T_B &= 2668^{\circ}\text{R} \\
 P_B &= 34.1 \text{ psia} - 34.1 (0.0664) = 31.84 \text{ psia} \\
 W_B &= 98 \text{ lb/sec} \\
 T_D &= 1093^{\circ}\text{R} \\
 P_D &= 34.1 \text{ psia} \\
 W_D &= 118.33 \text{ lb}_m/\text{sec}
 \end{aligned}$$

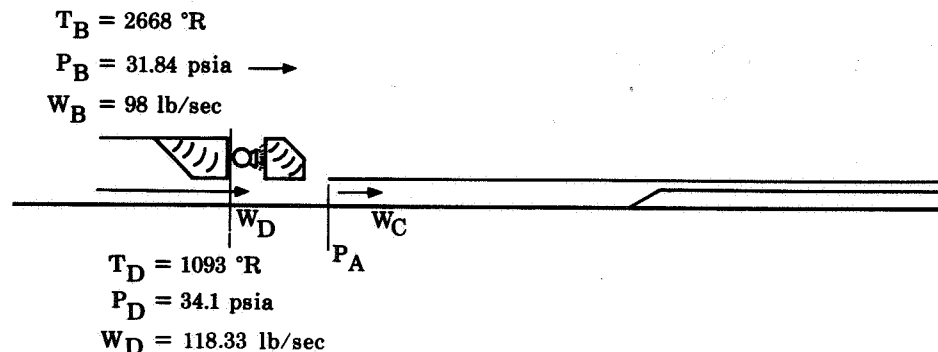


Figure IV-8. Calculation of Liner Entrance
Static Pressure

FD 13559 B

From the compressible flow tables, the ratio of static pressure to total pressure was found as a function of Mach number and compressible flow function:

$$\frac{W_D}{A_D} \frac{\sqrt{T_D}}{P_D} = \frac{118.23 \sqrt{1093}}{0.785(67.7^2 - 63.52^2)(34.1)} = 0.265$$

$$M_D = 0.305 \text{ and } p_D/P_D = 0.9375$$

Therefore,

$$p_D = 0.9375(34.1) = 32 \text{ psia}$$

The pressure at Station A was assumed to be equal to the pressure at Station D, 32 psia, because the length required for mixing between the two streams was very short and the static pressures of both streams vary by only 0.16 psi.

In calculating liner static pressures at the combustion section exit, the following quantities were used. (Refer to figure IV-9.)

Exit total pressure	=	$34.1 - 34.1 (0.1417) = 29.27 \text{ psia}$
Exit temperature	=	3820°R
Specific heat ratio (γ)	=	1.295
Airflow rate	=	$309 \text{ lb}_m/\text{sec}$
Fuel/air ratio	=	0.05
Exit gas area	=	$1/4 \pi (D_o^2 - D_i^2)$
	=	$0.785(67.7^2 - 44.975^2) = 2020 \text{ in.}^2$

$$\begin{aligned}\text{Flow rate } (W_g) &= \text{airflow rate} \times [\text{fuel/air ratio} + 1.0] \\ W_g &= 309(1.05) = 324.5 \text{ lb}_m/\text{sec}\end{aligned}$$

From compressible flow tables, the ratio of static pressure to total pressure was found as a function of Mach number at the exit and mass flow function. The mass flow function was calculated from:

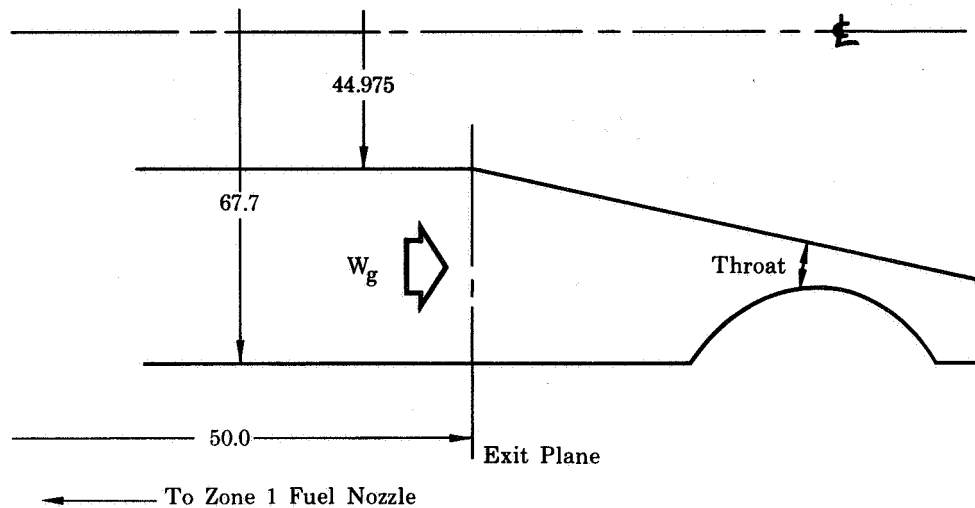


Figure IV-9. Calculation of Liner Exit Static Pressure

FD 13550

$$D = \frac{W_g}{A_g} \frac{\sqrt{T_r}}{P} \sqrt{\frac{R}{\gamma g}}$$

$$D = \frac{324.5}{2020(29.27)} \sqrt{\frac{3820}{1.295 \times 32.2}} = 0.386$$

$$M = 0.43$$

$$p/P = 0.888$$

$$p = 0.888(29.27) = 26.0 \text{ psia}$$

Using the numerical quantities that were summarized previously and applying equations (A-22), (A-19), (A-16), (A-23), (A-15), and (A-24), the following geometric values were computed:

Unblocked Section

$$\begin{aligned}A_c &= 117.4 \text{ in.}^2 \\ D_{HC} &= 0.975 \text{ in.} \\ l_p &= 216 \text{ in.}\end{aligned}$$

Blocked Section

$$\begin{aligned}A_c &= 57.6 \text{ in.}^2 \\ D_{HC} &= 0.478 \text{ in.} \\ l_p &= 216 \text{ in.}\end{aligned}$$

The duct burner gas flow area distribution is presented in figure IV-10. Using the geometric values given above and an entrance pressure of 32.0 psia, values of $W_c = 10, 12, 14,$ and 16 were processed through the pressure drop program. The results are plotted in figure IV-11. For a calculated liner exit pressure of 26.0 psia, the coolant airflow was found to be 14.95 lb/sec. This represented 4.85% of the total fan duct airflow rate.

The scrubbing gas was defined as that layer of gas between the liner wall and hot core (figure IV-1). The analytical prediction of the scrubbing gas profile was complex because it underwent combustion along with the normal mixing process. For design purposes, a scrubbing gas temperature profile was calculated. The assumptions used were considered conservative.

It was assumed that the scrubbing gas approximated the case of tangential injection into a turbulent stream. The air bypassing the burner can was mixed with fuel at the spraybar. Turbulent mixing of the cold scrubbing gas and hot mainstream occurred with a subsequent increase in the scrubbing gas temperature. After a short ignition time delay, spontaneous ignition occurred, and the heat release was gradual as the gas flowed axially. It was assumed that the scrubbing gas temperature rose to the average mainstream temperature at the nozzle exit plane, and that a 2.0 millisecond ignition time delay occurred. The Mach number over the forward portion of the liner was approximately equal to that calculated at Station D from figure IV-8. Therefore:

$$M = 0.265$$

$$c = 1608 \text{ ft/sec (sonic velocity for air at } 1093^\circ\text{R)}$$

$$V = 418.6 \text{ ft/sec}$$

To obtain the axial position at which ignition occurs, it was assumed that the velocity computed was an average value:

$$\begin{aligned} L_{\text{ignition}} &= L_{\text{fuel nozzle}} + \bar{V} \times \tau_{\text{ignition}} \\ &= 13.63 + 418.6 \times 2.0 \times 10^{-3} \times 12 \\ &= 23.63 \text{ in. (referenced to Zone-1 fuel nozzle} \\ &\quad \text{or 10 inches from the Zone-2 spraybar)} \end{aligned}$$

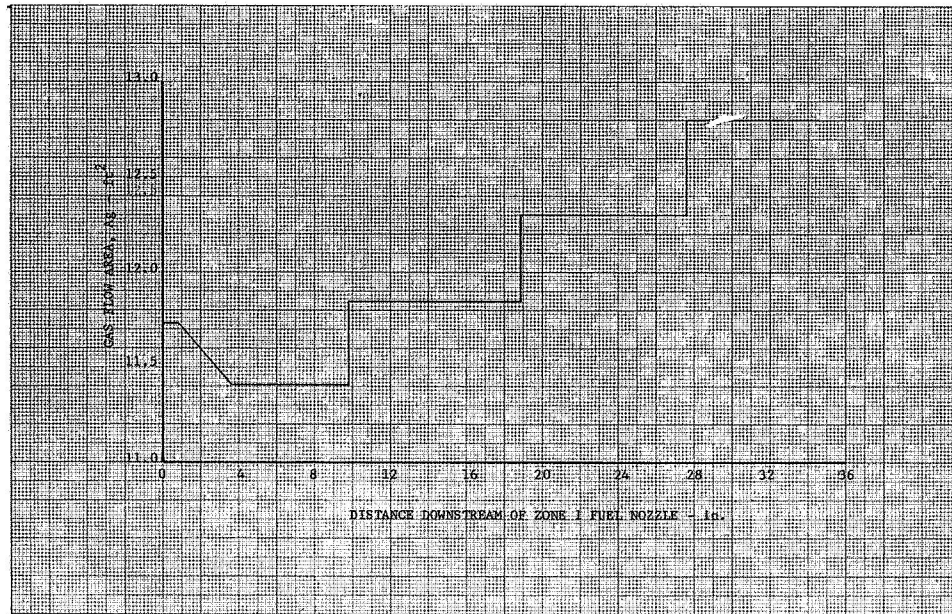


Figure IV-10. Duct Burner Gas Flow Area Distribution

DF 42452

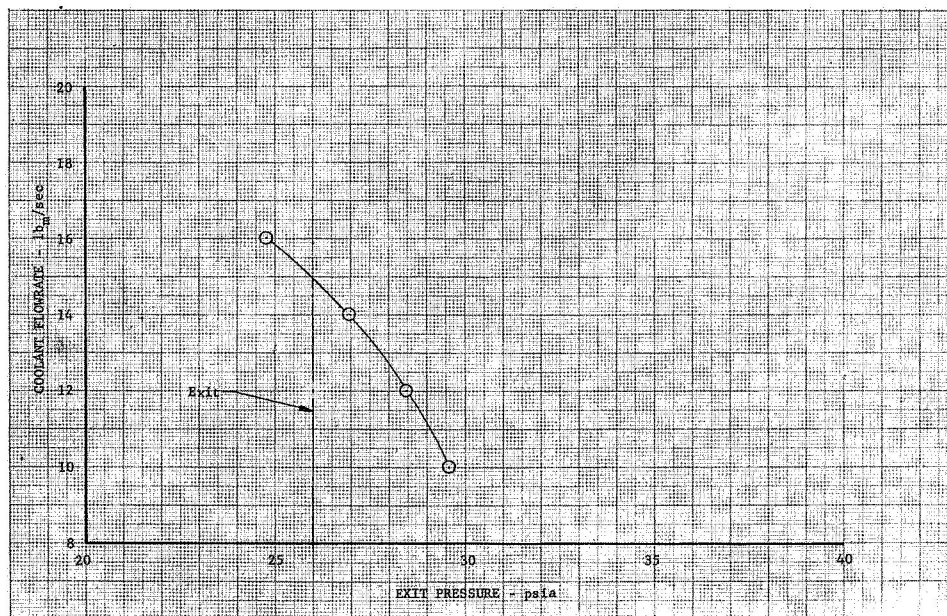


Figure IV-11. Determination of Liner Coolant Flow Rate

DF 42360

To obtain the scrubbing gas temperature in the region of turbulent mixing, P&WA applied a film slot correlation. Unpublished experimental data gave film average temperature as a function of the product of the mass velocity ratio and the ratio of distance to slot height.

$$\frac{T_{gs} - T_o}{T_g - T_o} = f\left(\frac{G_B x}{G_S S}\right)$$

The symbols are shown in figure IV-12 and numerical values follow.

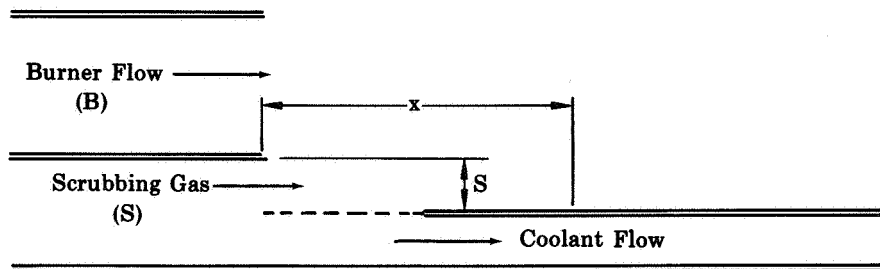


Figure IV-12. Equivalent Film Slot

FD 13555A

$$W_B = 98 \text{ lb/sec}$$

$$p_B = 31.84 \text{ psia}$$

$$T_B = 2668^\circ\text{R}$$

$$G_B = 0.082 \text{ lb/in.}^2 \text{ sec}$$

$$A_B = 1195 \text{ in.}^2$$

$$W_S = 118.23 \text{ lb/sec}$$

$$p_S = 32 \text{ psia}$$

$$T_S = 1093^\circ\text{R}$$

$$G_S = 0.376 \text{ lb/in.}^2 \text{ sec}$$

$$A_S = 315 \text{ in.}^2$$

$$S = 1.88 \text{ in.}$$

The temperature in the turbulent mixing region is shown in figure IV-13.

After spontaneous ignition had occurred, the temperature rise was predicted using figure IV-14. The data presented in the curve were based upon J-57 engine experimental data and were used to describe the heat release, which was rate-limited.

$$\frac{T_{gs} - T_o}{T_1 - T_o} = f\left(\frac{x}{L}\right) \quad (20)$$

In this instance,

$$T_o = 1560^\circ\text{R}$$

$$T_1 = 3890^\circ\text{R}$$

$$L = 60 - 23 = 37 \text{ in.}$$

DF 42361

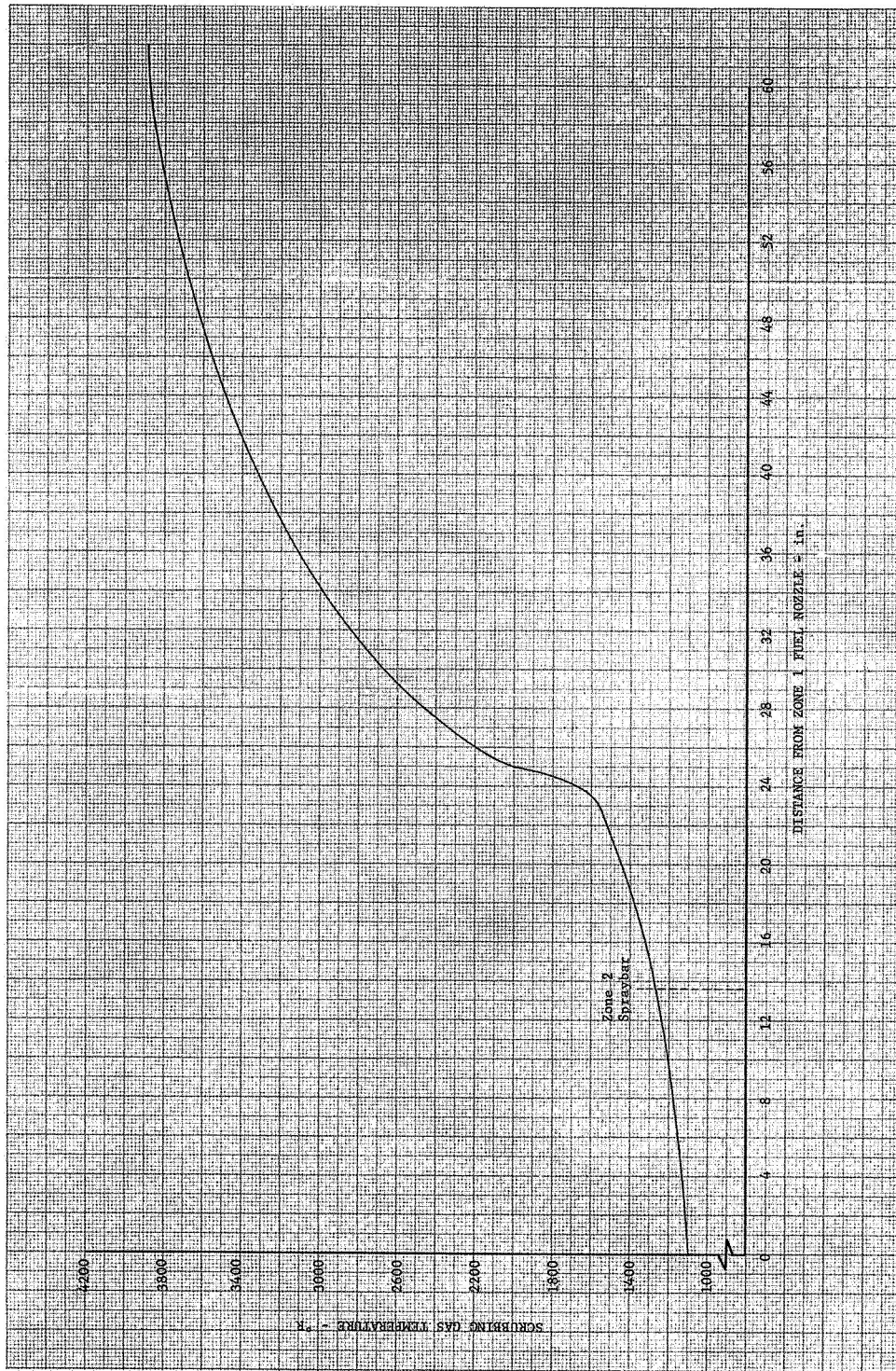


Figure IV-13. Duct Burner Liner Scrubbing Gas Temperature

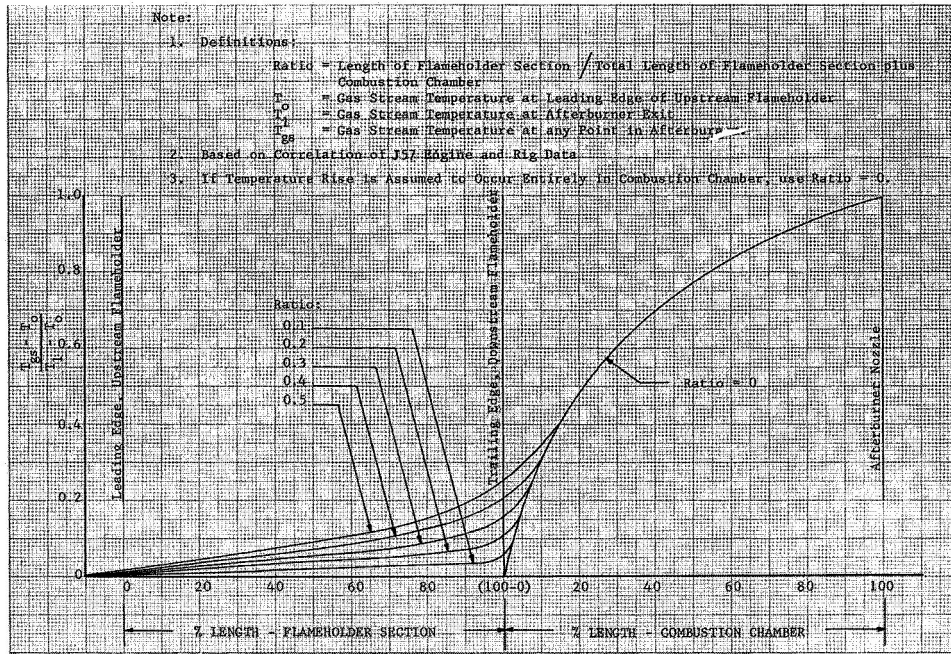


Figure IV-14. Design Temperature Rise Curve

DF 42529

The calculations for emissivity, ϵ_g , and absorptivity, α_g , followed the methods of Reference 3. It is well known that CO_2 and H_2O are the major components in the products of combustion that give rise to gas radiation. The molar concentration of each component was obtained with the aid of an IBM 7090 combustion program for an air/JP5 mixture at $F/A = 0.05$. The concentrations (as mole fractions) of these components were:

$$N_{\text{CO}_2} = 0.0971$$

$$N_{\text{H}_2\text{O}} = 0.0922$$

The above mole fractions were assumed to exist along the entire combustion chamber. An average chamber pressure of 29.7 psia was used. Thus, the partial pressure of each component was:

$$P_{\text{CO}_2} = \frac{29.7}{14.7} (0.0971) = 0.196 \text{ atm}$$

$$P_{\text{H}_2\text{O}} = \frac{29.7}{14.7} (0.0922) = 0.1861 \text{ atm}$$

The effective beam length was approximated by an expression presented in Reference 4. Using the dimensions given in figure IV-5,

$$\begin{aligned}\hat{L} &= 3.4 \frac{\text{Volume}}{\text{Surface Area}} \\ &= 1.211 \text{ ft}\end{aligned}$$

Therefore,

$$(\hat{P}_{\text{CO}_2} \hat{L}) = 0.237 \text{ ft atm}$$

$$(\hat{P}_{\text{H}_2\text{O}} \hat{L}) = 0.225 \text{ ft atm}$$

These values for the product of partial pressure and beam length were used with the axial temperature profile given in figure IV-6 to calculate α_g and ϵ_g . The resulting values are plotted as a function of the distance from the Zone-1 fuel nozzle in figure IV-15.

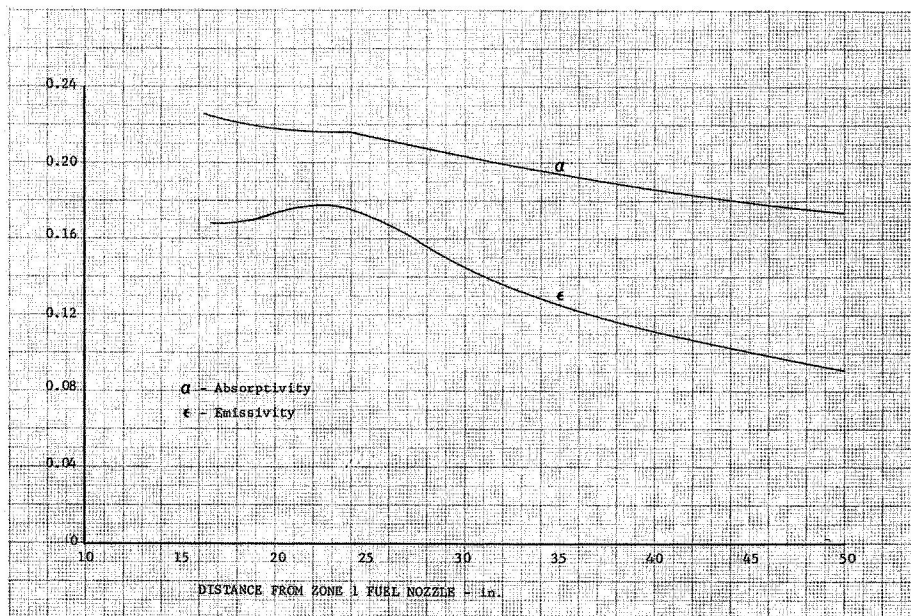


Figure IV-15. Duct Burner Hot Gas Emissivity and Absorptivity

DF 42358

(d) Solution of General Equations

Having calculated the various geometric quantities, coolant flow rate, emissivities, absorptivities, and the scrubbing gas temperature profile, equation (13) and (16) were solved. The calculated liner wall axial temperature profile and coolant temperature rise are plotted in

figure IV-16. The temperature discontinuity represents an abrupt area change because of the ramp. Figure IV-17 presents the coolant side, gas side, and effective radiation heat transfer coefficients. The effective radiation heat transfer coefficient was defined as:

$$h_{gr} = \frac{\sigma \left(\frac{1 + \epsilon_w}{2} \right) \left[\epsilon_g T_{gr}^4 - \alpha_g T_w^4 \right]}{T_{gr} - T_w} \quad (21)$$

As shown in figure IV-18, the coolant heat transfer coefficient doubled while the others remained relatively constant. The maximum predicted liner wall temperature was found to be 2248°R (or 1788°F). The exit coolant air temperature was calculated to be 1390°R.

(e) Nomenclature

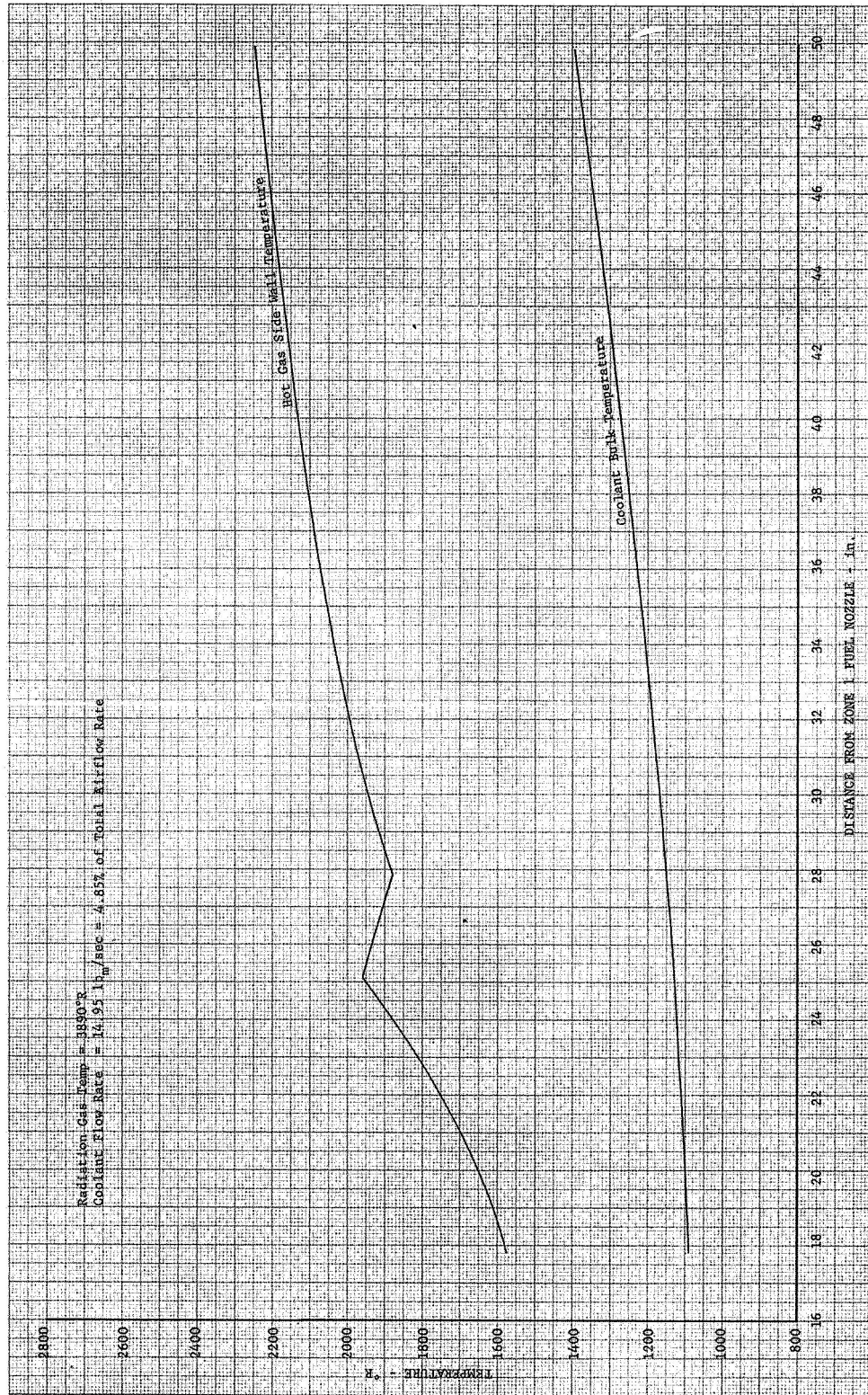
Symbol	Description	Units
A	Area	in.
A _{BLK}	Blocked area	in. ²
C _f	Friction coefficient	
C _p	Specific heat at constant pressure	Btu/lb _m °R
D	Mass flow function	$\frac{W}{A} \frac{T}{P} \sqrt{\frac{R}{\gamma g}}$
D _{HC}	Hydraulic diameter	in.
D _i	Inside diameter of duct burner	in.
D _o	Outside diameter of duct burner	in.
F _{ws}	Radiation view factor	
F/A	Fuel/air ratio	
f	Friction factor	
f _i	Isothermal friction factor	
g _c	Gravitational constant	32.2 lb _m ft/lb _f sec ²
G	Mass velocity	lb _m /in. ² sec
h	Heat transfer coefficient	Btu/hr ft ² °R
h	Convolution height of liner	in.
i	Enthalpy	Btu/lb _m

Symbol	Description	Units
k	Thermal conductivity	Btu/hr ft °R
\hat{L}	Beam length	ft
L	Liner length, also general length dimension	in.
ℓ	Distance from liner to Zone-1 fuel nozzle	in.
L_s	Liner length up to filler strip	in.
M	Mach number	
N	Number of convolutions	
\hat{P}	Partial pressure	atm
p	Static pressure	psia
P	Total pressure	psia
P_r	Prandtl number	$\frac{C_p \mu}{k}$
$q_{c,c}$	Convective heat flux (coolant-side)	Btu/hr ft ²
$q_{c,g}$	Convective heat flux (gas-side)	Btu/hr ft ²
$q_{r,g}$	Radiation heat flux (gas-side)	Btu/hr ft ²
$q_{r,w}$	Radiation heat flux (wall-side)	Btu/hr ft ²
Q	Total heat flow	Btu/hr
Re	Reynolds Number	$\rho V x / \mu$
T	Temperature	°R
T_{cf}	Coolant-side film temperature	°R
T_{gs}	Scrubbing gas temperature	°R
T_{gr}	Radiating gas temperature	°R
T_{gf}	Gas-side film temperature	°R
t_p	Metal thickness	in.
V	Velocity	ft/sec
VH	Velocity head	lb _f /in. ²
W	Flow rate	lb _m /sec
x	Variable distance along liner	in.
α	Absorptivity	
δ	Sidewall height	in.

Symbol	Description	Units
ϵ	Emissivity	
γ	Specific Heat Ratio	
ρ	Density	lb/ft ³
σ	Stefan-Boltzmann's Constant	
μ	Viscosity	lb/ft-sec
τ	Time, ignition delay	sec

Subscripts

c	Coolant
g	Gas
m	Mean
r	Radiation
s	Slot
u	Outer skin
w	Wall
x	Distance in x direction along liner
o	Reference station
1	Station number
2	Station number



DF 42382

Figure IV-16. Liner Temperature Profile for Duct Burner Rig

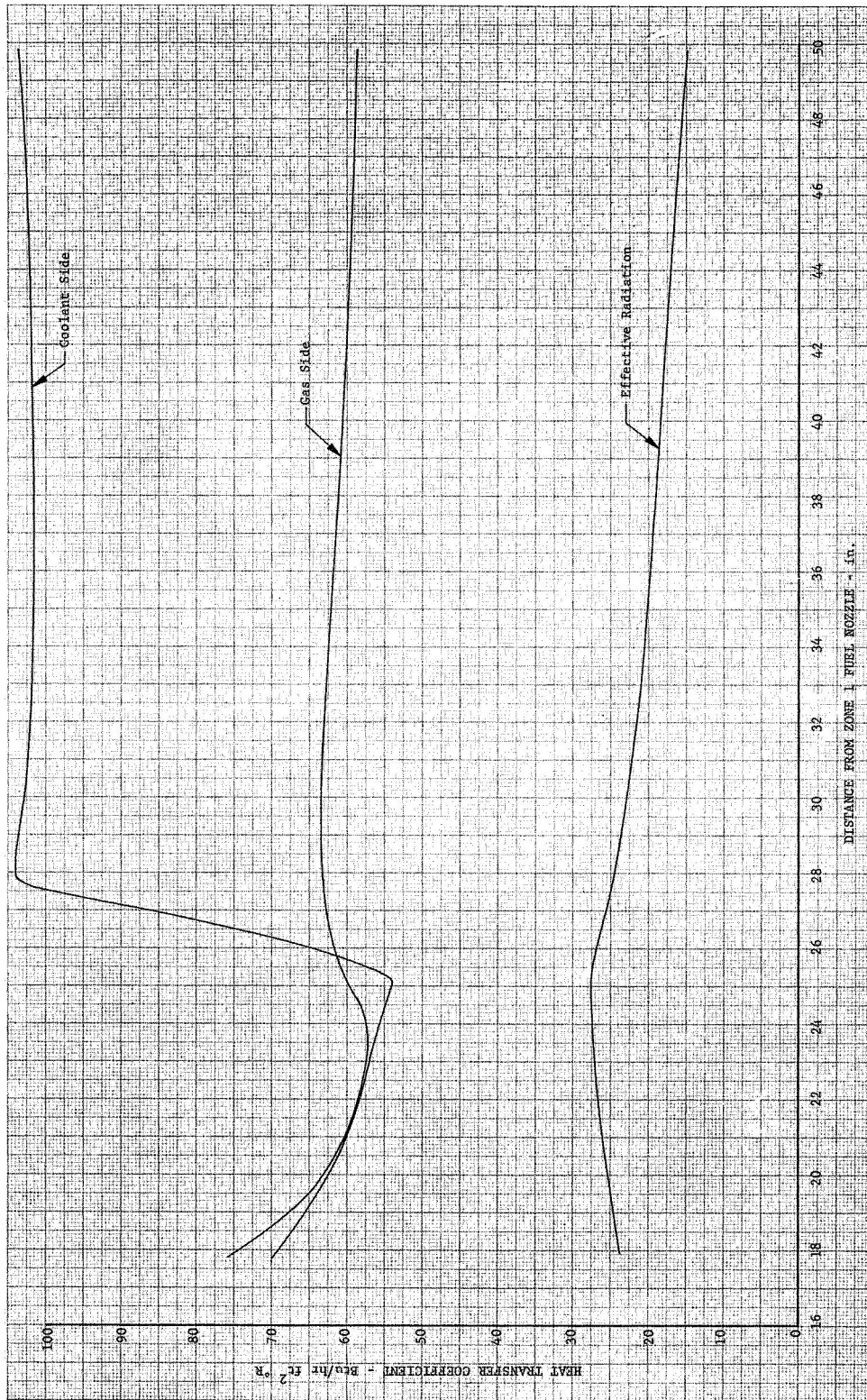


Figure IV-17. Liner Heat Transfer Coefficients for Duct Burner Rig

DF 42383

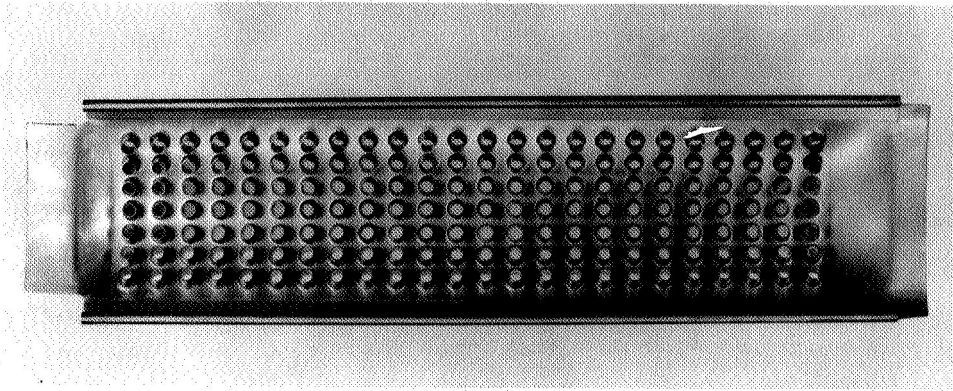


Figure IV-18. Acoustic Damping Outer
Liner Segment

FE 63618

2. Acoustic Damper Design

The outer cooling liners were redesigned during the test program to incorporate an acoustic suppressor system because of the occurrence of combustion instability. To place the acoustic suppressor in the proximity of the combustion, the forward section of the liner was designed to incorporate perforations and tubes, as shown in figures II-15, IV-18, and IV-19. This type of acoustic damper has proved to be highly successful in rocket chamber applications. The liner was to act as Helmholtz resonators, using the principle discussed in Appendix B. The curves in figure IV-20 show the estimated absorption coefficients at different frequencies and aperture velocities for this configuration. The absorption coefficient was the predicted percentage of the incident pressure wave that is not reflected from the liner. At the anticipated aperture velocity of 300 fps and acoustic frequency of 200 Hz, an absorption coefficient of 0.14 was obtained.

The aft section of the cooling liner was redesigned to incorporate corrugations (figure IV-21) to allow the top of the liner to expand more than the side areas, which were shielded by the tracks, creating thermal gradients during testing at high fuel/air ratios. A heat transfer analysis, similar to the one previously conducted on the original outer liners, showed the maximum skin temperature to be 40 degrees higher than the original outer liner while using only 2.26% of the total air flow rate. The predicted skin temperature is shown on figure IV-22.

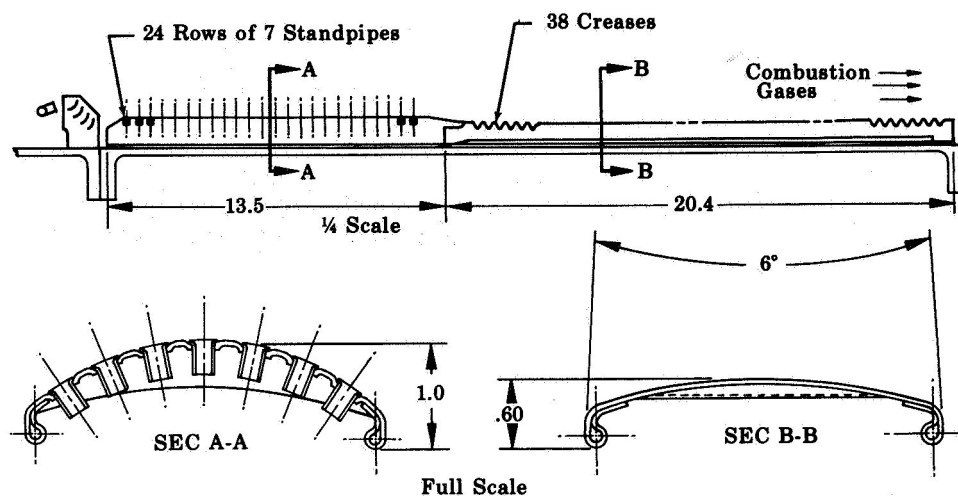


Figure IV-19. Revised Outer Cooling Liner Design

FD 18094A

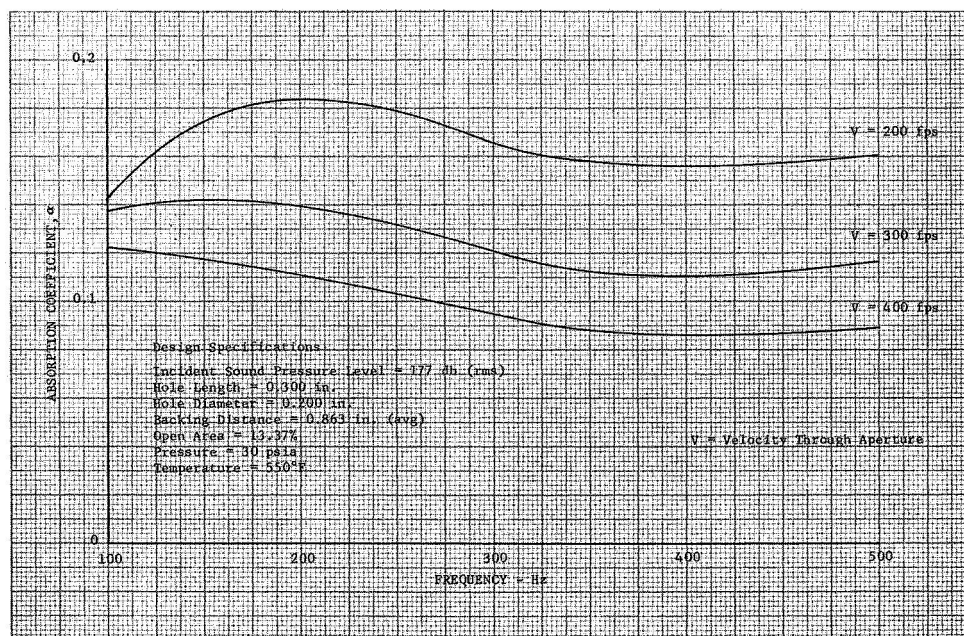


Figure IV-20. Expected Absorption Coefficient at Different Frequencies and Aperture Velocities

DF 55417

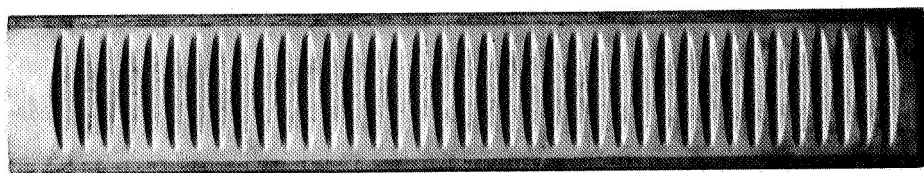


Figure IV-21. Corrugated Outer Liner Segment

FE 63615

DF 61096

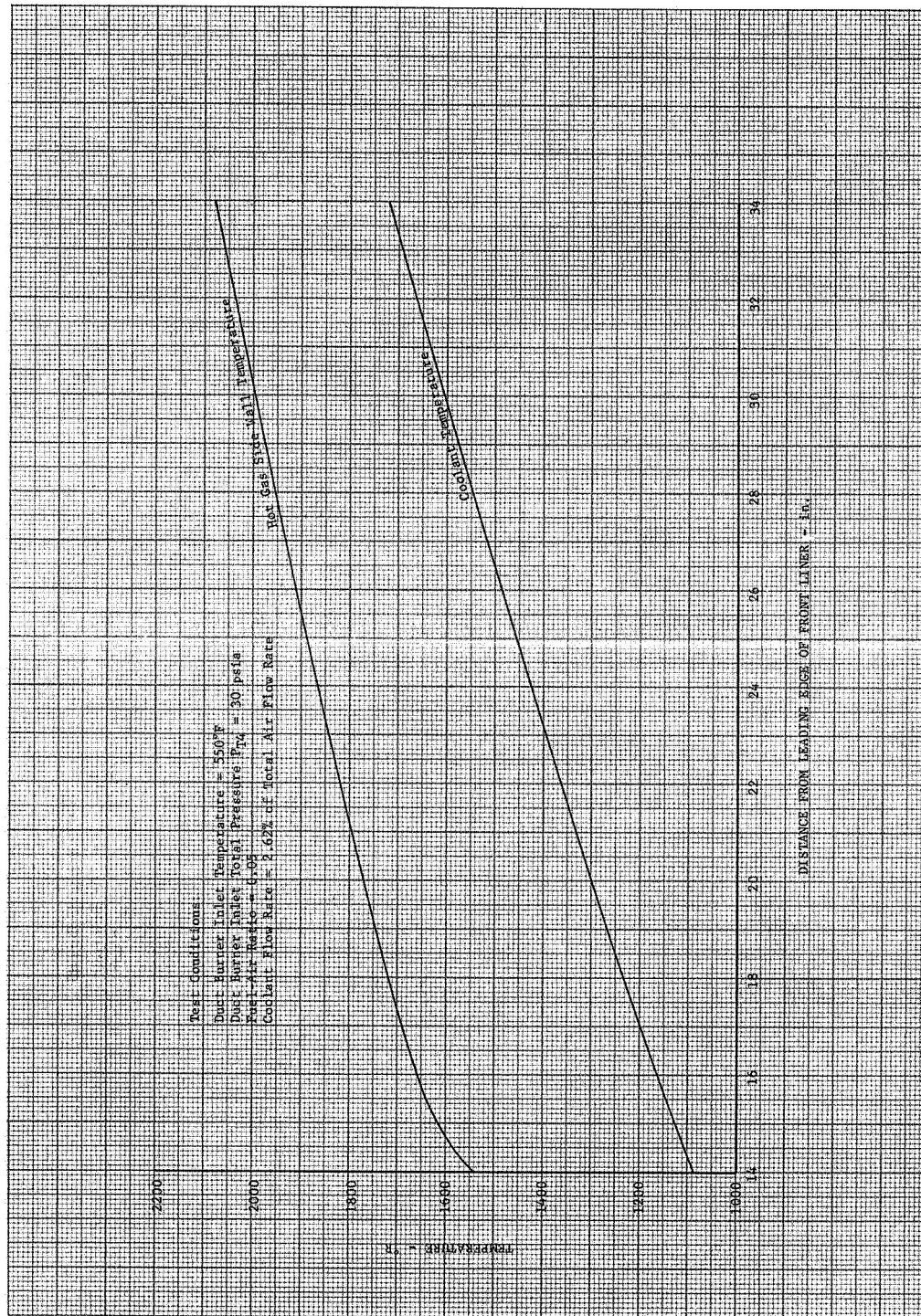


Figure IV-22. Calculated Outer Liner Temperature

B. INNER COOLING LINER

1. Film Cooling

The film-cooled inner cooling liner incorporated three narrow louvers and utilized cooling air obtained from the diffuser bleed. (Refer to figure II-17.) In an engine, the diffuser bleed air would flow in an annulus created by the duct burner inner casing and the compressor and main burner outer casings. In this rig, the bleed flow merely dumped into the internal centerbody volume for simplicity with no effect on performance. Approximately half of the bleed air re-entered the combustion area at the extreme upstream portion of the inner cooling liner. Some of this air aided inner liner cooling and some entered the combustion process.

2. Acoustic Damper Design

Since the outer cooling damping liners were not adequate in eliminating combustion instability and additional volume was available on the inner wall, it was decided to build additional absorption into this wall. This volume was also limited and performance data were not available on the configurations that could be incorporated, so tests were performed at the Florida Research and Development Center to optimize the design. The following paragraphs present the results of the studies and the predicted performance of the inner acoustic damper that was designed and constructed.

A Helmholtz resonator-type damper was designed using the inner wall volume shown in figure IV-23. The volume conveniently available was approximately 10 inches long and 1-1/8 inches deep and extended around the inner circumference of the duct. It was necessary to choose the best size, number, and depth of holes to bring the resonator frequency as near as possible to the 450-Hz instability frequency (to maximize the oscillating flow of air through the holes) and to provide the optimum resistance to flow through the holes: enough to absorb energy from flow oscillating in the holes, but not so much as to stop the oscillations. Optimum absorption occurs when the product of oscillating flow rate and resistance to flow reaches a maximum.

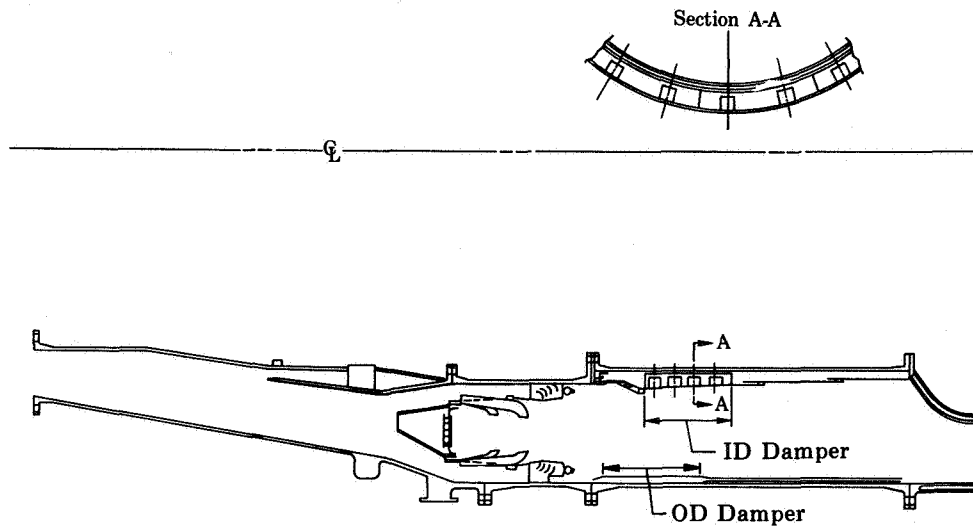


Figure IV-23. Location of Damping Liner

FD 19352B

From preliminary calculations, it was found that an open hole area small enough to obtain the right resonant frequency resulted in excessive resistance. Conversely, an open area large enough to provide optimum resistance resulted in the resonant frequency being too high. The resonant frequency depends upon the inertia of the air in the holes and the volume of the chamber. The inertia is increased and the frequency is decreased as the ratio of hole effective length to hole cross-sectional area per unit chamber volume is increased. To lower the resonant frequency without significantly increasing resistance, deep holes were desired. Tubes (standpipes) connected to the holes in the wall were extended until they approached the rear wall of the volume. In some previous cases, it had been found that locating the end of such a tube near a wall substantially increased the effective length, probably because of the velocity in the radial portion of the flow next to the wall. Thus, this tube location near the wall not only provided the maximum actual tube length but was expected to provide the maximum effective length as well. Large tubes were used, primarily because the use of fewer large tubes (96) rather than thousands of small tubes simplified construction. Also, large tubes have a somewhat longer effective length than small tubes of the same actual length and the maximum effective length was desired. Consideration was also given to use of concentric tubes, as shown in figure IV-24, which provide a longer effective length

but at the expense of higher resistance; however, the concentric tube design yielded very small values of absorption coefficient.

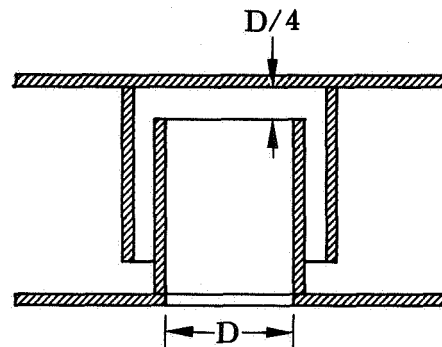


Figure IV-24. Concentric Tube Damper

FD 20594

Before choosing the hole diameter or percentage open area, tests were conducted using simulated cavities at several amplitudes and two frequencies. The results of these tests were used to obtain the effective length and resistance of these particular configurations, so that an optimum design could be calculated. In addition, actual absorption coefficients were measured and used as a check on the calculated predicted absorption.

The rig inner wall damper was therefore designed, based on the analytical and test results obtained, to provide a resonant frequency close to the observed 450 Hz rig frequency and to have good absorption characteristics over a wide band of frequencies near the resonance point.

The final design of the rig inner wall damper is shown in figure IV-25. It contained eight 1-inch diameter tubes in each 30-degree section of the volume. The damper was divided into 12 separate volumes by inserting dividing walls every 30 degrees. This was done to prevent crossflow, which might have occurred within the damper. The open area was 5.23% of the damper face area. The computed absorption characteristics are shown in figure IV-26. Although the predicted resonant frequency was 540 Hz, peak absorption fell at about 400 Hz at high sound amplitude and 450 Hz at intermediate amplitudes. The predicted absorption coefficient at 450 Hz varied from approximately 0.3 at high amplitudes to approximately 0.7 at very low amplitudes. These were about the desired values. The predicted characteristics that would have been obtained with a reduced number of holes are shown in figures IV-27 through IV-29.

The preceding design and computed performance were obtained from a computer program based on the ideal Helmholtz resonator theory supplemented with test data. Details are presented in Appendix B.

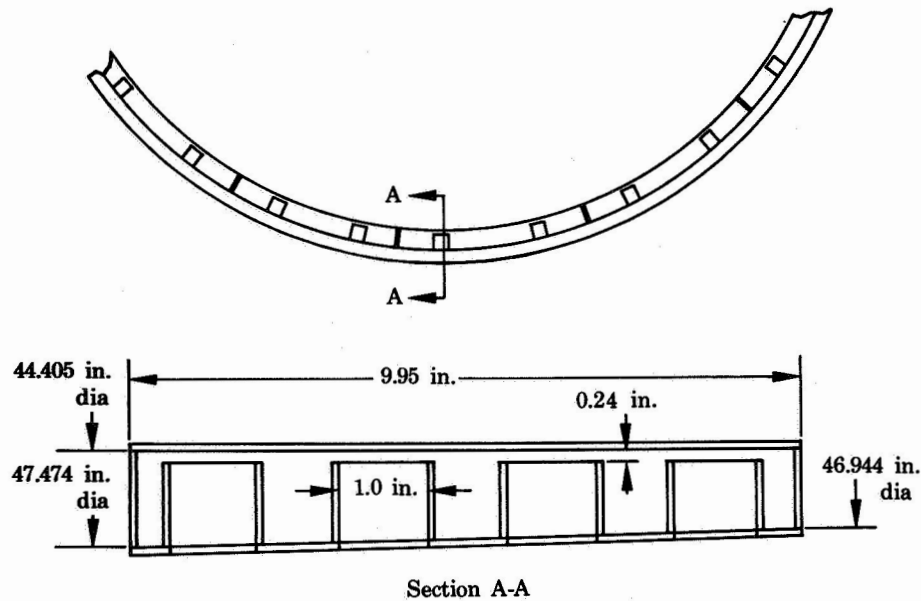


Figure IV-25 Inner Wall Damper Design

FD 20598A

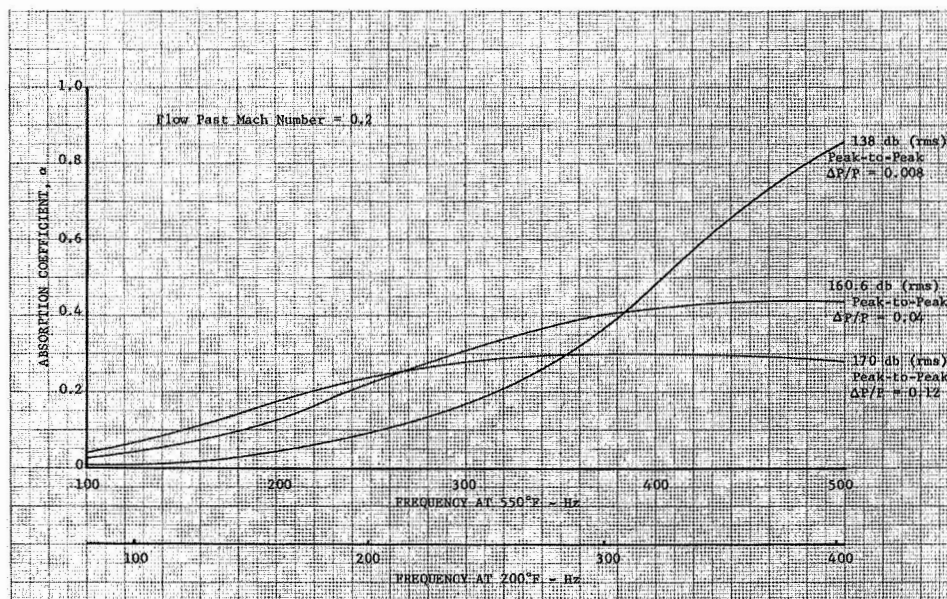


Figure IV-26. Estimated Burner Absorption Coefficient for Duct Burner Inner Wall Damper Design at Various Incident Sound Pressure Levels

DF 55418

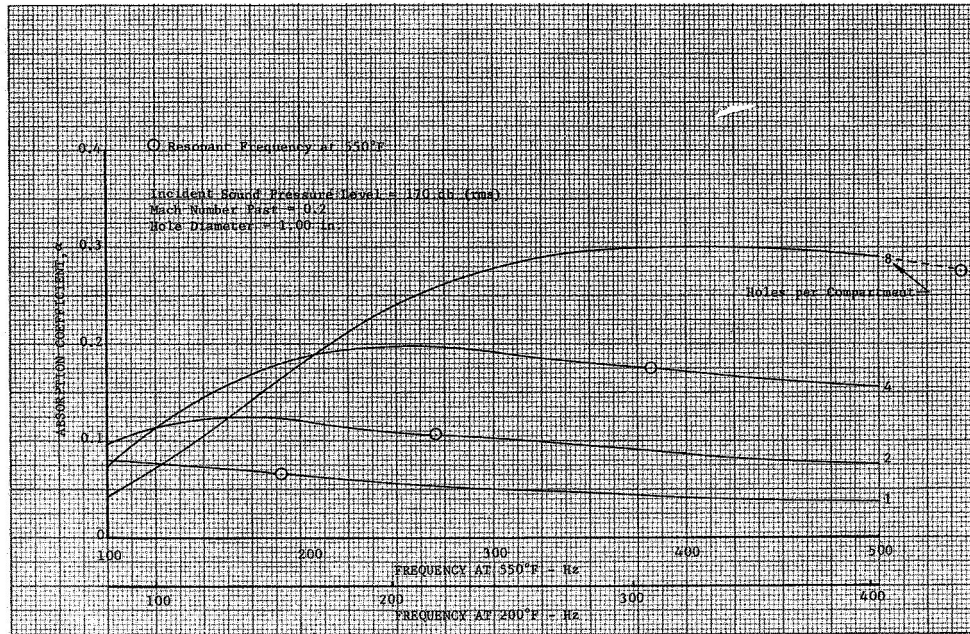


Figure IV-27. Estimated Absorption Coefficient for Duct Burner Inner Wall, Peak-to-Peak $\Delta P/P = 0.12$

DF 55419

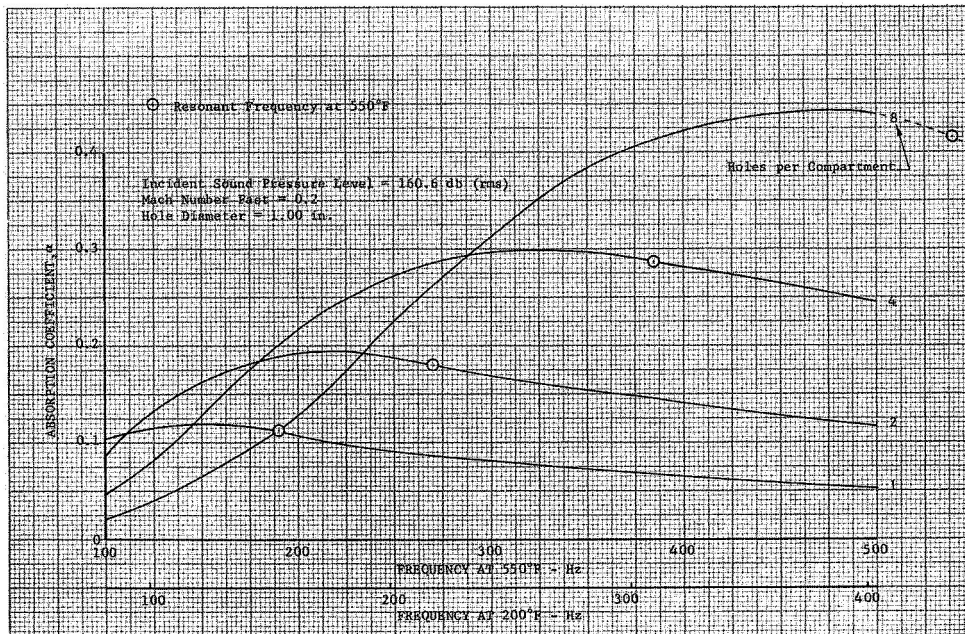


Figure IV-28. Estimated Absorption Coefficient for Duct Burner Inner Wall, Peak-to-Peak $\Delta P/P = 0.04$

DF 55420

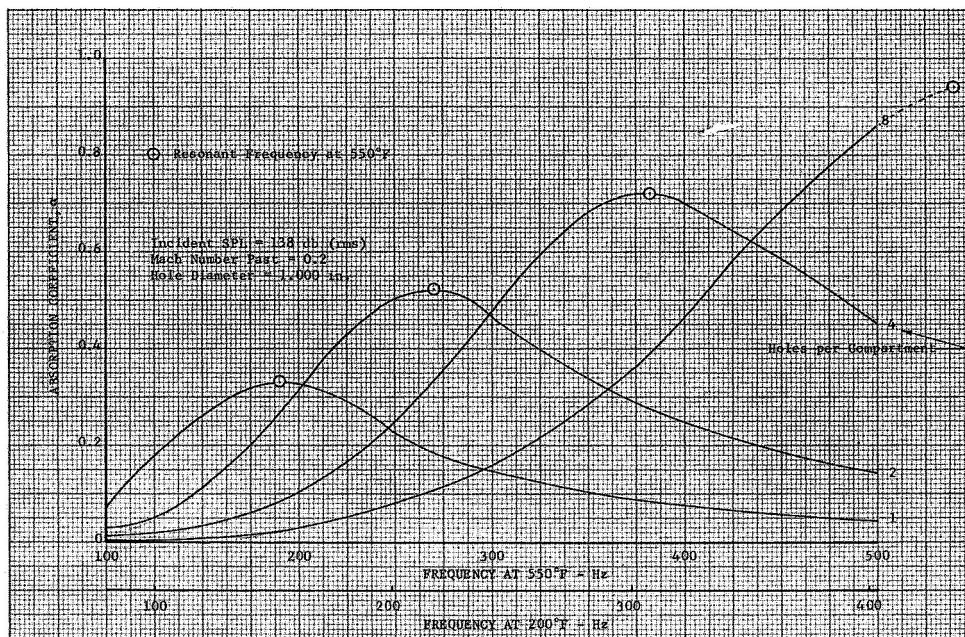


Figure IV-29. Estimated Absorption
Coefficient for Duct Burner
Inner Wall, Peak-to-Peak
 $\Delta P/P = 0.008$

DF 55421

SECTION V
PERFORMANCE CALCULATION PROCEDURE

A. PERFORMANCE CALCULATION PROCEDURE FOR DUCT BURNER RIG DATA

1. Assumptions

The following general assumptions were used in the performance calculations:

1. The ideal gas law ($P_s = \rho RT_s$) applied
2. The fluid throughout the system was homogeneous and compressible
3. All flow processes were isentropic and one-dimensional
4. Combustion took place with fuel and dry air. The products of combustion were mixed ideally with water vapor (from the inlet air) at the combustion temperature. (See figure V-1.)

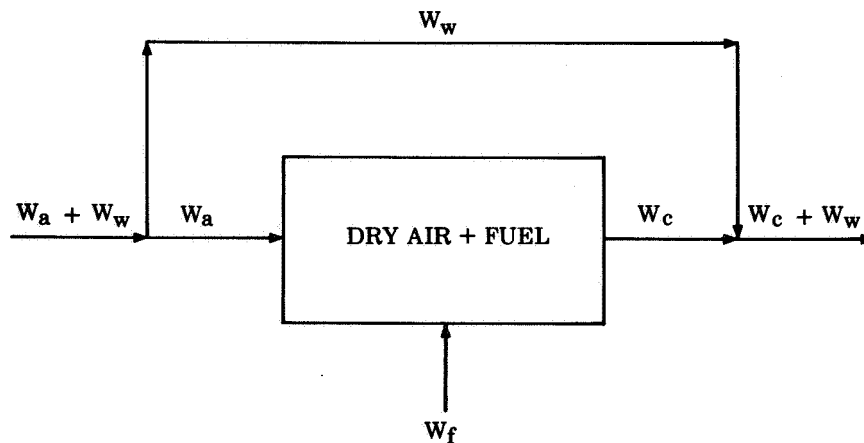


Figure V-1. Duct Burner Combustion Model

FD 12875 A

2. Inlet Airflow

A sharp-edged orifice in the facility inlet duct was used to determine the inlet airflow. The equation for the orifice was:

$$W_a + w = k \sqrt{\rho_m \Delta P} \quad (1)$$

As ΔP was measured, the only term that had to be calculated was the density of the air-water vapor mixture. The density of the mixture was defined as:

$$\rho_m = \rho_a + \rho_w \quad (2)$$

$$\rho_m = \frac{P_s}{R_a T_s} + \left(\frac{X}{0.622 + X} \right) \frac{P_s}{R_w T_s} \quad (3)$$

where P_s is the upstream orifice pressure and $X = W_w/W_a$. Here, X can be taken to be equal to 0.004.

It was assumed that the Mach number upstream of the orifice was negligible, and thus $T_s = T_T$.

3. Diffuser Bleed Flow

The diffuser bleed flow was determined from

$$\frac{W_b}{A} = \sqrt{\frac{\gamma_m g_c}{R_m T_T}} P_s M \sqrt{1 + \frac{\gamma_m - 1}{2} M^2} \quad (4)$$

The measurements made at the bleed location were the total and static pressures.

Because the bleed point was close to the diffuser exit instrumentation section, the total temperature measured at that location was used.

The specific heat ratio (γ) for the mixture of air and water vapor was determined in the following manner:

$$\gamma_m = \frac{C_{p_m}}{C_{v_m}} \quad (5)$$

where

$$C_{P_m} = \frac{W_a}{W_a + w} C_{P_a} + \frac{W_w}{W_a + w} C_{P_w} \quad (6)$$

$$C_{V_m} = \frac{W_a}{W_a + w} C_{V_a} + \frac{W_w}{W_a + w} C_{V_w} \quad (7)$$

$$C_{V_a} = \frac{C_{P_a}}{\gamma_a} \text{ and } C_{V_w} = \frac{C_{P_w}}{\gamma_w} \quad (8)$$

Combining the above gave

$$\gamma_m = \frac{\frac{W_a C_{P_a}}{C_{P_a}} + \frac{W_w C_{P_w}}{C_{P_w}}}{\frac{W_a}{\gamma_a} + \frac{W_w}{\gamma_w}} \quad (9)$$

Rearranging and substituting for X

$$\gamma_m = \frac{\gamma_w \gamma_a (C_{P_a} + X C_{P_w})}{\gamma_w C_{P_a} + X \gamma_a C_{P_w}} \quad (10)$$

The Mach number was determined from

$$M = \sqrt{\left[\left(\frac{P_T}{P_s} \right)^{\frac{\gamma_m - 1}{\gamma_m}} - 1 \right] \frac{2}{\gamma_m - 1}} \quad (11)$$

The gas constant (R_m) was defined as:

$$R_m = \frac{W_a R_a + W_w R_w}{W_a + w} \quad (12)$$

or

$$R_m = \frac{R_a}{X + 1} + R_w \frac{X}{X + 1} \quad (13)$$

4. Duct Reference Mach Number

The duct reference Mach number was defined as the Mach number of the gases based on the maximum duct cross-sectional area (the area in the duct, assuming that the burner was removed). The properties of the air were based on the measurements taken at the burner inlet.

The applicable equation to calculate the duct reference Mach number was:

$$\frac{W_a + w}{A_{ref}} = \sqrt{\frac{\gamma_m g_c}{R_m T_T}} \frac{P_T M_{ref}}{\left(1 + \frac{\gamma_m - 1}{2} M_{ref}^2\right) \frac{\gamma_m + 1}{2(\gamma_m - 1)}} \quad (14)$$

All values were measured except for the gas constant and the specific heat ratio, which were evaluated in the same manner as presented in paragraph 3 (Diffuser Bleed Flow).

5. Actual Nozzle Throat Temperature

The actual total temperature at the nozzle throat was determined from the following equation:

$$T_{T5} = \left(\frac{A_t P_{T5}}{W_t}\right)^2 \frac{\gamma_m g_c}{R_m \left(1 + \frac{\gamma_m - 1}{2}\right) \frac{\gamma_m + 1}{\gamma_m - 1}} \quad (15)$$

To evaluate the gas constant and the specific heat ratio, a new humidity ratio was defined.

$$Y = \frac{W_w}{W_a + W_f} \quad (16)$$

Thus:

$$R_m = \frac{R_c}{Y + 1} + R_w \left(\frac{Y}{Y + 1}\right) \quad (17)$$

and

$$\gamma_{m_c} = \frac{\gamma_w \gamma_c (C_{p_c} + Y C_{p_w})}{\gamma_w C_{p_c} + Y \gamma_c C_{p_w}} \quad (18)$$

Note that A_t was the nozzle effective open area and was determined by subtracting the blockage of the nozzle plugs from the total nozzle open area, defined by the inner and outer nozzle casings, and multiplying this difference by the nozzle discharge coefficient. Also, an adjustment was made for thermal expansion. The maximum thermal growth of the exit nozzle occurred with Condition 3 of Table II-1. This growth caused an approximate 0.36% increase in nozzle throat area. If this change was not accounted for, the calculated combustion efficiency would be somewhat lower (approximately 1%) than the actual combustion efficiency.

6. Theoretical Throat Temperature

The theoretical total temperature at the nozzle throat was determined from a theoretical performance deck included in the duct burner computer program. This deck calculated a value for the temperature just upstream of the nozzle throat and assumed isentropic expansion through the nozzle. Thus, the calculated temperature upstream of the nozzle was the same as that at the nozzle throat. This value was corrected for the water vapor that was present in the incoming airflow. The correction was made as follows:

From an enthalpy balance:

$$H_{out} = H_{w_{in}} + H_a + H_f = H_{w_{in}} + H_c \quad (19)$$

Note that the enthalpy of the water was considered constant; this resulted from assumption 4. The enthalpies used in the above equation were total enthalpies, which included the static enthalpy and the kinetic energy associated with each component.

Thus:

$$(WC_p T_T)_{out} = W_w C_{p_w} T_w + W_c C_{p_c} T_c \quad (20)$$

rearranging (20)

$$T_{T_{out}} = T_{T_c} \frac{C_{p_c}}{C_{p_m}} \frac{W_c}{W_t} + T_{T_w} \frac{C_{p_w}}{C_{p_m}} \frac{W_w}{W_t} \quad (21)$$

where:

C_{p_m} was determined from

$$C_{p_m} = C_{p_c} \left(\frac{W_t - XW_a}{W_t} \right) + C_{p_w} \left(\frac{XW_a}{W_t} \right) \quad (22)$$

7. Combustion Efficiency

Combustion efficiency is defined here as the actual total temperature rise between the burner inlet and nozzle throat divided by the ideal (theoretical) temperature rise.

In the actual temperature rise, the actual momentum pressure loss due to combustion was taken into account because the total pressure at the throat is measured. The efficiency thus described, however, did not account for the heat lost to the cooling water upstream of the nozzle throat (heat lost downstream of the nozzle throat does not enter into the efficiency calculation). The heat absorbed by the cooling water was unavailable to the combustion gases for conversion into kinetic energy. The efficiency thus calculated was based on an ideal temperature rise that assumed no heat loss. To obtain accurate results, the combustion efficiency was corrected as follows:

$$\text{Total Heat Release} = W_f \Delta H_{c_f} = Q_{\text{released}} \quad (23)$$

where ΔH_{c_f} = heat of combustion of the fuel

Heat lost to the cooling water was calculated from the coolant temperature rise and coolant flow rate.

$$(\eta_c)_{\text{corrected}} = (\eta_c)_{\text{uncorrected}} + \frac{Q_{\text{lost}}}{Q_{\text{released}}} \quad (24)$$

8. Burner Pressure Loss

The burner pressure loss was defined as:

$$\frac{P_{T4} - P_{T5}}{P_{T4}} \times 100 \quad (25)$$

B. NOMENCLATURE

Symbol	Description	Units
A	Area	in. ²
A _{ref}	Duct reference area	in. ²
A _t	Effective area of nozzle throat	in. ²
C _p	Specific heat at constant pressure	Btu/lb _m °R
C _{p_a}	Specific heat at constant pressure for air	Btu/lb _m °R
C _{p_c}	Specific heat at constant pressure for dry combustion products	Btu/lb _m °R
C _{p_m}	Specific heat at constant pressure for air-water vapor mixture	Btu/lb _m °R
C _{p_w}	Specific heat at constant pressure for water vapor	Btu/lb _m °R
C _v	Specific heat at constant volume	Btu/lb _m °R
C _{v_a}	Specific heat at constant volume for air	Btu/lb _m °R
C _{v_m}	Specific heat at constant volume for air-water vapor mixture	Btu/lb _m °R
C _{v_w}	Specific heat at constant volume for water vapor	Btu/lb _m °R
f/a	Fuel/air ratio	Dimensionless
g _c	Universal gravitational constant (32.17)	lb _m -ft/lb _f -sec ²
H _a	Total enthalpy of dry air	Btu/lb _m
H _c	Total enthalpy of dry combustion products	Btu/lb _m
H _f	Total enthalpy of fuel	Btu/lb _m
H _{out}	Total enthalpy of wet combustion products	Btu/lb _m
H _{w_{in}}	Total enthalpy of inlet water	Btu/lb _m
k	Constant	
M	Mach number	Dimensionless
M _{ref}	Duct reference Mach number	Dimensionless
P _T	Total pressure	lb _f /in. ²
P _{T4}	Total pressure at burner inlet	lb _f /in. ²
P _{T5}	Total pressure at nozzle throat	lb _f /in. ²

Pratt & Whitney Aircraft

PWA FR-2542

Symbol	Description	Units
P_s	Static pressure	lb_f/in^2
Q_{lost}	Heat lost to cooling water	Btu/sec
Q_{released}	Heat released due to combustion	Btu/sec
R	Gas constant	$\text{ft-lb}_f/\text{lb}_m \text{ } ^\circ\text{R}$
R_a	Gas constant for air	$\text{ft-lb}_f/\text{lb}_m \text{ } ^\circ\text{R}$
R_c	Gas constant for dry combustion products	$\text{ft-lb}_f/\text{lb}_m \text{ } ^\circ\text{R}$
R_m	Gas constant for air-water vapor mixture	$\text{ft-lb}_f/\text{lb}_m \text{ } ^\circ\text{R}$
R_w	Gas constant for water vapor	$\text{ft-lb}_f/\text{lb}_m \text{ } ^\circ\text{R}$
T_T	Total temperature	$^\circ\text{R}$
T_{T_c}	Total temperature of combustion products	$^\circ\text{R}$
T_{T_w}	Total temperature of water vapor	$^\circ\text{R}$
T_{T5}	Total temperature at nozzle throat	$^\circ\text{R}$
T_s	Static temperature	$^\circ\text{R}$
W	Flow rate	lb_m/sec
W_a	Flow rate of dry air	lb_m/sec
$W_a + w$	Flow rate of air-water vapor mixture	lb_m/sec
W_b	Flow rate of diffuser bleed	lb_m/sec
W_c	Flow rate of dry combustion products	lb_m/sec
W_f	Flow rate of fuel	lb_m/sec
W_t	Total flow rate of air-water vapor and fuel	lb_m/sec
W_w	Flow rate of water vapor	lb_m/sec
X	Humidity ratio	Dimensionless
Y	Humidity ratio in burner	Dimensionless
ΔH_{c_f}	Heat of combustion of fuel	Btu/lb _m
ΔP	Pressure drop	lb_f/in^2

Symbol	Description	Units
γ_a	Specific heat ratio of dry air	Dimensionless
γ_c	Specific heat ratio of dry combustion products	Dimensionless
γ_m	Specific heat ratio of air-water vapor mixture	Dimensionless
γ_{mc}	Specific heat ratio of combustion products - water vapor mixture	Dimensionless
γ_w	Specific heat ratio of water vapor	Dimensionless
η_c	Combustion efficiency	Dimensionless
ρ	Density	lb_m/ft^3
ρ_a	Density of air	lb_m/ft^3
ρ_m	Density of air-water vapor mixture	lb_m/ft^3
ρ_w	Density of water vapor	lb_m/ft^3

SECTION VI TEST MODIFICATIONS

During the course of the test program, the following changes or modifications (table VI-1) were made to the apparatus to do the following:

1. Reduce inlet noise and inlet flow profile distortion (Section VIII)
2. Reduce combustion oscillation (Section VIII)
3. Improve combustion efficiency (Section VII)
4. Improve durability of test apparatus (Section VII)

These modifications were not necessarily permanent, and a detailed, chronological discussion of all testing and modifications is given in Appendix D.

Table VI-1. Test Modifications

A. Facility, Diffuser and Centerbody

Modification	Reason	Effect
Installation of a perforated cylinder at plenum inlet	To reduce inlet pressure fluctuations	Substantial improvement
Installation of acoustic suppressing boxes in the plenum inlet	To reduce inlet noise	Boxes failed structurally
Increased the flow distribution plate flow area	To reduce inlet noise	Minor reduction in noise; inlet flow profile adversely affected
Removed the flow distribution plate	To improve inlet flow profile	Substantially reduced mechanical vibrations and improved inlet flow profile.
Installation of radial vanes in the diffuser	To reduce the facility/rig interface effect on combustion instability	Effective (at 60-deg angle) in eliminating combustion instability in some cases
Installation of a 3-mesh inlet screen	To reduce the facility/rig interface effect on combustion instability	None
Installation and modification of a 4-mesh inlet screen	To reduce the facility/rig interface effect on combustion instability	Minor effect

Table VI-1. Test Modifications (Continued)

Modification	Reason	Effect
Installation of a center-body damping plate	To eliminate possible longitudinal oscillations in the centerbody	None detected
Diffuser bleed static pressure rise eliminated	To eliminate possible oscillation driving force through the bleed area	None detected
Installation of radial fins in the centerbody	To eliminate possible transverse oscillations in the centerbody	None detected
Blockage of diffuser bleed and opening the inlet nose	To determine if diffuser bleed contributed to oscillations	Diffuser bleed not involved
B. Burner and Cooling Liner Changes		
Modification	Reason	Effect
Increased the cooling air to the firewall while fabricating a replacement burner for the failed one	To cool the firewall	Satisfactory, no effect on burner performance
Trimmed the No. 2 scoops	To prevent burning	Successful
Relocated the primary liner support tabs	To allow increased axial clearance for thermal growth	No further interferences detected
Removed the trailing edge of the No. 3 scoop	To prevent thermal cracking	Successful
Increased cooling air to the ID vortex generator	Cool trailing edge	Successful, no effect on burner performance
Installed blockage plates in the annulus surrounding the ID and OD of the burner	To increase ΔP through the burner to check facility rig interface effect on combustion instability	Negligible effect
Removed the vortex generators	To eliminate combustion instability	Successful at 30-psia tests but combustion efficiency decreased; ineffective at other test conditions

Table VI-1. Test Modifications (Continued)

Modification	Reason	Effect
Installed newly designed turbulators at location vortex generators had occupied	To increase combustion efficiency at 30-psia test conditions	Successful when compared to geometry with vortex generator removed, but instability occurred.
Removed every other turbulator	To eliminate combustion instability	Slight improvement
Circumferentially reindexed the outer secondary liner assembly, outer Zone-2 spraybars, and vortex generators	To eliminate combustion instability	None
Redesigned and fabricated the outer cooling liners to incorporate acoustic damping	To eliminate combustion instability	None
Redesigned and modified the inner cooling liner to incorporate acoustic damping	To eliminate combustion instability	Minor suppression of 450 Hz instability

C. Fuel Injector Changes

Modification	Reason	Effect
Structurally modified the Zone-1 fuel nozzles	To eliminate cracking in the secondary supply tube	No further cracking detected
Fabricated and installed 4 additional Zone-2 ID spraybar supports	To eliminate bowing of spraybar	Successful
Restricted flow to every other Zone-1 fuel nozzle	To eliminate combustion instability	Increased the stable combustion range
Restricted flow to the Zone-2 ID spraybars	To reduce combustion instability	No effect on instability, although combustion efficiency was reduced
Circumferentially unbalanced the flow to the Zone-2 OD spraybars	To reduce combustion instability	None

SECTION VII PERFORMANCE AND DURABILITY DISCUSSION

A. EXIT NOZZLE CALIBRATION

It was necessary that the rig exit nozzle discharge coefficient be known with accuracy because the burner exit total temperature, and therefore combustion efficiency, was calculated from the choked flow parameter from this nozzle area. Figure VII-1 shows the variation of cold flow calibration exit nozzle discharge coefficient (based on the facility orifice airflow) with the nozzle pressure ratio P_{s5}/P_{T5} at the nozzle minimum area with an inlet temperature of approximately 100°F. The choked flow coefficient varies 7%, from 1.01 to 0.94, which is excessive and too large a variation to be entirely due to instrumentation error. It was determined that moisture in the air that vaporized between the orifice and the nozzle could account for this variation and would also cause a drop in air temperature; this was observed during tests.

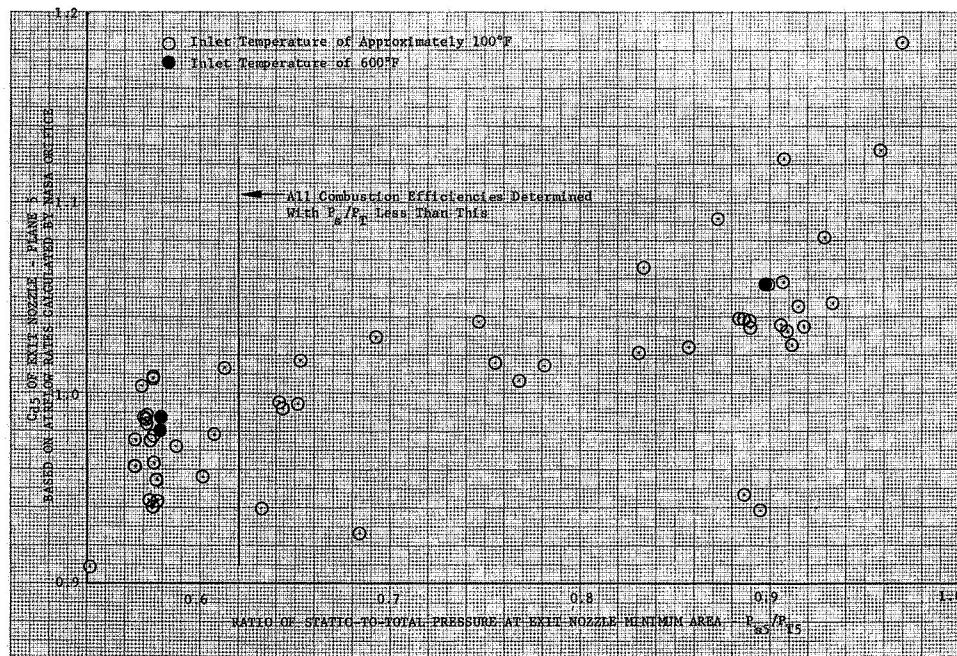


Figure VII-1. Exit Nozzle Discharge Coefficient: DF 58514
Cold Calibration

This effect was eliminated when the 600°F heated inlet cold flows were performed, as shown in figure VII-1. A discharge coefficient of 0.985 was determined from the heated inlet test and used in reduction of data from the combustion tests.

Static pressures, figure II-26 and II-27, were measured in an axial direction on the exit nozzle OD wall from the minimum area plane. These static pressures were used to indicate when supersonic flow occurred downstream of the minimum area, indicating that the exit nozzle was choked. The nozzle was observed to be choked when the ratio P_{s5}/P_{T5} was less than 0.62. The minimum P_{s5}/P_{T5} ratio obtained is somewhat higher than the ideal one-dimensional P_{s5}/P_{T5} ratio, and is the result of being unable to correctly measure the nozzle throat static pressure and/or not having the static taps in the plane of minimum effective area. However, this was of little consequence because nozzle throat static pressure was not used in the data reduction since all combustion efficiency results presented were calculated with a choked nozzle.

B. DIFFUSER PERFORMANCE

The diffuser total pressure loss was only 36% of the anticipated value, as shown in figure VII-2. The diffuser pressure loss was found to be affected by the diffuser bleed flow. The diffuser bleed flow increased as the burner fuel/air ratio was increased, as shown in figure VII-3. As the burner exit temperatures increased and the burner static pressure decreased the differential pressure across the diffuser bleed area increased. The original diffuser configuration had bleed flows varying from 8.5% to 12% of the total airflow, which was near the design flow of 10%. When acoustical damping was incorporated into the inner cooling liner, one of the three cooling louvers was eliminated, being replaced by the enclosed volume for the damping. This resulted in a reduction of diffuser bleed flow by approximately 2% of the total airflow, as shown in figure VII-3. The total pressure drop through the diffuser increased considerably, as shown in figure VII-2. This increase in total pressure loss could not be explained by an increase of airflow in the diffuser

downstream of the bleed. This was substantiated with test data which showed that when the bleed was flowing an equal amount for the two configurations, the diffuser total pressure loss was greater with the inner cooling liner that had decreased cooling flow.

Velocity profiles were plotted for the diffuser inlet and exit by using an average of the rig instrumentation at the diffuser inlet and exit, and are shown in figure VII-4. For the two configurations under consideration, no appreciable difference was noted. The inlet profile was peaked toward the ID, and the general shape of the radial profile carried through to the diffuser exit. Hence, the radial profiles measured gave no indication as to the reason for the increase in the diffuser total pressure drop.

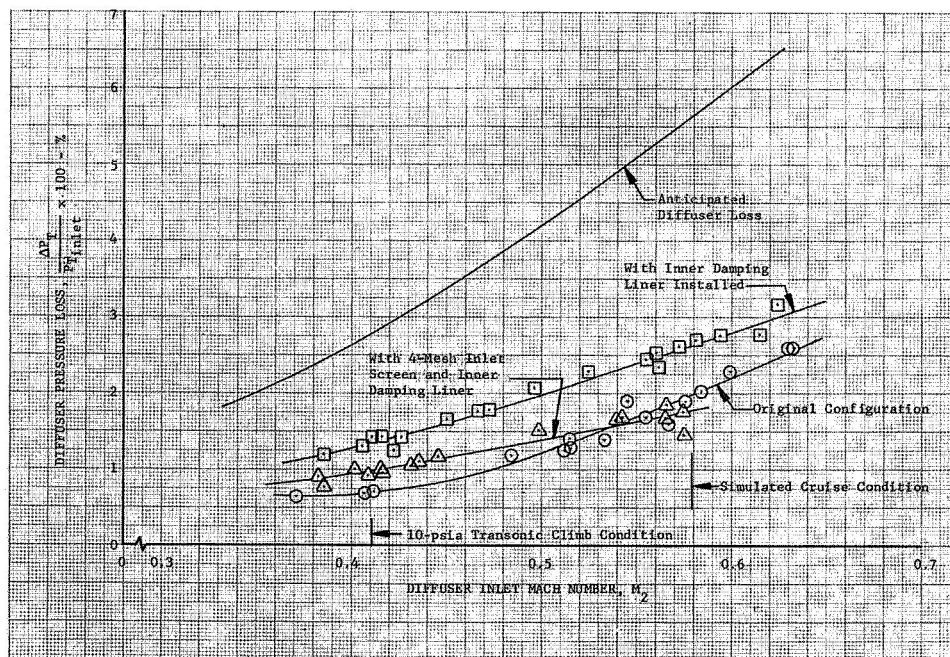


Figure VII-2. Diffuser Pressure Loss vs
Diffuser Inlet Mach No.

DF 58515

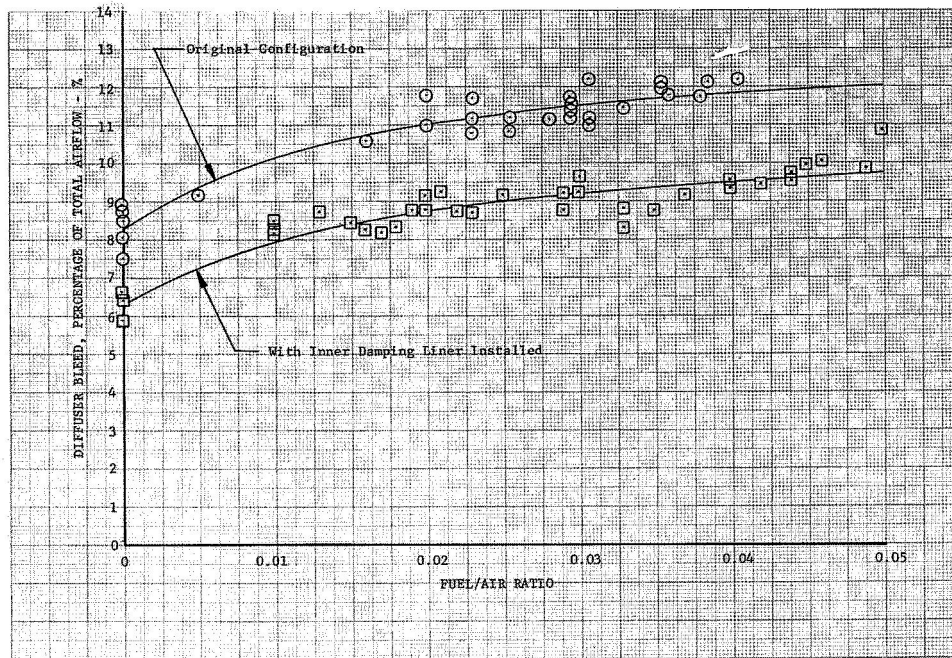


Figure VII-3. Diffuser Bleed Airflow vs Fuel/Air Ratio

DF 58516

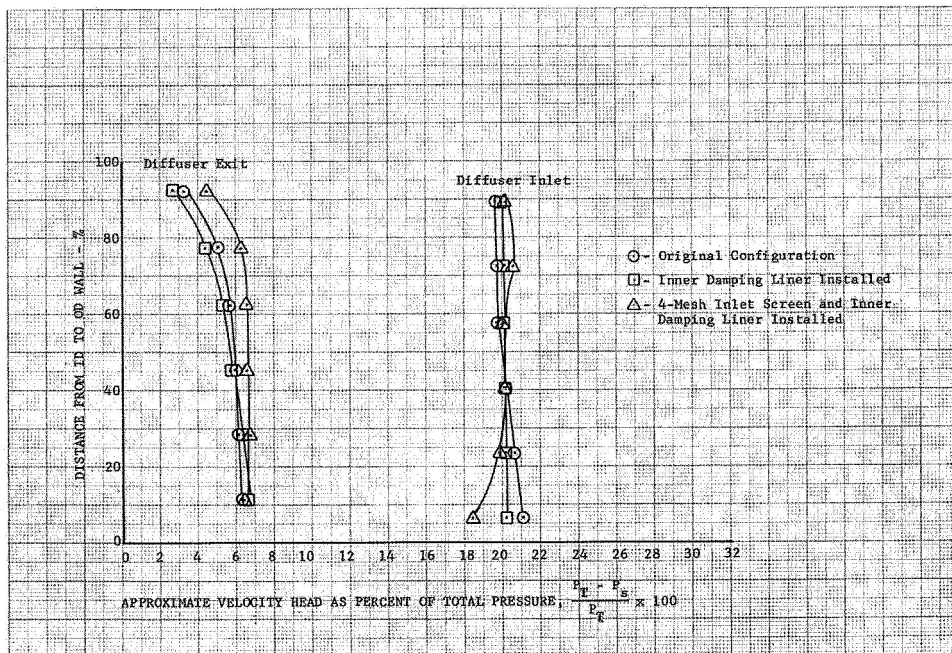


Figure VII-4. Average Radial Velocity Profiles in the Diffuser

DF 58517

It was theorized that the airflow along the ID wall separated at the bleed lip when it was flowing only 6.5% of the total airflow with no combustion occurring, and this resulted in the increased total pressure drop. Although the bleed flow increased when the fuel/air ratio was increased, the flow did not reattach to the ID wall and the diffuser total pressure drop remained high. The instrumentation used did not verify a flow separation, but the pressure was not recorded closer than 0.57 inch to the ID wall at the diffuser exit.

When a 4-mesh screen was installed upstream of the diffuser inlet, the inlet radial profile peaked toward the OD, as shown in figure VII-4. The diffuser total pressure drop decreased (figure VII-2), showing the effect of the radial profile. It is likely that decreasing the flow on the ID lessened the flow separation on the ID at the bleed lip, and improved the total pressure loss.

C. COOLING LINERS

1. Outer Cooling Liner

Two configurations of outer cooling liners were tested.

The original configuration was of one-piece construction, and is shown in figure II-11. This liner was tested with fuel/air ratios as high as 0.040 at simulated cruise conditions. Higher fuel/air ratios were not tested because of combustion instability. Figure VII-5 shows the metal temperatures recorded, and figure VII-6 shows the rate of cooling airflow. The cooling airflow exceeded the design flow rate of 4.85% of the total airflow. The liners rippled slightly due to thermal differences (see figure D-7). The portion of the liner that was shielded by the installation tracks were cooler than the metal at the maximum height of the liner, which was the portion closest to the combustion area. The ripples did not appear to be detrimental to the structural life of the liners, having accumulated 15.0 hours of combustion test time.

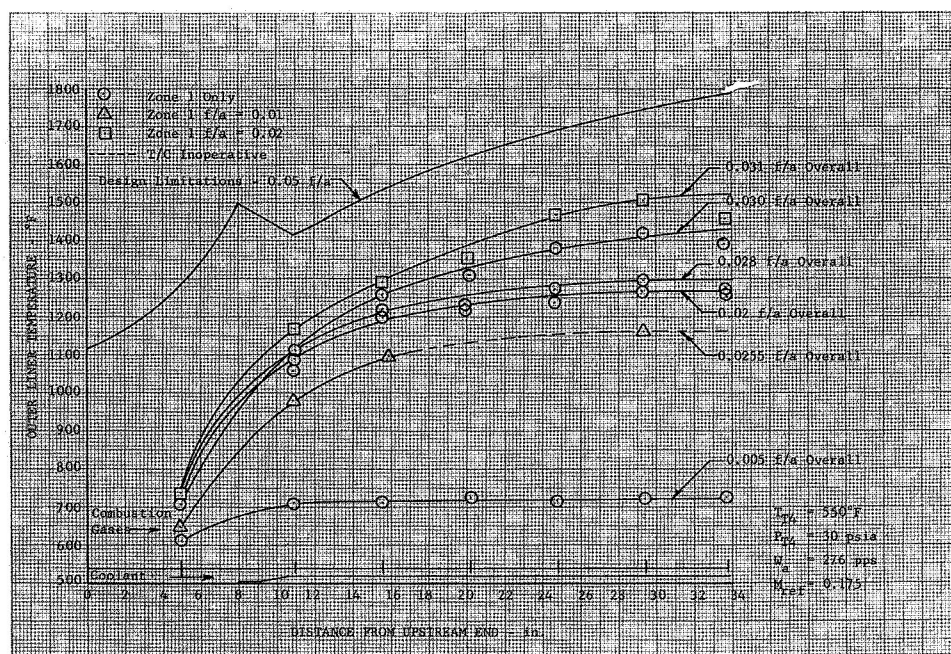


Figure VII-5. Original Design Outer Liner Temperature vs Distance

DF 50486

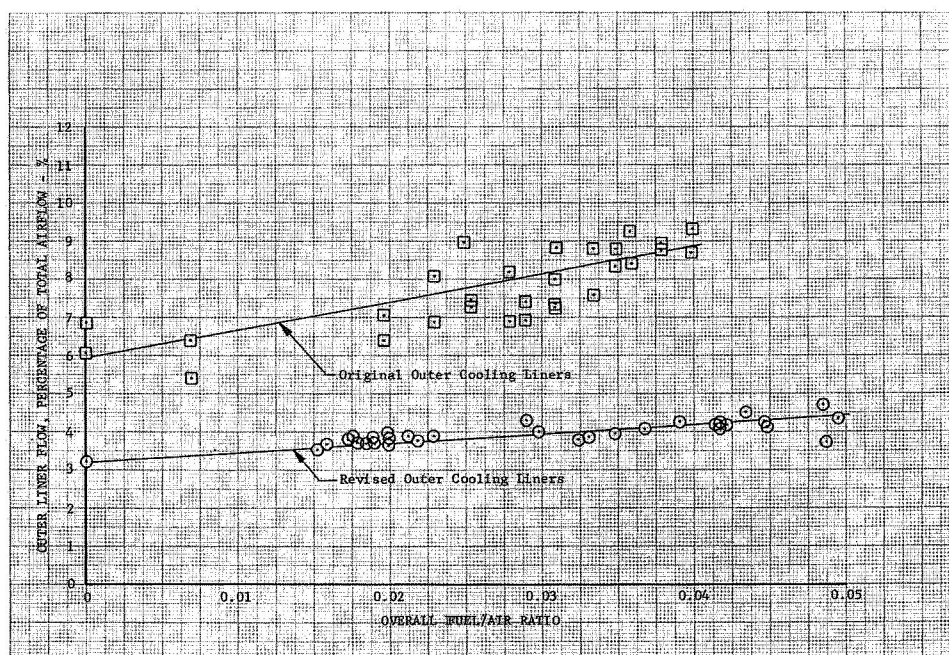


Figure VII-6. Outer Cooling Liner Airflow Rates

DF 58518

The outer liners were redesigned to include acoustical damping and are shown in figures II-15 and IV-19. The liners were fabricated in 2 axial sections. The upstream section incorporated the acoustical damping, and the downstream section was changed to include ripples in the design because of the thermal gradients.

Figure VII-7 shows the metal temperatures recorded on a typical outer liner while operating at simulated cruise-approach conditions, which produces the most severe test conditions for the liners. The metal temperatures were very close to the predicted temperatures. It should be noted in figure VII-6 that the rate of cooling airflow was reduced approximately 50% from the original configuration. This is because the cross-sectional cooling flow area was reduced by the added ripples. The ripples apparently increased the cooling effectiveness.

The liners were polished before testing. The resulting metal temperature pattern confirmed the temperatures recorded with thermocouples.

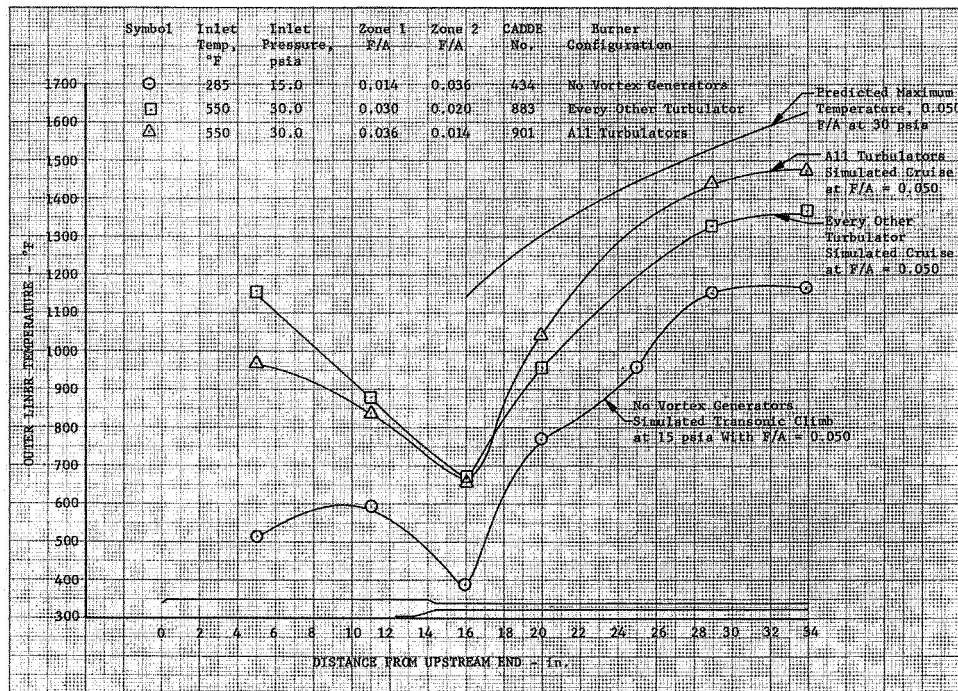


Figure VII-7. Outer Liner Temperature vs Length DF 58519

A final inspection of the outer liners at the conclusion of the program showed them to be in excellent structural condition. No cracking or warping of any kind was observed. The liners performed in an excellent manner, and the complete set was tested for a total of 81.2 hours of combustion time.

It appears that the originally designed liners would have performed satisfactorily for the duration of the program; however, ripples should be incorporated. One other suggested change would be to loosen the fit between the outer liners and the tracks that retain them. It was found that assembly and disassembly of the liners was difficult when dirt particles from the facility became imbedded in the tracks.

2. Inner Cooling Liner

The inner cooling liner performed as designed. Figure VII-8 shows the metal temperatures recorded with fuel/air ratios up to 0.0487, with a maximum temperature of less than 1100°F. The rate of cooling airflow through the three louvers is shown in figure VII-9. It is obvious from the low metal temperatures that the inner liner was more than adequately cooled by the diffuser bleed flow.

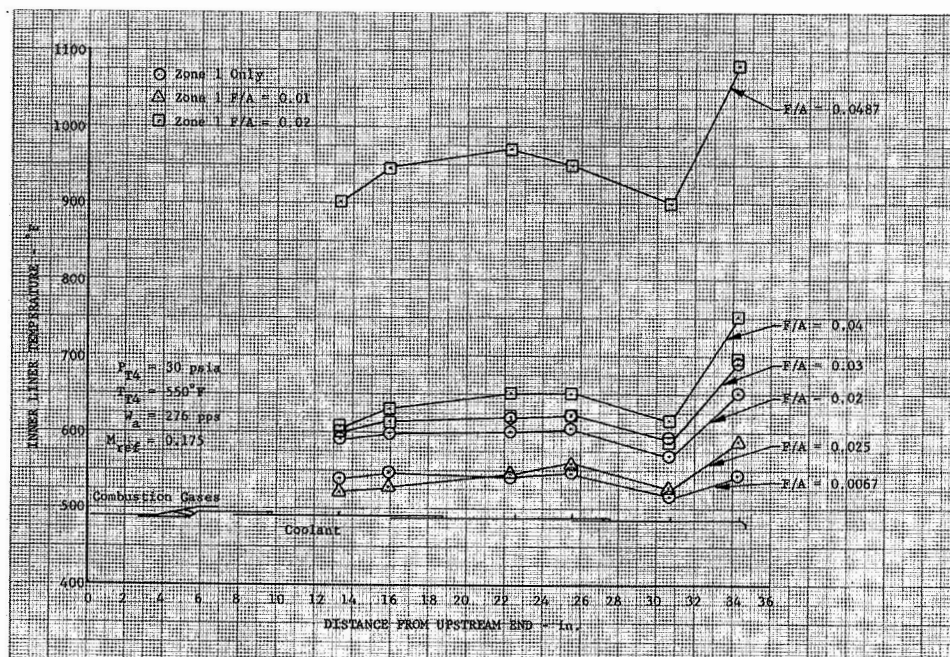


Figure VII-8. Inner Liner Temperature vs Distance From Upstream End

DF 58520

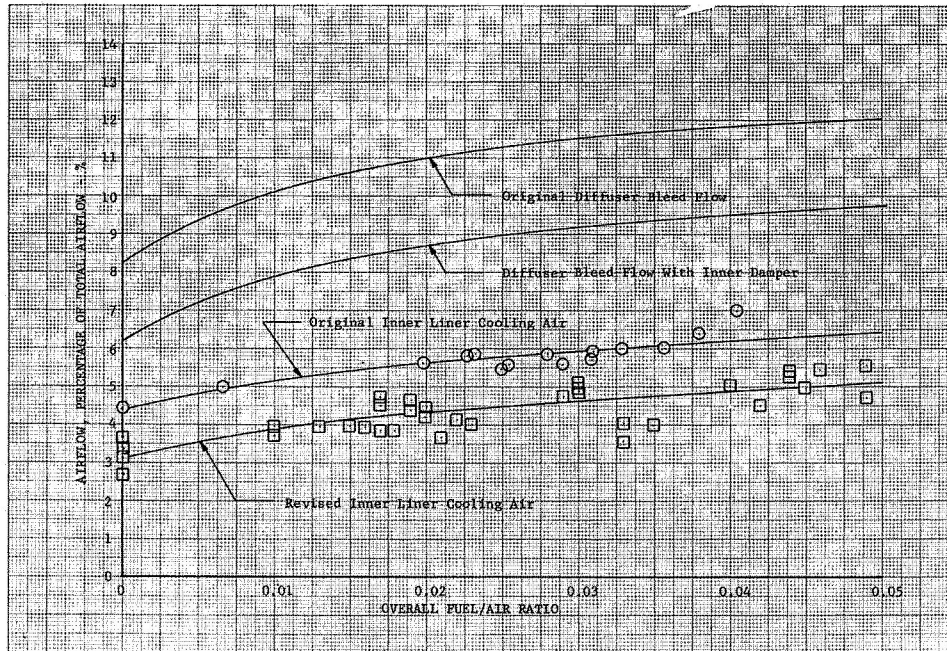


Figure VII-9. Inner Liner Airflow vs Fuel/Air Ratio

DF 58521

The inner liner accumulated 25.23 hours of combustion test time when an internal fuel leak occurred (caused by a faulty seal in the ID manifold of the Zone-2 fuel system) that resulted in burning of the inner cooling liner, as shown in figure VII-10.

The burned area was cut away and replaced with a section incorporating acoustical damping (figure II-18). The metal temperatures recorded are shown in figure VII-11, and are similar to the original liner temperatures. The rate of cooling airflow shown in figure VII-9 was lower than the original inner liner because one cooling louver was removed.

Final inspection of the inner cooling liner when the program was terminated showed the inner liner to be in perfect structural condition. The inner liner accumulated a total of 97.2 hours of combustion test time with the upstream louver and panel being replaced with a section incorporating acoustical damping after 25.23 hours of combustion test time.

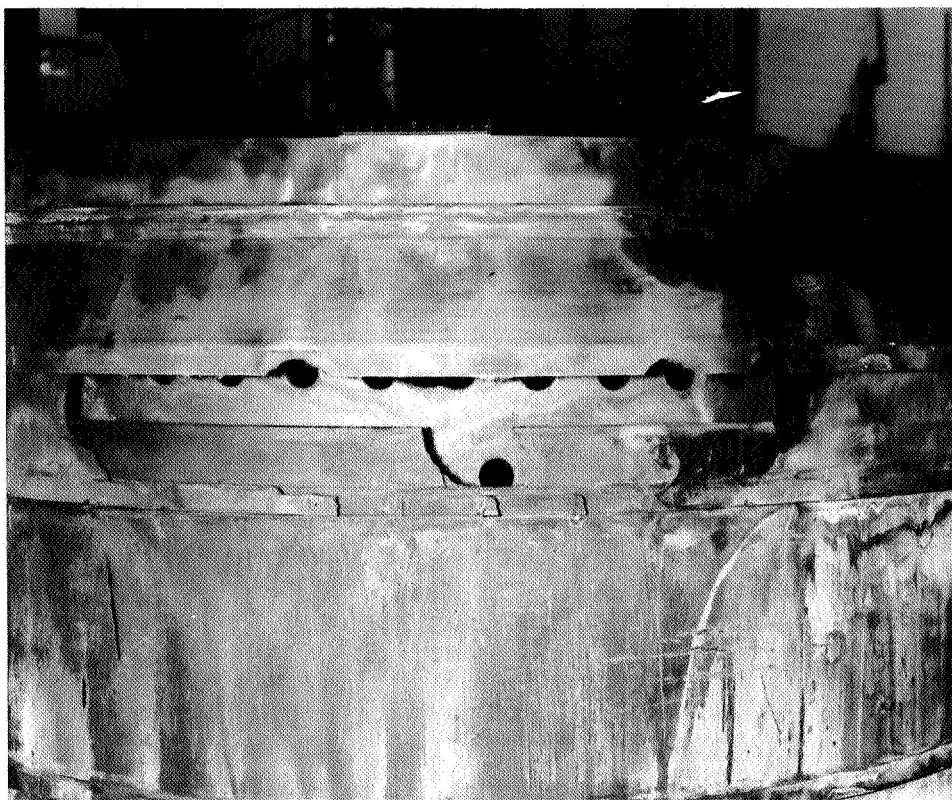


Figure VII-10. Inner Cooling Liner

FE 66617

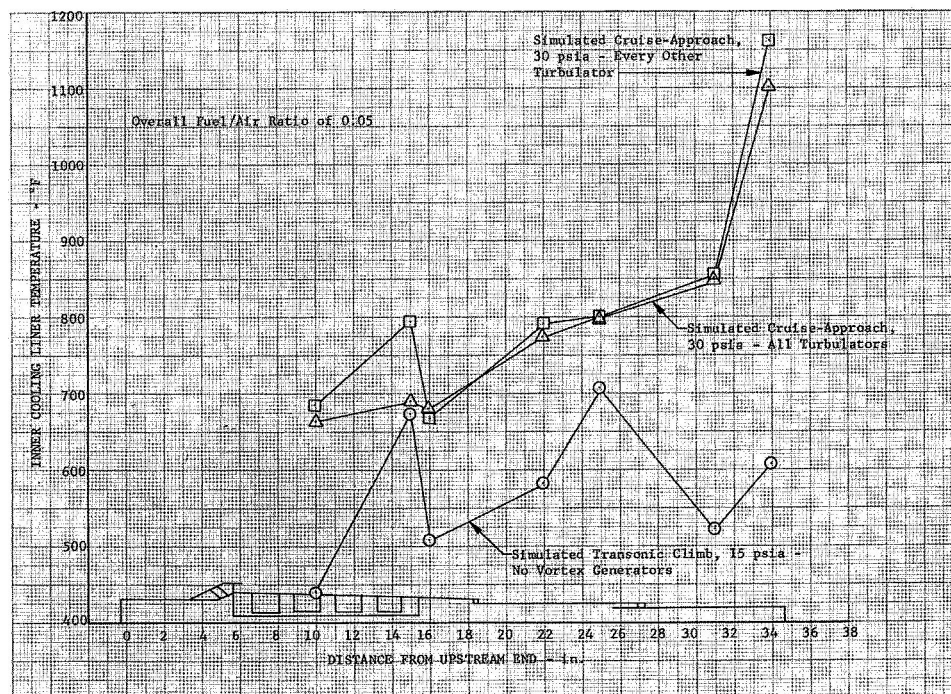


Figure VII-11. Inner Cooling Liner Temperature
vs Length

DF 58522

D. DUCT BURNER

1. Durability and Cooling

The original duct burner was tested for 15.0 hours of combustion testing and 84.10 hours of cold flow when a failure occurred. Four of the twenty firewall panels became detached from the dome assembly (figure VII-12). Two swirlers also failed, as shown in figure VII-13. Sixteen of the liner support tabs were torn out of the primary liner (figure VII-14). Cracking also occurred at the trailing edge of the scoops in the secondary liner, as shown in figure VII-15. The dome and primary liner assembly was scrapped, because it was impossible to make a satisfactory weld repair.

The failure of the original burner can be attributed in part to subjecting the burner to test conditions that were much more severe than those that an engine would produce. The burner was subjected to extremely turbulent inlet airflow during the exit nozzle cold calibration. In choking the exit nozzle, the diffuser became choked and shocks existed in the divergent section. This subjected the burner to excessive vibrations while a choked diffuser condition existed for a total of 6 hours during the cold flow calibrations.

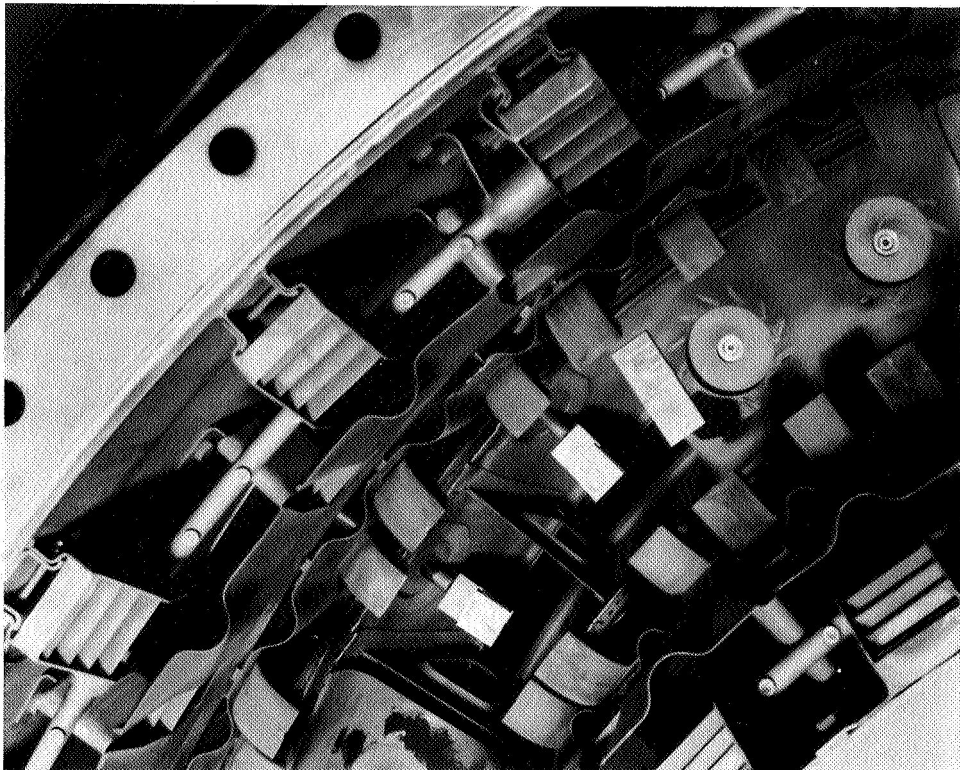


Figure VII-12. Duct Burner Firewall Failure

FE 62644



Figure VII-13. Duct Burner Swirler Failure

FE 62643



Figure VII-14. Duct Burner Liner Support
Tab Failure

FE 62642

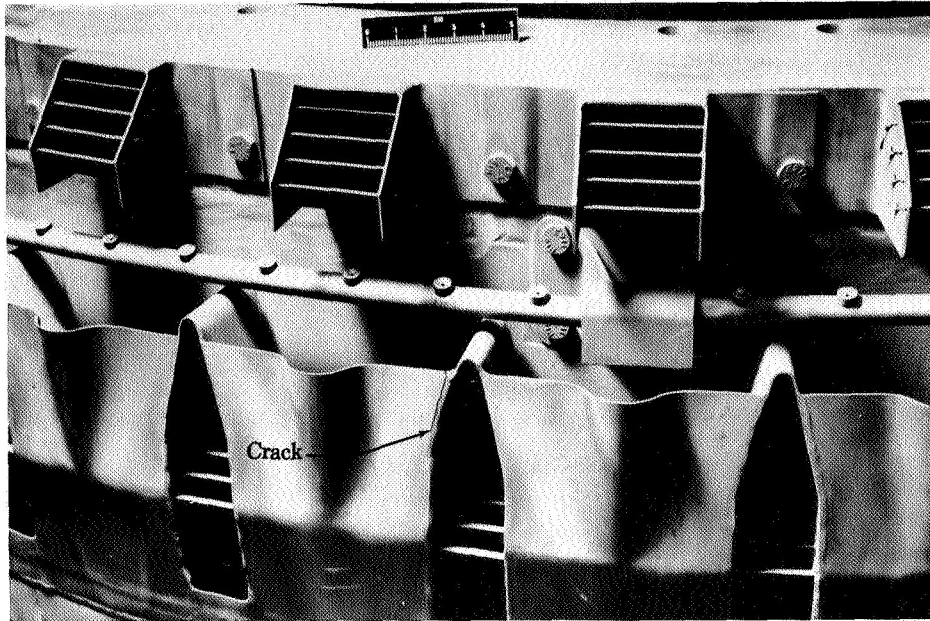


Figure VII-15. Duct Burner Secondary Liner
Failure

FD 22561

After several hours of combustion testing, the firewall lip began to distort and the circumferential gaps between the firewall segments narrowed because of thermal stresses between the hot firewall panels and the cooled support spacers connecting the segments to the burner dome. Metal discoloration indicated that the firewall temperature had greatly exceeded the 900°F design point.

Due to a facility operation error, the burner was quenched with water while operating with a 550°F inlet.

The burner was also subjected to extreme vibrations and pressure pulsations when combustion instability occurred. The rig was not adequately instrumented initially, and the potential damage from instability was not fully recognized. Hence, the burner was initially weakened during the cold calibrations, further weakened due to the firewall overheating, and finally failed while being subjected to severe combustion instability.

A new dome and primary liner assembly was fabricated with provision for increased cooling airflow. Five hundred fifty 0.150-inch diameter holes were drilled along the firewall ID, six hundred forty 0.150-inch diameter holes were drilled along the firewall OD, and eight hundred eighty 0.175-inch diameter holes were drilled around the swirlers, (figure VII-16). The downstream side of the swirler holes was covered by a deflector that caused a cooling air scrubbing action prior to entering the burner. The additional firewall cooling represented approximately 0.5%, 0.6%, and 0.5% of the total airflow for the ID holes, OD holes, and the swirler holes, respectively. The firewall was instrumented with skin thermocouples in the locations shown in figure VII-17. The metal temperature never exceeded a recorded 950°F for the remainder of the program, as shown in figure VII-18. The added cooling air had no detected effect on ignition or performance.

Slight burning had been noticed on the No. 2 scoops on the original burner. The scoop tip was cut at a slightly greater angle (figure VII-19) and no further burning was detected on the second burner.

The second burner primary liners had the rear support tabs located 0.1-inch farther forward to provide a 0.20-inch axial clearance for thermal growth between the primary and secondary liners.

Slight overheating on the downstream side of the ID vortex generator was indicated by metal discoloration and modifications were made (figure VII-20) when the second burner was fabricated. Additional cooling airflow, representing approximately 0.7% of the total airflow, was provided by cutting slots in the vortex generator end plate. The modification was completely satisfactory and no further overheating was detected.

The duct burner secondary liners were weld repaired, but cracks continued to develop and after 25.23 hours of combustion, half of the OD secondary scoops were modified by cutting away the trailing edge to relieve the stress concentration, as shown in figure VII-21. Continued combustion tests for 7.83 hours showed that the modified scoops were in excellent condition, while some of the nonmodified scoops continued to develop cracks. The remainder of the No. 3 OD scoops and all No. 3 ID scoops were modified. No further cracking was detected during the remainder of the program.

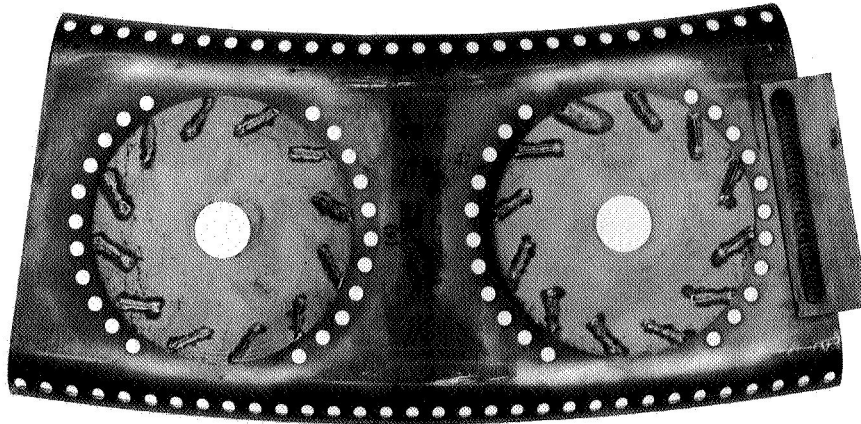


Figure VII-16. Modified Firewall With Provisions
for Additional Cooling Airflow
(Looking Downstream) FE 63617

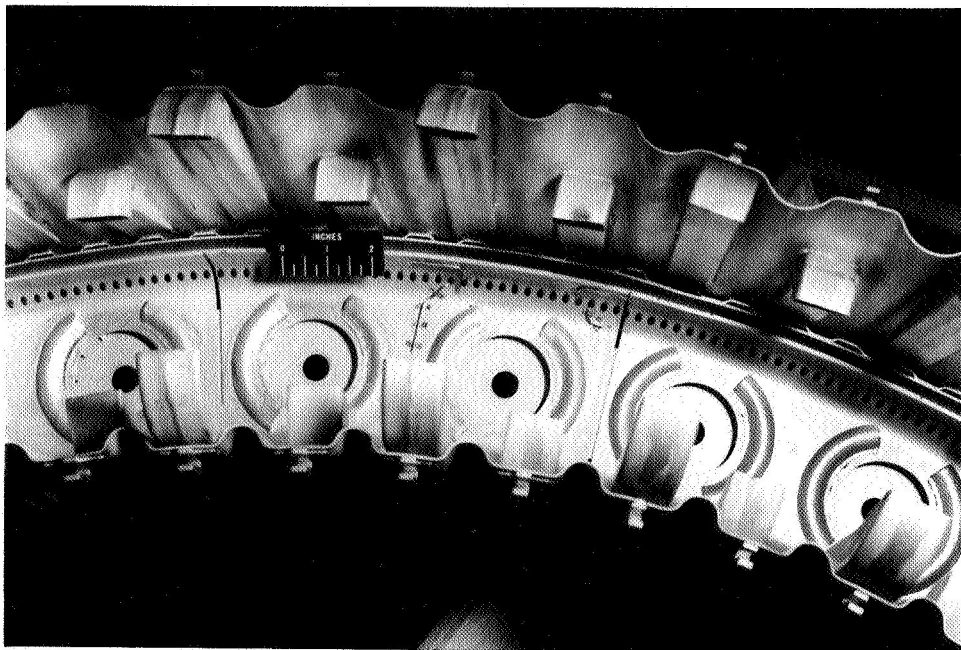
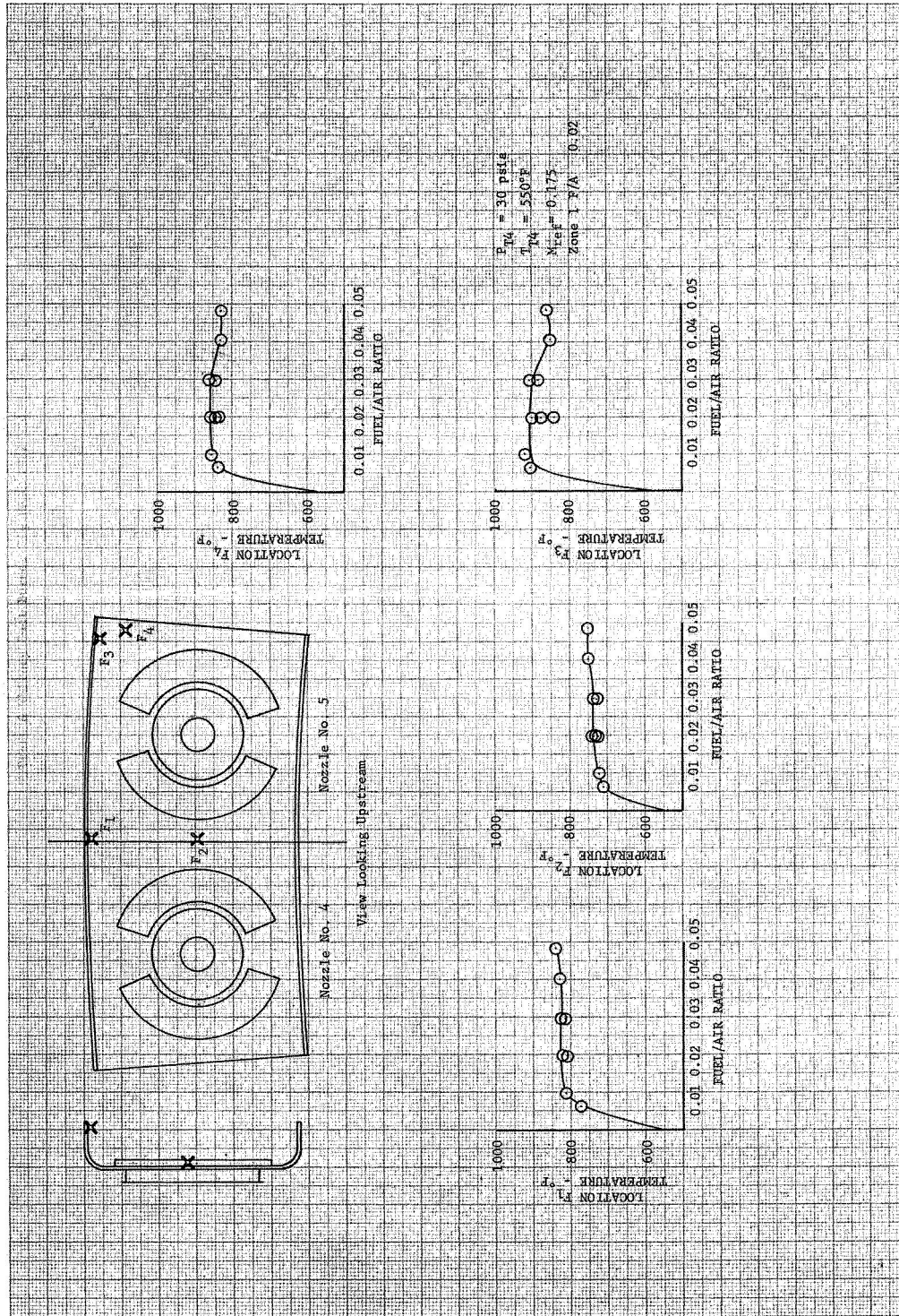


Figure VII-17. Thermocouple Installation on
the Modified Firewall FE 71986



DF 58523

Figure VII-18. Burner Firewall Temperature vs Fuel/Air Ratio

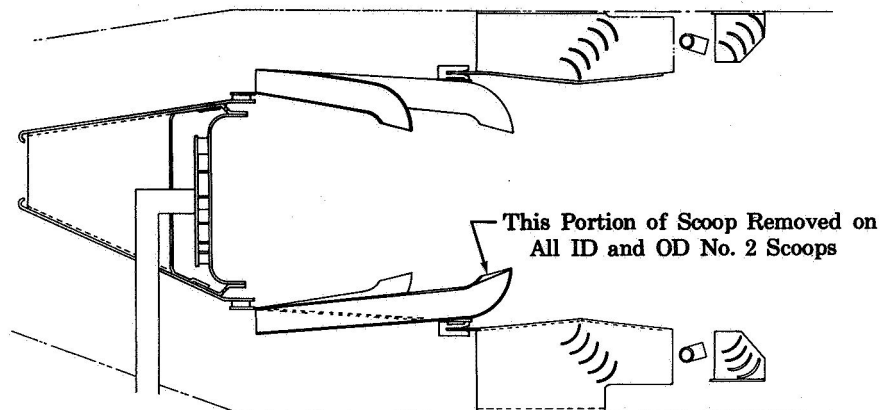


Figure VII-19. Schematic of No. 2 Scoop
Modification

FD 13591A

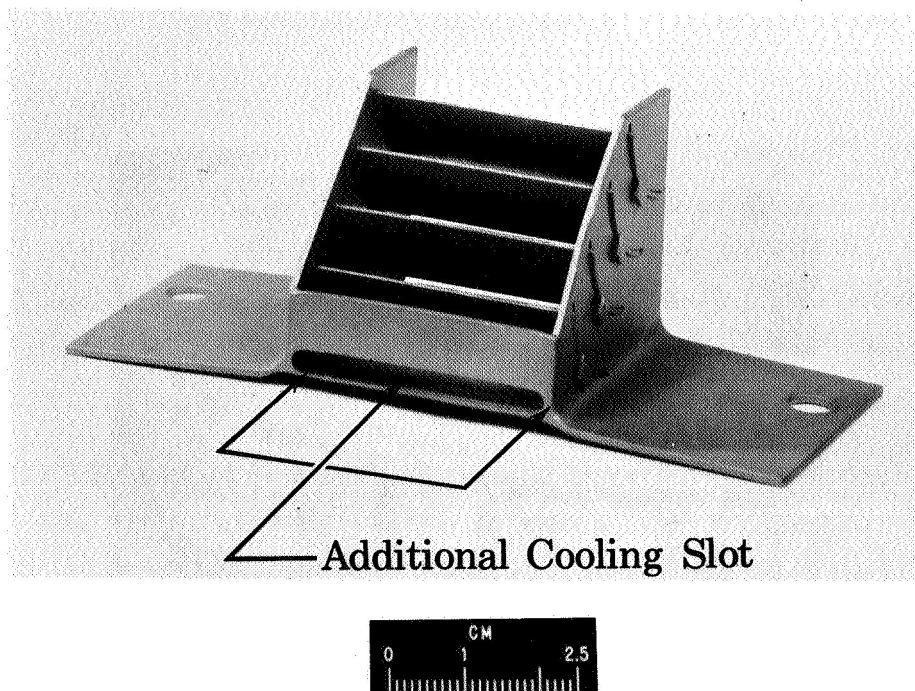


Figure VII-20. Modification to ID Vortex
Generators

FD 22560

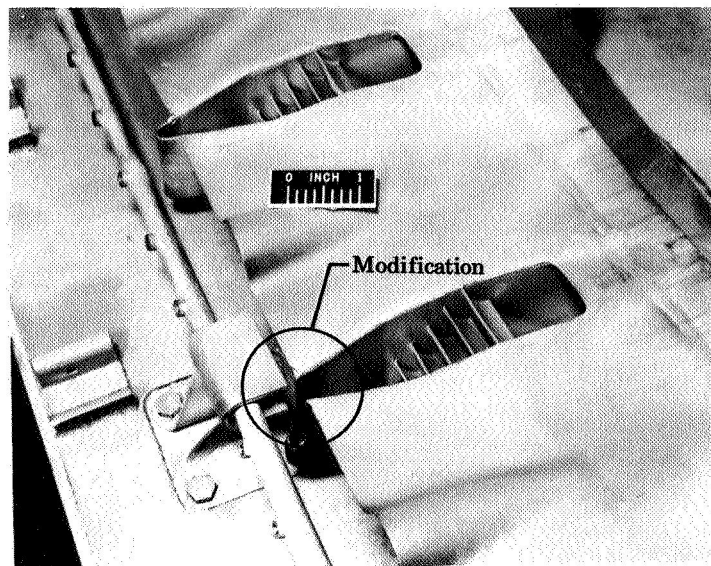


Figure VII-21. No. 3 Scoop Trailing Edge
Modification

FD 19524

At this time additional supports for the ID Zone-2 spraybars were installed (figure VII-22). The ID spraybars consisted of four segments, and were experiencing slight bowing due to air loading.

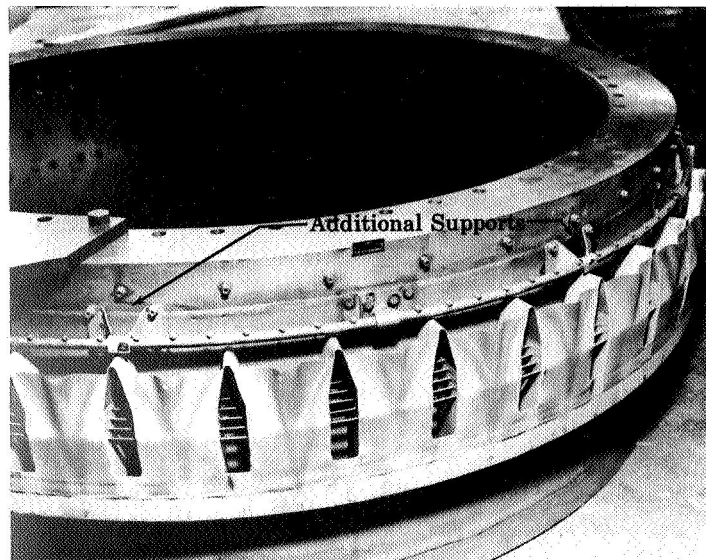


Figure VII-22. ID Spraybar Supports

FD 19525

After 16.77 hours of combustion testing with the second burner, the No. 36 Zone-1 fuel nozzle secondary supply tube failed and this resulted in burning of the primary and secondary liners (figures VII-23 and VII-24). The liners were repaired as shown in figure VII-25. The Zone-1 nozzles were strengthened by adding supports, as shown in figure VII-26, and no further Zone-1 fuel problems were encountered.

The vortex generators were eventually replaced by turbulators (figure II-10) intended to maintain high combustion efficiency while suppressing combustion instability.

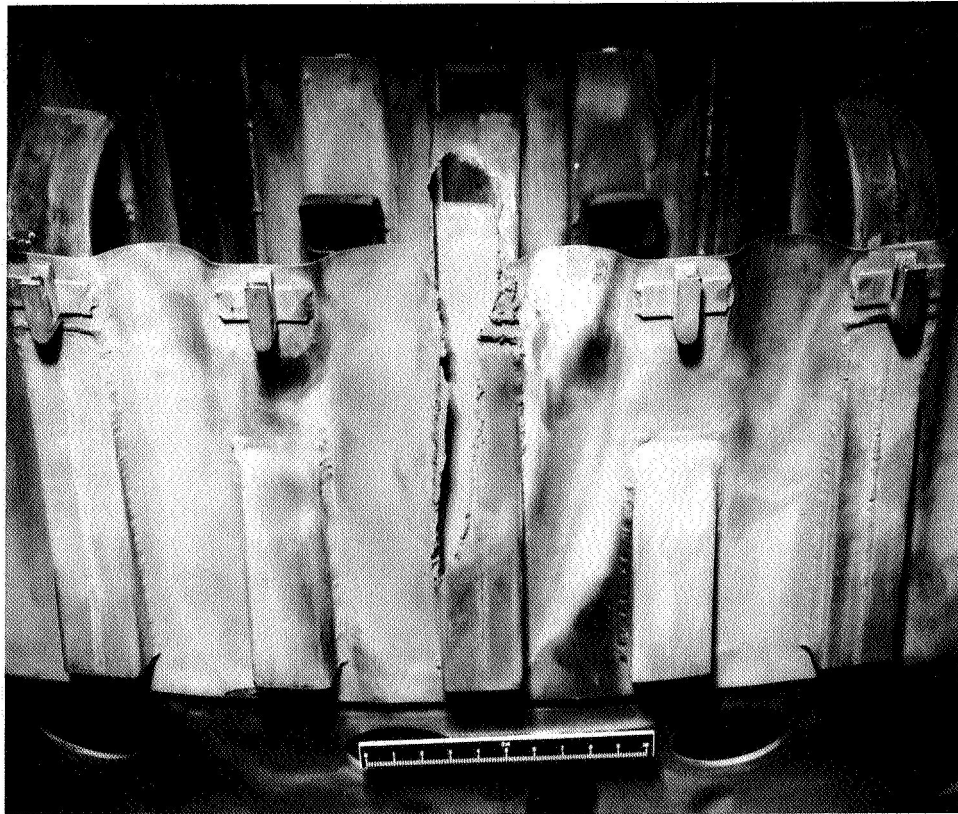


Figure VII-23. Primary OD Burner Panel
Burned Scoop

FE 67933

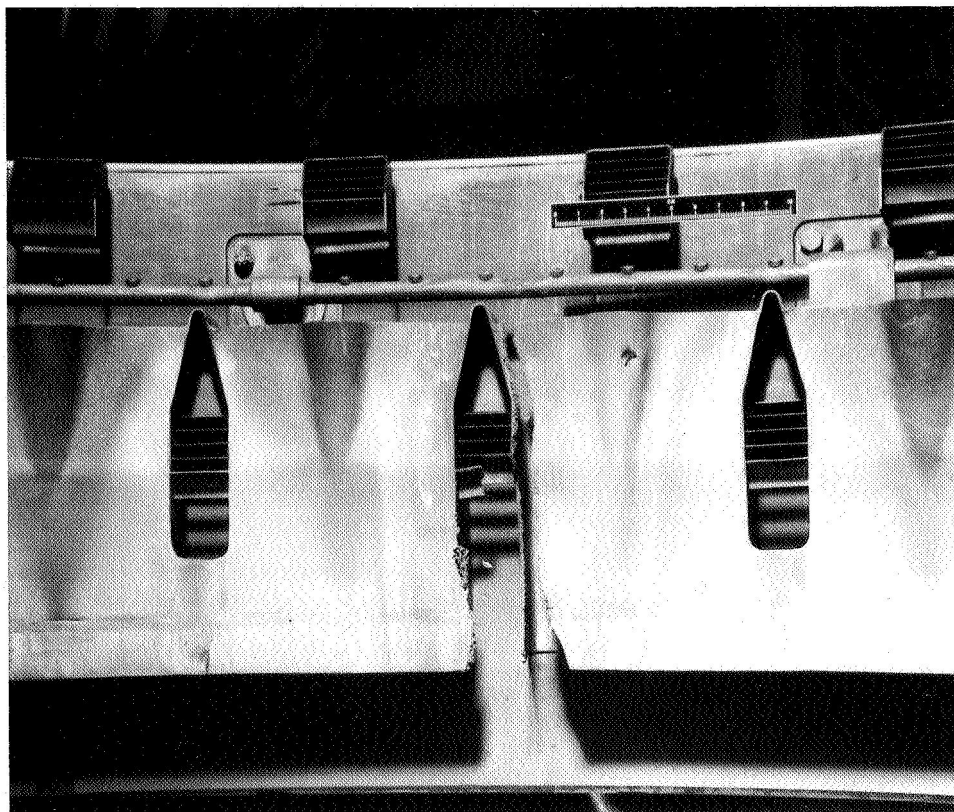


Figure VII-24. Secondary OD Burner Panel Burned Scoop FE 67934

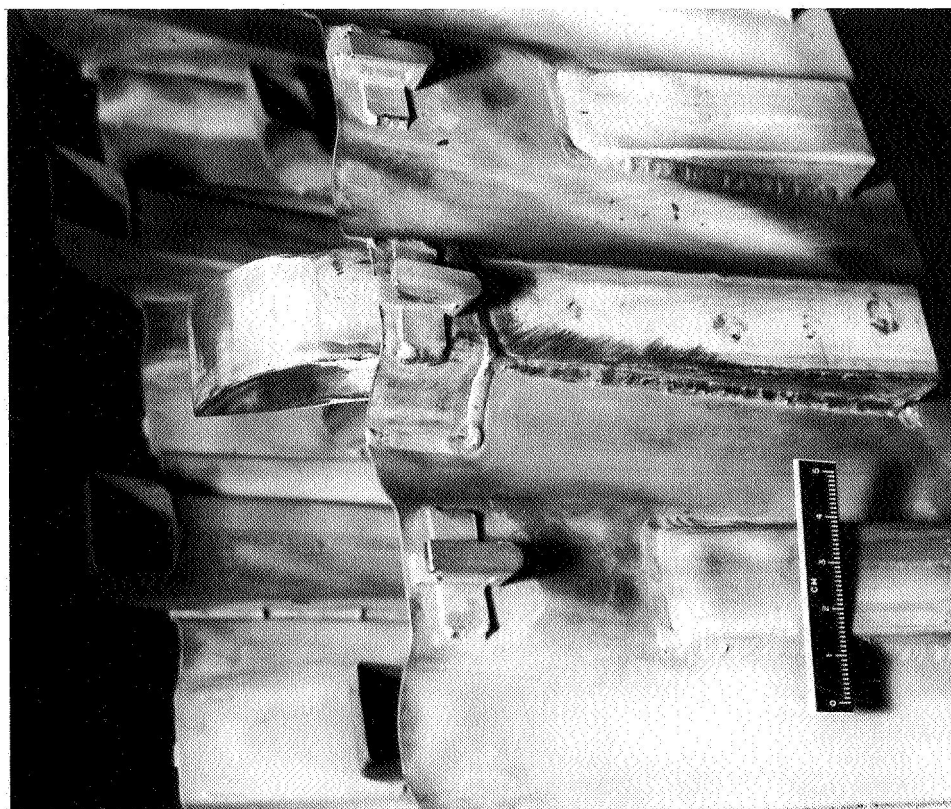


Figure VII-25. Repaired Primary OD Burner
Panel Scoop

FE 67935

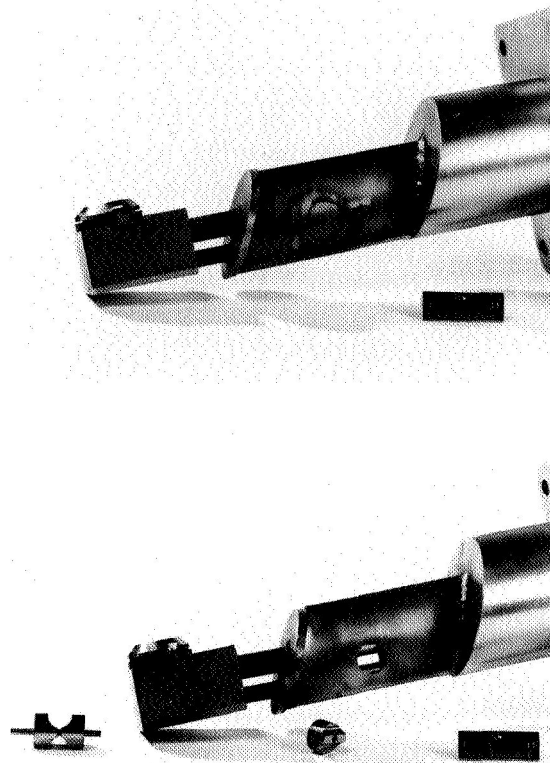


Figure VII-26. Structural Modification to
Zone-1 Nozzles

FD 20604

Good structural durability of the final ram-induction burner design was demonstrated as follows. A final inspection of the duct burner at the termination of the program showed that the burner was in excellent structural condition. No burning or cracks were found. The burner was cycled at least 54 times (the number of documented ignitions) while accumulating 81.20 hours of combustion testing and 92.66 hours of cold flow, as shown in figure VII-27. Furthermore, the burner was subjected to combustion instability 216 times, with an accumulated time of approximately 20 minutes. The secondary burner liners endured the entire test program for 97.20 hours of combustion testing and 175.70 hours of cold flow, while the burner was ignited 66 times and subjected to combustion instability 226 times.

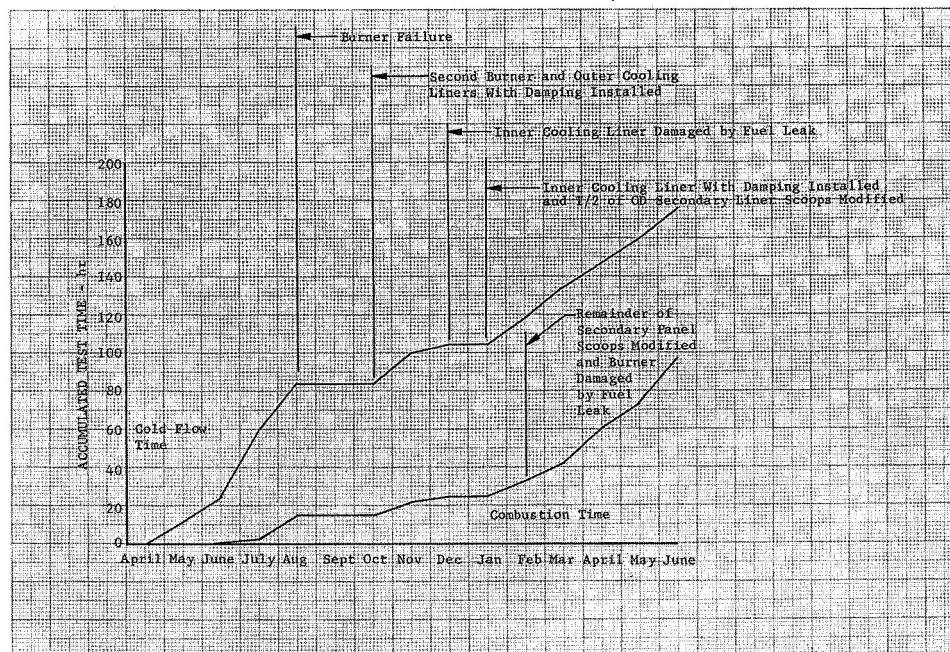


Figure VII-27. Program Test Times

DF 58524

2. Ignition and Blowout

The ignition and blowout characteristics of the duct burner were excellent. Although no specific instrumentation was employed to determine the ignition characteristics, the burner was observed to ignite at the minimum fuel flow limit of the fuel flow turbine meters, which was a fuel/air ratio of 0.0004 at the 30-psia simulated cruise test condition, and a fuel/air ratio of 0.0012 at a 10-psia simulated transonic climb test condition. The ignitions were achieved with no noticeable burner exit total pressure change when observing those parameters on a mercury manometer. When ignition was accomplished at 10 psia employing only every other Zone-1 secondary fuel nozzle, smooth and instantaneous ignition was achieved at a fuel/air ratio of 0.0037, which was the lowest fuel/air ratio that could be determined.

Burner blowout was never incurred unless testing at some point with combustion instability present.

3. Pressure Loss

The isothermal pressure loss of the ram-induction burner (figure VII-28) indicates that the design goal was achieved. Total burner pressure loss for the conditions tested is listed in table VII-1.

4. Combustion Efficiency

One hundred sixty-five test points produced valid data from which the performance of the duct burner could be determined. These test points are listed in table VII-1.

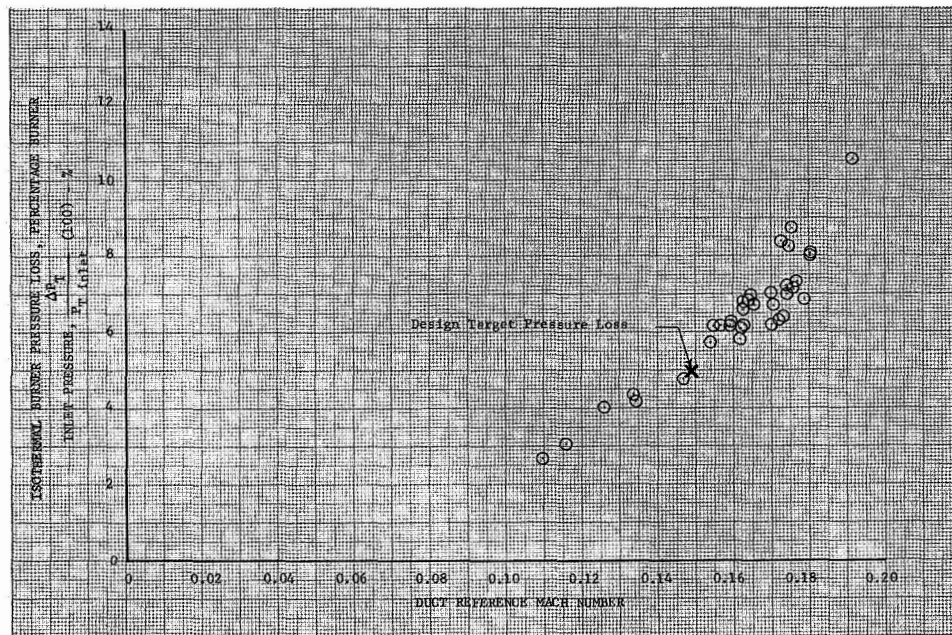


Figure VII-28. Isothermal Burner Pressure Loss (Percent Burner Inlet Pressure) vs Duct Reference Mach No. DF 58541

Table VII-1. Recorded Performance Test Conditions

Test Point	Date	CADD Number	Burner Inlet Conditions			Duct Reference Mach Number	Fuel/Air Ratio			Overall	Combustion Efficiency, %	Instability	Total Burner Pressure Loss, $\frac{\Delta P_{4-5}}{P_{T4}}$
			Airflow, \dot{W}_a , lb/sec	Pressure, P_{T4} , psia	Temperature, T_{T4} , °F		Zone 1 Primary	Zone 1 Secondary	Zone 2				
79	8-5-66	223-224	281.8	30.0	546	0.178	0.007	0.013	0.010	0.030	91.6	No	10.56
80	8-5-66	225-226	282.2	30.0	549	0.178	0.007	0.013	0.010	0.030	90.7	No	10.59
81	8-5-66	227-228	283.4	29.9	544	0.180	0.007	0.022	--	0.029	90.5	Yes	11.02
83	8-6-66	235-236	276.5	30.1	550	0.175	0.006	0.013	0.011	0.030	94.0	No	10.45
84	8-6-66	237-238	276.8	30.0	548	0.176	0.006	0.013	0.011	0.030	91.9	No	10.42
88	8-9-66	246-247	275.8	30.2	521	0.170	0.007	0.016	--	0.023	90.9	Yes	11.00
89	8-9-66	248-249	275.3	30.2	522	0.168	0.004	0.019	--	0.023	90.7	Yes	9.47
90	8-9-66	250-251	275.8	30.2	505	0.170	0.007	0.003	0.016	0.026	81.7	No	9.08
98	8-24-66	271-272	279.7	29.7	553	0.181	0.007	0.013	0.016	0.036	95.3	No	11.42
100	8-25-66	278-279	278.7	29.0	547	0.183	0.007	0.013	0.018	0.038	96.9	Yes	12.65
101	8-25-66	280-281	278.5	29.2	543	0.181	0.007	0.011	0.018	0.036	97.5	Yes	11.28
102	8-25-66	282-283	278.1	29.2	544	0.181	0.007	0.015	0.016	0.038	95.0	No	11.71
103	8-25-66	284-285	278.6	29.2	542	0.181	0.007	0.015	0.019	0.041	96.6	Yes	12.00
New burner* installed with diffuser bleed plates* and nose cone damper plate* and new outer absorption liners* installed.													
109	11-4-66	315-316	281.5	29.7	550	0.175	0.006	0.011	--	0.017	95.0	No	9.60
110	11-4-66	317-318	283.2	29.8	555	0.175	0.006	0.013	--	0.019	94.0	No	10.05
Removed flow distribution plate* in the rig inlet, installed radial fins in the rig centerbody, and removed the vortex generators.													
147	12-16-67	407	215.6	24.1	546	0.170	0.009	0.011	0.024	0.044	96.9	No	11.96
148	12-16-67	408	215.7	24.1	549	0.170	0.008	0.011	0.030	0.049	96.8	No	12.10
Radial fins in the rig centerbody removed, vortex generators removed, new inner absorption liner* installed, and 20 OD secondary scoops were modified.													
150	2-8-67	417-418	275.4	29.8	532	0.174	0.007	0.013	--	0.020	87.0	No	8.84
151	2-8-67	419	274.2	29.4	537	0.176	0.007	0.012	--	0.019	87.8	No	8.86
152	2-8-67	420	275.5	29.1	534	0.179	0.007	0.011	--	0.018	87.5	No	8.81
153	2-8-67	421	276.0	28.8	533	0.181	0.007	0.010	--	0.017	87.0	No	9.22
154	2-8-67	422	277.0	28.4	532	0.185	0.007	0.009	--	0.016	87.8	No	9.12
155	2-8-67	423	275.3	28.0	532	0.186	0.007	0.008	--	0.015	87.7	No	9.30
156	2-8-67	424	276.1	29.5	534	0.177	0.007	0.014	--	0.021	86.5	No	8.99
157	2-8-67	425	276.3	29.8	532	0.175	0.007	0.015	--	0.022	86.5	No	8.86
158	2-8-67	426	275.8	30.1	533	0.173	0.007	0.016	--	0.023	86.3	No	8.94
161	2-9-67	434	137.7	15.3	286	0.146	0.014	--	0.036	0.050	86.3	Yes	9.25

*This change was incorporated for the duration of the program.

NOTE: Cold flow calibration points and instability data points are NOT included.

Table VII-1. Recorded Performance Test Conditions (Continued)

Test Point	Date	CAME Number	Burner Inlet Conditions			Fuel/Air Ratio			Overall	Combustion Efficiency, %	Instability	Total Burner Pressure Loss, $\frac{\Delta P_{A-5}}{P_{t4}}$
			Airflow, \dot{W}_a , lb/sec	Pressure, P_{t4} , psia	Temperature, T_{t4} , °F	Duct, Reference Mach Number	Zone 1, Primary	Zone 2, Secondary				
175	2-10-67	448	226.6	24.6	543	0.175	0.008	0.011	0.042	93.2	No	11.86
176	2-10-67	449	226.9	24.7	531	0.174	0.008	0.011	0.042	94.0	No	17.00
177	2-10-67	450	227.8	24.8	546	0.175	0.008	0.011	0.042	93.7	No	17.08
178	2-10-67	451	217.9	24.9	556	0.167	0.009	0.011	0.050	94.2	No	11.30
179	2-10-67	452	295.0	28.9	547	0.195	0.006	0.013	0.033	84.4	No	13.11
180	2-10-67	453	296.3	29.3	543	0.193	0.006	0.012	0.035	85.4	No	12.80
181	2-10-67	454	296.2	30.0	543	0.188	0.006	0.012	0.035	88.4	No	12.62
182	2-10-67	455	296.9	30.7	540	0.184	0.006	0.013	0.037	91.1	No	12.23
183	2-10-67	456	296.5	33.1	540	0.170	0.006	0.012	0.045	96.8	No	11.45
184	2-10-67	457	296.2	32.3	540	0.174	0.006	0.012	0.041	95.4	No	11.99
185	2-10-67	458	295.2	32.9	540	0.170	0.006	0.013	0.045	96.6	No	9.11
Vortex generators removed. The fuel lines capped off on every other Zone 1 secondary fuel nozzle, and modified the secondary scoops on the ID and the remaining 20 secondary scoops on the OD.												
241	3-28-67	558	134.6	15.2	288	0.143	--	0.016	0.028	90.9	No	11.42
242	3-28-67	559	134.5	15.3	289	0.143	--	0.016	0.028	90.3	No	9.76
243	3-28-67	560	134.4	15.4	289	0.142	--	0.016	0.030	90.0	Yes	9.05
Vortex generators removed, fuel lines capped off on every other Zone 1 secondary fuel nozzle, and the diffuser vanes installed at 60 degrees from rig centerline.												
278	4-13-67	596	138.8	16.1	285	0.139	--	0.015	0.029	91.2	No	9.26
279	4-13-67	597	135.7	16.1	285	0.137	--	0.016	0.033	90.2	Yes	8.99
280	4-13-67	598	135.9	15.7	286	0.140	--	0.018	0.027	89.8	No	9.27
281	4-13-67	599-600	133.5	16.2	286	0.133	--	0.018	0.032	89.2	No	9.06
282	4-13-67	601-602	135.0	16.3	286	0.134	--	0.020	0.031	88.5	No	9.07
Vortex generators removed, fuel lines capped off on every other Zone 1 secondary fuel nozzle, and the diffuser vanes installed at 30 degrees from rig centerline.												
309	4-14-67	635	132.4	15.3	284	0.140	--	0.016	0.026	89.5	No	8.82
310	4-14-67	636	132.1	15.1	284	0.142	--	0.016	0.029	90.3	Yes	9.18
311	4-14-67	637	132.3	15.2	284	0.141	--	0.018	0.028	90.5	No	9.19
312	4-14-67	638	132.5	15.7	284	0.137	--	0.018	0.033	88.1	Yes	9.13
313	4-14-67	639-640	132.4	15.3	284	0.140	--	0.020	0.027	89.7	No	9.37
314	4-14-67	641-642	132.2	15.6	283	0.136	--	0.020	0.031	88.8	No	9.23
326	4-14-67	657	90.8	10.5	218	0.133	--	0.012	0.039	76.5	Yes	9.55
Vortex generators removed, fuel lines capped off on every other Zone 1 secondary fuel nozzle, 3-mesh screen installed in the rig inlet, and the diffuser vanes installed at 30 degrees from the rig centerline.												

*This change was incorporated for the duration of the program.

Table VII-1. Recorded Performance Test Conditions (Continued)

Test Point	Date	CADD Number	Burner Inlet Conditions			Fuel/Air Ratio			Overall	Combustion Efficiency, %	Instability	Total Burner Pressure Loss, $\frac{\Delta P_{5-4}}{P_{T4}}$
			Airflow, \dot{W}_a , lb/sec	Pressure, P_{T4} , psia	Temperature, T_{T4} , °F	Duct Reference Mach Number	Zone 1 Primary	Zone 2 Secondary				
342	4-20-67	685	135.1	15.4	291	0.142	0.013	--	0.027	0.040	91.3	8.92
346	4-20-67	689	135.4	15.4	291	0.143	--	0.016	0.024	0.040	91.0	8.93
347	4-20-67	690	135.1	15.1	290	0.145	--	0.016	0.026	0.042	90.1	9.59
348	4-20-67	691	135.2	15.4	290	0.143	--	0.018	0.026	0.044	91.4	9.56
349	4-20-67	692	135.2	16.0	290	0.138	--	0.018	0.032	0.050	90.01	9.22
350	4-20-67	693	135.1	15.4	290	0.143	--	0.020	0.024	0.044	90.3	9.67
351	4-20-67	694	135.4	16.0	290	0.138	--	0.020	0.030	0.050	89.5	9.41
354	4-20-67	697	91.0	10.2	218	0.137	0.010	--	0.038	0.048	77.4	8.39
357	4-20-67	700	91.1	10.4	217	0.135	--	0.016	0.032	0.048	80.9	9.56
358	4-20-67	701	91.1	10.4	216	0.135	--	0.020	0.028	0.048	82.9	9.38
Vortex generators removed, fuel lines capped off on every other Zone 1 secondary fuel nozzle, 4-mesh screen installed in the rig with an OD ring, (3-mesh screen was removed) and the diffuser vanes installed at 30 degrees from rig centerline.												
373	4-28-67	728	133.9	15.9	285	0.136	--	0.016	0.033	0.049	88.6	9.01
374	4-28-67	729	133.5	15.7	285	0.138	--	0.018	0.028	0.046	90.5	9.04
375	4-28-67	730	133.8	15.6	285	0.138	--	0.020	0.026	0.046	90.1	8.94
376	4-28-67	731	133.3	15.7	286	0.137	--	0.022	0.025	0.047	89.8	8.99
378	4-28-67	733	133.8	15.6	284	0.138	--	0.020	0.032	0.052	89.4	9.47
379	4-28-67	734	133.7	15.6	283	0.138	--	0.020	0.032	0.052	89.2	9.44
Installed the turbulators, fuel lines capped off on every other Zone 1 secondary fuel nozzle, 4-mesh screen with OD ring, in the rig inlet, and the diffuser vanes installed at 30 degrees from rig centerline.												
417	5-5-67	788-789	91.2	11.1	200	0.126	--	0.020	0.032	0.052	91.2	8.04
419	5-5-67	791	89.9	10.9	204	0.126	--	0.020	0.032	0.052	89.3	8.09
423	5-5-67	795	134.7	15.1	286	0.144	--	0.018	0.022	0.040	95.3	9.88
424	5-5-67	796	134.4	16.4	286	0.133	--	0.018	0.023	0.051	94.7	9.55
425	5-5-67	797	134.1	14.9	287	0.146	--	0.020	0.020	0.040	95.4	9.76
426	5-5-67	798	134.0	16.1	287	0.135	--	0.020	0.031	0.051	95.3	9.52
429	5-8-67	807	264.7	31.8	550	0.158	0.007	0.014	0.007	0.028	88.7	8.41
430	5-8-67	808	264.3	30.7	552	0.164	0.007	0.014	0.004	0.025	88.2	8.77
431	5-8-67	809	264.7	30.4	551	0.165	0.007	0.016	--	0.023	91.8	8.66
432	5-8-67	810	264.7	29.5	550	0.171	0.007	0.014	--	0.021	91.0	8.17
434	5-8-67	812	264.3	29.6	550	0.170	0.003	0.017	--	0.020	91.1	8.80

Table VII-1. Recorded Performance Test Conditions (Continued)

Test Point	Date	QADDE Number	Burner Inlet Conditions			Duct Reference Mach Number	Fuel/Air Ratio			Combustion Efficiency, %	Instability	Total Burner Pressure Loss, $\frac{\Delta P_{4-5}}{P_{t4}}$	
			Airflow, W_a lb/sec	Pressure, P_{t0} , psia	Temperature, T_{t0} , °F		Zone 1 Primary Secondary	Zone 1 Zone 2 Overall					
435	5-8-67	813	264.6	30.5	549	0.165	0.004	0.017	0.003	0.024	88.3	No	8.80
436	5-8-67	814	265.5	31.0	550	0.163	0.003	0.017	0.005	0.025	87.0	No	8.73
437	5-8-67	815	265.9	30.5	548	0.165	0.003	0.009	0.013	0.025	83.6	No	8.75
438	5-8-67	816	265.1	30.6	550	0.165	0.007	0.008	0.009	0.024	86.4	No	8.88
Turbulators installed, Zone 1 secondary fuel nozzles restored to 40, 4-mesh screen, with OD ring, in the rig inlet, and the diffuser vanes removed.													
469	5-15-67	857	276.9	29.7	545	0.178	0.003	0.025	0.012	0.040	92.2	No	12.35
Every other turbulator removed on both the ID and OD, Zone 1 secondary fuel nozzles restored to 40, diffuser vanes removed, and 4-mesh screen in the rig inlet with OD ring.													
481	6-10-67	879	277.5	30.7	560	0.173	0.007	0.017	0.020	0.044	94.3	Yes	11.57
484	6-10-67	882	277.7	31.0	560	0.172	0.007	0.021	0.019	0.047	91.2	No	11.79
485	6-10-67	883	278.1	31.4	558	0.169	0.007	0.023	0.020	0.050	89.5	No	11.69
Every other turbulator installed, Zone 1 secondary fuel nozzles restored to 40, diffuser vanes removed, 4-mesh screen in the rig inlet with OD ring, and Zone 2 spraybars capped off on the ID.													
493	6-10-67	892	276.8	30.6	559	0.173	0.007	0.023	0.020	0.050	82.7	No	11.93
All turbulators installed, 6 low flow Zone 2 OD spraybars installed, and 4-mesh screen in the rig inlet with OD ring, Zone 1 secondary fuel nozzles restored to 40.													
495	6-16-67	899-900	279.6	30.4	545	0.175	0.007	0.029	0.008	0.044	88.6	No	12.54
496	6-16-67	901	279.5	31.5	546	0.169	0.007	0.029	0.014	0.050	87.5	No	12.30
497	6-16-67	902	278.1	31.3	549	0.169	0.007	0.027	0.015	0.049	88.7	No	12.02
498	6-16-67	903	277.7	30.8	550	0.171	0.007	0.025	0.014	0.046	90.1	No	12.24
499	6-16-67	904	278.0	31.5	550	0.168	0.007	0.025	0.018	0.050	89.8	No	11.87
505	6-16-67	910	277.8	30.1	541	0.175	0.007	0.021	0.015	0.043	91.1	Yes	11.90
All turbulators installed, Zone 1 secondary fuel nozzles restored to 40, diffuser vanes removed, 4-mesh screen in the rig inlet with OD ring.													
510	6-20-67	922-923	275.4	29.0	557	0.182	0.007	0.009	--	0.016	92.6	No	12.55
511	6-20-67	924	275.4	29.4	557	0.180	0.007	0.010	--	0.017	94.2	No	10.81
512	6-20-67	925	274.9	29.8	557	0.177	0.007	0.011	--	0.018	92.3	No	9.39
513	6-20-67	926	275.7	29.8	557	0.177	0.007	0.012	--	0.019	92.1	No	9.57
514	6-20-67	927	275.3	29.8	557	0.177	0.007	0.013	--	0.020	93.7	No	9.82
515	6-20-67	928	275.3	29.7	558	0.177	0.007	0.014	--	0.021	92.4	No	10.07
516	6-20-67	929	275.4	30.1	558	0.175	0.007	0.015	--	0.022	93.1	No	9.88
517	6-20-67	930	275.0	30.3	558	0.173	0.007	0.016	--	0.023	91.9	No	9.86

Table VII-1. Recorded Performance Test Conditions (Continued)

Test Date Point	CADDE Number	Airflow, W_a , lb/sec	Burner Inlet Conditions		Duct Reference Match Number	Fuel/Air Ratio			Overall	Combustion Efficiency, %	Instability	Total Burner Pressure Loss, $\frac{\Delta P_{4-5}}{P_{T4}}$
			Pressure, P_{T4} , psia	Temperature, T_{T4} , °F		Zone 1 Primary	Zone 1 Secondary	Zone 2				
518	6-20-67	931	30.8	558	0.171	0.007	0.017	--	0.024	91.9	No	9.76
519	6-20-67	932	31.0	557	0.169	0.007	0.018	--	0.025	91.8	No	9.78
520	6-20-67	933	31.4	558	0.168	0.007	0.019	--	0.026	91.6	No	9.55
521	6-20-67	934	31.6	557	0.167	0.007	0.020	--	0.027	91.2	No	9.25
522	6-20-67	935	32.0	557	0.164	0.007	0.021	--	0.028	91.1	No	9.51
523	6-20-67	936	31.7	556	0.165	0.007	0.013	0.008	0.028	89.6	No	9.51
Turbulators installed, Zone 1 secondary fuel nozzles restored to 40, and 4-mesh screen in the rig inlet with OD rings.												
536	6-23-67	968	280.8	512	0.173	0.006	0.023	0.012	0.041	91.8	No	13.01
537	6-23-67	969	280.8	512	0.171	0.007	0.023	0.014	0.044	91.7	No	11.88
538	6-23-67	970	31.0	513	0.168	0.007	0.023	0.016	0.046	92.2	No	12.02
539	6-23-67	971	31.0	512	0.169	0.007	0.023	0.016	0.046	91.5	Yes	12.06
540	6-23-67	972	30.6	516	0.172	0.007	0.025	0.012	0.044	90.5	No	12.20
541	6-23-67	973	30.9	511	0.169	0.007	0.025	0.014	0.046	90.2	No	12.11
543	6-23-67	975	31.7	509	0.165	0.007	0.025	0.018	0.050	90.0	No	11.81
544	6-23-67	976	30.8	508	0.170	0.007	0.025	0.018	0.050	91.3	No	12.28
545	6-23-67	977	30.4	507	0.172	0.007	0.027	0.010	0.044	88.6	No	12.41
546	6-23-67	978	30.6	506	0.170	0.007	0.027	0.012	0.046	89.1	No	12.15
547	6-23-67	979	31.2	508	0.168	0.007	0.027	0.014	0.048	88.2	No	12.11
548	6-23-67	980	30.7	508	0.170	0.007	0.027	0.016	0.050	89.7	No	12.58
549	6-23-67	981	30.3	511	0.173	0.006	0.030	0.008	0.044	87.3	No	12.42
550	6-23-67	982	30.7	510	0.171	0.007	0.029	0.010	0.046	87.9	No	12.09
551	6-23-67	983	31.0	511	0.169	0.007	0.029	0.012	0.048	87.3	No	12.04
552	6-23-67	984	30.6	512	0.172	0.007	0.029	0.014	0.050	88.5	No	12.60
553	6-23-67	985	31.3	510	0.167	0.007	0.029	0.014	0.050	87.2	No	11.87
Turbulators installed, every other Zone 1 secondary fuel nozzles capped off, and 4-mesh screen in the rig inlet with OD ring and 3 additional rings evenly spaced.												
558	6-26-67	996	89.4	209	0.130	--	0.014	0.030	0.044	89.0	Yes	9.07
559	6-26-67	997	89.7	211	0.126	--	0.014	0.035	0.049	88.9	Yes	8.36
560	6-26-67	998	89.7	209	0.131	--	0.014	0.035	0.049	89.1	Yes	9.10
561	6-26-67	999	91.7	208	0.138	--	0.016	0.021	0.037	89.8	No	8.91

Table VII-1. Recorded Performance Test Conditions (Continued)

Test Point	Date	QADDE Number	Airflow, M_a , lb/sec	Burner Inlet Conditions		Duct Reference Mach Number	Fuel/Air Ratio				Combustion Efficiency, %	Instability	Total Burner Pressure Loss, $\frac{\Delta P_{4-5}}{P_{t4}}$
				Pressure, P_{t4} , psia	Temperature, T_{t4} , °F		Zone 1 Primary	Zone 1 Secondary	Zone 2	Overall			
562	6-26-67	1000	91.8	10.4	209	0.135	--	0.016	0.024	0.040	90.8	No	8.47
564	6-26-67	1002	92.0	10.4	207	0.136	--	0.016	0.025	0.041	91.6	No	8.63
565	6-26-67	1003	91.6	10.5	207	0.133	--	0.016	0.028	0.044	90.9	No	8.51
566	6-26-67	1004	92.0	10.7	207	0.132	--	0.016	0.029	0.045	90.4	No	8.63
567	6-26-67	1005	91.6	10.5	207	0.134	--	0.016	0.030	0.046	91.5	No	8.74
569	6-26-67	1007	92.1	10.7	207	0.131	--	0.016	0.033	0.049	89.6	No	8.65
572	6-26-67	1010	91.8	10.8	206	0.129	--	0.022	0.027	0.049	92.1	No	8.90
574	6-26-67	1012	91.9	10.1	207	0.140	--	0.018	0.022	0.040	91.6	Yes	9.25
575	6-26-67	1013	91.8	11.1	208	0.126	--	0.012	0.037	0.049	85.3	Yes	9.35
578	6-27-67	1021	133.9	15.2	292	0.143	--	0.012	0.024	0.036	91.5	No	10.32
579	6-27-67	1022	134.1	15.5	295	0.141	--	0.012	0.026	0.038	92.9	No	9.97
580	6-27-67	1023	133.8	15.8	293	0.138	--	0.012	0.028	0.040	92.5	No	10.11
581	6-27-67	1024	133.9	15.2	293	0.144	--	0.012	0.028	0.040	93.2	No	10.43
582	6-27-67	1025	133.7	15.4	294	0.142	--	0.012	0.030	0.042	92.5	No	10.27
583	6-27-67	1026	133.9	15.6	293	0.139	--	0.012	0.032	0.044	92.9	No	10.15
584	6-27-67	1027	133.7	15.9	293	0.137	--	0.012	0.034	0.046	92.9	No	10.04
585	6-27-67	1028	133.9	16.1	293	0.136	--	0.012	0.036	0.048	91.3	Yes	10.21
586	6-27-67	1029	134.0	16.2	290	0.134	--	0.012	0.038	0.050	91.0	Yes	9.87
588	6-27-67	1031	134.2	15.6	285	0.140	--	0.014	0.024	0.038	93.4	No	10.18
589	6-27-67	1032	134.2	15.8	285	0.137	--	0.014	0.026	0.040	94.0	No	9.88
590	6-27-67	1033	134.3	15.2	284	0.143	--	0.014	0.026	0.040	93.4	No	10.32
596	6-27-67	1039	134.0	16.2	285	0.134	--	0.012	0.038	0.050	90.6	Yes	10.16
598	6-27-67	1041	133.6	15.2	284	0.142	0.012	--	0.026	0.038	93.9	No	10.51
599	6-27-67	1042	134.0	15.2	284	0.142	0.012	--	0.028	0.040	93.5	No	10.68
601	6-27-67	1043	133.9	15.5	285	0.140	0.012	--	0.030	0.042	93.5	No	10.48
602	6-27-67	1045	133.5	15.7	285	0.138	0.012	--	0.032	0.044	93.7	No	10.25
603	6-27-67	1046	133.9	16.0	285	0.136	0.012	--	0.034	0.046	93.2	No	9.94
604	6-27-67	1047	133.5	16.2	286	0.135	0.012	--	0.036	0.048	92.5	No	10.05
606	6-27-67	1049	133.5	14.9	288	0.133	0.012	--	0.038	0.050	91.4	No	10.13
607	6-27-67	1050	133.4	15.1	287	0.143	0.014	--	0.024	0.038	94.5	No	9.63
608	6-27-67	1051	133.6	15.4	287	0.141	0.014	--	0.026	0.040	94.6	No	10.13
609	6-27-67	1052	133.7	15.6	287	0.139	0.014	--	0.028	0.042	94.5	No	9.72
610	6-27-67	1053	133.6	15.8	286	0.137	0.014	--	0.030	0.046	93.7	No	9.43
611	6-27-67	1054	133.6	16.0	286	0.135	0.014	--	0.034	0.048	92.9	No	9.72

Figure VII-29 shows the performance obtained with the original burner design at simulated cruise conditions. This burner gave combustion efficiency values of 92.5% to 95% in the 0.016-0.020 fuel/air ratio range, and exceeded 95% combustion efficiency in the 0.036-0.041 fuel/air ratio range. The burner experienced combustion instability and was not tested with fuel/air ratios greater than 0.041. It was noted that the occurrence of combustion instability had little effect on the combustion efficiency, probably because the combustion efficiency level was already high. The higher overall fuel/air ratio points were tested with the Zone-1 fuel/air ratio in the 0.020 range. This was the design point for the Zone-1 fuel/air ratio. The detrimental effect of reducing the Zone-1 fuel/air ratio is shown by the 82% combustion efficiency obtained with a Zone-1 fuel/air ratio of 0.010.

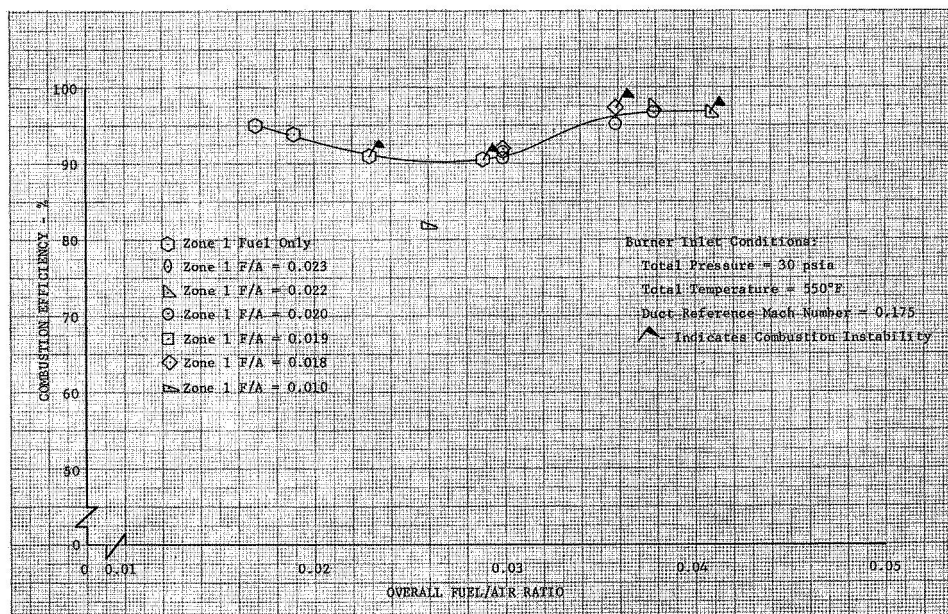


Figure VII-29. Combustion Efficiency vs Fuel/Air Ratio

DF 58525

Figure VII-30 illustrates how the mixing process downstream of the burner reduces the core temperature for the nearly stoichiometric combustion gases discharged from the Zone-1 region of burning. Analysis of the profile indicated that had the profile been flat, the combustion efficiency as defined in Section V would have been several percent higher than the value of 94% presented in table VII-1.

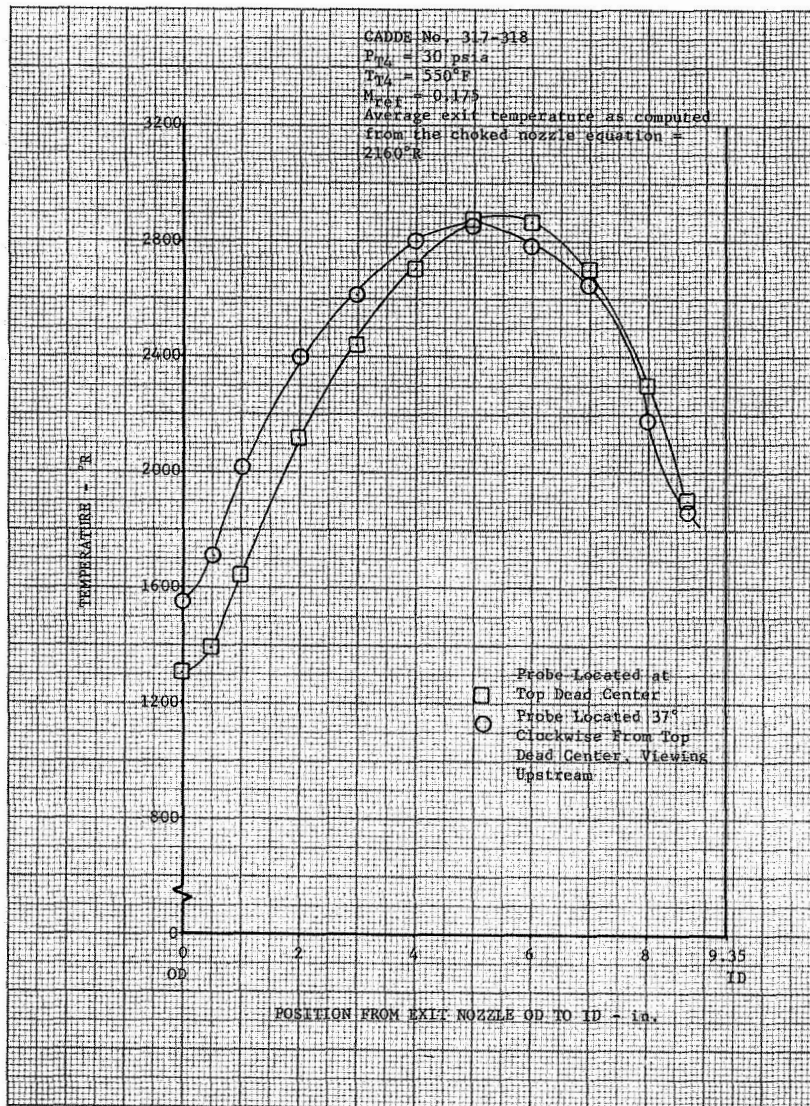


Figure VII-30. Traversed Burner Exit Temperature Profile at Cruise Conditions DF 61116

A No. 2 scoop was slightly burned when a Zone-1 fuel/air ratio of 0.029 was tested; subsequent tests of long duration were restricted to a Zone-1 fuel/air ratio of less than 0.025. It was found later in the program that the burning could be attributed to the combustion instability incurred during the test, and later tests were successfully conducted with Zone-1 fuel/air ratios as high as 0.036.

The vortex generators were removed and the ensuing combustion efficiencies are shown in figures VII-31 through VII-34. Figure VII-31 shows that the combustion efficiency was less than 90% until a fuel/air ratio of 0.036 was reached. This indicated that some type of mixing devices were required to mix the burner bypass air with the main combustion

mixture in the Zone-2 region. The lowered combustion efficiency could be a result of actual loss in chemical efficiency, a profile efficiency loss, or more likely a combination of both. Combustion efficiencies higher than 95% were obtained with a fuel/air ratio greater than 0.040. This was probably caused by increased mixing due to the additional burning of the Zone-2 mixture and also a flattening of the burner exit temperature profile.

Figure VII-32 shows the burner performance was not affected by reducing the burner inlet pressure to 24 psia (the data were obtained when facility limitations would not allow a test at the desired 30-psia level).

Performance with the vortex generators removed at simulated transonic climb test conditions at 15 and 10 psia are shown in figures VII-33 and VII-34, respectively. Little effect was seen due to fuel zone splits, although the higher efficiencies shown in figure VII-33 were generally those with higher Zone-1 fuel/air ratios. At 10-psia inlet pressure conditions (figure VII-34), there was a clear indication that the Zone-1 fuel/air ratio should be at least as high as 0.020. While testing at 10- and 15-psia inlet pressures, combustion instability occurred when the Zone-1 fuel/air ratio reached approximately 0.015 and 0.019, respectively. It was possible to increase the Zone-1 operation range by utilizing only every other Zone-1 fuel nozzle.

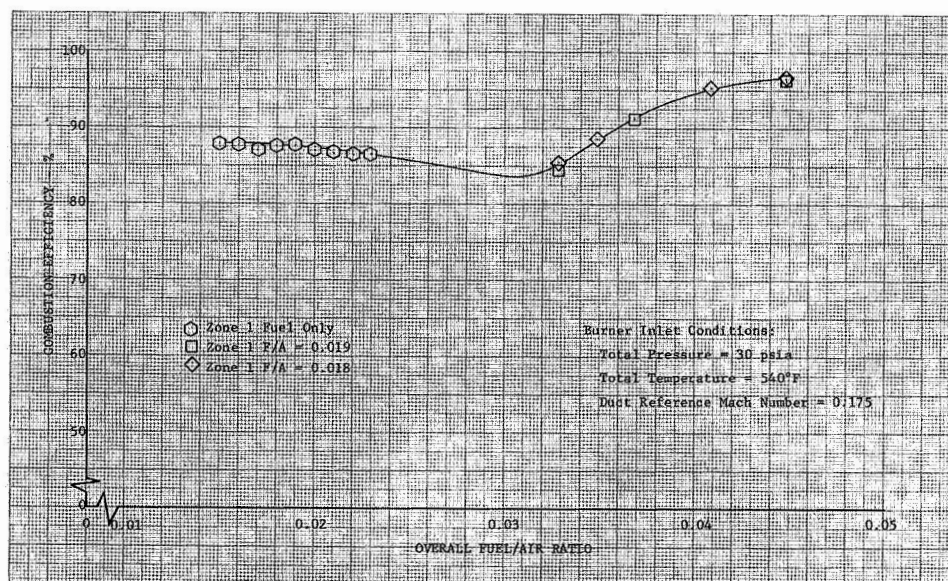


Figure VII-31. Combustion Efficiency at Simulated DF 58526
Cruise Conditions With Vortex
Generators Removed

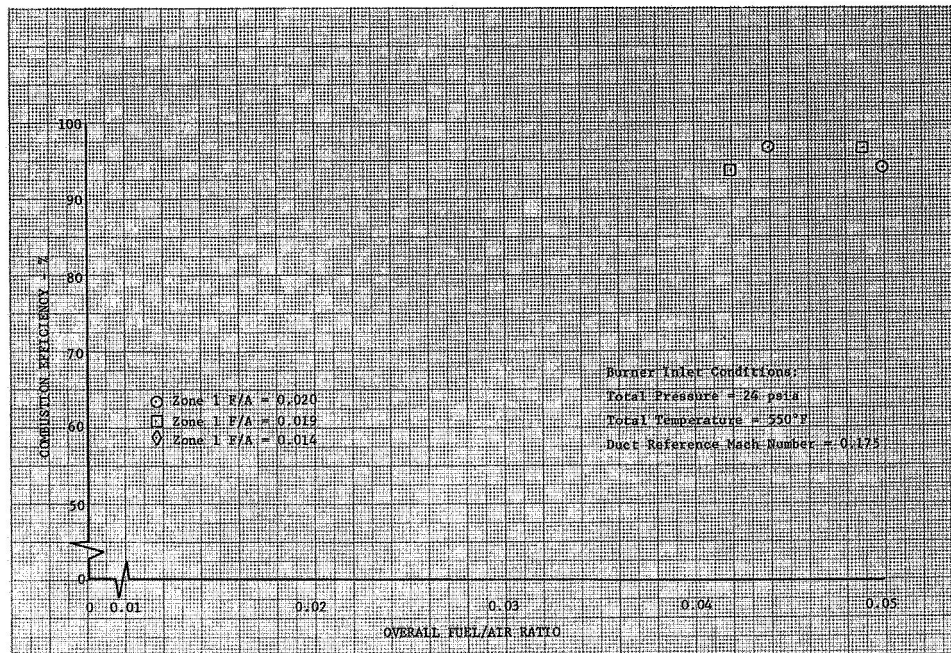


Figure VII-32. Combustion Efficiency at Simulated DF 58527
Cruise Conditions With Vortex
Generators Removed

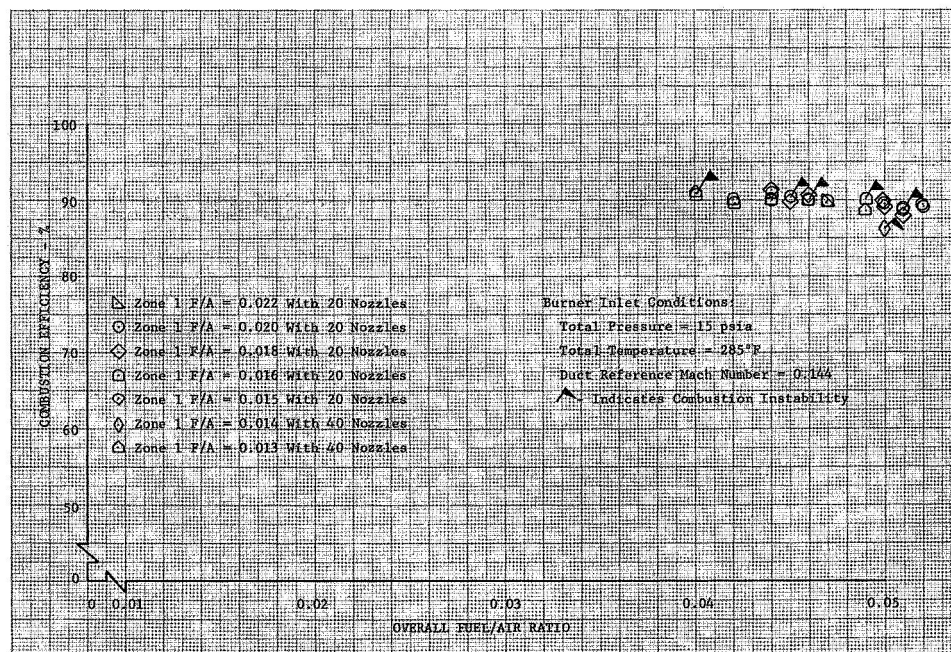


Figure VII-33. Combustion Efficiency at Simulated DF 58528
Climb Conditions With Vortex
Generators Removed

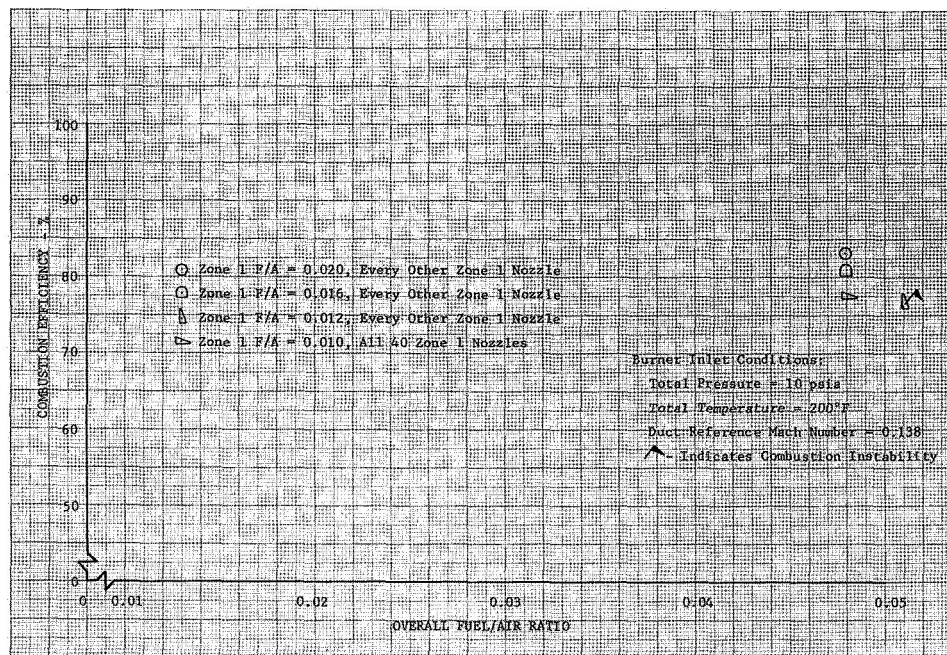


Figure VII-34. Burner Performance at Simulated
Climb Conditions With Vortex
Generators Removed

DF 58529

The effect of the turbulators installed in place of the vortex generators at simulated cruise conditions is shown in figure VII-35. Combustion efficiencies higher than 90% were shown for the full range of tested fuel/air ratios. In order to test an overall fuel/air ratio of 0.05, it was necessary to employ a Zone-1 fuel/air ratio of 0.032 to prevent combustion instability from occurring. As the Zone-1 fuel/air ratio was increased, a noticeable drop in combustion efficiency was seen. The optimum Zone-1 fuel/air ratio for maximum combustion efficiency was obviously less than the employed 0.030, and probably was much closer to the design point of 0.020.

Figure VII-36 shows the performance of the burner with the turbulators installed at the 15-psia simulated transonic climb test conditions. Very little difference was seen on combustion efficiency when employing 20 or 40 Zone-1 fuel nozzles. It was necessary, however, to use only 20 Zone-1 fuel nozzles to obtain stable combustion at Zone-1 fuel/air ratios higher than 0.019. The use of 20 nozzles had little overall effect on the combustion efficiency when compared to 40 nozzles. Again, it was shown that the optimum Zone-1 fuel/air ratio is at least 0.020, and a satisfactory 95% combustion efficiency was obtained at an overall fuel/air ratio of 0.051.

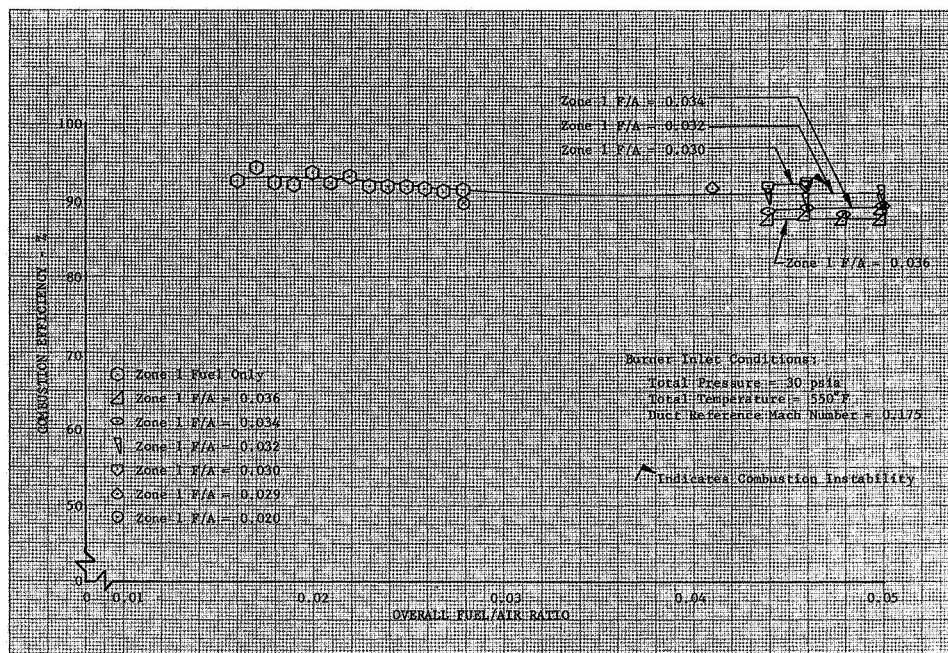


Figure VII-35. Combustion Efficiency at Simulated DF 58530
Cruise Conditions With Turbulators
Installed

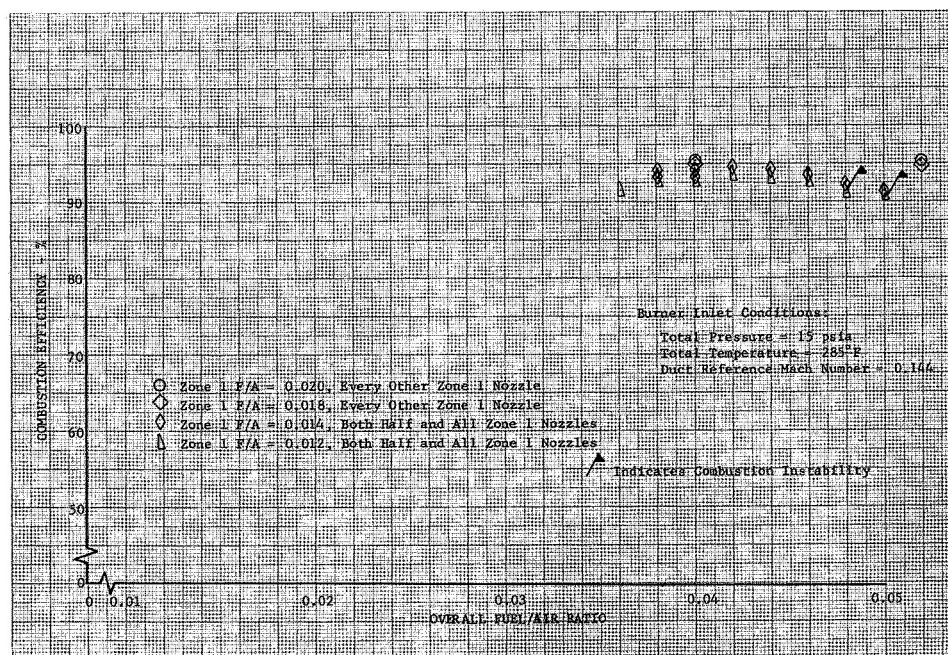


Figure VII-36. Combustion Efficiency at Simulated DF 58531
Climb Conditions With Turbulators
Installed

Figure VII-37 shows the burner with turbulators to follow the trend established at the 15-psia inlet pressure when tested at 10 psia simulated transonic climb conditions. Every other Zone-1 fuel nozzle was employed and a maximum combustion efficiency of 92% was recorded. The optimum Zone-1 fuel/air ratio may have been greater than 0.022 in this case. Combustion stability characteristics were very similar to those at the 15-psia inlet pressure conditions.

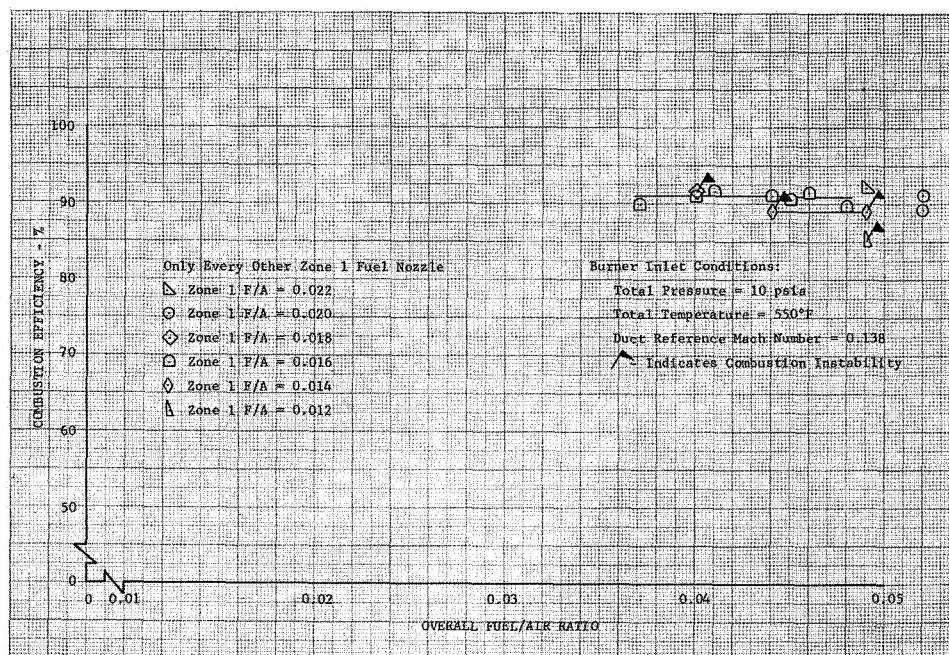


Figure VII-37. Combustion Efficiency at Simulated DF 58532
Cruise Conditions With Turbulators
Installed

In an attempt to eliminate the transverse mode of combustion instability, 6 of the 10 OD Zone-2 spraybar segments were replaced with segments having flow rates only 37% as high as the corresponding high flow rate segments. The location of these spraybars is shown in figure VII-38. The spraybar change caused a circumferential unbalance of the Zone-2 OD fuel injection and also caused the Zone-2 ID to flow higher than the OD. The local OD circumferential average Zone-2 fuel/air ratio was 0.020 and the ID average fuel/air ratio was 0.033 with an injector pressure differential of 160 psid on tests with an overall Zone-2 fuel/air ratio of 0.015. When all the high flow spraybars were normally used, the average ID and OD local Zone-2 fuel/air ratio was 0.026 with an injection pressure differential of 100 psid at an overall Zone-2 fuel/air ratio of 0.015.

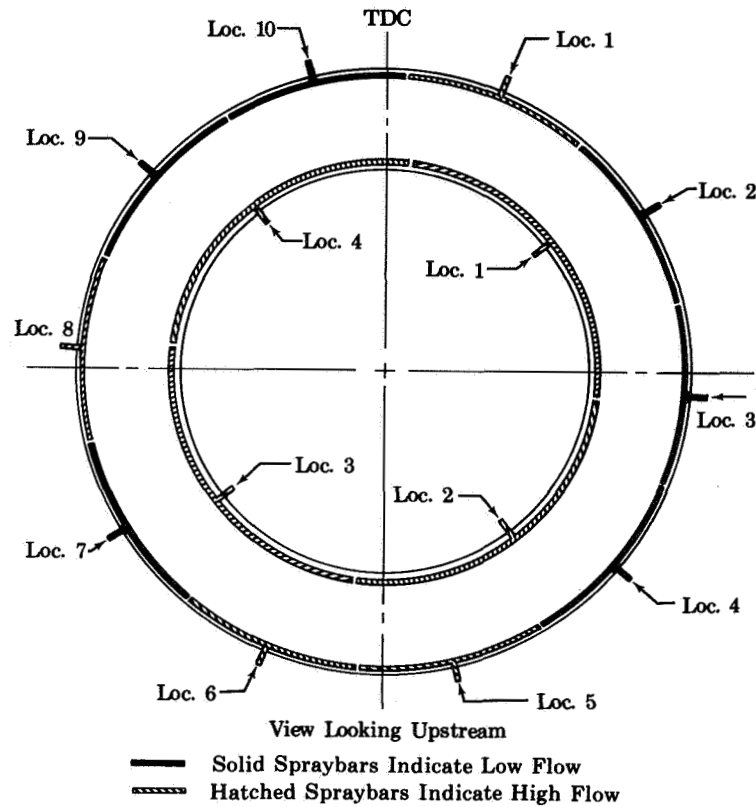


Figure VII-38. Zone-2 Spraybar Installation

FD 22822

Figure VII-39 shows the results obtained with the above configuration. Comparison of figures VII-35 and VII-39 show that the unbalance of the Zone-2 fuel injection had no noticeable effect on the combustion efficiency at an overall fuel/air ratio of 0.05. This indicates that for the particular burner design, the Zone-2 combustion area was flexible enough to allow considerable mismatch of individual nozzles in the Zone-2 system before any effect was seen on the burner performance.

The results obtained with every other turbulator installed at the simulated cruise conditions are shown in figure VII-40. Although precise points for comparison were not available, it was indicated that removing

every other turbulator reduced the combustion efficiency slightly. Figure VII-40 also shows the effect of testing with all Zone-2 fuel being injected on the OD only. At an overall fuel/air ratio of 0.05, the combustion efficiency was 82.7%, a drop of 7%.

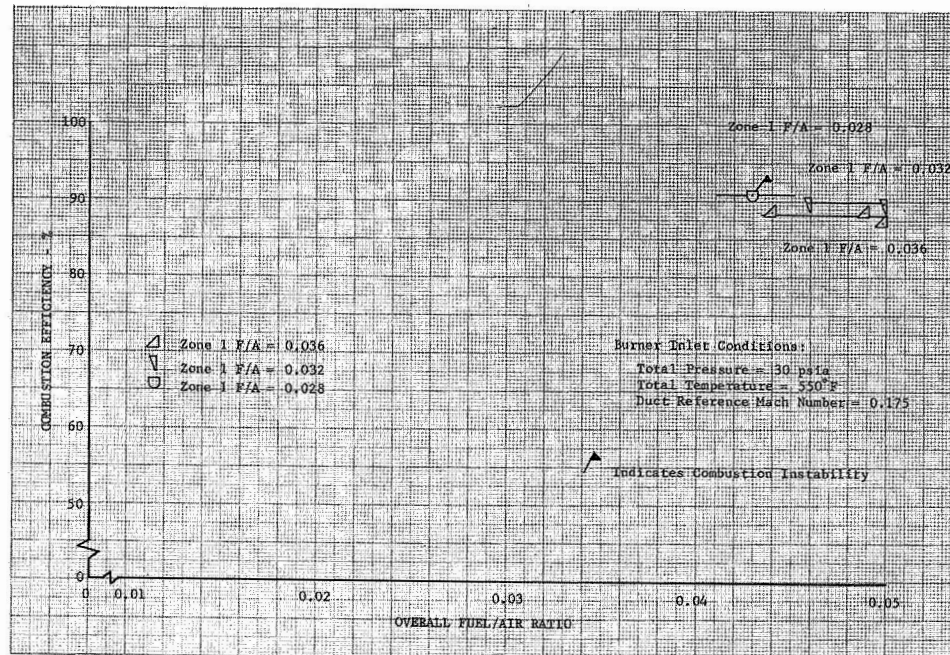


Figure VII-39. Combustion Efficiency at Simulated DF 58533 Cruise Conditions With Circumferentially Unbalanced Zone-2 Fuel Injection and With Turbulators Installed

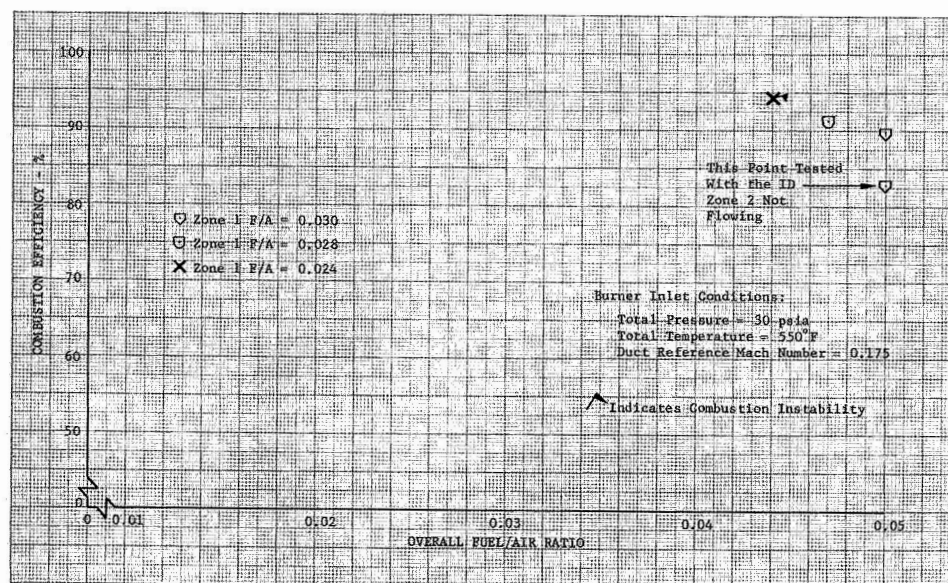


Figure VII-40. Combustion Efficiency at Simulated DF 58534 Cruise Conditions With Every Other Turbulator Removed

Comparisons of the three tested configurations are shown in figure VII-41. This was the only test condition in which comparisons of all three configurations could be made. The combustion efficiencies of the original burner and the one with turbulators were nearly identical up to a fuel/air ratio of 0.030. At higher fuel/air ratios, the original burner produced combustion efficiencies higher than the burner with the turbulators. However, the two burners were not operated at identical fuel zone splits at fuel/air ratios higher than 0.030. The original burner was tested with a Zone-1 fuel/air ratio of approximately 0.02 (the original design point), whereas the burner with the turbulators was tested with Zone-1 fuel/air ratios of 0.030-0.036. This was done to allow a stable overall fuel/air ratio of 0.05 to be tested. Data show (figure VII-35) that increasing the Zone-1 fuel/air ratio from 0.030 to 0.036 was done at a 4.5% sacrifice in combustion efficiency. It was concluded, therefore, that the turbulators performed similarly to the original vortex generators, and had both burner configurations been tested at identical test conditions, the results probably would have been very similar. The burner with the vortex generators removed was tested in a manner similar to the original burner, but did not match the original burner performance until an overall fuel/air ratio of 0.042 was reached. Although the burner was free of combustion instability at this test condition, the need for mixing devices in the Zone-2 injection area was clearly evident.

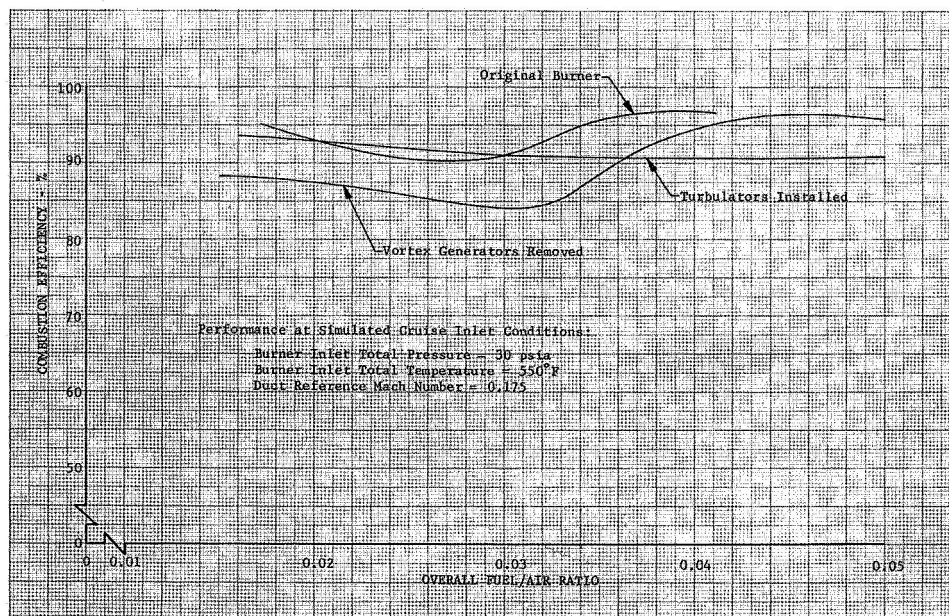


Figure VII-41. Combustion Efficiency Comparisons at Simulated Cruise Conditions DF 58535

Transverse mode combustion instability that occurred at the 30-psia test conditions was apparently associated with the Zone-2 combustion area, almost always occurring when the Zone-2 fuel/air ratio exceeded 0.015.

Figures VII-42 and VII-43 present comparisons of the burner with vortex generators removed and the burner with turbulators at simulated transonic climb conditions with inlet total pressures of 15 and 10 psia, respectively. These curves were partially drawn by extrapolation and interpolation of some data test points. This was done with confidence, due to the good repeatability displayed by the burners (see figures VII-31 through VII-39 and table VII-1).

A comparison of figures VII-41 and VII-42 shows that the burner with turbulators gave higher combustion efficiencies at simulated transonic climb than at the simulated cruise-approach condition. This was due to the burner being operated at the Zone-1 fuel/air ratio design point of 0.020 at the transonic climb condition, and indicates that much higher combustion efficiencies could be expected with the burner at a 30-psia inlet pressure if it was operated with a Zone-1 fuel/air ratio closer to the design point. The combustion instability that occurred at the transonic climb condition differed considerably from that at a 30-psia inlet pressure. In this case, a transverse mode was associated with the Zone-1 combustion area and a longitudinal mode associated with the Zone-2 area. The transverse mode would not allow a Zone-1 fuel/air ratio higher than approximately 0.019 to be tested, but this was circumvented by utilizing only every other Zone-1 fuel nozzle. The longitudinal mode would not allow an overall fuel/air ratio of 0.05 to be tested, but this mode was eliminated by use of radial vanes to effect a pressure drop in the rig diffuser.

Comparisons at the 10-psia simulated transonic climb conditions are shown in figure VII-43. The same general trend as that shown in figure VII-42 resulted at this test condition. The highest combustion efficiency (91%) was approximately 5% lower than that demonstrated at the 15-psia inlet pressure condition, indicating that the lower pressure and temperature levels were beginning to have noticeable effects on the

burner performance. The combustion instability incurred was generally similar to the 15-psia inlet pressure condition, except the instability occurred at lower fuel/air ratios.

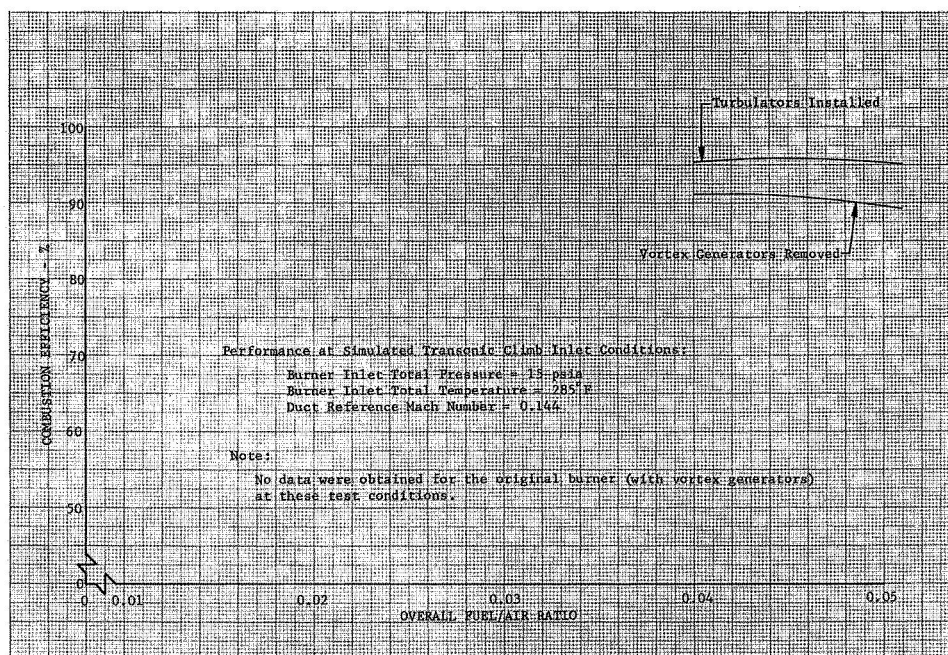


Figure VII-42. Combustion Efficiency Comparisons DF 58536
 at Simulated Transonic Climb
 Conditions (15 psia)

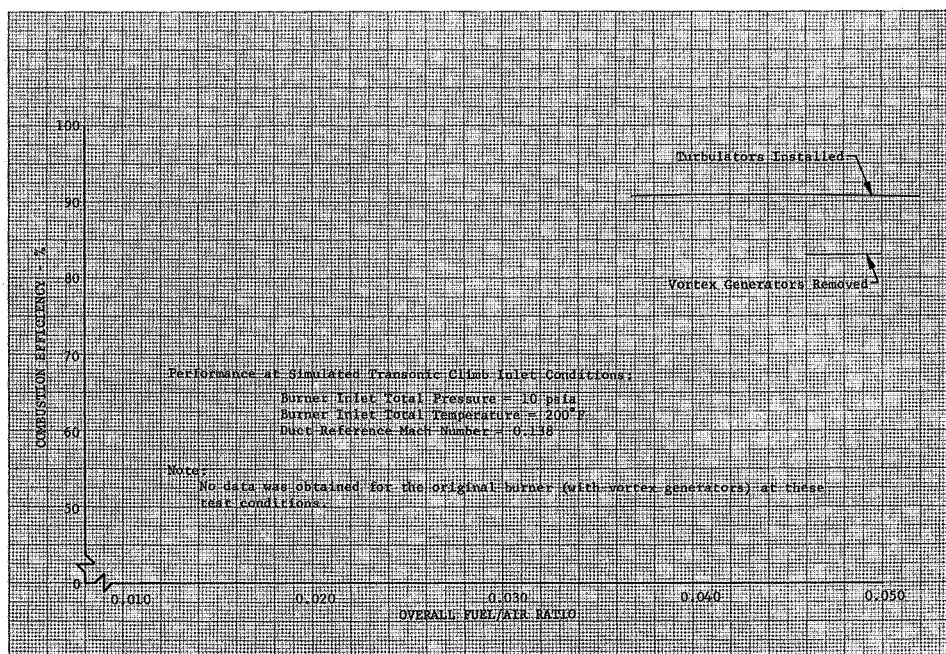


Figure VII-43. Combustion Efficiency Comparisons DF 58537
 at Simulated Transonic Climb
 Conditions (10 psia)

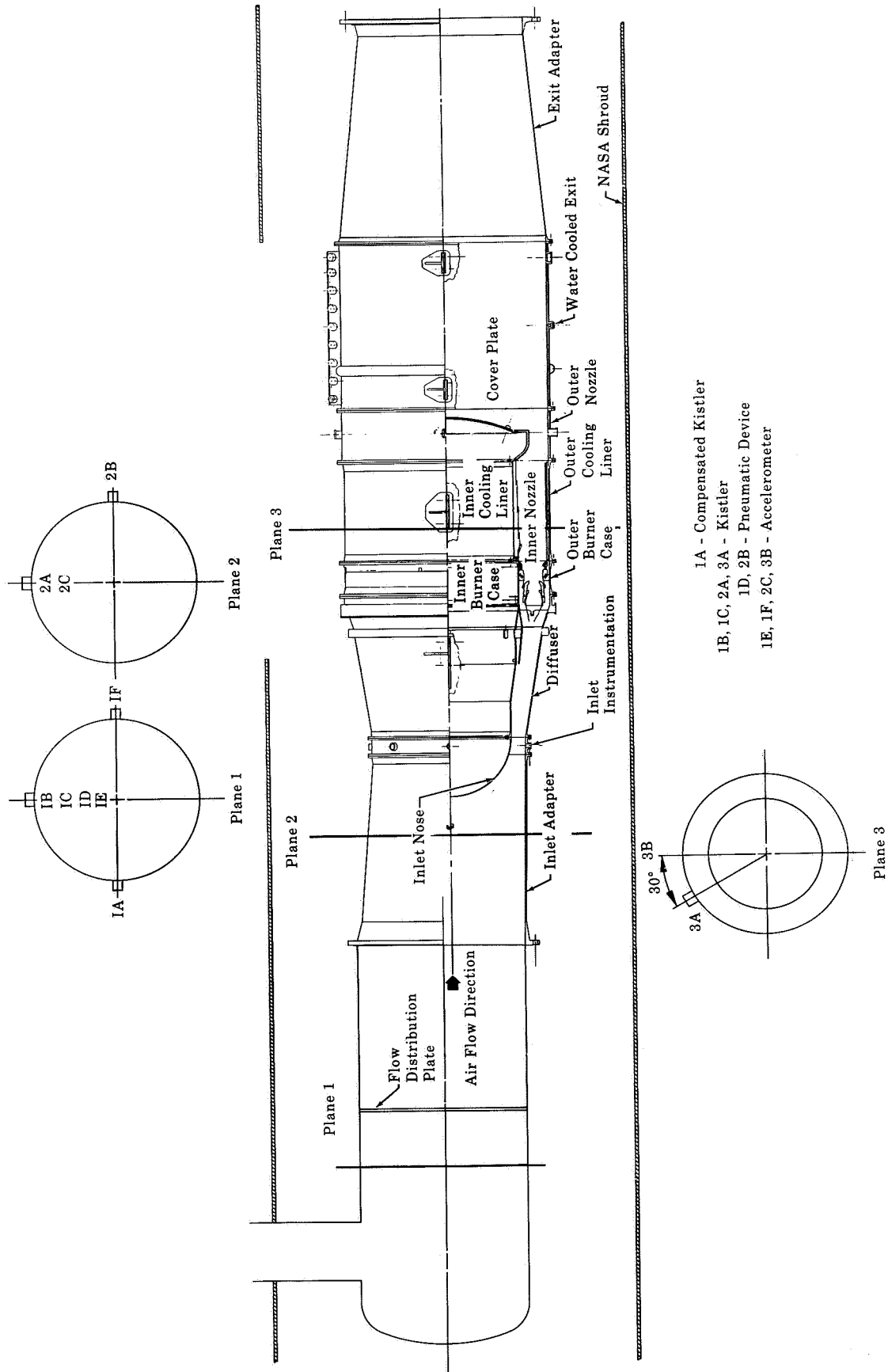
Although only one duct burner modification, installation of the turbulators, was made to improve combustion efficiency (the majority of the program development was devoted to the combustion instability area), one burner configuration was able to produce combustion efficiencies higher than 90% throughout the entire specified operating range.

SECTION VIII
COMBUSTION INSTABILITY

Prior to the burner tests that revealed combustion oscillations, several mechanical failures of the facility and test hardware were experienced. (All failures are documented in Appendix D, Test Chronology.) Most failures were attributed to the intense turbulence and large pressure drops produced in the inlet piping and plenum. The highly turbulent flow (white noise) and resulting mechanical vibration of the hardware necessitated changes to the baffling in the inlet plenum. Some baffle changes produced poor velocity profiles. Combustion oscillation was first encountered during the period in which different types of baffles were being examined. Since it is possible that the combustion oscillation could be affected by flow behavior in the plenum, design changes to the plenum were made concurrently with some of the burner modifications intended to damp the combustion oscillation. Both types of hardware changes and their effects on combustion oscillation are presented in this section.

During the exit nozzle nonburning calibrations, the dynamic pressure transducer mounted through and under the outer cooling liners indicated that high frequency pressure fluctuations existed with a peak-to-peak amplitude approximately equal to 10% of the measured static pressure. The rig and facility were then instrumented as shown in figure VIII-1 to obtain more data on these fluctuations.

Further testing did not pinpoint the source of the white noise that was observed; however, the primary sources were believed to be the discharge of high velocity air from the 24-in. diameter supply pipe into the plenum chamber, and, to a lesser extent, the noise generated within the pipe due to high velocities around the turns. Some noise may have been generated by the flow distribution plate, which had large holes with very high velocities, and some noise may have been generated by the inlet butterfly valve. Also, the piezoelectric (Kistler) pressure transducer, used to evaluate both white noise and combustion instability, were somewhat sensitive to mechanical vibration, hence the transducer output signals were not entirely from acoustical sources. A typical frequency spectrum analysis, obtained with a panoramic wave analyzer is shown in figure VIII-2.



- 1A - Compensated Kistler
- 1B, 1C, 2A, 3A - Kistler
- 1D, 2B - Pneumatic Device
- 1E, 1F, 2C, 3B - Accelerometer

FD 19179D

Figure VIII-1. Rig and Facility Instrumentation

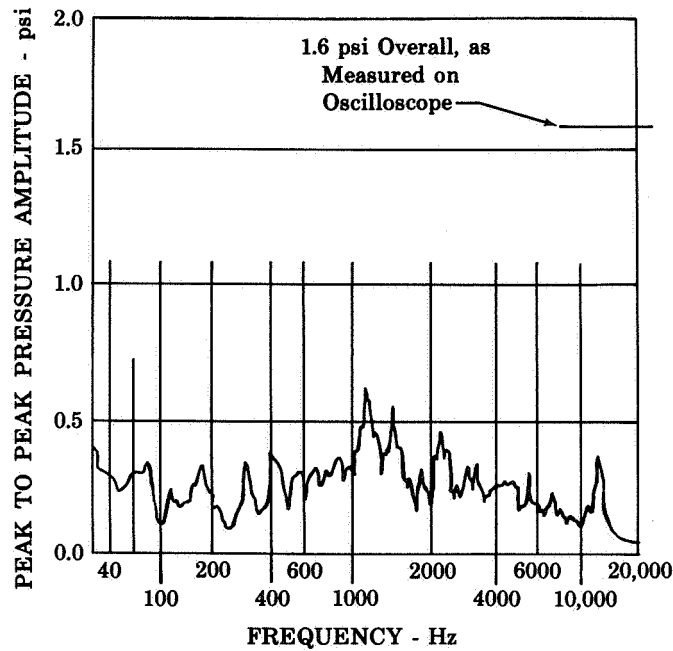
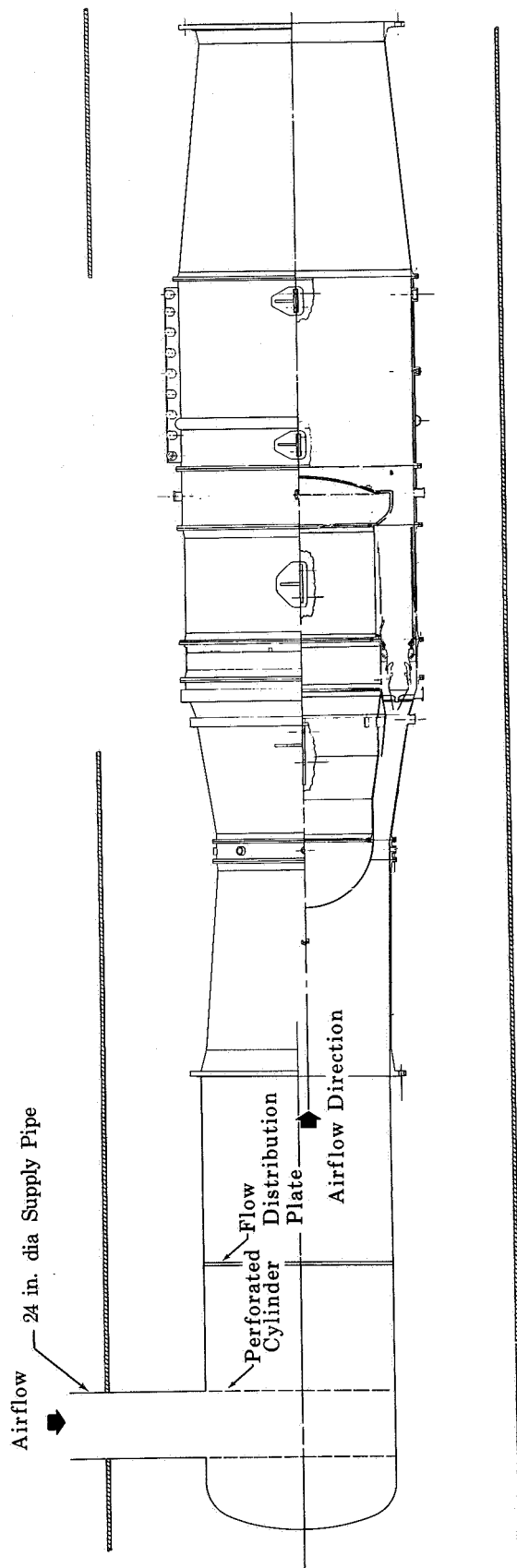


Figure VIII-2. Panoramic Wave Analyzer Display FD 22848
Obtained at Diffuser Inlet -
Airflow, 150 lb/sec

An attempt was made to reduce the noise by installing a perforated cylinder, which extended from the 24-inch diameter supply line to the bottom of the 54-inch diameter duct (figure VIII-3). Subsequent airflow tests showed the pressure fluctuations had been substantially reduced, although absolute levels could not be determined due to inadequate instrumentation. All burning tests were made after installation of the perforated pipe.

Combustion instability occurred during the sixth combustion test (Test Point 81, table D-2) during testing at simulated cruise conditions. (All instability test points referred to are listed in table D-2 of Appendix D.) Combustion instability occurred six more times until the burner failed (Test Point 103). High peak-to-peak pressure amplitudes were noted (figure VIII-4), with the frequency in the 150-180 Hz range. These dynamic pressure transducer signals were recorded on a Visacorder (self-developing strip-chart recorder) in the test cell control room. Pressure was displayed as a function of time. The vibration level of the rig was extremely high (figure VIII-5).



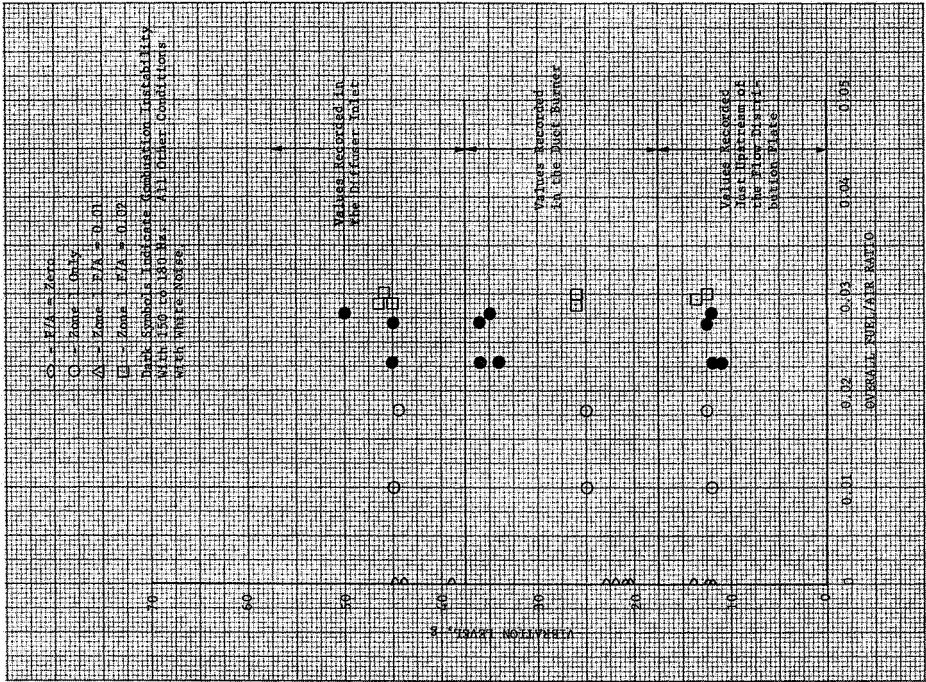
VIII-4

Figure VIII-3. Facility Inlet Modification

FD 19179A

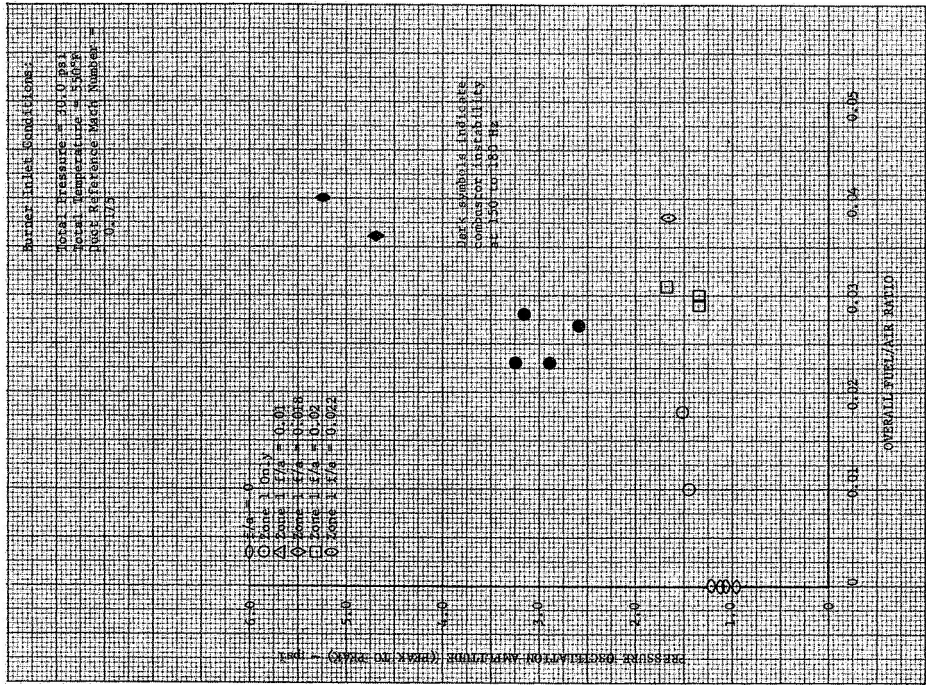
DF 58538

Figure VIII-5. Rig and Facility
Vibrations - Instru-
ments Mounted on
Casing Flanges



DF 58544

Figure VIII-4. Burner Pressure
Oscillations



Although the data recorded during the previous tests were limited in quality and quantity, the observed frequency was that which would be expected for a combustion induced, first tangential mode of pressure oscillation for this burner. New outer cooling liners were then fabricated and installed with forward segments that incorporated perforations and tubes to act as Helmholtz resonators to damp out pressure oscillations and thus act as an acoustic suppressor. The liners are shown in figures II-15 and IV-19. The predicted absorption coefficient (that portion of the incident pressure wave not reflected from the liner) is shown in figure IV-20. The existing analytical techniques of acoustic suppression do not provide for determination of the level of suppression required to suppress pressure instability effectively. The evaluation of any design is therefore difficult and dependent upon previous experience. The installed acoustic liners were therefore considered to be effective, although the absorption coefficient was approximately 0.14.

It was also possible that longitudinal oscillations existed, as the pressure amplitude did not fall off rapidly with distance upstream of the burner, and the frequency and occurrence was controlled only in part by the burner.

To eliminate longitudinal instability that might be coupled with rig centerbody pressure oscillations (the theoretical frequency of the second longitudinal mode of oscillation within the inner body was 150 Hz) a damping plate incorporating the Helmholtz resonator principle was installed as shown in figures VIII-6 and VIII-7. To eliminate a possible driving force for centerbody oscillations that could result from the diffuser bleed air, the diffuser bleed static pressure rise was eliminated by installing restrictions at the diffuser bleed exit, also shown in figures VIII-6 and VIII-7.

At this point in the test program the new burner was installed, and the operation procedure was revised to minimize damage produced by combustion instability. In previous tests, a full set of recorded data was obtained when instability occurred. Approximately 20 seconds were required to obtain these data. The new burner was spared this relatively long exposure to vibration by being operated at the instability condition only long enough to garner the most pertinent data. This was done in a period of several seconds.

FD 14326B

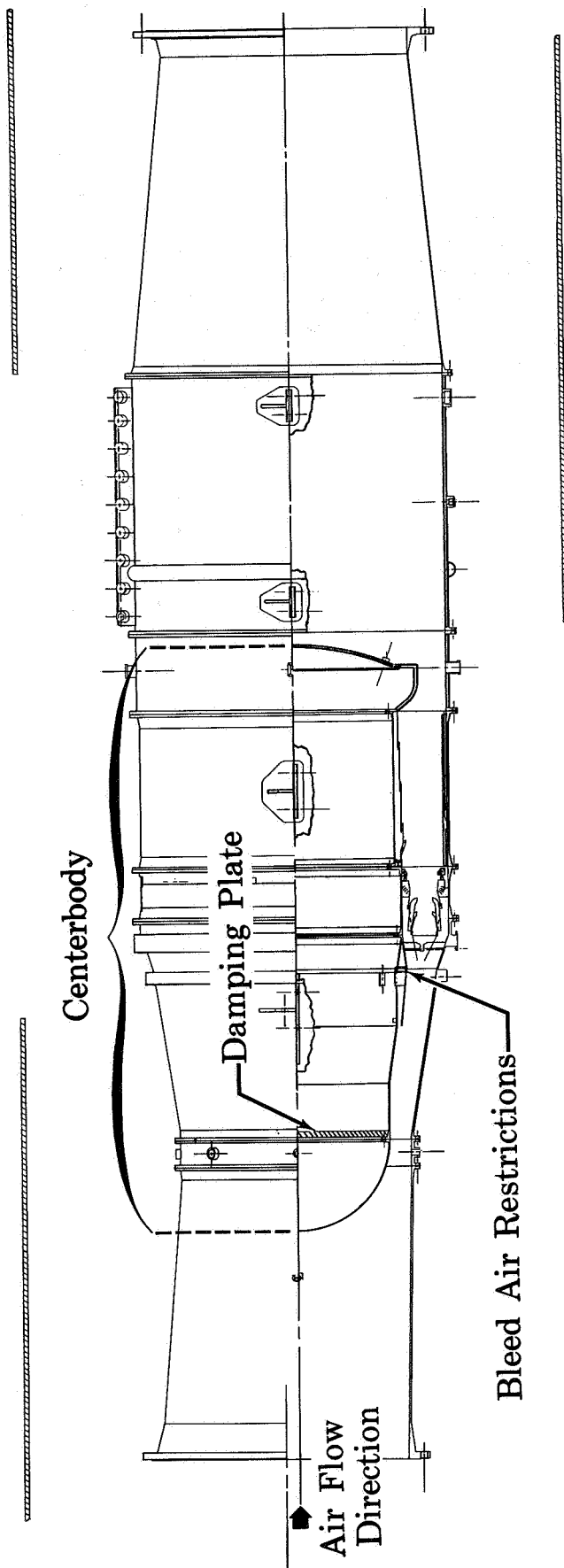


Figure VIII-6. Rig Centerbody Modifications

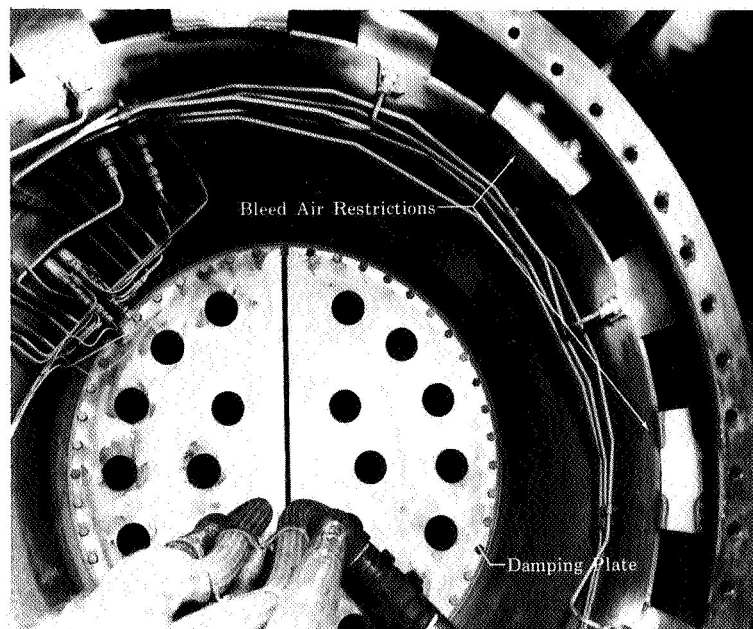


Figure VIII-7. Rig Centerbody Modifications

FD 18858

Combustion Test Points 115 through 117 showed these modifications to be ineffective in reducing combustion instability, which was occurring predominantly at a frequency of 450 Hz. The instability was only noted when the Zone-2 fuel/air ratio exceeded 0.01 while augmenting the Zone-1 combustion. The burner pressure amplitude was modulated at a frequency of 5 Hz (figure VIII-8) and the two burner pressure transducers spaced 90-deg apart were not in phase, indicating a rotation. There was a definite decrease in pressure amplitudes in the diffuser inlet and the burner exit. The increase in the frequency from 150-180 to 450 Hz indicated that the first transverse mode was probably replaced by the third transverse mode.

An effort was made to reduce the cold flow white noise peak-to-peak inlet pressure amplitudes of 1 to 2 psia at 30 psia by the installation of damping devices in the facility inlet duct. These inlet damping devices consisted of three steel boxes, perforated to act as Helmholtz resonators, which were welded to the inlet duct wall between the flow

distribution plate and the rig. The boxes failed during nonburning operation due to the extreme pressure oscillations (noise) present in the inlet (figure VIII-9).

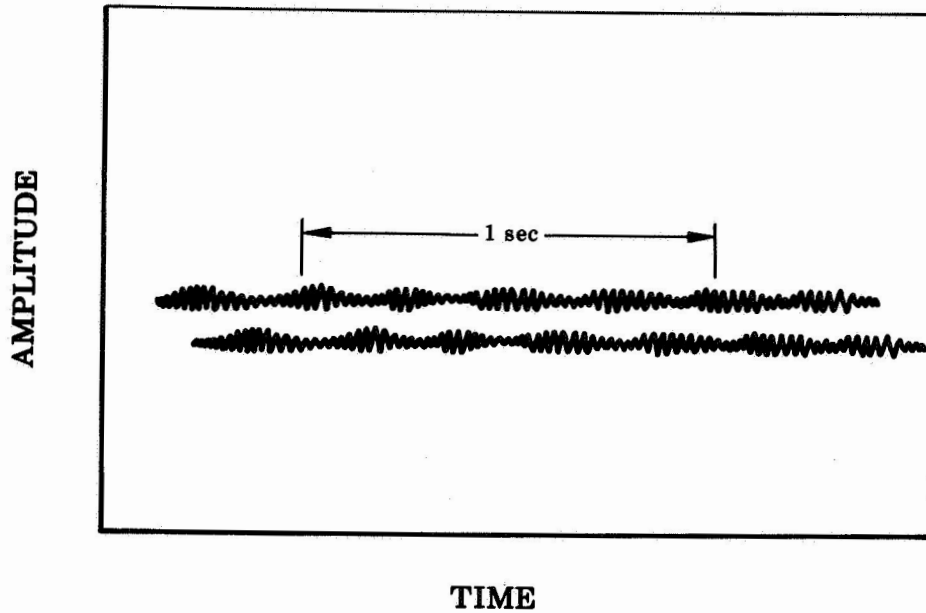


Figure VIII-8. Schematic of Burner Oscillations FD 23703

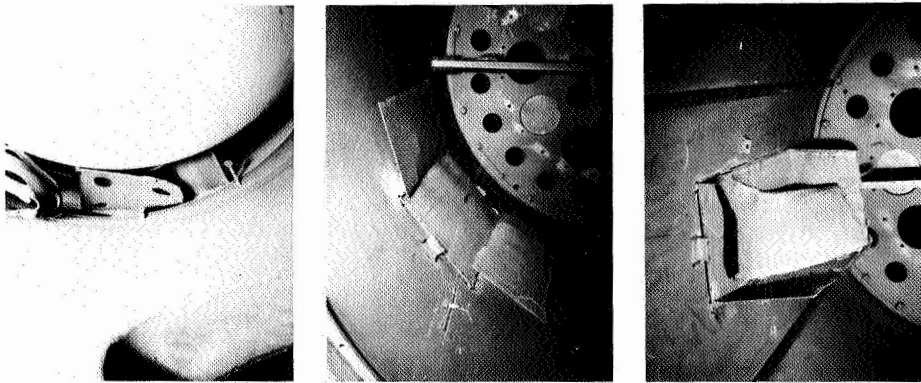
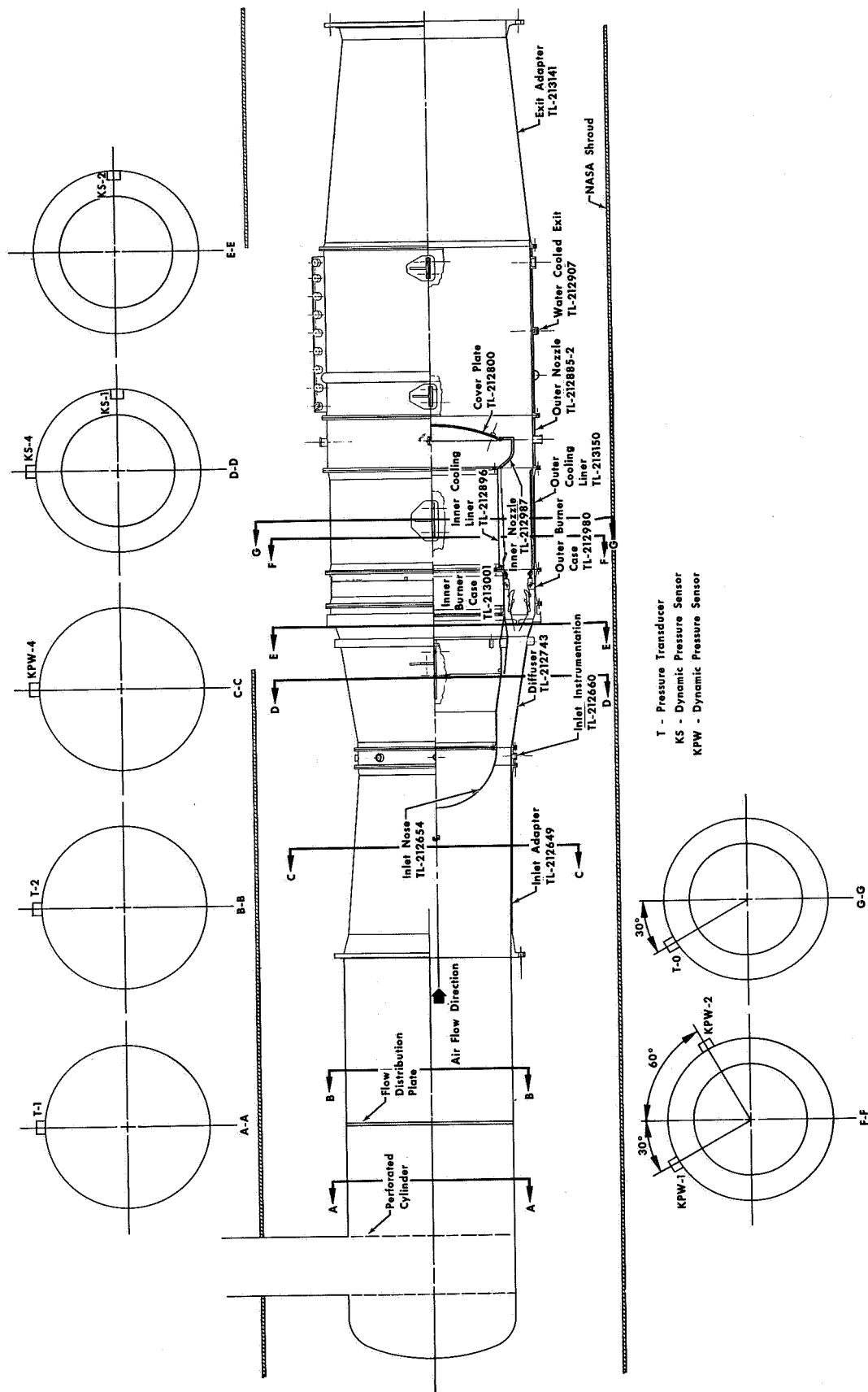


Figure VIII-9. Failure of Inlet Damping Devices FD 19148

Another attempt to improve the inlet flow conditions was made by increasing the inlet flow distribution plate open area to reduce the jet velocity. This modification produced a poor rig inlet velocity profile and did not affect combustor oscillations.

The rig was further instrumented as shown in figure VIII-10, and combustor pressure oscillations of the same amplitudes and frequencies as those measured in the inlet duct were measured in the centerbody.



VIII-10

FD 19179

Figure VIII-10. Instrumentation Location

It was still suspected that the pressure oscillations were associated with the diffuser air bleed and the centerbody. Consequently, radial fins were installed to suppress a transverse mode in the centerbody (figure VIII-11). Although the character of the pressure oscillations in the centerbody was substantially changed as a result of this modification there was no observable effect on combustion instability in the duct burner. The following values of pressure oscillations were recorded at a typical 30-psia test condition:

Location	Peak-to-Peak Amplitude, psi
Diffuser Bleed, ID Wall	3-4
Diffuser Bleed, OD Wall	7-10
Centerbody	2-3
Burner	5-6

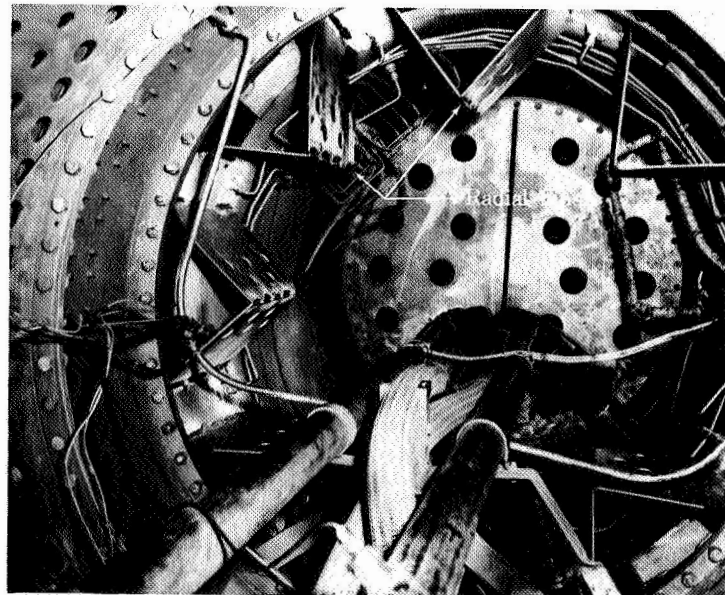


Figure VIII-11. Radial Fins in Centerbody

FD 22553

At this time the relative magnitudes of the oscillations indicated that the burner oscillation was the primary one. When oscillations occur in the burner, the velocity must also oscillate in the diffuser, and, since the velocity in the diffuser was higher than that in the burner, a given pressure fluctuation in the burner would cause a larger static pressure fluctuation in the diffuser. The velocity in the diffuser bleed was controlled by the centerbody pressure rather than by the burner

pressure and, since the centerbody oscillations were of low amplitudes, the bleed velocity and static pressure oscillations were also of low amplitudes.

It was alternatively considered that the critical phenomena could have occurred where the amplitudes were the highest (at the diffuser bleed) and that the diffuser bleed was probably the immediate cause of the oscillations. The diffuser bleed air discharge passage was therefore blocked off temporarily and a hole cut in the inlet centerbody nose to provide cooling air for the inner cooling liner. In an attempt to improve inlet flow conditions, the flow distribution plate was removed at the same time.

The rig inlet flow velocity profile was improved and the white noise pressure amplitudes dropped from 2 to 1 psia, with no predominant frequency recorded up to 1600 Hz. Mechanical vibrations of the rig were greatly reduced, as shown in figure VIII-12. However, combustion instability behavior was unaffected. Hence, neither noise nor the diffuser bleed appeared to be associated with the observed type of combustion instability. During the rest of the program no further changes were made to the inlet plenum. Also, the diffuser bleed was restored to the configuration shown in figures VIII-6 and VIII-7, and no further changes were made within the centerbody.

The ID and OD vortex generators were then removed. At the cruise airflows, combustion instability was completely absent. This allowed an overall fuel/air ratio of 0.049 to be tested at the simulated cruise-approach conditions (Test Points 141 through 148). A subsequent test at cruise fuel/air ratios (Test Points 90 through 99) after the inner cooling liner with acoustic damping was installed, showed the combustion efficiency to be lowered to an unacceptable level because of the removal of the vortex generators. Also, combustion instability was found to occur at both the 10- and 15-psia simulated transonic climb test conditions. These were the first tests made at transonic climb conditions. The results showed the amount of acoustic damping provided by the outer and inner cooling liner to be inadequate.

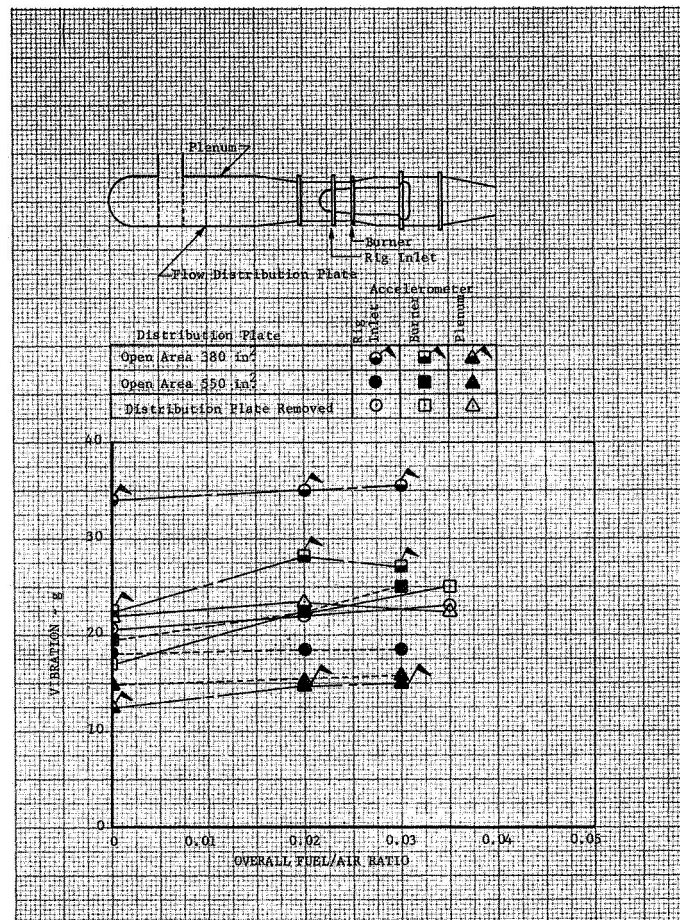
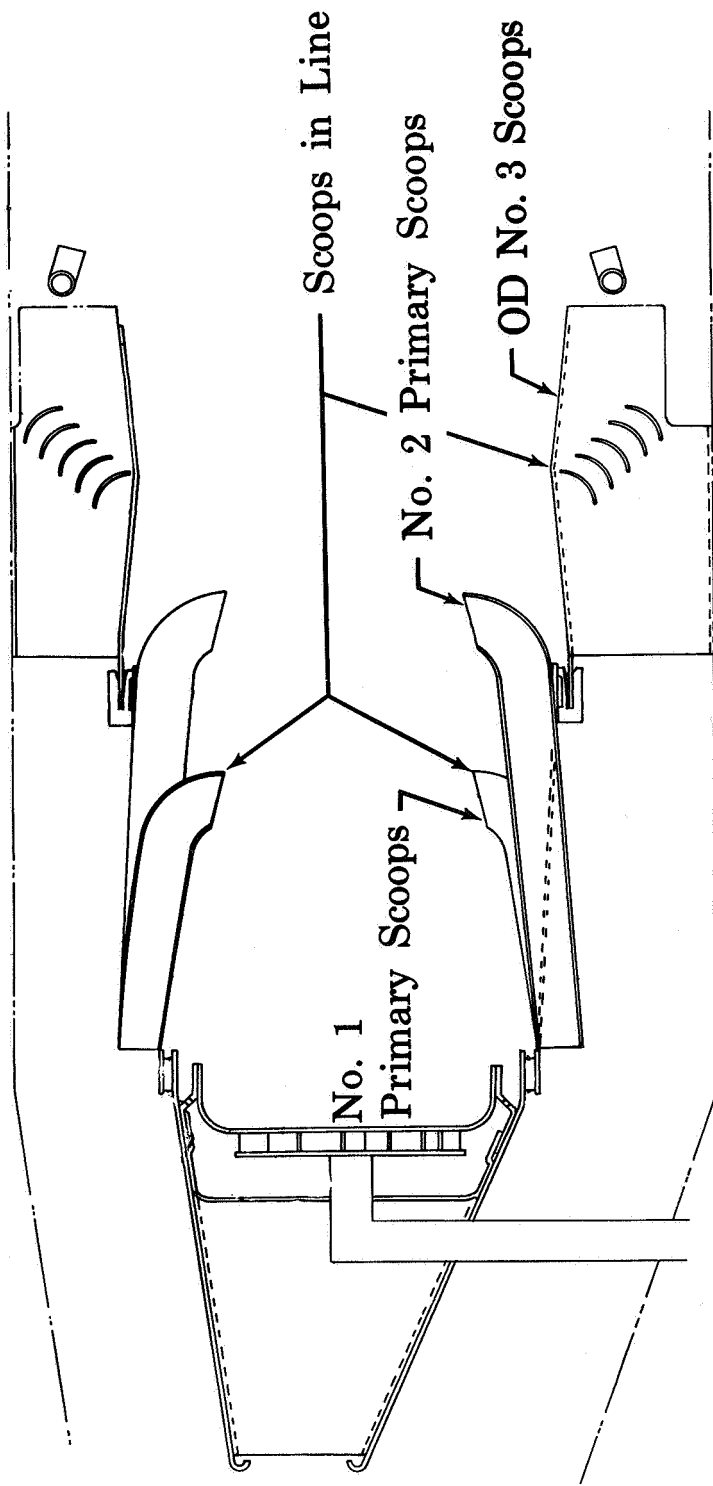


Figure VIII-12. Duct Burner Rig Mechanical
Vibration With Stable Burning

DF 53349

The outer secondary burner panel was then rotated so that the OD No. 3 scoops no longer opposed the ID No. 3 scoops, figure VIII-13, but this had no effect on combustion instability at the 10- and 15-psia simulated transonic climb conditions (Test Points 194 through 203).



FD 13591C

Figure VIII-13. Burner Schematic

Dynamic pressure instrumentation was installed on the Zone-1 secondary fuel manifold, encircling and mounted on the test rig at the top and bottom. This was installed to determine if the vibrations incurred by the rig were causing manifold pressure pulsations that would affect fuel flow at the fuel nozzles and cause combustion instability. Test data showed the fuel manifold to have maximum peak-to-peak pressure amplitudes of 4% of the mean manifold pressure at frequencies of 200, 600, and 800 Hz. This was considered to cause an insignificant change in fuel flow.

Combustion instability encountered at the simulated transonic climb conditions was of an entirely different nature than that previously encountered at the simulated cruise condition. While the cruise condition encountered a probable third transverse mode due to the Zone-2 combustion region, a 100 Hz longitudinal mode was encountered at the simulated transonic climb conditions, which was associated with the larger fuel/air ratios tested. A 160 to 180 Hz instability, apparently a combination of a first transverse mode and a longitudinal mode, was evident at the simulated transonic climb airflows and Zone-1 fuel injection.

It did not appear likely that the 100 Hz longitudinal mode was directly associated with the combustion process. It was theorized that the connection of a large facility volume to the rig with extremely low resistance in the connection resulted in longitudinal pressure oscillations involving the facility and the rig, which were of relatively low frequency and were poorly damped. These oscillations were then easily driven by the combustor. It was believed that this effect could be reduced by increasing the pressure drop at the facility/rig interface.

The first attempt to check this theory was made by installing blockage plates in the inner and outer annuli surrounding the duct burner, as shown in figure VIII-14. This attempt was ineffective, as the blockage plates upset the airflow distribution in the duct burner and the combustion characteristics were unsatisfactory.

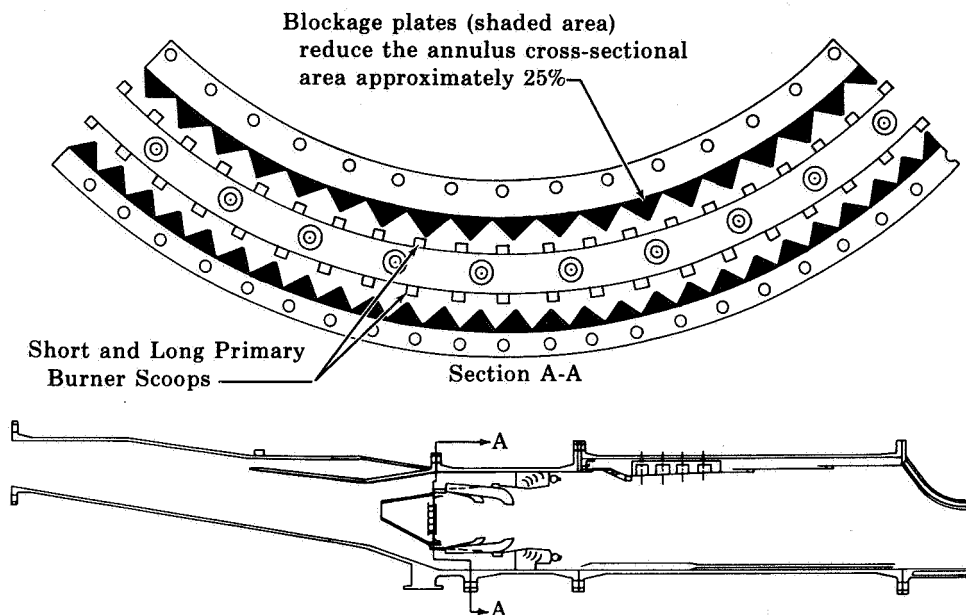


Figure VIII-14. Burner Annulus Blockage Plate Installation

FD 20593

Testing with only alternate Zone-1 fuel nozzles flowing did not eliminate combustion instability at the simulated transonic climb conditions, but it did increase the operating range over which the Zone-1 fuel/air ratio could be tested without combustion instability. This was significant since combustion instability had previously occurred with the Zone-1 fuel/air ratio lower than the desired design ratio (0.015 as opposed to 0.020) for maximum combustion efficiency. The 100 Hz longitudinal pressure oscillations were occasionally observed when augmenting with the Zone-2 nozzles while testing at simulated transonic climb conditions at high overall fuel/air ratios. Fuel/air ratios at the onset of combustion instability are shown in figure VIII-15. The data presented on the lower portion of the figure were obtained by setting the Zone-1 primary fuel flow and then increasing the Zone-1 secondary fuel flow. While the fuel/air ratio was being increased, the burner pressure was held constant by regulating the butterfly exhaust valve. The data shown on the upper portion of the figure were obtained in a similar manner, i.e., Zone-1 fuel flow was held constant and Zone-2 fuel flow was increased.

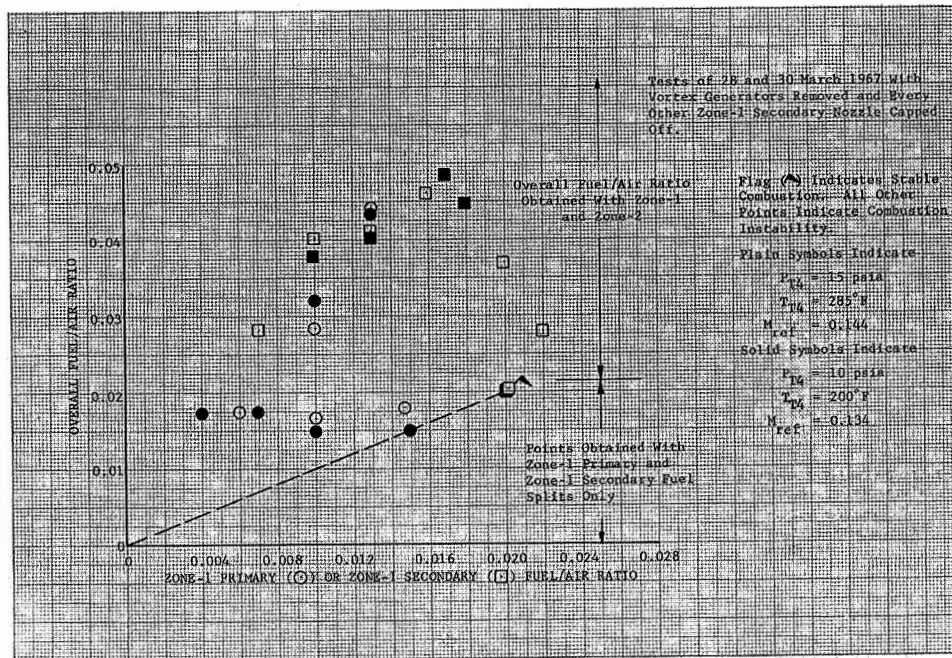


Figure VIII-15. Effect of Zone-1 Fuel Flow on Combustion Stability DF 58542

To study further the effect of facility/rig interface on combustion oscillation 36 radial blockage vanes were fabricated for installation in the diffuser (figure VIII-16). The vanes could be rotated 90 deg (in 10-deg increments) from their axial position to give various pressure drops through the diffuser. This was desirable since it allowed the additional flow resistance to be positioned close to the burner inlet. It was unrealistic in that it was not applicable to a flight engine because of the increased diffuser pressure loss. Diffuser pressure loss vs diffuser inlet Mach number is plotted for two vane angles of attack in figure VIII-17.

The diffuser vanes were initially installed with a 60-deg angle of attack (every other vane was turned in the opposing direction to prevent swirl in all vane tests). The diffuser vanes created an additional 9.1% drop in pressure, giving the diffuser a total pressure drop of 10.5% with an inlet Mach number of 0.4 (figure VIII-17). The installation of the diffuser vanes had no effect on the simulated transonic climb combustion

stability limit obtained with Zone-1 fuel flow only. However, there was a definite improvement when flowing only alternate Zone-1 nozzles, because the Zone-1 fuel/air ratio exceeded 0.016 and was further augmented by the Zone-2 fuel. An overall fuel/air ratio of 0.050 was thus obtained with the Zone-1 fuel/air ratio set between 0.017 and 0.022. Stable combustion with an overall fuel/air ratio of 0.050 at simulated transonic climb conditions was thus accomplished for the first time. As shown in figure VIII-18, the Zone-1 fuel/air ratio had to be greater than 0.017 if an overall fuel/air ratio of 0.050 was to be obtained with stable combustion. Testing with 20 Zone-1 nozzles did not reveal a Zone-1 maximum fuel/air ratio limit due to combustion instability. The stable points shown in figure VIII-18, at Zone-1 fuel/air ratios of 0.007 and 0.010 and overall fuel/air ratios of 0.054 and 0.051, respectively, did not necessarily define the stability limits. The stable combustion at these high overall fuel/air ratios at 10 psia may have been due to the Zone-1 pilot flame having a heat release insufficient to burn the augmented Zone-2 fuel efficiently. Operation at higher efficiencies might have been unstable.

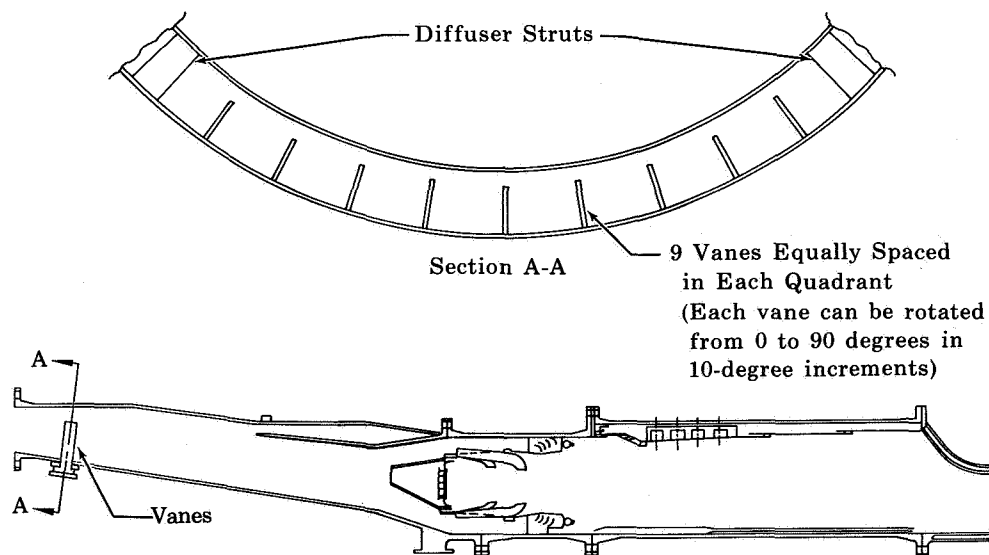


Figure VIII-16. Diffuser Radial Vane
Installation

FD 20597A

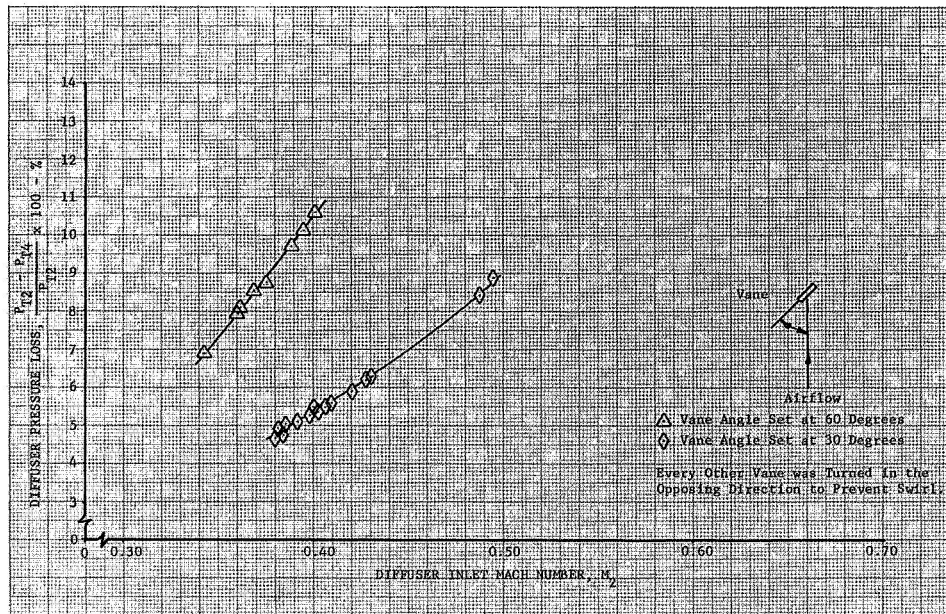


Figure VIII-17. Diffuser Pressure Loss
vs Diffuser Inlet Mach
Number

DF 56595

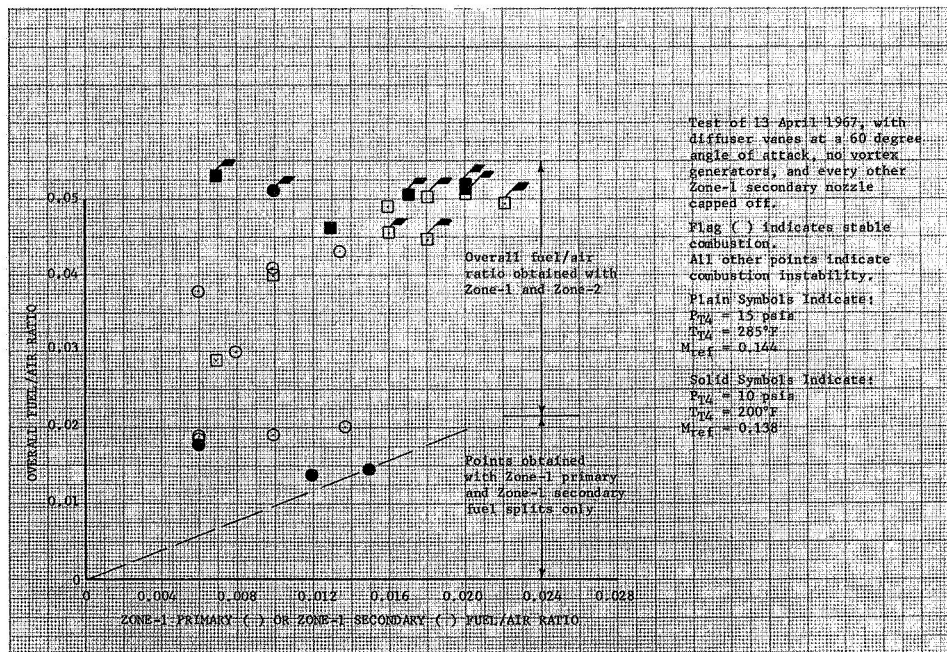


Figure VIII-18. Effect of 60-deg Diffuser
Vaness on Combustion Stability

DF 61933

At 10 psia there was an indication that operation with 20 Zone-1 fuel nozzles provided a broader region of stable combustion than did operation with 40 nozzles.

The diffuser vanes disturbed the flow through the diffuser since they did not extend across the complete diffuser annulus to the ID wall. With the vanes at a 60-degree angle of attack, the airflow was diverted toward the ID wall and apparently separated on the diffuser bleed lip. This resulted in an unacceptable burner inlet radial profile that had an erratic flow that peaked toward the ID wall.

The diffuser vanes were repositioned to a 30-deg angle of attack to determine if the radial flow distribution could be corrected while maintaining the improvement in the facility/rig interface attributed to the presence of the vanes.

The pressure drop created by the diffuser vanes was 4.0%, decreased from 9.1% in the previous test, resulting in a diffuser total pressure drop of 5.4% at an inlet Mach number of 0.4, (figure VIII-17). The radial flow distribution was improved but the stable combustion range was narrowed. The combustion stability limits are shown in figure VIII-19. At the 15-psia simulated transonic climb condition, the region of combustion stability was narrowed when compared to the previous test, as instability occurred when the Zone-1 fuel/air ratio was increased to 0.022. A more noticeable deterioration in the stable combustion range occurred at 10 psia, where a stable burning region with a fuel/air ratio of 0.05 was obtained only over a very narrow range of Zone-1 fuel/air ratio.

Since a significant facility/rig interface pressure drop was shown to be effective and the diffuser vanes were not completely satisfactory, a heavy inlet screen assembly was installed in front of the diffuser as shown in figure VIII-20. The diffuser vanes were left at a 30-deg angle of attack and the resulting total pressure drop across the screen was 4.2% at a diffuser inlet Mach number of 0.4. The inlet screen was completely ineffective with no apparent change of the combustion stability limits.

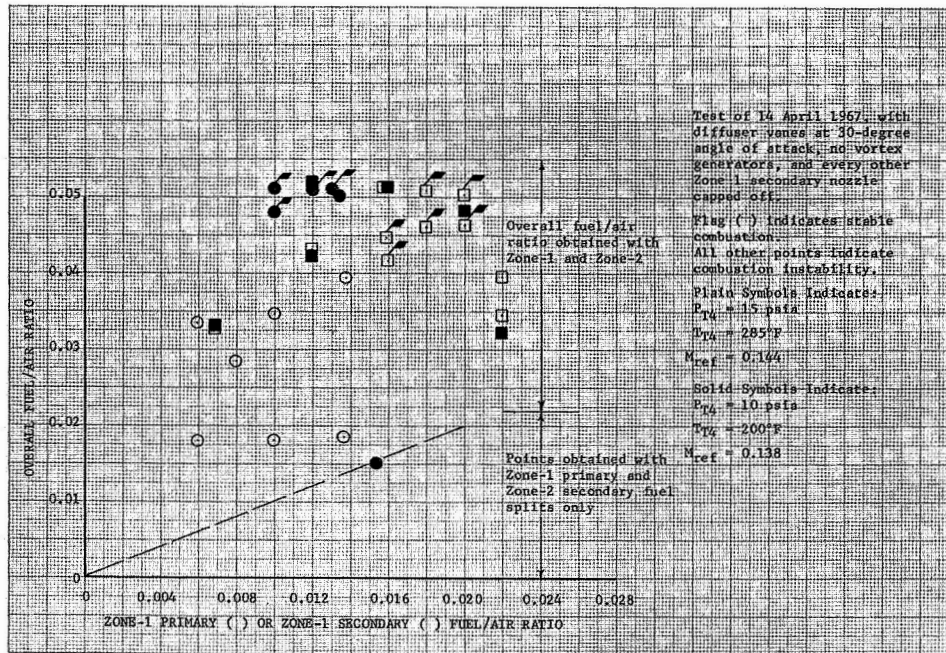


Figure VIII-19. Effect of 30-deg Diffuser Vanes on Combustion Stability DF 61932

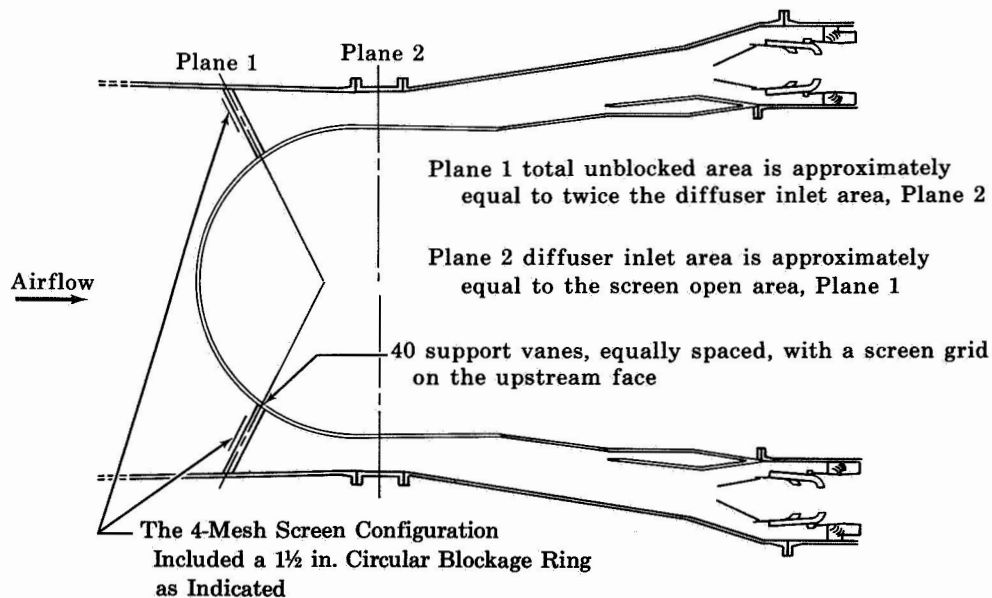


Figure VIII-20. Rig Inlet Screen Installation FD 20599A

This original 3-mesh inlet screen with 47% blockage area was replaced with a 4-mesh inlet screen with 60% blockage area. The 4-mesh inlet screen provided a significant increase in pressure drop (figure VIII-21) but had no significant effect on the combustion stability limit. The

simulated transonic climb conditions that resulted in combustion instability are shown plotted on figure VIII-22. During this test, the diffuser vanes were set at 30-degree angle of attack.

Testing was then conducted at the simulated transonic climb conditions using all 40 Zone-1 secondary fuel nozzles. The test results are shown plotted on figure VIII-23. The combustion stability region with 40 Zone-1 secondary nozzles was decreased, compared to that with 20 Zone-1 secondary nozzles. Stable combustion was not obtained at a Zone-1 fuel/air ratio greater than 0.018, compared to a previously obtained fuel/air ratio of 0.023 with 20 Zone-1 secondary nozzles.

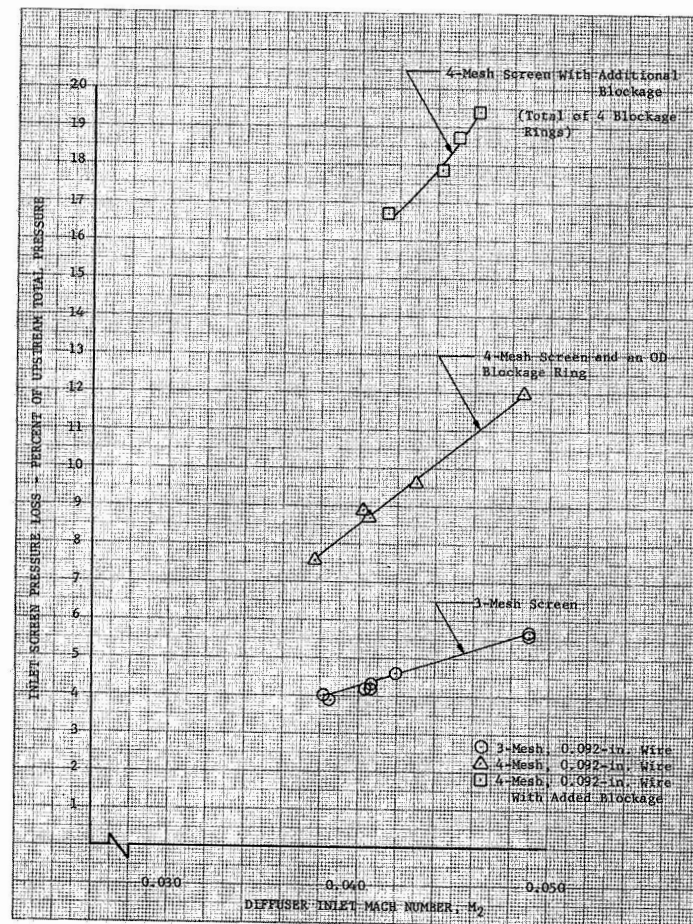


Figure VIII-21. Inlet Screen Pressure Loss
vs Diffuser Inlet Mach Number

DF 58543

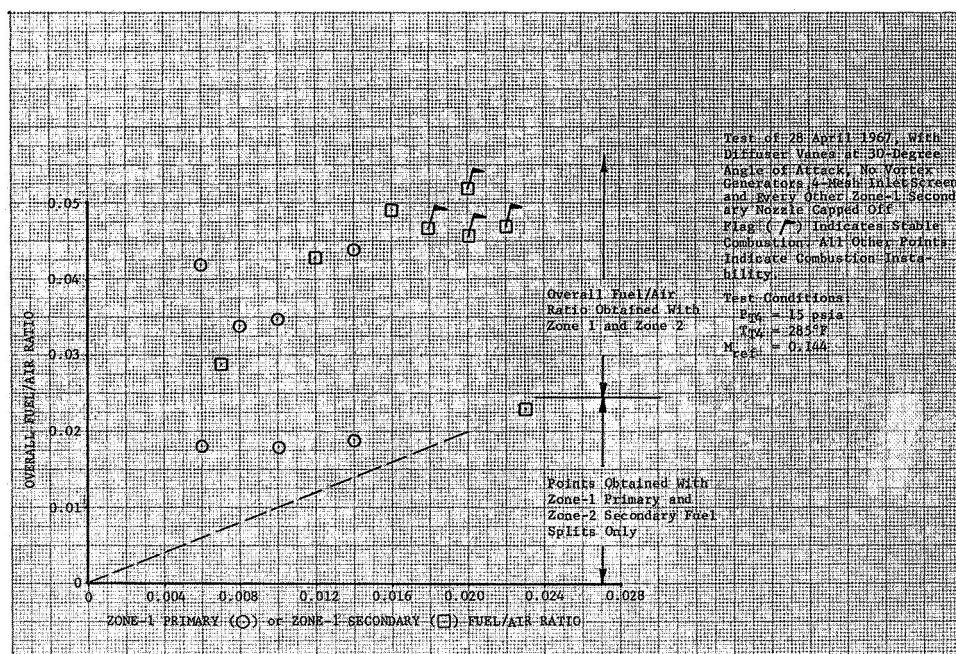


Figure VIII-22. Effect of Inlet Screen on Combustion Stability

DF 56594

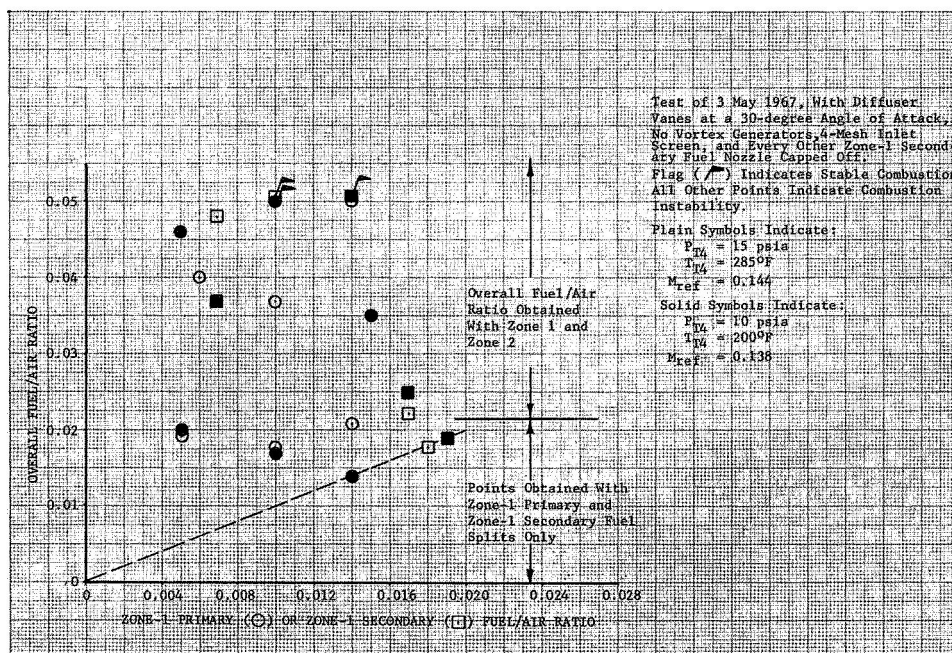


Figure VIII-23. Effect of Zone-1 Secondary Fuel Flow on Combustion Stability

DF 56596

New design turbulators (figure II-10) were then installed in the burner in the vortex generator locations. The results of a simulated transonic climb test, plotted on figure VIII-24, show that combustion instability occurred at slightly lower overall fuel/air ratios than without vortex generators. Data also showed that the combustion efficiency was increased with the turbulators installed.

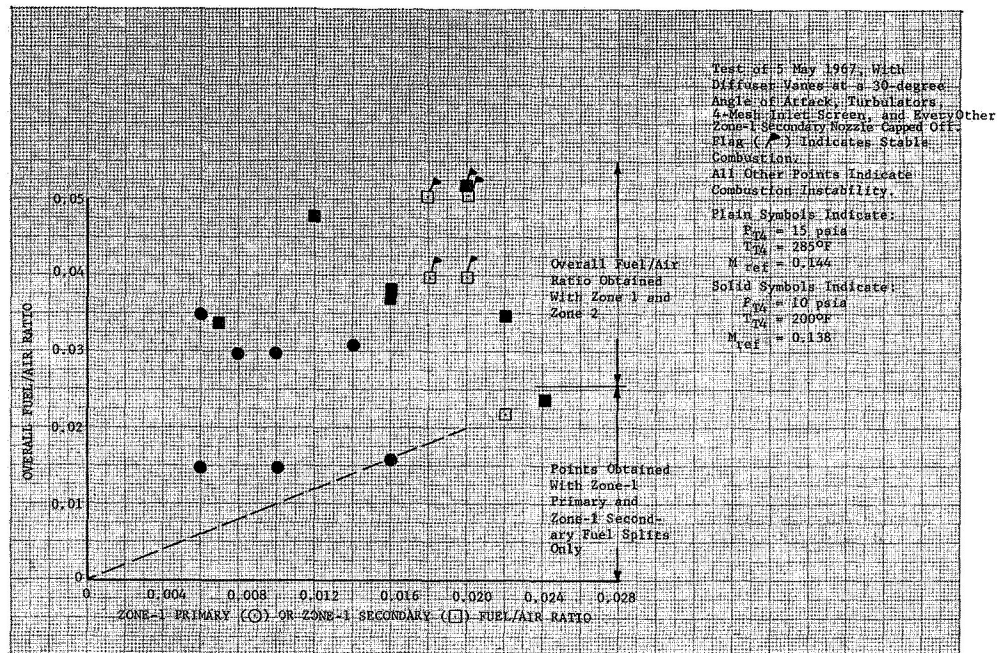


Figure VIII-24. Effect of Turbulators on Combustion Stability at Transonic Climb

DF 56597

The effect of the turbulators at simulated cruise conditions is shown in figure VIII-25. It was noted that combustion instability always occurred when the Zone-2 fuel/air ratio reached 0.015, indicating that the Zone-2 fuel injection and/or combustion zone affected the stability region. This was not the case at the 10- and 15-psia test conditions.

With every other turbulator removed, the combustion stability range at the simulated cruise conditions was slightly improved, showing that it was possible to obtain a stable overall fuel/air ratio of 0.05 by increasing the Zone-1 fuel/air ratio to 0.030, as shown in figure VIII-26.

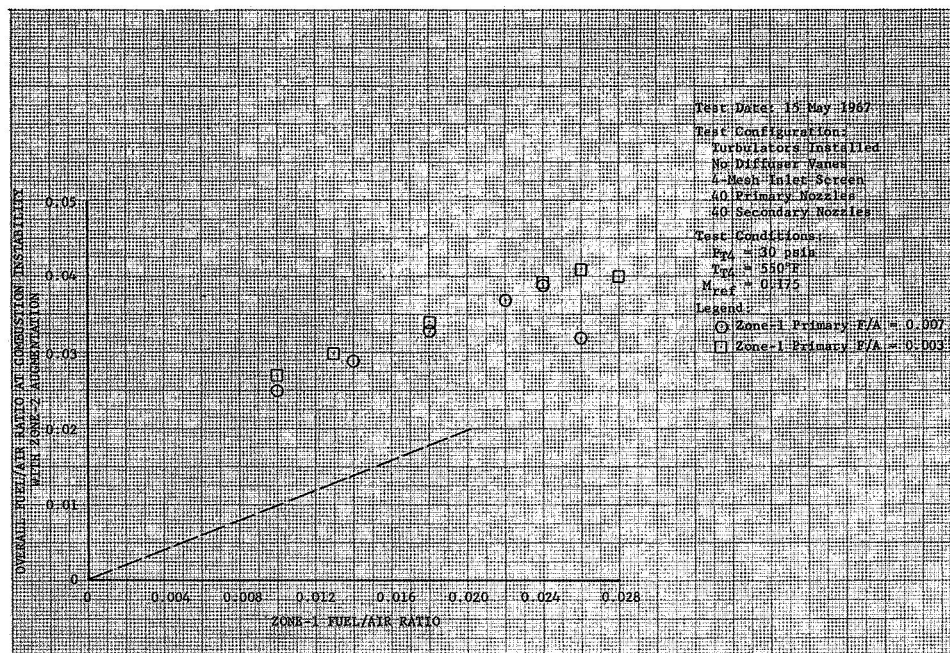


Figure VIII-25. Effect of Turbulators on
Combustion Stability at Cruise

DF 56599

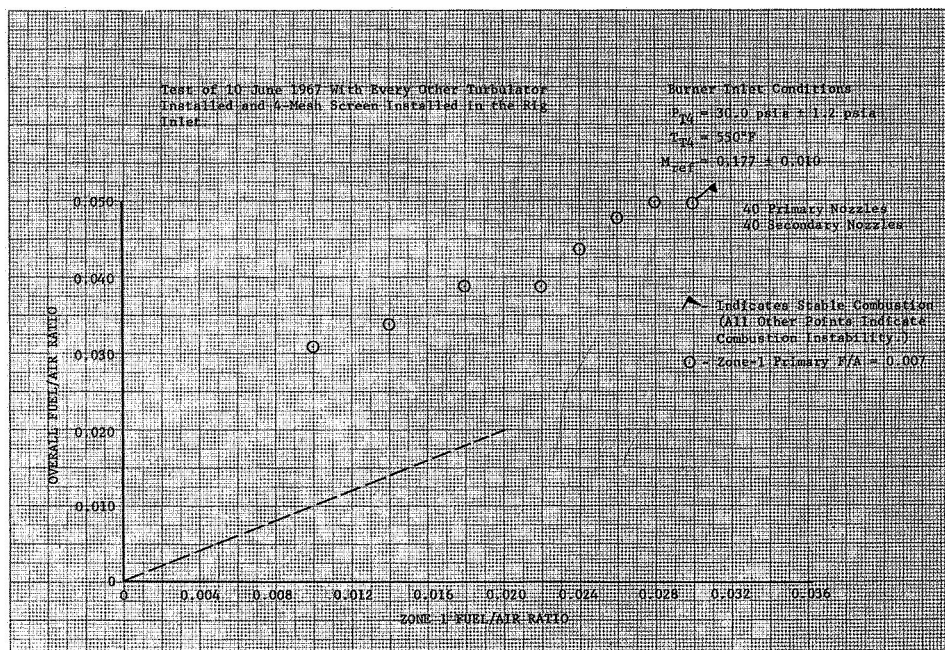


Figure VIII-26. Effect of Alternate Turbulators
on Combustion Stability

DF 58539

No appreciable effect was seen on the combustion stability range at simulated cruise-approach conditions when all the Zone-2 augmentation was performed by flowing Zone-2 fuel on the OD only. However, combustion efficiency dropped considerably (Test Point 493).

No effect was seen on the stable operating range at the simulated cruise condition when the Zone-2 OD fuel was injected in a circumferentially unbalanced manner (Test Points 504 through 518).

The inlet screen was further reduced in flow area by adding 3 blockage rings (figure VIII-27); the resulting total pressure loss is shown in figure VIII-21. Although the pressure loss was greater than that achieved with the diffuser vanes, a comparison of figure VIII-28 and previously presented data shows the fuel/air ratio range of stable combustion was much lower for this last configuration tested. At the simulated 15-psia transonic climb test condition, an overall fuel/air ratio of 0.05 was obtained at a Zone-1 fuel/air ratio of 0.02 by manipulating the fuel/air ratios in the manner shown in figure VIII-28. At the 15-psia test condition, the combustion instability was a sudden, violent type, not previously experienced.

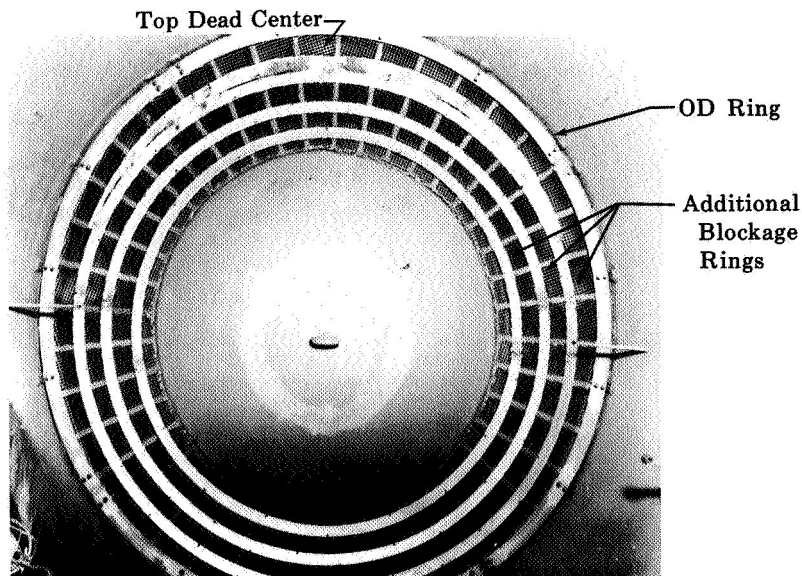


Figure VIII-27. Inlet Screen Modification

FD 23720

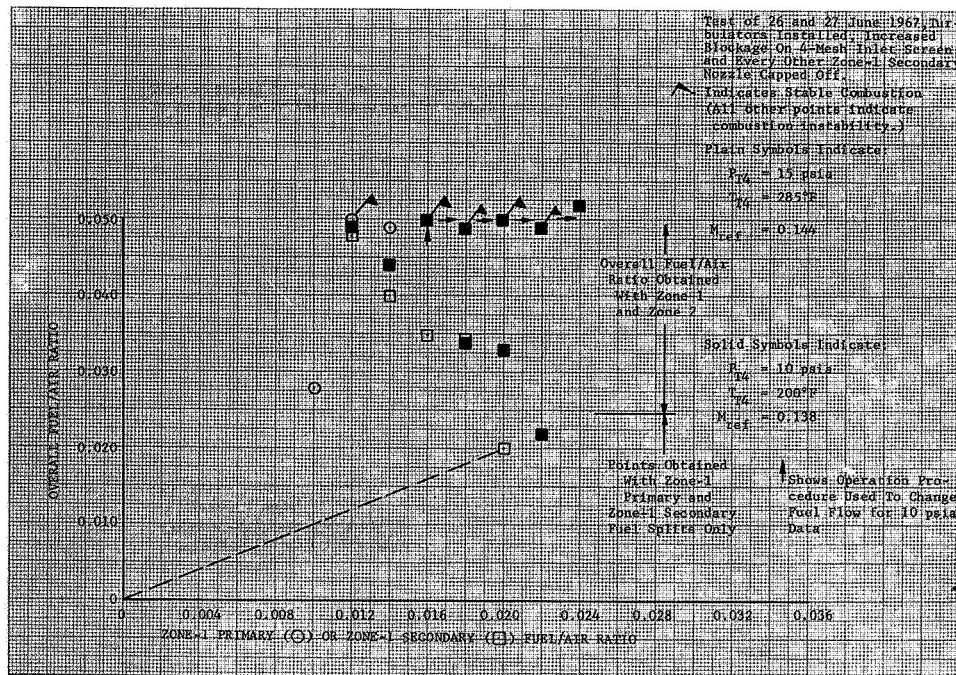


Figure VIII-28. Effect of Inlet Screen Blockage on Combustion Stability DF 58540

There were therefore considerable data to show that the combustion instability was not completely and independently involved with the duct burner. The results of the tests with increased pressure drops upstream of the duct burner showed that there is an effect due to the facility/rig interface with Zone-2 fuel present at the transonic climb airflows.

The following duct burner modifications were considered during the program for improving stability, and hardware was procured in each case, but none of the schemes were tested:

1. Removal of the Secondary Burner Liner - Supports for the rear of the primary burner section were fabricated (figure VIII-29). These were required if the secondary liner was removed, as the secondary liner supported the rear of the primary liner. The third burner scoop, located in the secondary liner position, was similar to the vortex generators. Removal of the vortex generators had eliminated the 300 Hz pressure oscillations and it was considered that elimination of the No. 3 scoop might also be effective. A separate increased-area third scoop was fabricated that could be installed, left out, or modified as required.
2. Diffuser Axial Vanes - Seven axial vanes were fabricated (figure VIII-30). These vanes were intended to provide damping of transverse pressure oscillations in the diffuser.

3. Burner Secondary Panel Scoop Extensions - Scoop extensions of 1-inch height were fabricated to install on the third scoops (figure VIII-31). Segment rig tests had shown that this extension improved flame stability at low pressures and might reduce burner instability driving force.

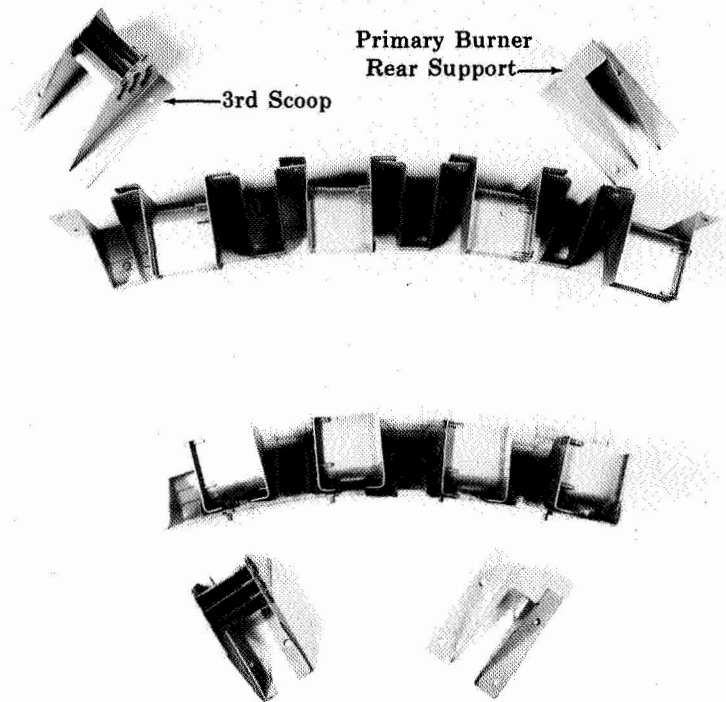


Figure VIII-29. Secondary Panel Replacement

FD 20603

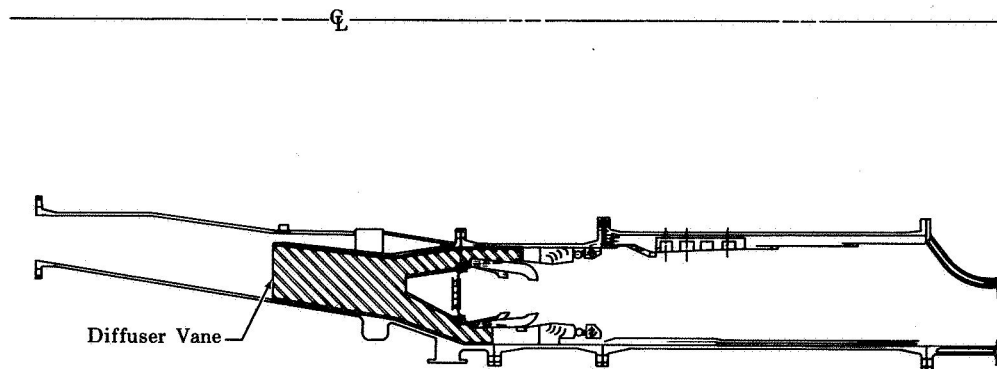


Figure VIII-30. Diffuser Axial Vanes

FD 20560



Figure VIII-31. Secondary Panel Scoop
Extension

FE 68722

SECTION IX
CONCLUSIONS

1. The ram-induction duct burner demonstrated good combustion efficiency while meeting the required isothermal total pressure loss of 5% at a reference Mach number of 0.150.

Test Condition	Fuel/Air Ratio	Combustion Efficiency Goal, %	Combustion Efficiency Burner with Turbulators, %	Highest Combustion Efficiency Obtained, %
30-psia Cruise	0.02	95	93	93
30-psia Cruise-Approach	0.05	95	91	95
15-psia Transonic Climb	0.05	95	95	95
10-psia Transonic Climb	0.05	95	91	91

The occurrence of combustion instability limited the operating range of the duct burner but it was possible to test at all of the required conditions with one configuration. The combustion efficiencies demonstrated by the duct burner with the turbulators at all test conditions is shown above. The highest combustion efficiency obtained at each test condition, regardless of the burner configuration, is also shown.

2. The burner demonstrated excellent ignition characteristics, igniting at fuel/air ratios as low as 0.0004 with no detectable burner exit total pressure change. No blowouts occurred during stable combustion.

3. The second duct burner was tested for 81.2 hours. This included subjecting the burner to severe conditions while operating with combustion instability 216 times for an accumulated time of approximately 20 minutes during the program. The ram-induction duct burner was in excellent structural condition as the program ended, demonstrating the durability level to be quite high.

4. Combustion instability occurred with both transverse and longitudinal modes. The transverse mode was generally associated with the Zone-2 combustion region and could be altered by modifying that region of the burner. The longitudinal mode generally occurred with 100 Hz and was thought to be associated with the rig and facility. This mode of instability could be altered by changing the pressure drop at the facility/rig interface. It was possible to operate without instability at all required test conditions with particular combinations of configuration and operating procedure.

APPENDIX A
ADDITIONAL CALCULATIONS
FOR OUTER COOLING LINER

1. DERIVATION OF GAS SIDE HEAT TRANSFER COEFFICIENT

The Colburn Analogy, Reference 4, was the starting point in establishing the gas-side heat transfer coefficient. Thus,

$$\left(\frac{Nu_x}{Re_x Pr} \right)_f P_{rf}^{2/3} = \frac{C_{fx}}{2} \quad (A-1)$$

where,

$$Nu_x = \frac{h_g X}{k_f}, \quad Re_x = \frac{\rho_f V X}{\mu_f} \quad (A-2)$$

It was assumed that a turbulent boundary over a flat plate, with zero pressure gradient, existed on the liner wall panel. It was also assumed that the boundary layer has no laminar starting length due to the very turbulent mainstream conditions induced by the burner, vortex generators and spraybar. For Re_x between 5×10^5 to 10^7

$$C_f = \frac{0.0576}{(Re_x)^{0.2}} \quad (A-3)$$

Substituting equations (A-3) and (A-2) into (A-1) and solving for h_g :

$$h_g = 0.0288 \frac{k_f}{X} \left(\frac{\rho_f V X}{\mu_f} \right)^{0.8} (Pr_f)^{1/3} \quad (A-4)$$

but

$$V = \left(\frac{W_g}{A_g} \right) \frac{1}{\rho}$$

If the velocity were evaluated at the overall average gas stream temperature, the velocity in the scrubbing gas region would have been excessively high because of the large temperature difference between the gas stream and the scrubbing gas. Because the scrubbing gas was in immediate contact with the liner wall, the scrubbing gas temperature was used to evaluate the velocity. Substituting the velocity relationship into equation (A-4) gave

$$h_g = 0.0288 \frac{k_f}{X} \left(\frac{W_g}{A_g} \frac{X}{\mu_f} \frac{\rho_f}{\rho_{gs}} \right)^{0.8} (P_{rf})^{1/3}$$

Letting

$$f(T_{gf}) = \left[\frac{k (P_r)^{1/3}}{(\mu)^{0.8}} \right]_{T = T_{gf}}$$

$$\frac{\rho_f}{\rho_{gs}} = \frac{T_{gs}}{T_f}$$

$$X = x - \ell \quad (\text{references distance to Zone 1 fuel nozzle})$$

The final resulting equation for h_g was,

$$h_g = 0.0288 \left(\frac{W_g}{A_g} \frac{T_{gs}}{T_{gf}} \right)^{0.8} \frac{f(T_{gf})}{(x - \ell)^{0.2}} \quad (A-5)$$

Using assumption (2) for the gas and noting that properties at atmospheric pressure could be used because of the low system pressure, figure A-1 was used to evaluate $f(T_{gf})$.

DF 40496

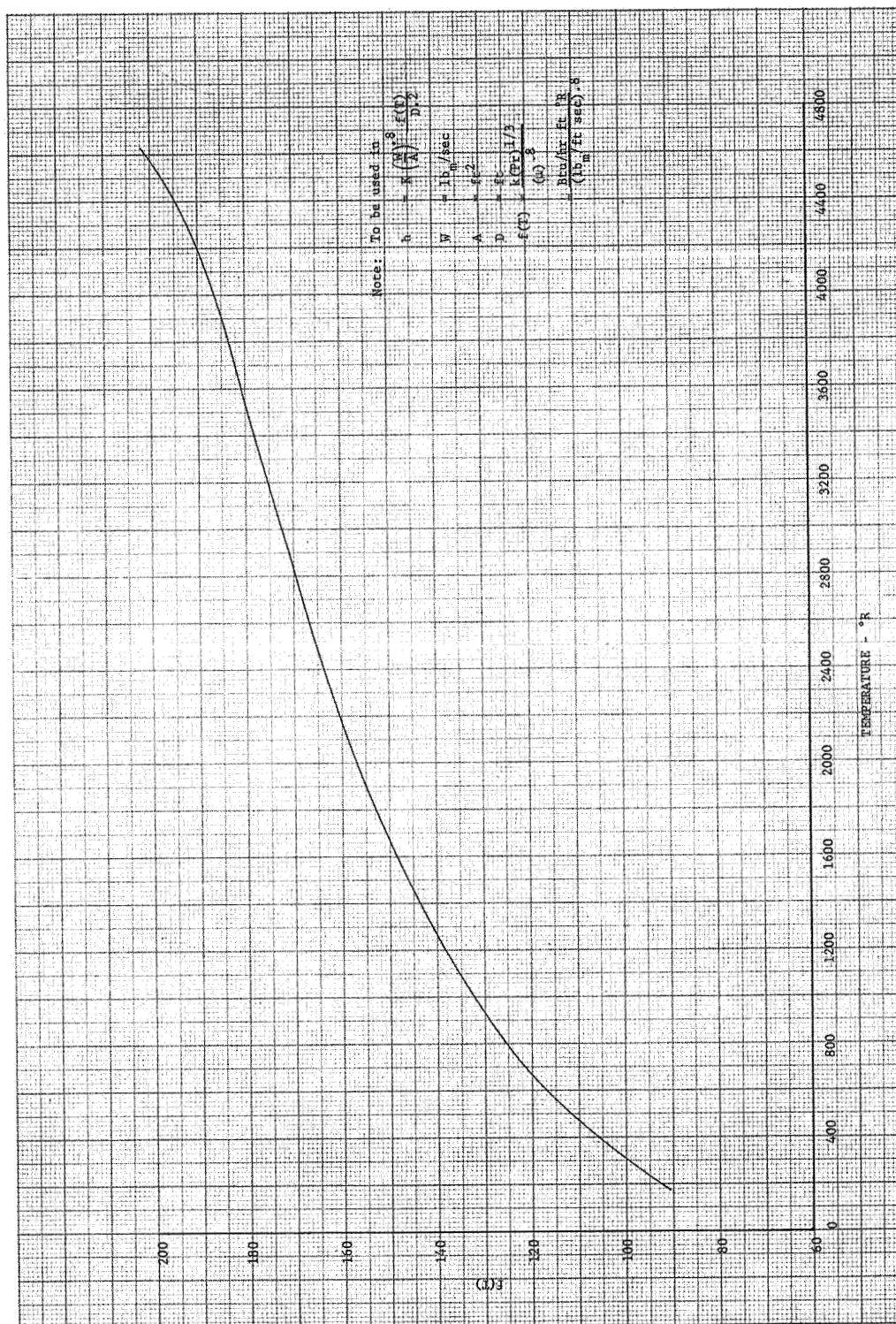


Figure A-1. Property Parameter for Air

2. DUCT BURNER GEOMETRIC RELATIONSHIPS

The duct burner cooling liner geometric relationships were derived on the basis of one convolution. As illustrated in figure A-2, the fasteners and the filler strip are not shown but were considered as an area blockage. The cross-sectional area per convolution was

$$\frac{A_c}{N} = A_\delta + A_\Delta + A_D - (\ell_p + 2\delta) t_p - A_{BLK} \quad (A-6)$$

Area of Segment A_D :

$$\begin{aligned} A_D &= \pi R_p^2 \left(\frac{\theta}{2\pi} \right) - 2 \left[\frac{1}{2} R_p \sin \frac{\theta}{2} R_p \cos \frac{\theta}{2} \right] \\ &= R_p^2 \left(\frac{\theta}{2} - \sin \frac{\theta}{2} \cos \frac{\theta}{2} \right) \end{aligned} \quad (A-7)$$

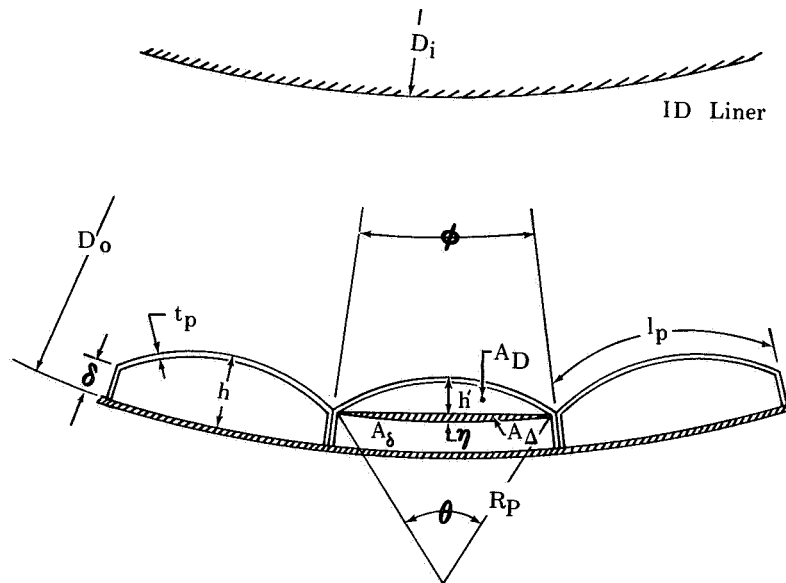
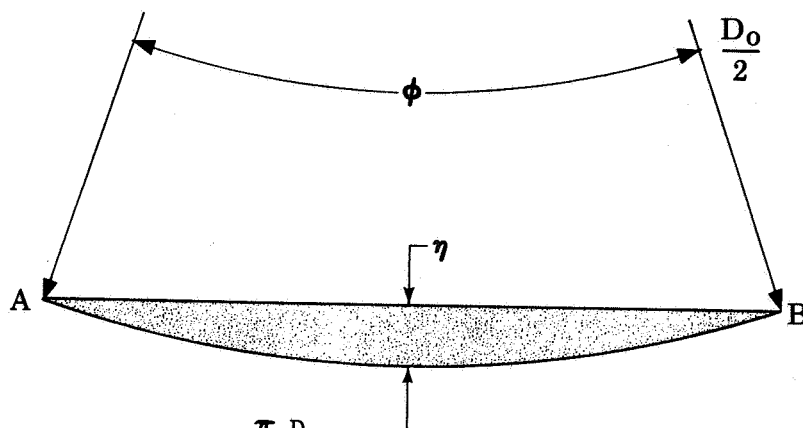


Figure A-2. Symbols Used in Deriving Geometric Equations

Substituting the trigonometric identity below into equation (A-7).

$$\sin \frac{\theta}{2} \cos \frac{\theta}{2} = \frac{1}{2} \sin \theta$$

$$A_D = \frac{R_p^2}{2} (\theta - \sin \theta) \quad (A-8)$$

Area of Segment A_{Δ} :

$$\text{Arc AB} = \widehat{AB} = \frac{\pi D_o}{N} \quad (\text{A-9})$$

$$\phi = \frac{360}{N} \quad (\text{A-10})$$

$$\text{Line AB} = \overline{AB} = D_o \sin \frac{180}{N} \quad (\text{A-11})$$

$$\begin{aligned} A_{\Delta} &= \pi \left(\frac{D_o}{2} \right)^2 \frac{\phi}{2\pi} - 2 \left[\frac{1}{2} \frac{D_o}{2} \sin \frac{\phi}{2} \frac{D_o}{2} \cos \frac{\phi}{2} \right] \\ &= \frac{D_o^2}{4} \left[\frac{\pi}{N} - \frac{1}{2} \sin \frac{360}{N} \right] \end{aligned} \quad (\text{A-12})$$

Length η :

$$\eta = \frac{D_o}{2} \left(1 - \cos \frac{\phi}{2} \right) = \frac{D_o}{2} \left(1 - \cos \frac{180}{N} \right) \quad (\text{A-13})$$

Area of Annular Element A_{δ} :

$$A_{\delta} = \frac{\pi}{4} \left[D_o^2 - (D_o - 2\delta)^2 \right] \frac{1}{N} \quad (\text{A-14})$$

$$l_p = R_p \theta \quad (\text{A-15})$$

Substituting (A-15), (A-14), (A-12), and (A-8) into (A-6) and solving for A_c .

$$\begin{aligned} A_c &= \frac{\pi}{4} \left[D_o^2 - (D_o - 2\delta)^2 \right] + \frac{D_o^2}{4} \left[\pi - \frac{N}{2} \sin \frac{360}{N} \right] \\ &\quad + \frac{R_p^2 N}{2} (\theta - \sin \theta) - N (R_p \theta + 2\delta) t_p - A_{\text{BLK}}(N) \end{aligned} \quad (\text{A-16})$$

In examining equation (A-16), it became apparent that R_p and θ must be defined in terms of the known quantities D_o , N , and h . From figure A-2,

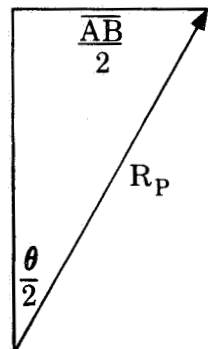
$$\begin{aligned} h' &= h - \eta - \delta \\ &= h - \frac{D_o}{2} \left[1 - \cos \frac{180}{N} \right] - \delta \end{aligned} \quad (A-17)$$

$$\begin{aligned} R_p &= R_p \cos \frac{\theta}{2} + h' \\ R_p &= \frac{h'}{1 - \cos \frac{\theta}{2}} \end{aligned} \quad (A-18)$$

Substituting equation (A-17) into (A-18) yielded,

$$R_p = \frac{h - \frac{D_o}{2} \left(1 - \cos \frac{180}{N} \right) - \delta}{1 - \cos \frac{\theta}{2}} \quad (A-19)$$

A relationship for θ was obtained with the aid of the sketch below.



$$\sin \frac{\theta}{2} = \frac{\overline{AB}}{2 R_p} \quad (A-20)$$

Substituting (A-11) and (A-19) into (A-20)

$$\begin{aligned} \sin \frac{\theta}{2} &= \frac{D_o \sin \frac{180}{N} \left(1 - \cos \frac{\theta}{2} \right)}{2 \left[h - \frac{D_o}{2} \left(1 - \cos \frac{180}{N} \right) - \delta \right]} \\ \frac{\sin \frac{\theta}{2}}{1 - \cos \frac{\theta}{2}} &= \frac{D_o \sin \frac{180}{N}}{2 \left[h - \frac{D_o}{2} \left(1 - \cos \frac{180}{N} \right) - \delta \right]} \end{aligned} \quad (A-21)$$

Using the following trigonometric identity,

$$\tan \frac{A}{2} = \frac{1 - \cos A}{\sin A}$$

in equation (A-21) and solving for θ .

$$\theta = 4 \arctan \left[\frac{h - \frac{D_o}{2} \left(1 - \cos \frac{180}{N}\right) - \delta}{\frac{D_o}{2} \sin \frac{180}{N}} \right] \quad (A-22)$$

The hydraulic diameter was calculated from the usual equation,

$$D_{HC} = \frac{4 A_c}{(WP)_c} \quad (A-23)$$

where the term $(WP)_c$ was calculated independently.

The following is a summary of the pertinent geometric equations.
The known values were N , D_o , and h .

$$\theta = 4 \arctan \left[\frac{h - \frac{D_o}{2} \left(1 - \cos \frac{180}{N}\right) - \delta}{\frac{D_o}{2} \sin \frac{180}{N}} \right] \quad (A-22)$$

$$R_p = \frac{h - \frac{D_o}{2} \left(1 - \cos \frac{180}{N}\right) - \delta}{1 - \cos \frac{\theta}{2}} \quad (A-19)$$

$$A_c = \frac{\pi}{4} \left[D_o^2 - (D_o - 2\delta)^2 \right] + \frac{D_o^2}{4} \left[\pi - \frac{N}{2} \sin \frac{360}{N} \right] \\ + \frac{R_p^2 N}{2} (\theta - \sin \theta) - N (R_p \theta + 2\delta) t_p - A_{BLK} (N) \quad (A-16)$$

$$D_{HC} = \frac{4 A_c}{(WP)_c} \quad (A-23)$$

$$l_p = R_p \theta \quad (A-15)$$

$$A_g = \frac{\pi}{4} (D_o^2 - D_i^2) - A_c \quad (A-24)$$

3. PRESSURE DROP

From the differential momentum equation, an expression for pressure drop along the length of a flow passage, using average cross section area (A_c), was derived using figure A-3.

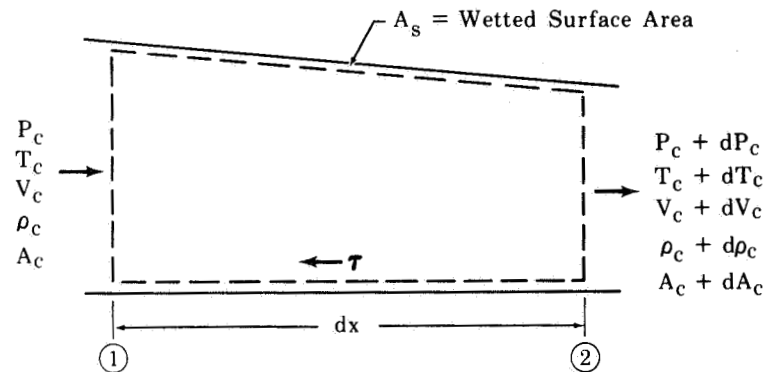


Figure A-3. Control Volume Within a Duct

FD 13554A

ΣF_x = Net change in momentum from section 1
to section 2

$$- A_c \frac{d p_c}{dx} - \tau_w \frac{d A_s}{dx} = \frac{W_c}{g_c} \frac{d V_c}{dx} \quad (A-25)$$

but

$$\tau_w = f_m \frac{\rho_{cm} V_m^2}{2 g_c}$$

where m = mean between sections 1 and 2.

$$\frac{d A_s}{dx} = \frac{4 A_c}{(D_{HC})}$$

where D_{HC} = Hydraulic diameter.

Substituting into equation (A-25) and simplifying, the following equation was obtained.

$$\frac{d p_c}{dx} = - \frac{4 f_m}{(D_{HC})_m} \frac{\rho_{c_m} V_m^2}{2 g_c} - \frac{W_c}{A_c g_c} \frac{dV_c}{dx} \quad (A-26)$$

but $\frac{W_c}{A_c} = G_c$

Therefore,

$$\frac{d p_c}{dx} = - \frac{4 f_m}{(D_{HC})_m} \frac{\rho_{c_m} V_m^2}{2 g_c} - \frac{G_c}{g_c} \frac{dV_c}{dx} \quad (A-27)$$

Writing equation (A-27) in finite difference form and letting $(VH) = \rho_c V^2 / 2 g_c$,

$$\frac{d p_c}{dx} = - \left(\frac{4 f_m}{(D_{HC})_m} \right) (VH)_m - \frac{G_c}{g_c} \left(\frac{V_2 - V_1}{\Delta x} \right) \quad (A-28)$$

The bulk pressure at the next station (3) at an incremental distance x is,

$$p_{c,2} = p_{c,1} + \left(\frac{d p_c}{dx} \right) \Delta x \quad (A-29)$$

The following equation for the friction factor was obtained in Reference 3.

$$f_i = 0.0014 + (0.125) (Re_c)^{-0.32} \quad (A-30)$$

$$f = f_i \left(\frac{\mu_w}{\mu} \right)^{10 f_i} \sqrt{\frac{T}{T_w}} \quad (A-31)$$

$$Re_c = \frac{D_{HC} W_c}{\mu_c A_c} \quad (A-32)$$

$$f_m = \frac{1}{2} (f_1 + f_2) \quad (A-33)$$

$$V = \frac{W_c}{\rho_c A_c} \quad (A-34)$$

$$(VH)_m = \frac{1}{2} \left[(VH)_1 + (VH)_2 \right] \quad (A-35)$$

NOMENCLATURE

Symbol	Description	Units
A	Area	in.
A _{BLK}	Blocked area	in. ²
C _f	Friction coefficient	
D _{HC}	Hydraulic diameter	in.
D _i	Inside diameter of duct burner	in.
D _o	Outside diameter of duct burner	in.
f	Friction factor	
f _i	Isothermal friction factor	
g _c	Gravitational constant	32.2 lb _m ft/lb _f sec ²
G	Mass velocity	$\left[\frac{\text{lb}_m}{\text{in.}^2 \text{ sec}} \right]$
h	Heat transfer coefficient	$\left[\frac{\text{Btu/hr ft}^2 \text{ }^\circ\text{R}}{\text{in.}} \right]$
h	Convolution height of liner	in.
k	Thermal conductivity	Btu/hr ft [°] R
ℓ	Distance from liner to Zone 1 fuel nozzle	in.
N	Number of convolutions	
Nu	Nusselt Number	
p	Static pressure,	psia
P _r	Prandtl number	$\frac{C_p \mu}{k}$
Re	Reynolds Number	$\frac{\rho V x}{\mu}$
T	Temperature	[°] R
t _p	Metal thickness	in.
V	Velocity	ft/sec
W	Flowrate	lb _m /sec
WP	Wetted perimeter	in.
x	Variable distance along liner	in.
X	Variable distance difference	in.
δ	Sidewall height of liner	in.
ρ	Density	lb/ft ³
μ	Viscosity	lb/ft-sec
τ	Fluid shear stress	lb/in. ²

Symbol	Description	Units
--------	-------------	-------

Subscripts

c	Coolant
f	Film
g	Gas
gf	Gas-side film
gs	Scrubbing gas
m	Mean
s	Slot
w	Wall
x	Distance in x direction along liner
1	Station number
2	Station number

APPENDIX B DAMPING LINER DESIGN AND BENCH TESTS

1. IDEAL HELMHOLTZ ACOUSTIC RESONATOR THEORY

a. General

A damping liner is in principle an ideal Helmholtz acoustic resonator and its theory of operation can be formulated based on the same mathematical model as presented in Reference 5*. The model used for a Helmholtz acoustic resonator is a simple spring-mass system with one degree of freedom (figure B-1).

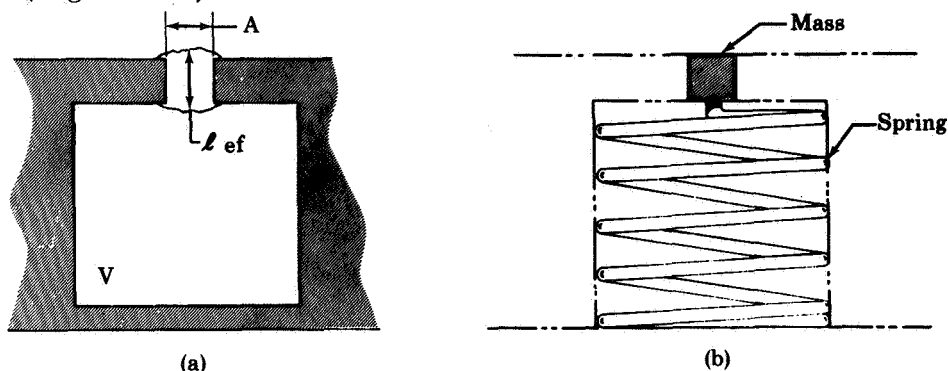


Figure B-1. Helmholtz Resonator and Analogous Mechanical System

FD 8464A

The mass of gas in the neck of the resonator is assumed to remain constant. The kinetic energy of the system is assumed to be centered in this mass. The oscillatory motion of the mass acts as a piston, alternately compressing and rarefying the gas in the resonator volume. The volume is thus forced to act as a spring on which the mass is supported, hence the spring-mass analogy.

The mass is equal to $A\rho l_{eff}$, where A is the area of the neck, ρ is the density of the resonator gas, and l_{eff} is the effective length of the mass**. Using Newton's second law of motion:

$$\sum F_x = \frac{d(mv)_x}{dt}$$

*References are given in Appendix C.

**A list of symbols is presented in table B-1.

Since m is assumed constant,

$$\sum F_x = m \frac{d^2 x}{dt^2} = A \rho l_{\text{eff}} \frac{d^2 x}{dt^2}$$

where x is the coordinate of mass motion.

The resultant external force on the mass, $\sum F_x$, is made up of three components: the external pressure force, the frictional or damping force, and restoring or spring force.

External Pressure Force: If the equilibrium static pressure inside the resonator is assumed equal to the external equilibrium static pressure, the unbalanced external pressure force can be written $PA \sin \omega t$.

Damping Force: If the damping force is considered to be directly proportional to the velocity, the force may be expressed as

$$F_D = RA \frac{dx}{dt}$$

R , the damping constant, is composed of two parts: friction and turbulence losses, R_d ; reradiation of sound losses from the resonator neck, R_r . Therefore

$$R = R_r + R_d$$

If the mass in the neck of the resonator is considered as a piston which generates sound waves, the integrated momentum equation (see Reference 6) over a wave generated will yield

$$R_r = \frac{\rho c}{g_c}$$

Restoring Force: If it is assumed that the movement of the mass of air in the neck causes an instantaneous uniform pressure change in the body of the resonator, the restoring or spring force may be written

$$F_s = A \frac{dp}{dx} x$$

During compression of the volume in the body of the resonator, the change in volume may be expressed as $-dV = A dx$; and,

$$F_s = -A^2 \frac{dp}{dV} x$$

For adiabatic compression:

$$\frac{dp}{dV} = -\frac{\gamma p}{V}$$

Also: $c = \sqrt{g_c \gamma p / \rho}$ or $p = c^2 \rho / \gamma g_c$

Substituting: $F_s = \rho c^2 A^2 x / V g_c$

The term $\rho c^2 A^2 / V g_c$ becomes the equivalent of the mechanical spring constant, K.

Substituting the forces back into Newton's second law of motion yields the differential equation:

$$\frac{\rho \ell_{\text{eff}} A}{g_c} \frac{d^2 x}{dt^2} + \frac{RA}{g_c} \frac{dx}{dt} + \frac{\rho c^2 A^2}{V g_c} x = PA \sin \omega t$$

The solution of this equation yields several useful relationships.

The damped frequency is found to be:

$$\omega_d = \sqrt{\frac{c^2 A}{V \ell_{\text{eff}}}} - \left(\frac{R}{2 \rho \ell_{\text{eff}}} \right)^2$$

From this relationship it can be seen that when the damping is low the second term becomes negligible, and the natural frequency becomes:

$$\omega_o = c \sqrt{\frac{A}{V \ell_{\text{eff}}}}, \quad f = \frac{\omega}{2\pi}$$

The maximum amplitude of mass displacement becomes:

$$X_o = \frac{P}{\rho c^2 A / V g_c} \left\{ \frac{1}{\left[1 - \left(\frac{\omega}{\omega_o} \right)^2 \right]^2 + \left[\frac{R \omega}{\rho \ell_{\text{eff}} \omega_o^2} \right]^2} \right\}$$

The amount of power dissipated per unit area by the resonator due to friction and turbulence is:

$$P = \frac{1}{2} R_d \sigma \left(\frac{dx}{dt} \right)^2 = \frac{1}{2} R_d \sigma (\omega X_o)^2 / g_c$$

Dividing by the average incident intensity, $I = P_i^2 g_c / 2\rho c$, the fraction of energy absorbed becomes:

$$\alpha = R_d \sigma \rho c \left(\frac{\omega X_o}{g_c P} \right)^2$$

If the pressure amplitude at a wall is taken as twice the free field amplitude the equation becomes:

$$\alpha = \frac{4R_d \sigma \omega^2 V^2}{A^2 c^3 \rho} \left\{ \left[1 - \left(\frac{\omega}{\omega_o} \right)^2 \right]^2 + \left[\frac{(R_d + \sigma \rho c) \omega}{\rho l_{eff} \omega_o^2} \right]^2 \right\}^{-1}$$

Using the definition of the specific acoustic resistance,

$$\theta = R_d / \sigma \rho c$$

and the quality factor,

$$Q = \omega_o l_{eff} / \theta c \sigma$$

the above equation can be expressed as:

$$\alpha = \frac{4\theta}{(\theta + 1)^2 + Q^2 \theta^2 \left(\frac{\omega}{\omega_o} - \frac{\omega_o}{\omega} \right)^2}$$

$$\alpha = \frac{4\theta}{(\theta + 1)^2 + X^2}$$

where $X = Q\theta \left(\frac{\omega}{\omega_o} - \frac{\omega_o}{\omega} \right)$ is the acoustical reactance.

b. Empirical Corrections for Ideal Helmholtz Resonator Theory

(1) Nonlinear Resistance (Damping Resistance)

The total resistance was previously shown to be the sum of the damping resistance, R_d , and the reradiation resistance, R_r . The reradiation resistance was easily determined by integration. The damping resistance is a sum of the viscous losses and nonlinear turbulence losses. This sum cannot be analytically determined. For each resonator geometry (i.e., plane holes, standpipes, etc.) empirical information must be obtained for the damping resistance.

The damping resistance is expressed as:

$$R_d = 2(2\mu\rho\omega)^{1/2} (\epsilon + t/D)$$

For each new geometrical type the nonlinear resistance term, ϵ , can be determined experimentally (see paragraph 2a) for the case of no-flow velocity past or through the resonator aperture.

(2) No-Flow

The no-flow case most closely approaches the ideal case, and for that reason is a basis for the cases with flow. In addition to the damping resistance, only experimental determination of the effective length is required.

To obtain the effective mass in the resonator neck, the effective length must be known. A relationship can be established for a given geometrical type of resonator as a function of geometrical parameters such as diameter, open area ratio, and thickness. This can be accomplished by experimentally establishing the resonant frequency of various test samples and calculating the corresponding effective lengths.

$$l_{\text{eff}} = \left(\frac{c}{\omega_0}\right)^2 \left(\frac{A}{V}\right)$$

(3) Flow Through

Calculations for the flow through case are made using the no-flow parameters as a basis of correction. The no-flow resistance and reactance must be corrected for the effects of the flow through velocity. The relationships for these corrections must be experimentally established as functions of velocity.

(4) Flow Past

Once again using the no-flow parameters as a basis of correction the influence of flow past may be determined. First, the shift in resonant frequency must be determined by establishing experimentally the relationship between frequency shift and flow past velocity.

$$(f_0)_v = f_0(1 + \Delta f_0/f_0)$$

Where:

$$\frac{\Delta f_o}{f_o} = \text{function of velocity}$$

Next, the specific resistance with flow past must be calculated using experimental relationships for the effects of pressure amplitude and flow past velocity.

$$\frac{\theta_v}{\theta} = \text{function of velocity}$$

2. FORMULATION OF DESIGN PROCEDURE

a. Impedance Tube Calculations

Using the trace of peak-to-peak pressure amplitude versus distance to sample face (figure B-2) obtained from a sample test in the impedance tube apparatus (figure B-3), the desired information can be calculated. The relationships are the following:

$$\lambda = 2(D3 - D1), \text{ wave length}$$

$$\Delta P = P_{\max} - P_{\min}, \text{ in decibels}$$

Percentage absorption,

$$\alpha = \left\{ 1 - \left[\frac{10^{\Delta P/20} - 1}{10^{\Delta P/20} + 1} \right]^2 \right\} \times 100$$

Total acoustic resistance,

$$\theta = \frac{1 - \left[\frac{10^{\Delta P/20} - 1}{10^{\Delta P/20} + 1} \right]^2}{1 + \left[\frac{10^{\Delta P/20} - 1}{10^{\Delta P/20} + 1} \right]^2 + 2 \left[\frac{10^{\Delta P/20} - 1}{10^{\Delta P/20} + 1} \right] \cos \left\{ 2\pi \frac{D1}{D3 - D1} \right\}}$$

Acoustic reactance,

$$X = 2 \left[\frac{10^{\Delta P/20} - 1}{10^{\Delta P/20} + 1} \right] \sin \left\{ 2\pi \frac{D_1}{D_3 - D_1} \right\} \frac{\theta}{1 - \left[\frac{10^{\Delta P/20} - 1}{10^{\Delta P/20} + 1} \right]^2}$$

Nonlinear resistance term,

$$\epsilon = \frac{\sigma \rho c \theta}{4} \frac{1}{\sqrt{\pi \mu \rho f}} - \frac{t}{D_o}$$

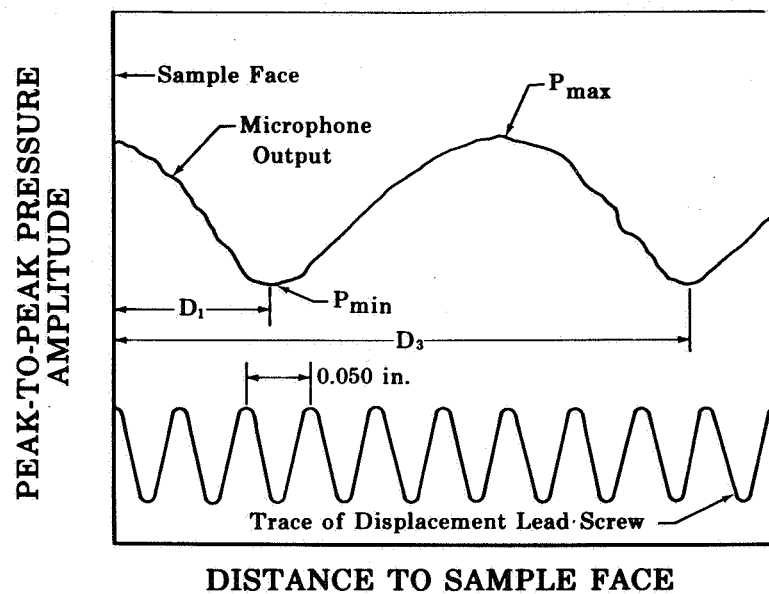


Figure B-2. Typical Impedance Tube Data

FD 20596

b. Analytical Design Program

The ideal Helmholtz resonator theory can now be used as a framework on which to place the experimentally obtained corrections. By conducting a relatively small number of tests on samples within a geometrical family of interest and under conditions of interest (i.e., no-flow, flow through, flow past, high sound pressure levels, multiple frequencies) the relationships for the corrections can be established. Once established, these relationships can be combined with the Helmholtz resonator theory in an analytical computer program. The program can be used to select a geometry and to optimize it for maximum possible absorption at the observed frequency of the combustion instability.

3. BENCH TESTS

a. Test Rig

The experimental data were obtained with the impedance tube apparatus shown in figure B-3. From the test results, information such as non-linear resistance corrections, absorption coefficient, resonant frequency, end corrections for effective length, and frequency shift due to flow past velocity can be determined for a given geometrical type. This was accomplished by conducting tests on many sample resonators within the geometrical family of interest and establishing the required relationships from correlation of the test data (see Reference 5).

Tests on the impedance tube were conducted in the following manner: First, the test frequency and sound pressure level were set on the sound source. A plane wave then formed in the tube, traveled down the tube to the sample face, and was reflected. The microphone probe traversed the tube, continually measuring the peak-to-peak pressure amplitudes. Simultaneously, the distance from the probe to the sample face was measured. This information yielded a strip chart trace of peak-to-peak pressure amplitude vs distance from the sample face. All the desired parameters were calculated from the information contained on the traces obtained by this procedure.

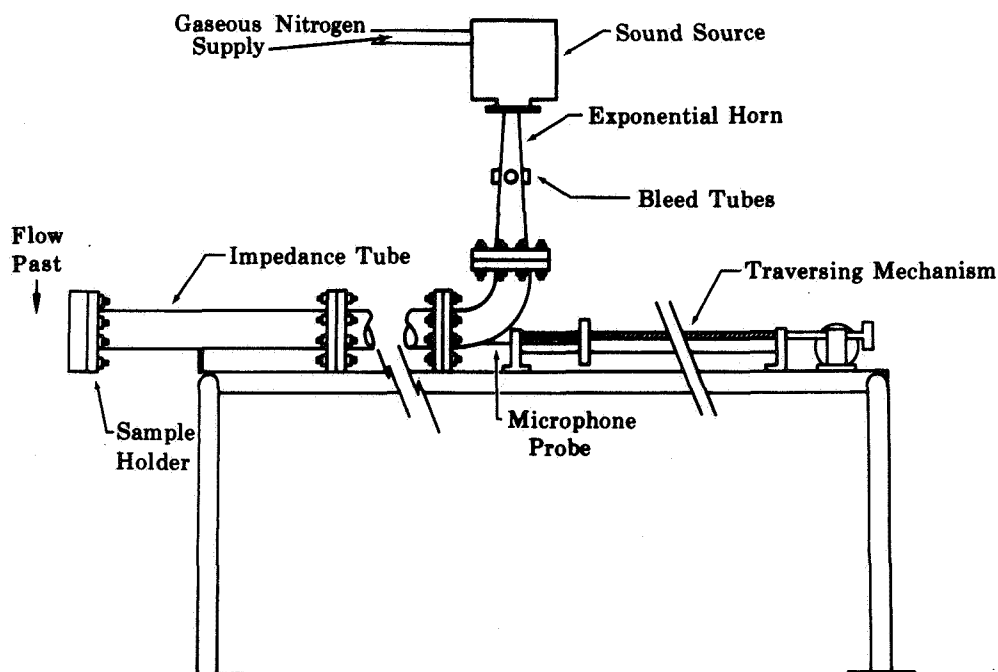


Figure B-3. Impedance Tube Apparatus

FD 15556C

b. Samples Tested

Tests were conducted on the inner liner damping tube configurations shown in figure B-4. These samples were standpipe configurations of 0.625- and 1.00-inch diameters. A concentric standpipe with a 0.625-inch inner diameter was also tested.

The surface area of the sample confronting the sound wave in the impedance tube was limited. To simulate the proper open area ratios, the sample standpipe diameters were scaled. The 1.00-inch diameter standpipe was scaled to 0.625 inch and the 1.25-inch diameter to approximately 1.00 inch.

The volume of the resonator was sized to simulate the proper volume for the given standpipe diameter by keeping the ratio of the volumes of the standpipe to the volume of the resonator constant. These samples were tested over a wide range of pressure amplitudes, frequencies of 200 and 400 Hz, and flow velocities of 0 to 400 fps.

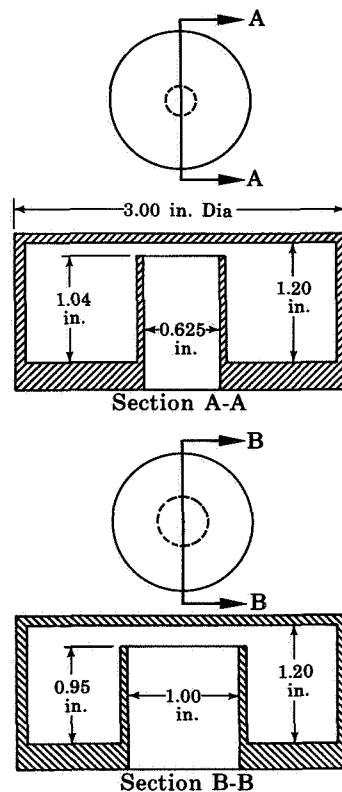


Figure B-4. Impedance Tube Test Sample Configurations

FD 20602

c. Results

The nonlinear resistance data are shown in figure B-5 as a function of sound pressure level. This information, along with test data for the end correction relationship (figure B-6) and the frequency shift ratio (figure B-7), provided the necessary supplemental information for the analytical computer program.

In addition, absorption coefficients were obtained for each sample. Figures B-8 and B-9 present the absorption coefficient vs the frequency for standpipes, and figure B-10 shows the same parameters for the concentric standpipe.

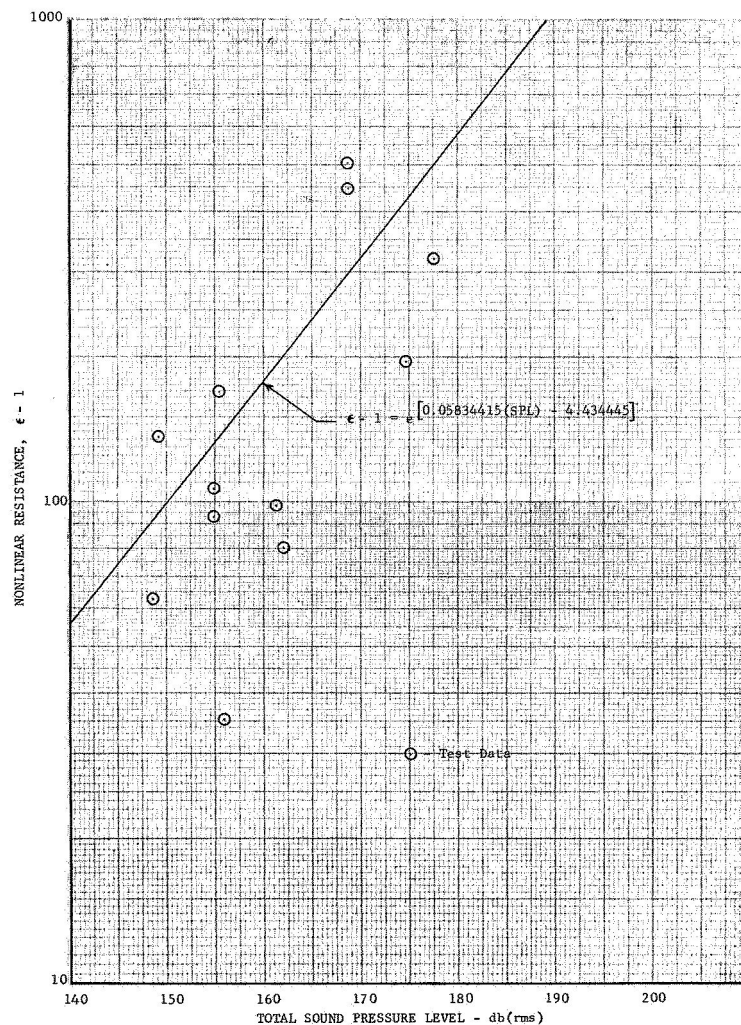


Figure B-5. Impedance Tube Test Results:
Nonlinear Resistance vs Total
Sound Pressure Level

DF 55422

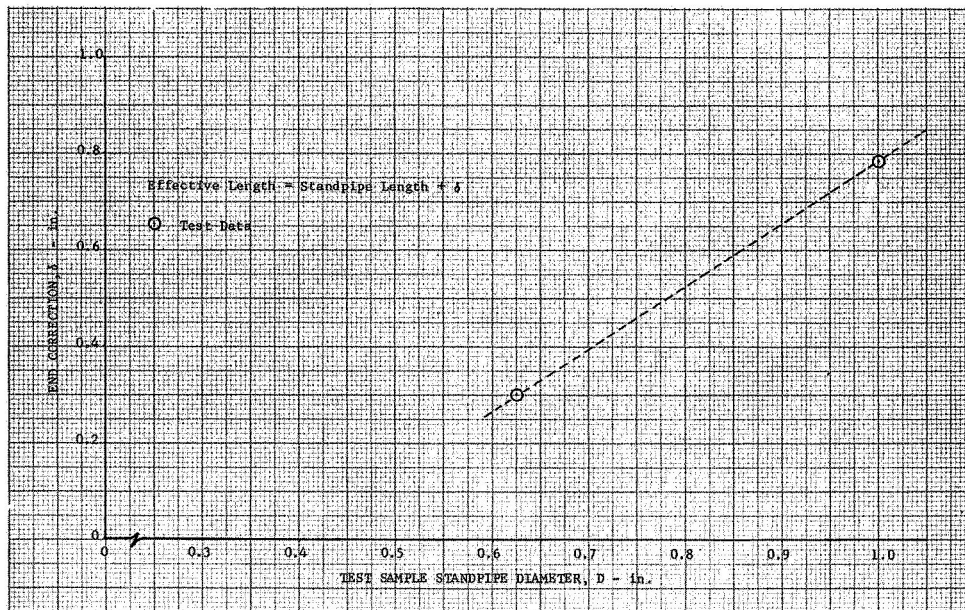


Figure B-6. Impedance Tube Test Results: End Correction vs Standpipe Diameter DF 55423

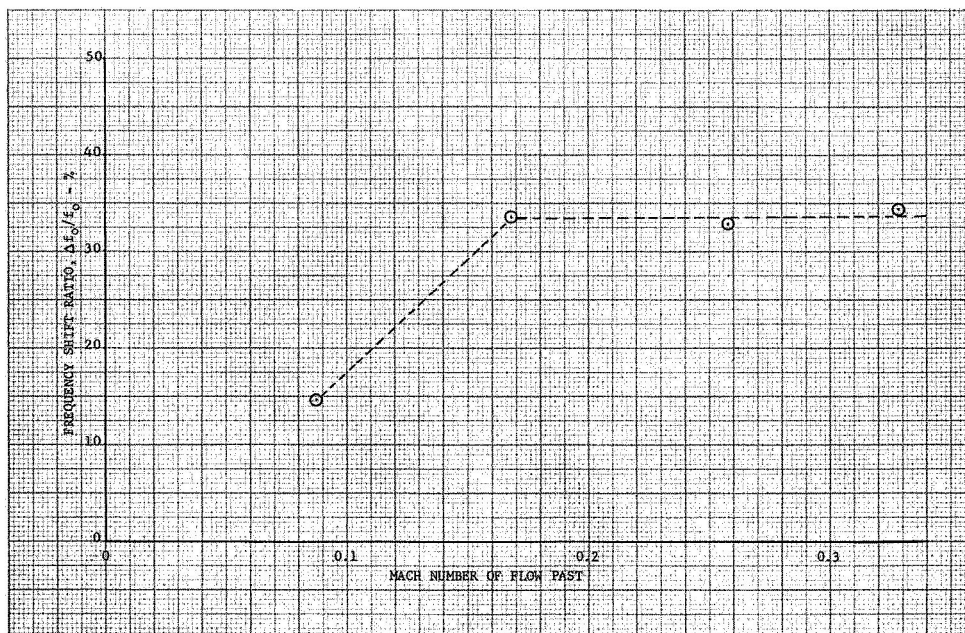


Figure B-7. Impedance Tube Test Results: Frequency Shift Ratio vs Flow Past Mach Number DF 55424

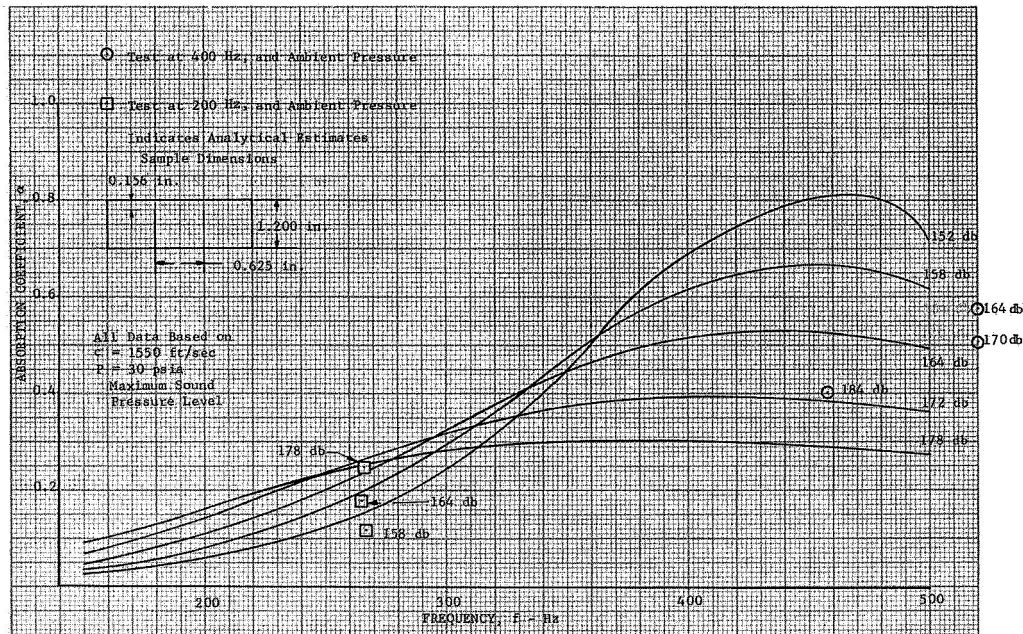


Figure B-8. Absorption Coefficient vs Frequency DF 55425
for 0.625-in. Diameter Standpipe

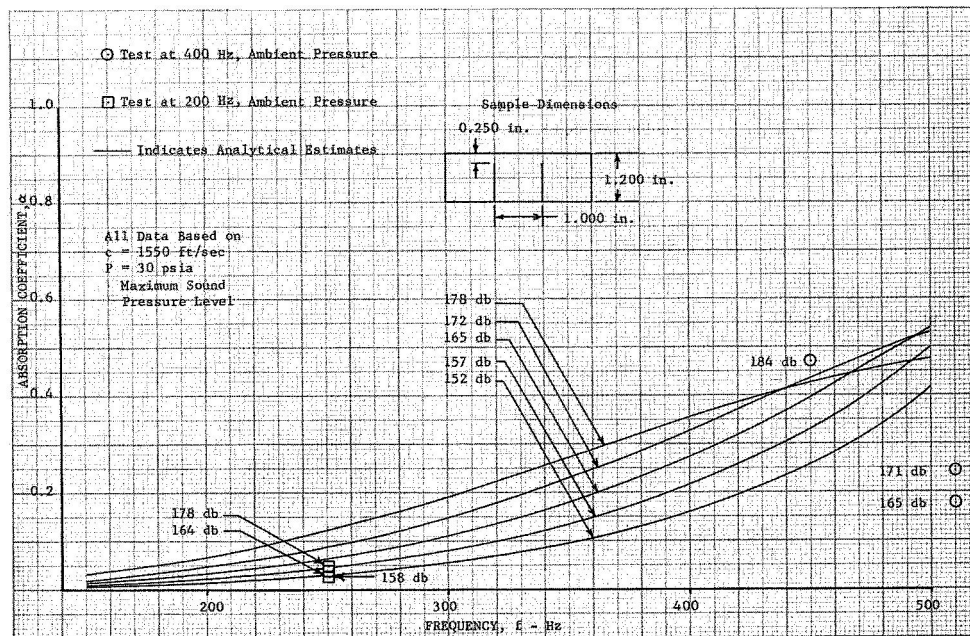


Figure B-9. Absorption Coefficient vs Frequency DF 55426
for 1.000-in. Diameter Standpipe

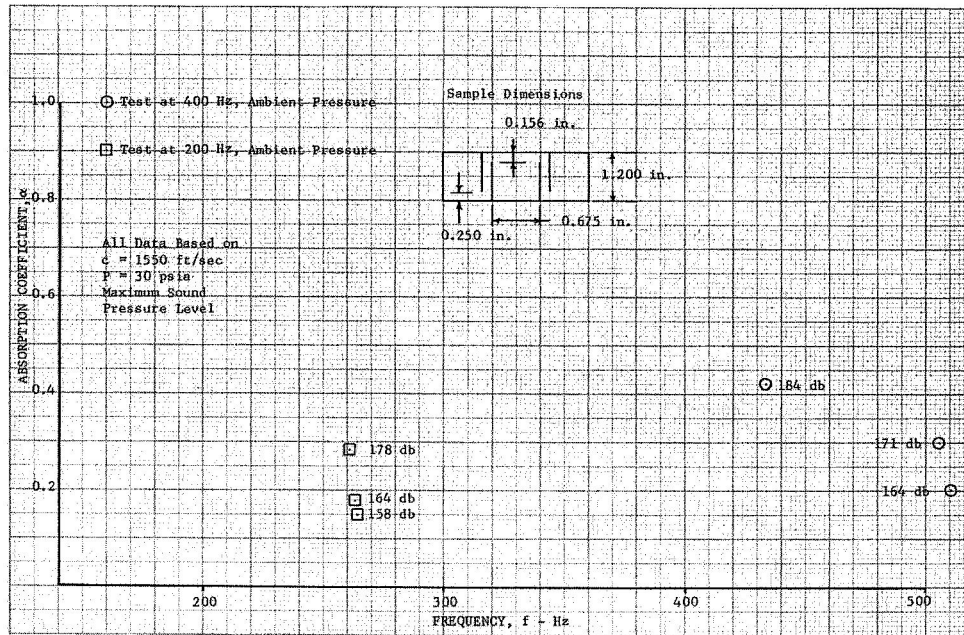


Figure B-10. Absorption Coefficient vs Frequency for Concentric Standpipes

DF 55427

Table B-1. Nomenclature

Symbol	Description	Units
A	Cross sectional area of resonator neck	ft ²
C	Sonic velocity	ft/sec
D	Aperture diameter	ft
D1	Distance to first node from sample face in impedance tube	ft
D3	Distance to second node from sample face in impedance tube	ft
F	Force	lb _f
f	Frequency	1/sec
g_c	Dimensional constant	lb _m ft/lb _f sec ²
m	Mass	lb _m
P	Pressure	lb _f /ft ²
P	Pressure amplitude	lb _f /ft ²
P_{max}	Maximum measured pressure amplitude	lb _f /ft ²
P_{min}	Minimum measured pressure amplitude	lb _f /ft ²
Q	Quality factor	

Table B-1. Nomenclature (Continued)

Symbol	Description	Units
R	Total resistance	$\text{lb}_f\text{-sec/ft}^3$
t	Time	sec
t	Wall thickness	ft
v	Velocity	ft/sec
V	Volume	ft^3
x	Coordinate of travel for oscillating mass	ft
X	Specific reactance	
X_0	Maximum mass displacement	ft
Z	Specific impedance	
α	Absorption coefficient	
γ	Specific heat ratio	
Δ	Differential	
ϵ	Nonlinear resistance	
θ	Specific resistance	
λ	Wave length	ft
μ	Viscosity	$\text{lb}_m/\text{ft sec}$
π	3.14159	
ρ	Density	lb_m/ft^3
σ	Open area ratio	
ω	Angular velocity or frequency	1/sec
Subscripts		
A	Apparent	
d	Friction plus turbulence	
d	Damped	
D	Damping	
eff	Effective	
i	Incident	
o	Natural	
r	Reradiation	
s	Spring	
v	Flow past	
x	Direction	

APPENDIX C
REFERENCES

1. "Effect of Pressure Level on Afterburner Wall Temperatures,"
NACA RM E58D01, 11 June 1958.
2. "Investigation of Heat Transfer Coefficients in an Afterburner,"
NACA RM E52D11.
3. McAdams, W.H., "Heat Transmission," 3rd Ed., McGraw-Hill,
New York, 1954.
4. Kreith, F., "Principles of Heat Transfer," 3rd Ed., International
Textbook Company, August 1960, p. 213.
5. "A Study of the Suppression of Combustion Oscillations With
Mechanical Damping Devices, Phase II Summary Report," Con-
tract NAS8-11038, PWA FR-1922, 15 July 1966.
6. Kinsler, E., and Austin R. Frey, "Fundamentals of Acoustics,"
2nd edition, Wiley, 1962.

APPENDIX D
TEST CHRONOLOGY

29 APRIL THROUGH 18 MAY 1966

The duct burner rig was installed in the SW-24 facility (figure II-1). The large-diameter inner exit nozzle was installed with all variable plugs in the retracted position.

19 MAY 1966

Test Point 1, table D-1*, was set to check out the test facility, instrumentation, and the automatic data recording system. It was found that sufficient test parameters could not be monitored by the test facility operator to safely conduct a test.

Cold Flow Time: 0.92 hour

20 MAY 1966

Pressure gages were installed in the control panel to allow the test facility operator to monitor the duct burner rig inlet and exit pressures. A facility and rig checkout was then conducted (Test Point 1).

Cold Flow Time: 2.25 hours

21 THROUGH 24 MAY 1966

The reduced data from the previous cold flows revealed that the facility automatic pressure recording system (DAMPR) was out of calibration. The DAMPR system was subsequently recalibrated.

25 MAY 1966

The first cold flow calibrations of the exit nozzle were conducted (Test Points 2 through 13) with an airflow rate of approximately 300 lb/sec. The object of the cold flow calibrations was to determine the discharge coefficient for the choked exit nozzle at several airflow rates and temperatures.

Cold Flow Time: 4.08 hours

*Tables D-1 and D-2 at the end of this Appendix present data for all cold calibration and combustion test points.

26 MAY 1966

Cold flow calibration test points 14 through 30 were obtained with airflow rates of approximately 150 lb/sec.

Cold Flow Time: 4.58 hours

1 JUNE 1966

Cold flow calibrations were resumed, but the test was terminated because of failures to the heater-burner located in the inlet plenum and to an air supply line bellows.

Cold Flow Time: 5.42 hours

2 THROUGH 19 JUNE 1966

The duct burner rig was removed by 2 June to permit removal of the failed heater-burner. Figure D-1 shows the 54-in. diameter inlet duct of the SW-24 facility looking upstream from the rig inlet. The inlet screen had failed and debris passed through the system. The heater-burner, which was used as a flow distribution device, had several burner cans dislocated from the rear mounts; some burner cans had structurally failed.

The diffuser pressure and temperature instrumentation sustained major damage from foreign object impact. The total pressure rakes were repaired and the total temperature probes were replaced. Eight of the Zone-1 fuel nozzles suffered damage to the aerodynamic heat shields, which are the only parts of the nozzle exposed to the airstream. The three most severely damaged heat shields were removed and a bent fuel supply tube was found on one nozzle. All 40 nozzles were returned to the manufacturer for flow checks and repair of the three most severely damaged.

A Zone-2 fuel spraybar was damaged by debris and required repairs.

Although the duct burner received only minor damage, much debris had become lodged in it. One OD scoop on the primary panel was bent; this was easily straightened. An ID scoop on the primary panel was cut on both edges. One ID secondary scoop wall was torn. The damaged scoops were straightened and weld-repaired.

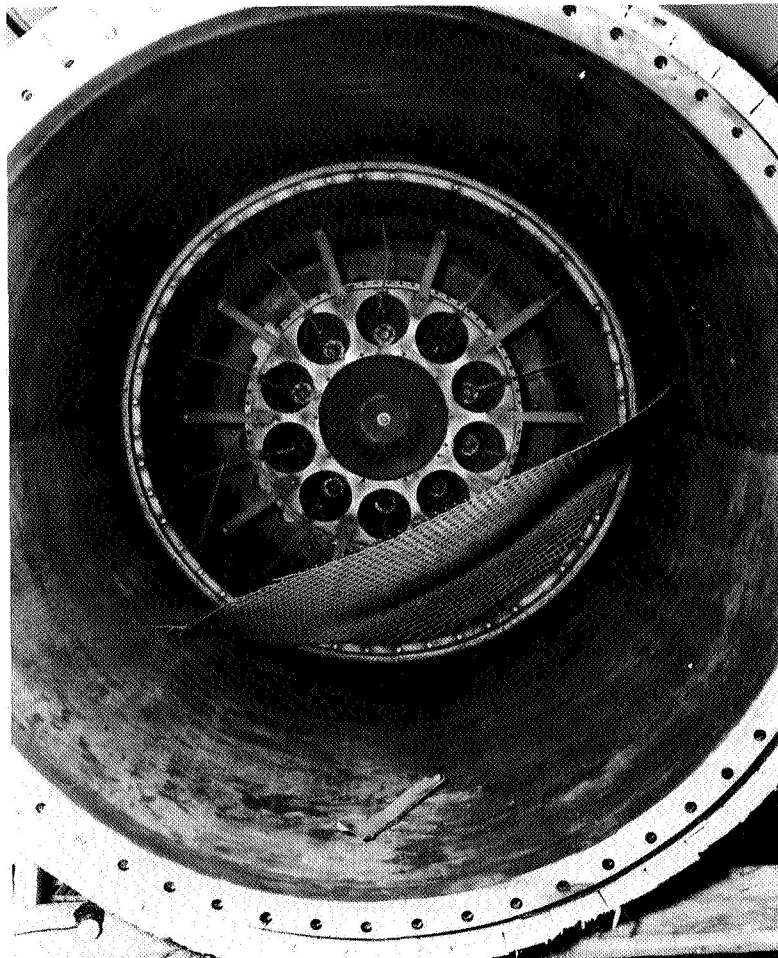


Figure D-1. SW-24 Facility Looking Upstream
from the 54-in. Diameter Duct
Burner Rig Inlet After the 1 June
Cold Flow Test

FE 60718

No damage was sustained by the water-cooled plugs or the water-cooled total pressure probes in the exit nozzle.

The screen downstream of the flow distribution plate was reinforced, (figure D-2). The heater-burner was disassembled and all parts except the 1-in. thick stainless steel support plate were removed. This plate was modified to provide the pressure drop previously supplied by the heater-burner assembly.

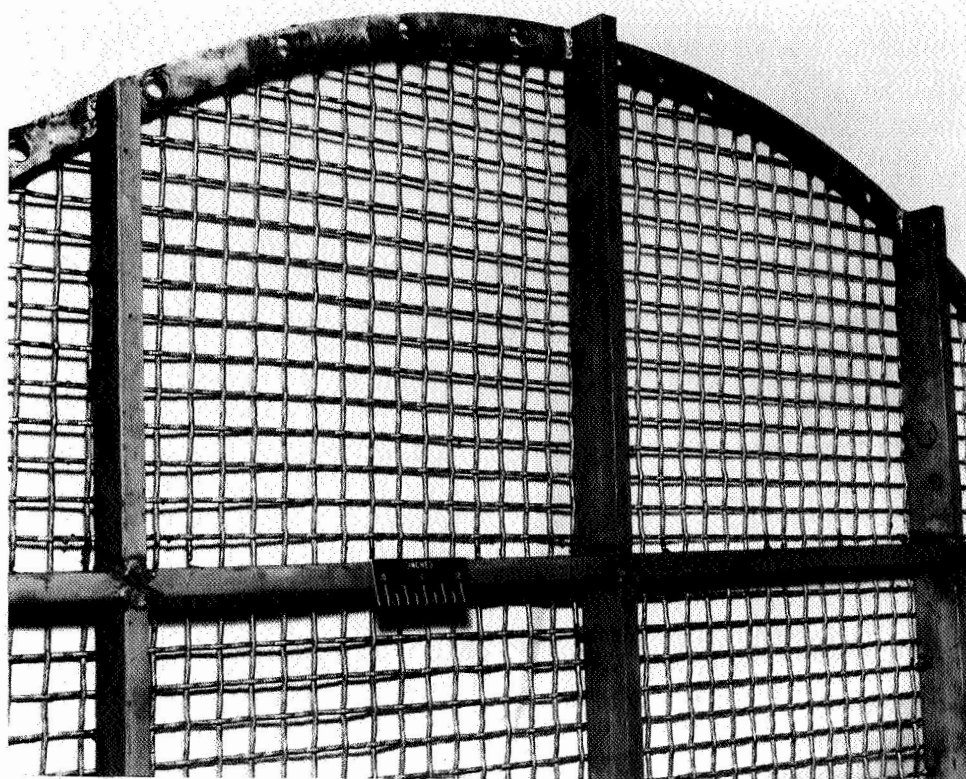


Figure D-2. SW-24 Screen Located Downstream
of the Heater-Burner

FE 60720

A new air supply line bellows section was installed. This bellows section had a sleeve that was spun rather than fabricated from two pieces, eliminating the weld that had previously failed. The sleeve thickness was approximately twice that of the old sleeve. For additional support, a 1- by 3-in. cross section x-member was welded in the downstream end of the bellows section.

An access hatch was installed in the rig inlet adapter to permit inspection of the downstream side of the flow distribution plate without rig disassembly.

The duct burner rig was reinstalled 13 - 16 June. X-ray inspection of the bellows section installation was completed on 20 June.

20 JUNE 1966

The cold flow calibration of the choked exit nozzle was resumed on 20 June (Test Points 31 through 34). A post-test inspection indicated that additional failure was imminent. Warpage of the flow distribution

plate (formerly the heater-burner upstream support plate) was the major problem. This plate was fastened by five bolts to a support ring. Pressure-loading caused the plate to warp 5/8-in. on the circumference between the bolts. In addition, the strands of the reinforced screen had many breaks. The clean strand breaks indicated that the wires were fatigued.

Cold Flow Time: 2.90 hours

21 THROUGH 28 JUNE 1966

Repairs were made inside the facility ducting without removing the duct burner rig. The screen was removed from the flow stream, cut in half inside the ducting, and dropped through the adjoining flange. The flow distribution plate was straightened and 20 more bolts were added on the circumference to secure the plate more rigidly in the duct. To provide additional support for the flow distribution plate, two large members (1 by 8 in. cross section) were welded across the 54-in. duct. The effective flow area of the plate had been 250 in.², resulting in choked flow through the plate and, consequently, a high pressure drop. To allow unchoked flow through the holes during normal operation, the effective flow area was increased to approximately 550 in.².

During the 20 June test, a pressure transducer, which was mounted slightly downstream of the duct burner, indicated that periodic pressure fluctuations existed with an amplitude approximately equal to 10% of the static pressure. Because these pressure fluctuations might have contributed to the facility failures, additional pressure transducers were installed both upstream and downstream of the flow distribution plate to obtain more data.

29 JUNE 1966

A test was made to check the rig inlet radial and circumferential total pressure profiles and to check for pressure fluctuations (Test Points 35 through 38). The rig inlet total pressure varied circumferentially by 5% and the indications of pressure fluctuations persisted. The test was terminated and an inspection of the rig and facility revealed that all parts were structurally sound.

30 JUNE 1966

Further instrumentation was installed in the duct burner rig and the SW-24 facility to provide data for a more complete analysis of the apparent pressure fluctuations. Dynamic pressure transducers and accelerometers were installed as shown in figure D-3.

1 THROUGH 11 JULY 1966

A test was conducted to investigate the pressure oscillations in the rig. Airflow and diffuser inlet Mach number were varied and data taken at Test Points 39 through 42 on 1 July. Although significant pressure fluctuations were shown to be present, the exact value could not be determined because the dynamic pressure sensors were also sensitive to rig vibration. The pressure oscillations were considered to have been at least partially caused by the 24-in. supply line dumping perpendicularly into the 54-in. inlet line.

A 24-in. diameter perforated cylinder was then installed extending from the 24-in. supply line to the bottom of the 54-in. duct; flow area of the perforated cylinder was 300 square inches.

Cold Flow Time: 4.40 hours

12 JULY 1966

Testing was resumed to continue investigation of the airflow characteristics (Test Points 43 through 46). Pressure fluctuations had been substantially reduced.

The diffuser inlet total pressure profile had a 5% variation between the bottom and top of the rig. This difference was considered to be excessive, since the inlet pressure on an engine would not be expected to vary more than 2%. Half the holes in the flow distribution plate were then blocked off to increase the pressure drop and improve mixing; the resulting open area was about 380 square inches.

Cold Flow Time: 3.99 hours

FD 19179

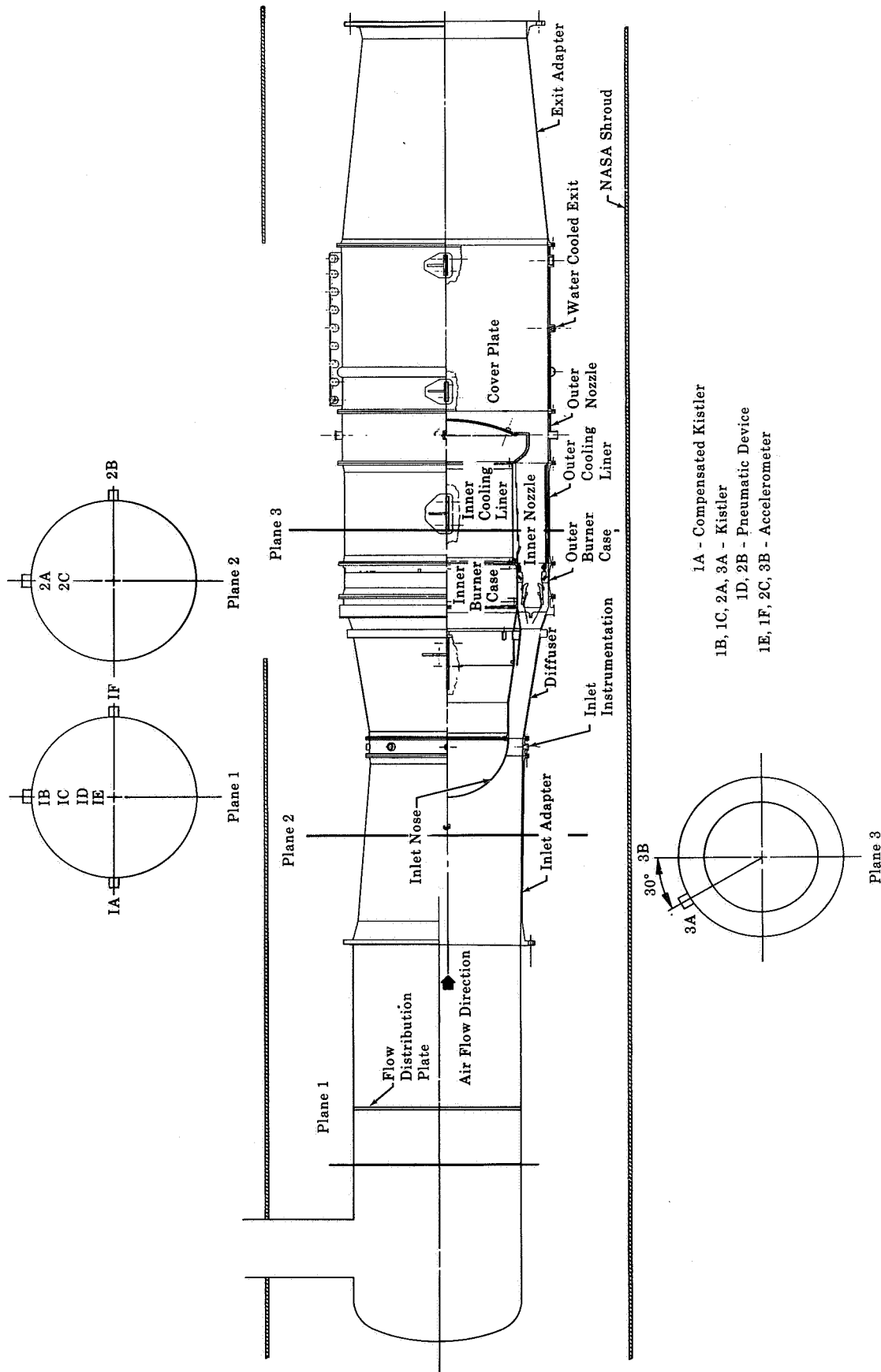


Figure D-3. Rig and Facility Instrumentation

13 JULY 1966

A test was conducted to check the inlet profile and make a heated inlet cold flow calibration (Test Points 47 through 53). The circumferential pressure profile appeared to be satisfactory although a radial profile that peaked toward the ID wall still existed. The heated inlet cold flow calibration was not made because the facility preheater could not sustain combustion.

Cold Flow Time: 4.00 hours

14 JULY 1966

Another attempt was made to obtain a heated inlet cold flow calibration (Test Points 54 through 56). An inlet temperature of 600°F was reached but could not be sustained by the facility preheater. Several attempts were made to maintain this temperature, but before the exit nozzle could be choked the facility exhausters began filling with water and the test was terminated.

Cold Flow Time: 4.17 hours

15 JULY 1966

Heated inlet cold flow calibration continued with satisfactory preheater performance (Test Points 57 through 59). While Test Point 59 was being recorded, it was noted that a total pressure probe at the diffuser exit was reading static pressure. The test was immediately terminated, and a check of the instrumentation revealed that two pressure probes at this location had broken off due to vibration fatigue. It was also noted that seven temperature probes had received internal damage and had open thermocouple junctions.

At 300 lb/sec airflow, exit nozzle choked, and 585°F inlet temperature (the test point at which the probes failed) the vibration level indicated by the accelerometer at the rig inlet (figure D-3) rose from 41 to 68 g, probably due to operation with supersonic flow in the diffuser. (The maximum diffuser Mach number in an engine is always less than approximately 0.6.)

Cold Flow Time: 4.03 hours

16 THROUGH 25 JULY 1966

The rig was disassembled to check for further damage and prepare for the first combustion tests. Three of the eight ID support plates on the diffuser exit were found to have suffered a fatigue failure in the weld area. The relationship of the support plates to the diffuser exit is shown in figure D-4, and a closeup of the failure is shown in figure D-5.

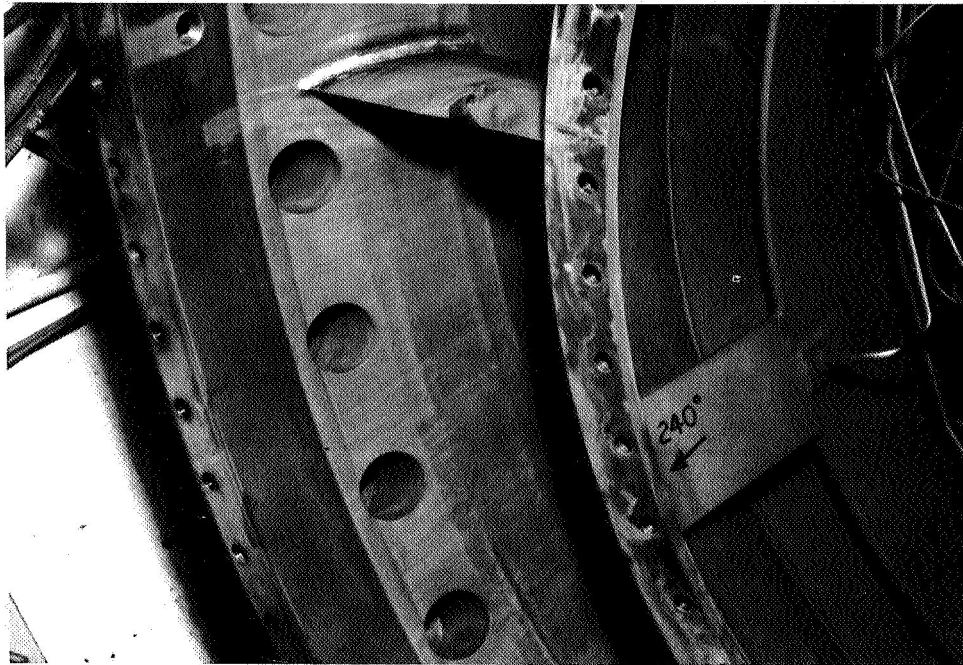


Figure D-4. Diffuser Exit Showing Position
of Failed Supporter Plate

FE 61878

The duct burner was also damaged. Three of the twenty firewall expansion plates (located radially on the upstream side of the firewall) had cracked on one side (figure D-6). One firewall expansion plate had cracked on both sides, had broken loose, and had lodged in the burner.



Figure D-5. Diffuser Support Plate Showing
Weld Fatigue Failure

FE 61879

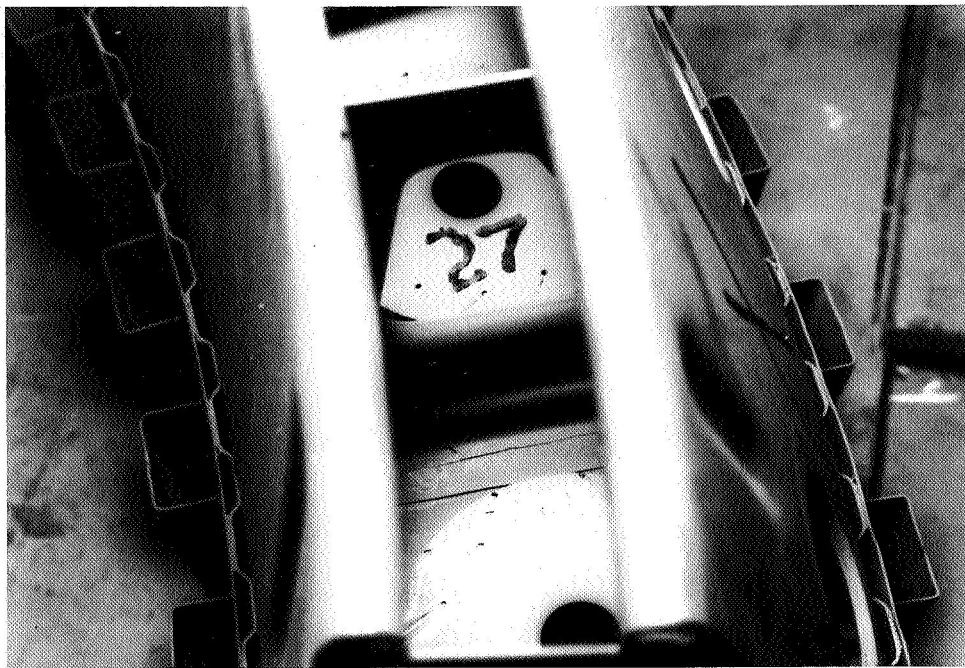


Figure D-6. Ram-Induction Burner Firewall
Expansion Plate Showing Fatigue
Failure

FE 61880

The cracked diffuser support plates were repaired by completely grinding out the cracks and rewelding. It was decided not to repair the burner firewall because of the complexity of the operation. Rig assembly with high flow Zone-2 fuel spraybars and the small diameter inner exit nozzle was completed by 25 July.

26 JULY 1966

The duct burner was ignited for the first time. (Test Point 60 of table D-2*.) The first attempt to ignite failed due to a fuel flow turbine meter overspeed abort caused by a time delay in filling the fuel manifold for the first time. The burner was ignited on the second attempt and ignition occurred at a fuel/air ratio of approximately 0.0004, simultaneously with the first indicated rise in the fuel manifold pressure. The exit nozzle total pressure change at ignition could not be detected on mercury manometers.

The burner was also ignited at Test Points 61 and 64. Test Point 64 represented a simulated cruise condition at low values of pressure and temperature (due to the inability of the facility preheater to maintain desired inlet temperature), a more difficult ignition condition than Condition C. Ignition was instantaneous.

Cold Flow Time: 4.36 hours

Combustion Time: 0.72 hour

27 JULY 1966

A test was conducted to obtain performance data at simulated cruise conditions. A maximum fuel/air ratio of 0.016 was obtained at the desired pressure and flow. (Test Point 8).

Testing was terminated with an improper shutdown procedure, which rapidly closed the inlet and exit valves to the rig. Quench water continued to be sprayed into the rig between these valves; before the water could be turned off the lower half of the rig was filled with cold water. The quench water valve was subsequently replaced with a remote control

*Table D-2, which gives combustion performance data for Test Points 60 through 612, appears at the end of this Appendix.

valve and coordinated with the abort system. Rig inspection revealed no apparent damage, although a metallurgical change may have contributed to later burner failure.

Cold Flow Time: 2.84 hours

Combustion Time: 0.68 hour

29 JULY 1966

The exit nozzle area was changed to obtain performance at a simulated cruise condition with a fuel/air ratio of 0.03. The burner was ignited and a fuel/air ratio of 0.0266 was obtained before the facility exhausters received too much water and had to be shut down. Another attempt was made to choke the exit nozzle while running hot, but the same problem was encountered.

Cold Flow Time: 4.33 hours

Combustion Time: 0.92 hour

30 JULY 1966

Post-test inspection showed the outer cooling liners had started to form a slight ripple across the convolution perpendicular to the axial centerline (figure D-7). This ripple occurred only on those liners immediately downstream of either a Zone-2 fuel spraybar manifold tee or end support. The liners downstream of an end support appeared to be getting hotter than those behind a tee.

Figure D-8 shows warpage that occurred in the water-cooled exit duct upstream of the quench water-spray nozzles. Because this warpage occurred just downstream of a window port through the duct water jacket, an additional water supply was added downstream. Later tests indicated that the warpage may have been caused by the addition of another water line connected to the cooling water supply, which reduced the local flow rate to the water-cooled exit duct.

2 AUGUST 1966

A test was conducted to determine the performance of the duct burner at a fuel/air ratio of 0.03 at simulated cruise conditions. Performance data were not obtained (Test Point 74); the test was terminated due to an inoperative water pump in the exit duct spray-cooler.

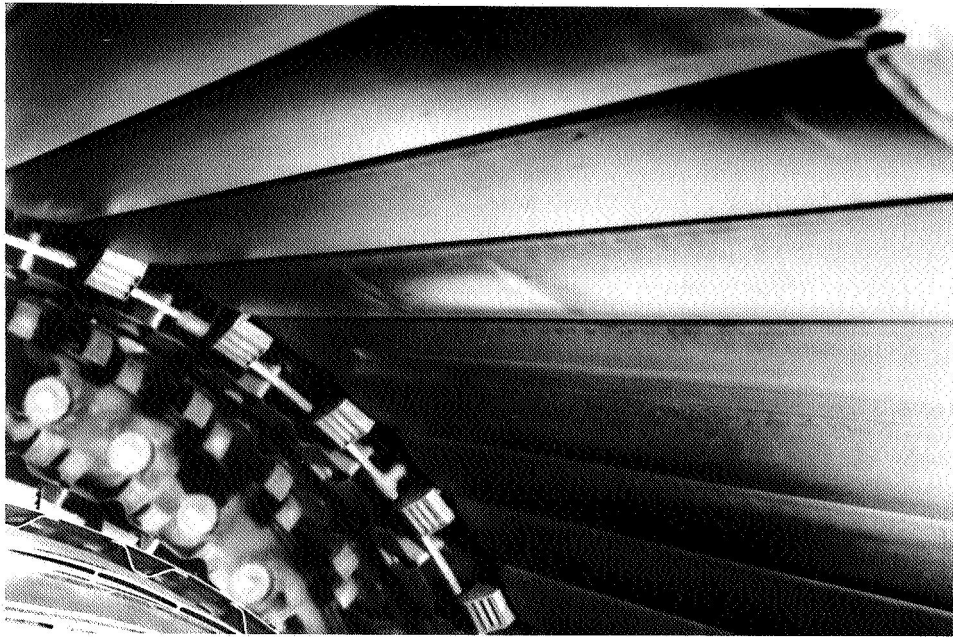


Figure D-7. Outer Cooling Liners After Test
at a Fuel/Air Ratio of 0.027

FE 61881



Figure D-8. Warpage of Water-Cooled Duct

FE 61882

Capacitors had been installed in the temperature instrumentation signal lines to the automatic data recording CADDE system prior to the test to filter out noise; a check at ambient conditions showed good correlation between the values recorded in the control room and those obtained with the CADDE system. During the test, however, there was disagreement between the two recording systems. There was also disagreement in the fuel and water measurements.

Cold Flow Time: 3.08 hours

Combustion Time: 0.50 hour

3 AUGUST 1966

A thorough checkout while testing at a fuel/air ratio of 0.03 was considered to be the only expedient way to correct the instrumentation and facility problems. Correction was necessary to allow all three fuel systems to operate at nominal flow rates and also to supply the facilities with typical conditions.

The maximum rig inlet temperature was reduced to 550°F for the remainder of the test program because of the performance limitations of the facility preheater.

The disagreement in liquid flow rates was traced to the presence of water in a bulkhead connector box in the test cell. The water was removed and the connector box dried. The wiring of the CADDE reference thermocouples in the test cell junction box was repaired.

Cold Flow Time: 3.47 hours

Combustion Time: 2.53 hours

4 AUGUST 1966

An instrumentation checkout test was terminated while only the Zone-1 primary fuel was being used (fuel/air ratio = 0.0067) when an expansion joint in the facility exit ductwork failed. Temperature and cooling water flow rate data obtained with the CADDE and control room recording systems were found to correlate.

Cold Flow Time: 2.44 hours

Combustion Time: 0.23 hour

5 AUGUST 1966

It was verified that all instrumentation problems had been corrected. Performance data were obtained at Test Points 79 through 81. The facility was shut down twice during the tests because of excessive water in the exhausters; at shutdown the rig was inadvertently overpressurized to approximately 80 psia, apparently without damage.

Cold Flow Time: 2.87 hours

Combustion Time: 2.80 hours

6 AUGUST 1966

Performance data were obtained at Test Points 83 and 84. Combustion instability occurred at Test Point 84. The instability was detected audibly and then observed on Kistler high-frequency response pressure transducers. The Zone-1 fuel/air ratio was set at 0.01 and the Zone-2 fuel/air ratio was gradually increased to 0.019 when combustion instability and a duct burner blowout occurred (Test Point 86). By controlling the quench water and staging the exhausters, it was possible to operate the facility continuously. It was found that the quench water supply line was not properly sized for the available pressure and would not deliver the required quench water for the higher fuel/air ratio operating conditions.

Cold Flow Time: 3.37 hours

Combustion Time: 1.58 hours

9 AUGUST 1966

Performance data were recorded for Test Points 88 and 89, with combustion instability again occurring. Data were then obtained at a Zone-1 fuel/air ratio of 0.01 and a Zone-2 fuel/air ratio of 0.016 (Test Point 90). During the test, preheater difficulty caused the rig inlet temperatures to be generally less than 520°F.

Cold Flow Time: 1.50 hours

Combustion Time: 1.58 hours

10 THROUGH 17 AUGUST 1966

Several outer cooling liner skin thermocouples (exposed to the highest temperatures) had become inoperative and the rig was partially disassembled for instrumentation repair while the quench water supply line modifications were being made.

The ram-induction burner was inspected. Figure D-9 shows the relative locations of the burner components as well as the numbering system used for identification. Figure D-10 shows warpage of the burner firewall at the OD between Zone-1 fuel nozzles 25 and 26. Other sections of the burner showed some overheating of the firewall lip, but only slight distortion (figure D-16). A flow check of Zone-1 fuel nozzles 25 and 26 verified that they were within calibration limitations.

There was slight burning on half the No. 2 (long) scoops in the primary liner; burning was limited to the upstream edge and sides of the truncated scoops. Figure D-10 shows the most severely burned scoops.

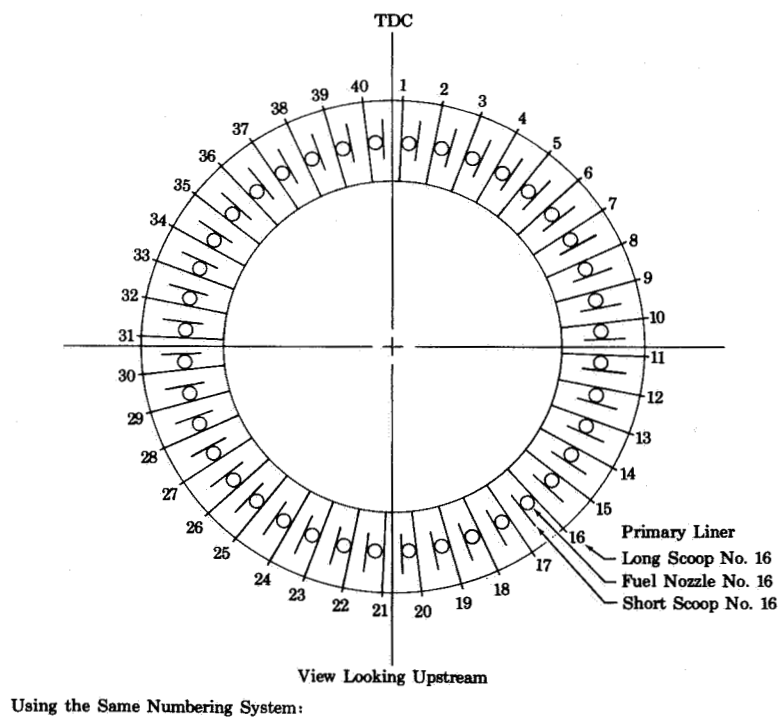


Figure D-9. Duct Burner Schematic Showing Relative Location and Numbering System of Scoops and Zone-1 Fuel Nozzles

FD 18092

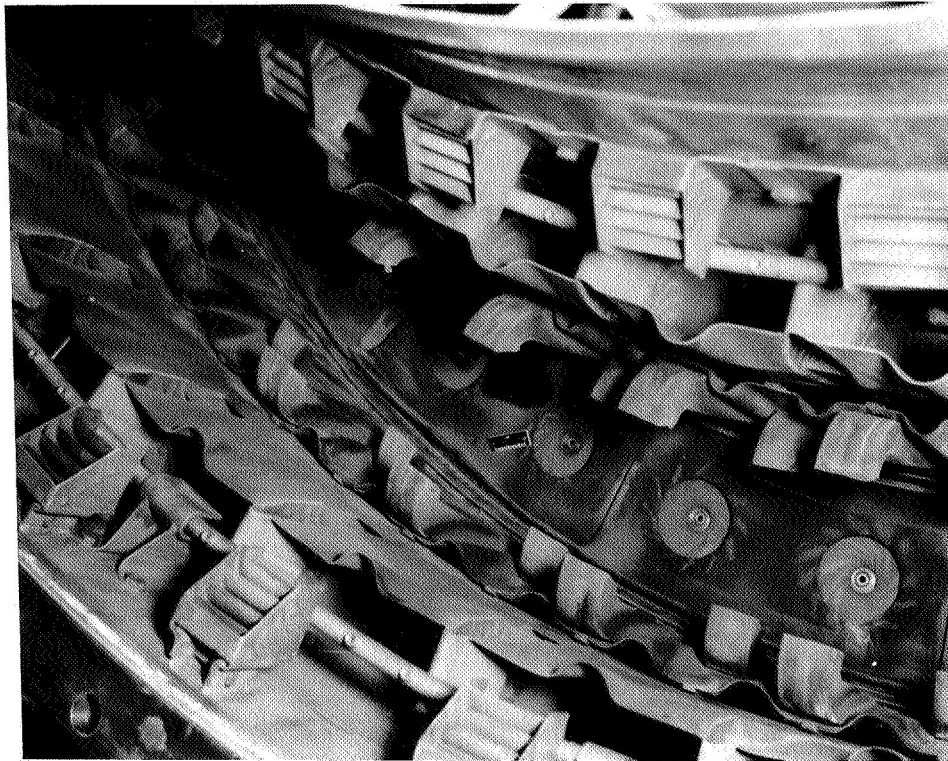


Figure D-10. Duct Burner Firewall Distortion FE 62639

Figure D-11 shows the condition of the outer cooling liners. Figure D-12 is a schematic showing the outer cooling liner location and numbering system. Four of the outer cooling liners, 90 degrees apart, were reinstrumented with skin thermocouples arc-welded to improve durability (originally, only 2 liners contained skin thermocouples). Four liners, No. 19 through 22, were polished to provide a base for a thermal discoloration pattern.

18 AUGUST 1966

A test at cruise inlet conditions was attempted; however, the duct burner rig filled with water because the quench water was erroneously turned on before the rig was supplied with facility air. Although performance data could not be obtained, it was verified that the new supply line substantially increased the quench water flow.

Cold Flow Time: 1.67 hours



Figure D-11. Outer Cooling Liners

FE 62645

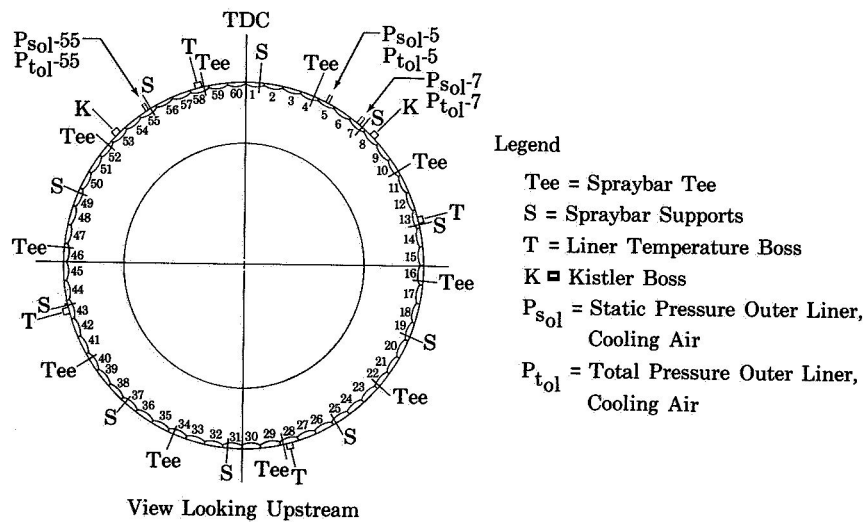


Figure D-12. Outer Cooling Liner Schematic
Showing Relative Location,
Numbering System, and
Instrumentation

FE 18093

19 THROUGH 23 AUGUST 1966

A test attempt on 19 August was terminated when the 24-in. facility inlet gate valve could not be opened. Several valve operating mechanisms were found to be damaged.

24 AUGUST 1966

Test Point 94 was set with the exit nozzle unchoked. It was found that the newly instrumented outer liner thermocouples indicated temperatures 300°F lower than in previous tests; this was attributed to the new type thermocouple installation used to improve durability. Data provided by the original thermocouple installation were considered to be more accurate.

Performance data were obtained at Test Point 98. The facility was shut down once due to excessive water carryover to the exhausters.

Cold Flow Time: 3.60 hours

Combustion Time: 1.73 hours

25 AUGUST 1966

A test was conducted to determine duct burner performance at a fuel/air ratio of 0.04. Data were recorded at Test Points 100 and 101, and combustion instability was again encountered. Test Point 102 was set and data recorded; no combustion instability was evident. While the Zone-2 fuel flow was being increased to reach Test Point 103, a vibration of approximately 100 g was noted as combustion instability occurred. The test was then terminated.

Cold Flow Time: 2.44 hours

Combustion Time: 1.73 hours

26 AUGUST THROUGH 31 OCTOBER 1966

Post-test inspection showed that some duct burner firewall segments had failed. The rig was disassembled and the ram-induction burner removed. Four of the firewall assemblies had broken out of the burner dome. Figure VII-12 shows a typical view at Zone-1 fuel nozzle locations 7 and 8. Similar failures occurred at fuel nozzle locations 3 and 4, 37 and 38, and 39 and 40. Failures were attributed to overheating of the firewalls, which were attached to relatively cool sections. Figure VII-13 shows two swirlers that failed.

Due to excessive vibrations, seventeen of the liner support tabs were torn out of the primary liner. The most severe failure is shown in figure VII-14, which also shows where the primary liner cracked adjacent to a long scoop. The only failures incurred by the secondary liners were eight cracks, similar to that shown in figure VII-15.

The dome and primary liner assembly were shipped to the Florida Research and Development Center.

A metallurgical examination showed the primary burner section material to be nonrepairable and it was scrapped. Fabrication of a new primary burner section was initiated. A redesigned firewall section with added cooling slots and holes was incorporated for improved cooling of the burner firewall. The ID vortex generators were modified as shown in figure VII-20 to solve the heating problem encountered during previous testing. The cracks that occurred on the trailing edge of the secondary liners were weld-repaired.

Seven of the eight diffuser struts that supported the burner dome assembly had small cracks, the worst of which is shown in figure D-13.

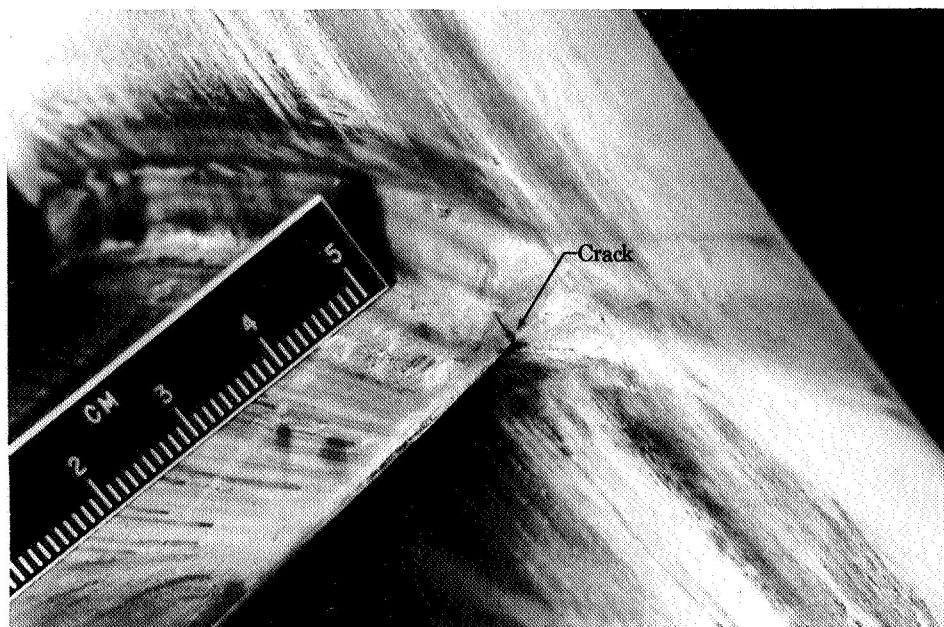


Figure D-13. Diffuser Strut Showing Crack

FD 22555

Three of the choked exit nozzle pressure probes received slight dents from the firewall sections that passed through the rig.

Two nozzle plugs also received slight dents. The outer cooling liners were not changed in appearance from figure D-11.

A centerbody damping plate was fabricated and installed between the inlet nose and the diffuser (figure VIII-6) to damp longitudinal pressure oscillations that might have been present in the rig centerbody.

Restrictions were placed at the bleed air diffuser exit to eliminate the bleed diffuser static pressure rise (figure VIII-6). These restrictions were intended to eliminate a possible driving force for centerbody oscillations. They would also slightly decrease the inner cooling liner airflow.

Two water-cooled traversing temperature and pressure probes, figure II-30, were installed in the duct burner rig exit nozzle at locations formerly occupied by eight-point total pressure rakes.

Redesigned outer cooling liners incorporating acoustic damping were installed. Four of these liners were instrumented with skin thermocouples. Three of the liners had holes enlarged to accept dynamic pressure sensors.

The replacement duct burner was received, skin thermocouples were installed on the modified burner firewall, and the rig was assembled.

1 AND 2 NOVEMBER 1966

Cold flow tests (Test Points 104 through 107) were conducted at simulated burner inlet conditions to determine the pressure loss through the new burner.

Cold Flow Time: 4.58 hours

4 NOVEMBER 1966

Combustion testing with the new burner was initiated at simulated cruise fuel/air ratios (Test Points 109 and 110).

Cold Flow Time: 4.17 hours

Combustion Time: 1.00 hour

9 NOVEMBER 1966

Combustion instability occurred when the overall fuel/air ratio was increased to 0.035 (Test Point 115). The objective of Test Points 116 and 117 was to determine the effect of different Zone-1 and Zone-2

fuel flow splits; combustion instability occurred at approximately 440 Hz frequency in both cases.

Cold Flow Time: 1.75 hours

Combustion Time: 2.33 hours

10 THROUGH 14 NOVEMBER 1966

An attempt to reduce the inlet pressure fluctuations was made by installing damping devices in the facility inlet duct. Before these devices were installed, a peak-to-peak pressure amplitude of 1 to 2 psi with no predominant frequency over a range up to at least 1600 Hz had been measured during 30 psia cold flow. The rig inlet damping devices consisted of three steel boxes, perforated to act as Helmholtz resonators, which were welded to the inlet duct wall between the flow distribution plate and the rig inlet.

15 NOVEMBER 1966

A cold flow test was made to evaluate the effectiveness of the damping devices. No useful data were obtained because the damping boxes failed structurally. Parts of the boxes passed through the diffuser, causing damage to pressure and temperature instrumentation (figure VIII-8).

Cold Flow Time: 1.33 hours

17 NOVEMBER 1966

In a further attempt to improve inlet flow conditions, the facility inlet jet velocity was reduced by increasing the inlet flow distribution plate open area to about 550 sq. in. (the area had been about 380 sq. in.). However, Test Point 122, at an overall fuel/air ratio of 0.035, indicated no change in the level of inlet pressure fluctuations or in combustion instability, which again occurred. Reductions in the inlet pressure and Mach number (Test Points 124 and 127) also had little effect on inlet pressure fluctuations, ignition, or combustion instability characteristics.

The area change to the flow distribution plate created an undesirable circumferential profile at the burner inlet.

Cold Flow Time: 2.75 hours

Combustion Time: 2.67 hours

18 THROUGH 28 NOVEMBER 1966

Additional pressure recording instruments, including diffuser bleed and centerbody pressure transducers, were added as shown in figure VIII-9.

29 NOVEMBER 1966

A combustion test was made (Test Point 131) with the revised pressure instrumentation, figure VIII-9. Pressure oscillations were measured in the centerbody having the same amplitude and frequency as those measured in the inlet duct.

Cold Flow Time: 1.17 hours

Combustion Time: 0.84 hour

1 DECEMBER 1966

A rig test was conducted with radial fins installed in the rig centerbody over the diffuser bleed air discharge openings (figure VIII-10) in an endeavor to suppress possible transverse oscillations. Combustion instability occurred when a fuel/air ratio of 0.035 was reached (Test Point 134). The radial fins had no observed effect on the pressure oscillations in the duct.

For these tests the flow distribution plate open area was decreased to 450 sq. in. Circumferential profile at burner inlet was still unsatisfactory.

Cold Flow Time: 1.25 hours

Combustion Time: 0.67 hour

2 THROUGH 7 DECEMBER 1966

The radial fins were removed. The diffuser bleed air discharge was blocked off and a hole cut in the inlet centerbody nose to provide cooling air for the inner cooling liner. In an attempt to further improve the inlet flow conditions, the flow distribution plate was removed.

8 DECEMBER 1966

A test showed that the inlet flow conditions had been improved. The circumferential distortion was practically eliminated and a very flat rig inlet radial velocity profile was recorded. Peak-to-peak pressure amplitudes of approximately 1 psi, with no predominant frequency up to

1600 Hz, were recorded. Mechanical vibrations of the burner were reduced (figure VIII-11). Combustion instability again occurred with an overall fuel/air ratio of 0.035 (Test Point 139). By increasing the fuel/air ratio of Zone-1 to 0.025, an overall fuel/air ratio of 0.038 was reached before combustion instability occurred (Test Point 140). These tests showed that the diffuser bleed flow did not have a significant effect on the occurrence of combustion instability.

Cold Flow Time: 1.18 hours

Combustion Time: 0.82 hour

9 THROUGH 15 DECEMBER 1966

The diffuser was restored to the original configuration of 1 November. The ID and OD vortex generators were removed from the duct burner to determine the effect of the vortex generators on burner performance and combustion instability. Analysis of previous tests indicated that burner operation affected the combustion stability characteristics whenever the Zone-2 fuel/air ratio significantly exceeded 0.010.

16 DECEMBER 1966

A test was conducted at reduced airflow and pressure levels because the facility fuel supply system could not deliver the flow rate required to test at fuel/air ratios greater than 0.04 with the standard 276 lb/sec airflow. Performance data were obtained at overall fuel/air ratios of 0.044 and 0.049 (Test Points 147 and 148) with no combustion instability occurring. This was the first time the duct burner had been tested at overall fuel/air ratios over 0.038.

This test showed that high combustion efficiency at high fuel/air ratios could be obtained without combustion instability by altering the Zone-2 combustion region.

Cold Flow Time: 2.22 hours

Combustion Time: 1.90 hours

17 DECEMBER 1966

A post-test inspection showed that the centerbody structure and the inner cooling liner had burned. Damage was incurred downstream of a fuel leak at the ID Zone-2 spraybar connection at 142 deg (figure D-31). There was no outer liner damage due to overheating. Liner No. 31 was

dented, probably by a fragment of the burned inner liner. The burned centerbody structural member and inner cooling liner are shown in figures D-14 and VII-10. The rear OD combustor liner had developed several cracks at the trailing edge in the vicinity of welds.

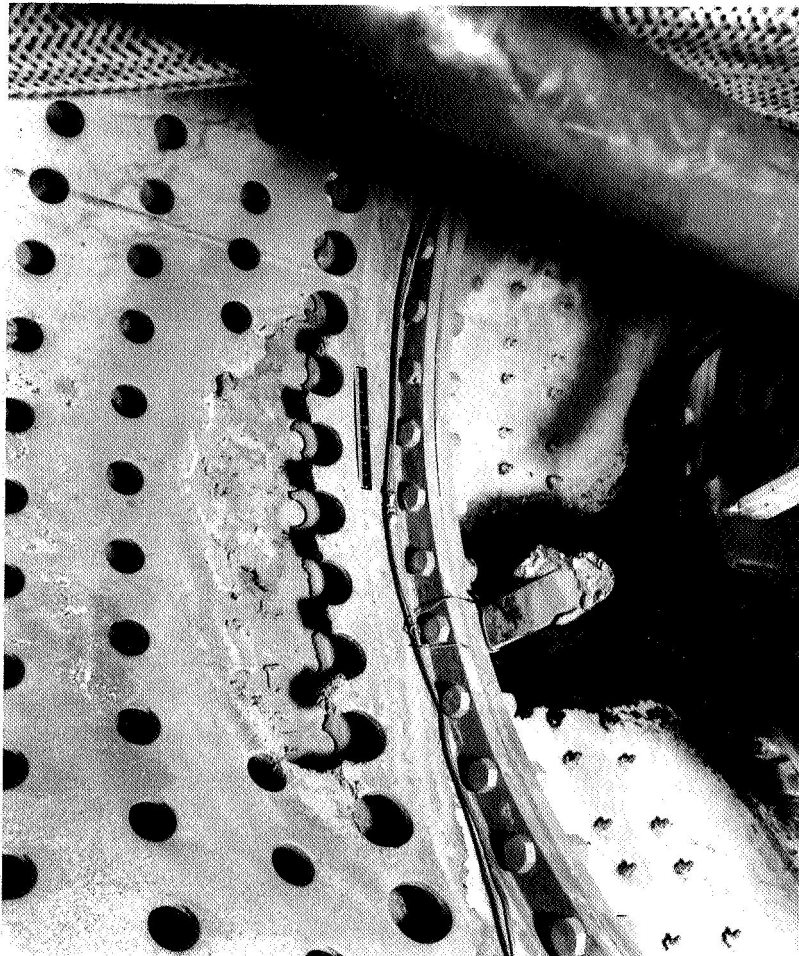


Figure D-14. Centerbody Burned Area

FE 66618

18 DECEMBER 1966 THROUGH 6 FEBRUARY 1967

The inner cooling liner was repaired and modified to incorporate an acoustical damper (figure IV-23). This is explained in more detail in Section IV.

Nozzle seal plates were fabricated to allow the spraybars and fuel lines to be pressurized for leak checks after installation in the rig.

The secondary OD combustor liner was modified by cutting away the trailing edge on 20 of the rear scoops (figure VII-21) to prevent cracks from occurring at the trailing edge near the welds.

Four additional ID Zone-2 spraybar supports were fabricated and installed between the tee and end supports (figure VII-22). These additional supports were necessary to prevent slight spraybar bowing, which had been observed following previous tests.

All fuel and water flow measuring turbine meters were sent to the Florida Research and Development Center for calibration.

The rig was assembled with the new inner damping liner (figure II-18) and with the vortex generators removed.

8 FEBRUARY 1967

A test was conducted at low fuel/air ratios, 0.015 to 0.023, at a simulated cruise condition to check out the facility and obtain burner performance. Data were obtained at Test Points 149 through 158 with Zone-1 fuel injection only.

Cold Flow Time: 1.36 hours

Combustion Time: 1.47 hours

9 FEBRUARY 1967

A test at the transonic climb condition was conducted with the vortex generators removed. Performance data were not obtained because of combustion instability (Test Points 160 through 162, 165, 167, and 170 through 173). Combustion instability was encountered when an overall fuel/air ratio of 0.02 was reached. Changes of the Zone-1 primary and secondary fuel flow split had no noticeable effect on the instability. When the Zone-1 fuel/air ratio remained relatively high, the addition of a small amount of Zone-2 fuel also produced instability. However, when the Zone-1 fuel/air ratio was reduced to 0.014, the Zone-2 fuel flow could be increased until an overall fuel/air ratio of 0.043 was obtained before instability was detected. Instability may have occurred at a lower fuel/air ratio, but it was not recorded. Audible instability occurred at a fuel/air ratio of approximately 0.016 when the inlet pressure and temperature were reduced to 10 psia and 200°F (Test Points 167 and 173). Increasing the inlet temperature to 480°F raised the instability threshold and allowed a fuel/air ratio of 0.05 to be attained. (Test Point 165).

Cold Flow Time: 3.47 hours

Combustion Time: 1.90 hours

10 FEBRUARY 1967

A test was conducted at high fuel/air ratios, 0.033 to 0.050, at the simulated cruise condition, and performance data were obtained at Test Points 175 through 185.

Cold Flow Time: 2.20 hours

Combustion Time: 2.35 hours

13 AND 14 FEBRUARY 1967

The vortex generators were reinstalled to allow determination of inner damping liner effectiveness.

15 FEBRUARY 1967

A test was conducted at the simulated cruise condition. Audible instability occurred with an overall fuel/air ratio of 0.03 (Test Points 188 and 192). An inaudible instability was detected with a fuel/air ratio of 0.025 regardless of the fuel flow distribution (Test Points 187 and 193). At a fuel/air ratio of 0.02 (Test Point 191) some pressure oscillations were detected. The recorded frequencies were somewhat lower than the normal 1700 Hz at cold flow, and the wave form was not fully established. This was considered a marginally stable condition. Instability was also detected at the transonic climb test condition (Test Point 190). Results of this test showed that the inner damping liner did have some effect on the instability characteristics. The damper was designed to suppress noise in the 450 Hz range, and no noise was recorded at that frequency. The vortex generators appeared to be associated with the instability at the cruise condition, but not at the transonic climb condition.

Cold Flow Time: 2.31 hours

Combustion Time: 0.82 hour

16 THROUGH 24 FEBRUARY 1967

Inspection of the burner showed burning of the primary and secondary OD liner scoops downstream of fuel nozzle 36 (figures VII-23 and VII-24). The burner was removed and repaired (figure VII-25). Zone-1 fuel nozzle No. 36 (figure D-9) was found to have a cracked secondary tube (figure D-15);

the burner scoop burning was caused by the resulting fuel leak. Zone-1 fuel nozzle No. 20 had a slight secondary tube crack; however, the leak was minor and no damage occurred. Thirty-seven primary fuel nozzle assemblies were returned to the manufacturer for a 1000-psi hydraulic pressure check. Necessary seal changes were made and the nozzle assemblies were returned and installed. The two fuel nozzle assemblies with cracked secondary tubes were repaired.

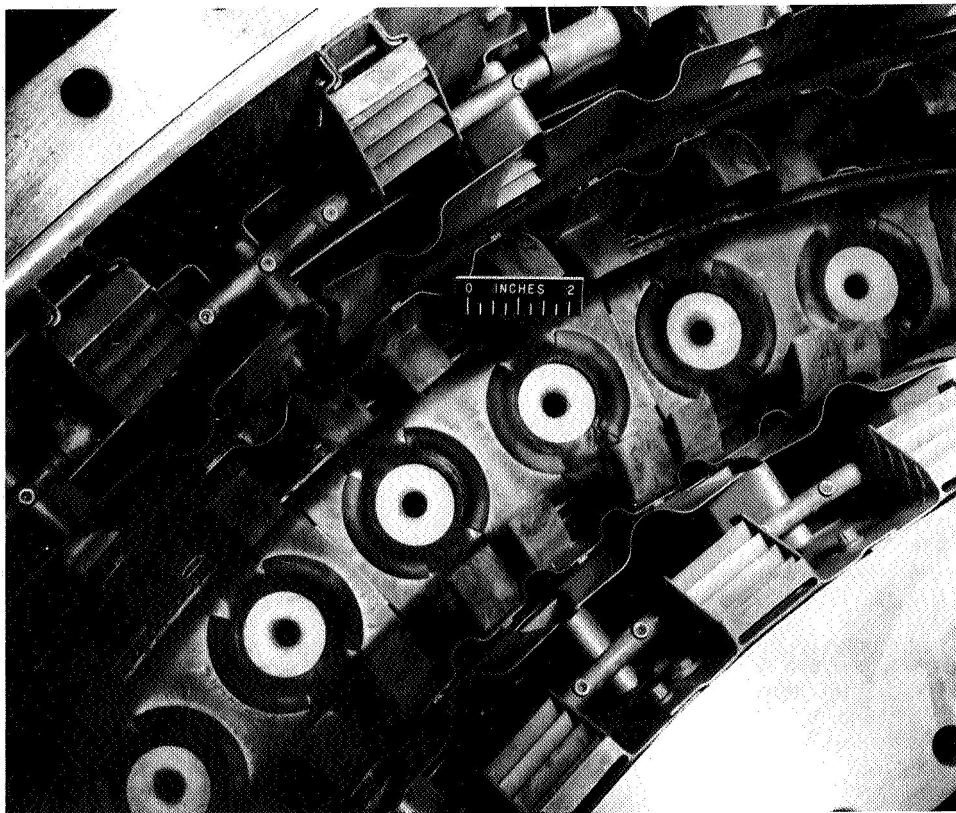


Figure D-15. Cracked Zone-1 Fuel Nozzle
Support Secondary Tube

FE 67936

During rig reassembly, the outer burner case with the attached secondary burner panel was rotated clockwise by one bolt hole. As a result, the OD secondary burner panel scoops no longer opposed the ID scoops; they were aligned axially with the front primary scoops, rather

than the rear primary scoops. The relative scoop locations were shown in figure VIII-12. The vortex generators were not installed. These changes were made to redistribute the burner airflow and determine if this had an effect on combustion stability.

25 FEBRUARY 1967

A test was conducted at the transonic climb condition. Instability occurred at a fuel/air ratio of 0.018 (Test Point 195). This test showed that rotation of the outer secondary burner panel had little effect on combustion stability at the transonic climb condition.

Cold Flow Time: 1.18 hours

Combustion Time: 2.12 hours

27 FEBRUARY 1967

A test was conducted at the transonic climb condition to check the effect of increasing the duct reference Mach number. Instability initially occurred at a fuel/air ratio of 0.015 (Test Point 197). Tests with the Mach number increased to 0.180 resulted in burner velocities too high to sustain combustion. The inlet temperature was increased to 400°F and instability occurred at a fuel/air ratio of 0.019 (Test Point 201). The Mach number was increased to 0.160 and instability occurred at a fuel/air ratio of 0.020 (Test Point 203). During this test a high-frequency response pressure pickup was installed in the Zone-1 primary fuel manifold to determine if any relationship existed between fuel pressure oscillations and combustion instability. Peak-to-peak pressure oscillations of 8 psi were recorded at both stable and unstable combustion conditions, indicating no such relationship in this instance.

Cold Flow Time: 2.41 hours

Combustion Time: 1.02 hours

28 FEBRUARY THROUGH 2 MARCH 1967

The Zone-1 fuel nozzles were removed for structural strengthening to add additional support to the supply tubes (figure VII-26). Two Zone-1 secondary tubes had failed during testing in February.

3 AND 6 MARCH 1967

Cold flow tests were conducted to check and calibrate the airflow measuring orifice differential pressures.

Cold Flow Time: 5.88 hours.

7 THROUGH 22 MARCH 1967

The rig was disassembled and the burner secondary panels removed. The inner and outer secondary liners were modified by cutting away the trailing edge of the rear scoops. This modification had been incorporated in January on half the outer scoops as a remedy for local cracking. The original scoops continued to crack while the modified scoops did not, showing that the modification was satisfactory. The rig was reassembled without the vortex generators and with blockage plates inserted in the inner and outer annuli surrounding the duct burner (figure VIII-13) to create additional pressure drop through the rig. The purpose of this modification was to test the effect of changing the facility/rig interface pressure drop. The blockage plate height was approximately half the annulus height and the plate blocked approximately 25% of the annulus.

23 MARCH 1967

A test was conducted at simulated transonic climb conditions at 10 and 15 psia. Combustion instability occurred at Test Points 207, 209, and 210. The blockage plate increased the isothermal burner pressure drop from 3.5 to 6.25% at a duct reference Mach number of 0.139.

Cold Flow Time: 3.06 hours

Combustion Time: 0.27 hour

24 MARCH 1967

The Zone-1 secondary fuel supply of every other nozzle was blocked off to determine the effect of changing the circumferential fuel distribution with the burner blockage plates installed in the rig.

A test was conducted at the transonic climb condition and with a Zone-1 primary fuel/air ratio of 0.006. The Zone-1 secondary fuel flow was increased to an overall fuel/air ratio of 0.015 when instability

occurred (Test Point 215). Test Points 217, 219 and 222 were run in a similar manner, with the Zone-1 primary fuel/air ratio set at 0.010, 0.012, and 0.004, respectively. The fuel flow splits were found to have little effect on the instability threshold.

The Zone-1 primary fuel flow was then shut off and the burner ignited on the Zone-1 secondary fuel flow. This resulted in fuel being injected only through every other nozzle (20 instead of the regular 40). Satisfactory ignition occurred and the Zone-1 secondary fuel/air ratio was increased to 0.02 with stable combustion. The Zone-2 fuel flow was increased until an overall fuel/air ratio of 0.045 was attained (Test Point 228) with indications of longitudinal instability developing.

Cold Flow Time: 1.18 hours

Combustion Time: 2.12 hours

25 THROUGH 28 MARCH 1967

The burner blockage plates were removed and a simulated transonic climb test at 15 psia was conducted on 28 March. The Zone-1 primary fuel/air ratio was set at 0.014, 0.010, and 0.007, and the Zone-1 secondary fuel flow (every other Zone-1 nozzle) was increased until combustion instability occurred at an overall fuel/air ratio of approximately 0.017 (Test Points 234, 235 and 244, respectively). These points showed little change in instability limits when compared to the 24 March test (with the burner blockage plates installed), although the frequency was changed.

The Zone-1 primary fuel/air ratio was reduced to zero and the Zone-1 secondary (every other Zone-1 nozzle in this test) was set at fuel/air ratios of 0.02, 0.022, and 0.016 (with overall fuel/air ratios increased to 0.037, 0.028 and 0.046, respectively, with Zone-2 augmentation) when instability occurred (Test Points 239, 243, and 245). Although instability frequencies were different in Test Points 239, 243 and 245, the same basic 95-Hz frequency was seen at a fuel/air ratio of 0.044 as that seen in Test Point 228 (fuel/air ratio = 0.045) when the burner blockage plates were installed. During this test, dynamic pressure instrumentation was installed on the Zone-1 secondary fuel manifold, encircling and mounted on the test rig at the top and bottom. The data from the test

showed the fuel to have maximum peak-to-peak pressure amplitudes of 4% of the mean manifold pressure at frequencies of 200, 600, and 800 Hz.

Cold Flow Time: 1.58 hours

Combustion Time: 2.00 hours

29 MARCH 1967

A test was attempted at simulated transonic climb conditions but was terminated due to a fuel leak in a cracked weld in the bypass line in the Zone-2 fuel system.

Cold Flow Time: 1.67 hours

Combustion Time: 0.25 hour

30 MARCH 1967

The fuel system crack was weld-repaired and testing was continued at simulated transonic climb conditions with the same rig configuration as in the previous test. With 15-psia inlet conditions, the 20 Zone-1 secondary fuel nozzles were set to provide fuel/air ratios of 0.013, 0.010, and 0.007 (with overall fuel/air ratios of 0.041, 0.040, and 0.028, respectively, with Zone-2 augmentation) before instability occurred (Test Points 249, 251 and 252). Test Points 256 and 257 showed the effect on stability limits of testing with the 40 Zone-1 fuel nozzles. Test Points 260 through 270 were made at 10 psia. Combustion instability occurred with a Zone-1 primary fuel/air ratio of 0.015 (Test Point 263). Higher fuel/air ratios were obtained by reducing the Zone-1 primary fuel/air ratio and augmenting with Zone-2 (Test Points 262 and 270). Various Zone-1 primary and secondary fuel flow splits were tested (Test Points 264, 265 and 266) with instability occurring at a fuel/air ratio of approximately 0.017. Higher fuel/air ratios were achieved by flowing fuel through the Zone-1 secondary nozzles (20 nozzles in this test) and through Zone-2. Test Points 260, 261, 267, 268 and 269 show the results of these tests.

Cold Flow Time: 3.43 hours

Combustion Time: 4.12 hours

31 MARCH THROUGH 12 APRIL 1967

The rig was disassembled to modify the diffuser to provide higher pressure drop by installing vanes with a 60-degree angle of attack (every other vane was turned in the opposing direction to prevent swirl). The vanes were installed 7-in. downstream of the diffuser inlet (figure VIII-15).

13 APRIL 1967

A test was conducted at simulated transonic climb conditions at 15 psia and 10 psia. The diffuser vanes caused an additional 9.1% drop in pressure, giving the diffuser a total pressure drop of 10.5% with an inlet Mach number of 0.4 (Test Point 271). The simulated transonic climb conditions that resulted in combustion instability are listed in table D-2, Test Points 275, 276, 277, 279, 284, 285, 286, 290, 293 and 299. The installation of the diffuser vanes had no effect on the combustion stability limit obtained with Zone-1 fuel only. However, a definite improvement was seen when flowing only every other Zone-1 nozzle, as the Zone-1 fuel/air ratio exceeded 0.016 and was further augmented by the Zone-2 fuel. This allowed an overall fuel/air ratio of 0.050 to be obtained with the Zone-1 fuel/air ratio set between 0.017 and 0.022. This was the first time that stable combustion with a fuel/air ratio of 0.050 at transonic climb conditions had been accomplished. (The Zone-1 fuel/air ratio had to be greater than 0.017 to obtain an overall fuel/air ratio of 0.050 with stable combustion.) Although testing with 20 nozzles did not reveal a Zone-1 maximum fuel/air ratio limit due to combustion instability, a decrease in combustion efficiency was noted as the Zone-1 fuel/air ratio reached 0.022.

At 10 psia there was an indication that operation with 20 Zone-1 fuel nozzles provided a broader region of stable combustion than did operation with 40 nozzles.

Results of this test showed that the stability of the burner was improved by increasing the facility/rig interface pressure drop with the diffuser vanes and thus implied that a facility/rig interface effect did exist. Although the diffuser vanes were helpful, they disturbed the radial flow distribution.

Cold Flow Time: 2.12 hours

Combustion Time: 5.23 hours

14 APRIL 1967

The diffuser vanes were repositioned to a 30-degree angle of attack to determine if the radial flow distribution could be corrected while maintaining the improved stable combustion range.

A simulated transonic climb test at 10 and 15 psia was conducted at Test Points 300 through 332. The pressure drop caused by the diffuser vanes was 4.0% (decreased from 9.1% in the previous test) resulting in a diffuser total pressure drop of 5.4% at an inlet Mach number of 0.4. At 15 psia the region of combustion stability was narrowed when compared to the previous test, as instability occurred when the Zone-1 fuel/air ratio was increased to 0.022. A more noticeable deterioration in the stable combustion range occurred at 10 psia where a stable burning region with a fuel/air ratio of 0.05 was obtained only over a very narrow range of Zone-1 fuel/air ratio.

Cold Flow Time: 2.50 hours

Combustion Time: 6.13 hours

15 THROUGH 18 APRIL 1967

Since a significant rig/facility interface pressure drop was desired and the diffuser vanes were not completely satisfactory, a heavy inlet screen assembly was installed as shown in figure VIII-19. The diffuser vanes were left as previously tested at a 30-deg angle of attack.

19 THROUGH 20 APRIL 1967

A test was made to investigate the effects of the inlet screen (Test Points 338 through 361). The total pressure drop across the screen was 4.2% with a diffuser inlet Mach number of 0.4. The results of the test did not differ significantly from the previous test of 14 April.

Cold Flow Time: 3.76 hours

Combustion Time: 4.12 hours

21 APRIL 1967

To further increase the total pressure drop across the inlet screen, the screen open area was decreased by welding tubes on the upstream side of the screen assembly. A cold flow test showed no significant increase in total pressure drop across the inlet screen, and no combustion test was made.

Cold Flow Time: 2.22 hours

22 THROUGH 27 APRIL 1967

The original three-mesh inlet screen with 47% blockage area was replaced with a four-mesh inlet screen with 60% blockage area and the diffuser vanes were left at a 30-deg angle of attack.

28 APRIL 1967

A test at the 15-psia transonic climb conditions was conducted using 20 Zone-1 secondary fuel nozzles and no vortex generators. The four-mesh inlet screen provided a significant increase in pressure drop, but it had no significant effect on the combustion stability limit, which remained unchanged from that obtained with the three-mesh inlet screen. The conditions that resulted in combustion instability are listed in table D-2, Test Points 366 through 375 and 379. During this test, the diffuser vanes were set at a 30-deg angle of attack.

Cold Flow Time: 2.00 hours

Combustion Time: 3.22 hours

1 MAY 1967

A test was attempted at 10- and 15-psia transonic climb conditions but was terminated due to a fuel leak on the Zone-1 secondary fuel system caused by a cracked weld just downstream of the pump discharge.

Cold Flow Time: 1.13 hours

Combustion Time: 0.25 hour

2 AND 3 MAY 1967

The fuel leak was weld-repaired and the Zone-1 fuel system was changed to employ all 40 Zone-1 secondary fuel nozzles. Test Points 383 through 407 were conducted on 3 May at the 10- and 15-psia transonic climb conditions. The combustion stability region with 40 Zone-1 secondary nozzles was decreased compared to that with 20 Zone-1 secondary nozzles. Stable combustion was not obtained at a Zone-1 fuel/air ratio greater than 0.018, as compared to a previously obtained fuel/air ratio of 0.023 with 20 Zone-1 secondary nozzles.

Cold Flow Time: 4.52 hours

Combustion Time: 3.08 hours

4 AND 5 MAY 1967

Inspection of the rig showed that the exit nozzle cover plate had warped on the inner wall and the weld on the inlet boss had cracked on the outer wall, as shown in figure D-16. The warpage was attributed to the inlet and outlet cooling water lines being reversed during the previous rig reassembly, causing overpressurization in the cooling passages. The damage was not considered to be detrimental to the cooling of the cover plate. To verify this, three thermocouples were installed on the outside wall as shown in figure D-16. These indicated the cover plate to be adequately cooled.

New-design turbulators (figure VII-27) were then installed in the burner at the vortex generator locations. Simulated 10- and 15-psia transonic climb tests (Test Points 409 through 429) were conducted on 5 May 1967. The results showed that combustion instability occurred at slightly lower overall fuel/air ratios than without vortex generators. When compared to configurations containing no vortex generators, data showed that the combustion efficiency was increased with the turbulators installed.

Cold Flow Time: 3.68 hours

Combustion Time: 3.00 hours

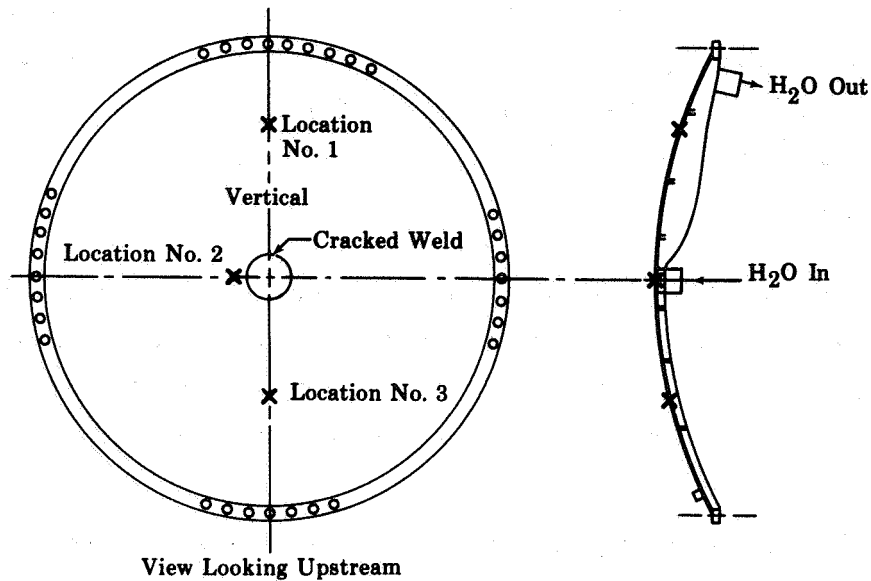


Figure D-16. Cover Plate Damage and T/C Installation

FD 22557

8 MAY 1967

A test was conducted to obtain performance data at simulated cruise conditions with the turbulators installed (Test Points 431 through 440). A total of 40 Zone-1 primary nozzles and 20 Zone-1 secondary nozzles were employed.

Cold Flow Time: 1.75 hours

Combustion Time: 1.83 hours

10 MAY 1967

A test was conducted at 30-psia cruise conditions (Test Points 442 through 458). Test results indicated that varying the Zone-1 fuel/air ratio had no obvious effect on the combustion instability region. It was noted that combustion instability always occurred when the Zone-2 fuel/air ratio reached 0.015, indicating that the Zone-2 fuel injection and/or combustion zone affected the stability region. This was not the case at the 10- and 15-psia test conditions. It was also noted that the dominant instability frequency was 470 Hz compared to the 300 Hz that occurred previously when the vortex generators were installed.

Cold Flow Time: 1.78 hours

Combustion Time: 2.42 hours

11 THROUGH 14 MAY 1967

The Zone-1 fuel system was changed to utilize all 40 primary and secondary nozzles to allow higher Zone-1 fuel/air ratios to be tested. The radial diffuser vanes were removed.

15 MAY 1967

A test was conducted at 30-psia cruise conditions (Test Points 460 through 471). Results show no significant change from the previous test. Increasing the Zone-1 fuel/air ratio to 0.028 had no effect on the combustion stability region. Removal of the 30-degree diffuser vanes also had no effect.

The test was terminated when the facility air supply line bellows failed.

Cold Flow Time: 0.84 hour

Combustion Time: 2.48 hours

16 MAY THROUGH 1 JUNE 1967

The facility air supply line bellows was removed and a new liner was installed with flow-straightening tubes (figure D-17). The rig geometry was changed by removing every other turbulator on both the ID and OD.

2 JUNE 1967

A test was conducted at simulated cruise conditions at reduced temperatures to investigate combustion instability with every other turbulator removed on both the ID and OD (Test Points 472 through 477). The test was terminated because the facility preheater would not work.

The range of stable operation was widened from previous tests. The test did not adequately demonstrate the effects of removal of every other turbulator because the burner inlet temperature of 550°F could not be obtained.

Cold Flow Time: 1.85 hours

Combustion Time: 2.40 hours

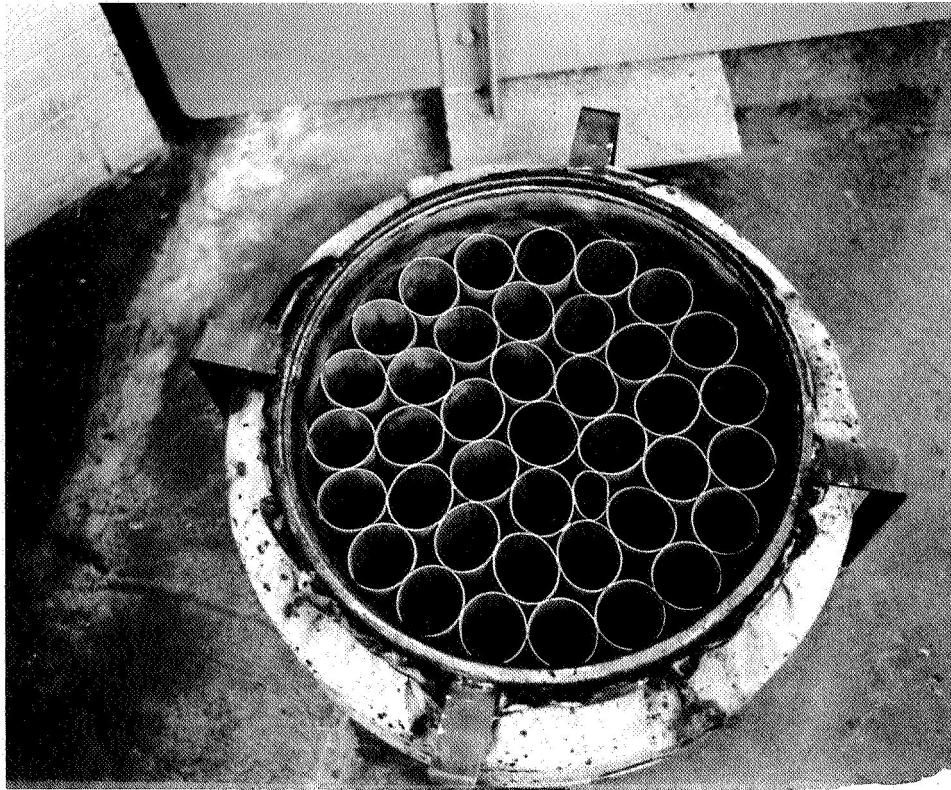


Figure D-17. Inlet Bellows Modification

FE 71983

3 THROUGH 9 JUNE 1967

The facility preheater was found to be failing structurally, allowing some of the heater air to bypass the heat exchanger tubes. This failure caused the preheater to give air temperatures too low while having excessive combustion gas temperature. Temporary repairs were made so that testing could be continued without delay.

10 JUNE 1967

A test was conducted at simulated cruise conditions to investigate combustion instability with every other turbulator removed on both the ID and the OD (Test Points 479 through 488). The range of stable operation was slightly improved by this configuration at Zone-1 fuel/air ratios less than 0.020. Performance data were obtained at Test Points 486 and 487.

The Zone-2 ID spraybars were blocked off to investigate unsymmetrical fuel injection into the burner at Test Points 490 through 495. The test results indicate that this variation in fuel injection did not improve the range of stable operation. With the Zone-1 fuel/air ratio at 0.030, a performance data point was obtained at an overall fuel/air ratio of 0.050 (Test Point 495).

Cold Flow Time: 2.55 hours

Combustion Time: 5.12 hours

11 THROUGH 15 JUNE 1967

The fuel injection system was changed by restoring the Zone-2 ID spraybars and replacing six of the ten OD high-flow spraybars with low-flow spraybars (figure VII-39). All turbulators were installed on both the ID and the OD.

16 JUNE 1967

A test was conducted at simulated cruise conditions (Test Points 497 through 509). The stable operating range was not improved over that of previous tests in the Zone-1 fuel/air ratio range of 0.01 to 0.030. However, a stable overall fuel/air ratio of 0.050 was achieved by operating Zone-1 above a fuel/air ratio of 0.030 and augmenting with the Zone-2 fuel. Performance data were obtained at Test Points 497, 499 through 501, and 507.

Cold Flow Time: 1.87 hours

Combustion Time: 3.73 hours

17 THROUGH 19 JUNE 1967

The six Zone-2 low-flow OD spraybars were removed and the original high-flow spraybars were installed, restoring the Zone-2 to the original design configuration.

20 JUNE 1967

A test was conducted at simulated cruise conditions and performance was obtained at cruise fuel/air ratios of 0.016 to 0.025, Test Points 512 through 526, table D-II.

Cold Flow Time: 1.87 hours

Combustion Time: 3.73 hours

21 JUNE 1967

Every other Zone-1 secondary fuel nozzle was capped off and a test at simulated transonic climb conditions at 10 psia was attempted but was terminated because of an ignition difficulty.

22 JUNE 1967

The ignition difficulty was found to be in the facility power system and was corrected. A test was conducted at simulated transonic conditions at 10 psia to obtain performance data (Test Points 528 through 536). Performance data were not obtained because of combustion instability. The range of stable operation was significantly reduced from previous tests (when the diffuser vanes were installed). The pressure drop produced by the screen in the rig inlet was apparently not as effective as the pressure drop produced by the vanes in the diffuser.

Cold Flow Time: 1.60 hours

Combustion Time: 1.57 hours

23 JUNE 1967

The number of Zone-1 secondary fuel nozzles were restored to 40 and a test was conducted at simulated cruise conditions to obtain performance data (Test Points 538 through 543 and 545 through 555). Combustion instability occurred at an overall fuel/air ratio of 0.046 with a Zone-1 fuel/air ratio of 0.030. With Zone-1 fuel/air ratios above 0.030, combustion instability was not encountered.

Cold Flow Time: 3.67 hours

Combustion Time: 2.50 hours

26 JUNE 1967

Every other Zone-1 secondary fuel nozzle was capped off and three additional blockage rings were added to the inlet screen to provide additional pressure drop (figure VIII-26).

A test was conducted at 10-psia transonic climb conditions (Test Points 557 through 578) to obtain performance data. Combustion instability occurred over a wide range of fuel/air ratios. With a Zone-1 fuel/air ratio of 0.016, stable operation at an overall 0.050 fuel/air ratio could

be achieved. Then by increasing the Zone-1 fuel/air ratio and decreasing the Zone-2 fuel/air ratio, stable operation was obtained at overall 0.050 fuel/air ratios with Zone-1 fuel/air ratios of 0.018, 0.020, and 0.022 (Test Points 572, 573, and 574, respectively). Performance data were obtained at Test Points 560 through 563, 565 through 569, 571, 574, 576, and 577.

Cold Flow Time: 1.85 hours

Combustion Time: 2.20 hours

27 JUNE 1967

A test was conducted at simulated 15-psia transonic climb conditions (Test Points 580 through 614). Performance data were obtained at Test Points 580 through 588, 590 through 592, 598, 601 through 606, and 608 through 613. Combustion instability was evident at some test points and the range of stable operation was significantly lower than the tests in which the diffuser vanes were installed. While testing with a Zone-1 secondary fuel/air ratio of 0.014, combustion instability occurred when an overall fuel/air ratio of 0.040 was reached.

Cold Flow Time: 1.70 hours

Combustion Time: 3.55 hours

28 THROUGH 30 JUNE 1967

The rig was disassembled for a final burner inspection. No failed or distressed parts were observed.

Table D-1. Cold Calibration Tests

Test Point	Date	CADDE No.	Burner Inlet Conditions					Diffuser Inlet Mach Number	Duct Reference Mach No.	P_{s5}/P_{T5}	C_{d5}
			Airflow, W_a , lb/sec	Pressure, P_{T4} , psia	Temperature, T_4 , °F						
1	5-19 & 20-66		200				0.500				
2	5-25-66	15	300	32.9	90		0.371		0.126	0.959	1.127
3	5-25-66	16	299	27.0	90		0.485		0.154	0.929	1.082
4	5-25-66	17	300	23.9	87		0.577		0.175	0.908	1.123
5	5-25-66	18	299	21.8	87		0.688		0.192	0.873	1.091
6	5-25-66	19	300	20.1	88		0.782		0.210	0.834	1.066
7	5-25-66	20	302	17.9	86		0.863		0.238	0.575	1.007
8	5-25-66	21	302	18.0	85		0.864		0.237	0.653	1.017
9	5-25-66	22	300	18.3	88		0.865		0.232	0.747	1.037
10	5-25-66	23	300	17.8	86		0.868		0.238	0.569	1.003
11	5-25-66	24	302	17.9	86		0.866		0.238	0.575	1.008
12	5-25-66	25	300	17.9	88		0.863		0.238	0.613	1.013
13	5-25-66	26	300	18.0	87		0.864		0.235	0.693	1.029
14	5-26-66	30	130	7.9	78		0.855		0.231	0.565	0.961
15	5-26-66	31	89	5.4	81		0.857		0.229	0.540	0.908
16	5-26-66	32	153	9.1	76		0.857		0.235	0.566	0.975
17	5-26-66	33	153	18.3	88		0.341		0.116	0.970	1.184
18	5-26-66	34	152	13.0	88		0.519		0.163	0.912	1.025
19	5-26-66	35	152	11.8	89		0.587		0.180	0.890	1.034
20	5-26-66	36	152	10.8	88		0.681		0.198	0.857	1.024

*Includes H₂O vapor present in combustor air

Table D-1. Cold Calibration Tests (Continued)

Test Point	Date	CADDE No.	Burner Inlet Conditions					Diffuser Inlet Mach Number	Duct Reference Mach No.	P_{s5}/P_{T5}	C_{d5}
			Airflow, W_a , lb/sec	Pressure, P_{T4} , psia	Temperature, T_{T4} , °F						
21	5-26-66	37	152	10.4	89			0.744	0.207	0.831	1.021
22	5-26-66	38	152	9.3	88			0.861	0.231	0.756	1.016
23	5-26-66	39	152	9.4	88			0.854	0.227	0.768	1.006
24	5-26-66	40	152	9.6	88			0.846	0.225	0.781	1.015
25	5-26-66	41	152	9.1	85			0.857	0.235	0.642	0.995
26	5-26-66	42	150	9.1	86			0.858	0.233	0.587	0.972
27	5-26-66	43	152	9.1	84			0.860	0.234	0.572	0.986
28	5-26-66	44	151	9.1	84			0.859	0.234	0.572	0.984
29	5-26-66	45	152	9.1	83			0.861	0.235	0.571	0.987
30	5-26-66	46	152	9.1	84			0.856	0.235	0.572	0.987
31	6-20-66	80, 81	314	26.6	76			0.531	0.162	0.909	1.032
32	6-20-66	82, 83	314	19.5	79			0.838	0.226	0.651	0.994
33	6-20-66	84, 85	314	19.5	78			0.838	0.225	0.576	0.977
34	6-20-66	86, 87	314	19.4	76			0.839	0.226	0.578	0.980
35	6-29-66	94	157	9.6	88			0.846	0.232	0.643	0.992
36	6-29-66	95	157	9.5	89			0.851	0.235	0.607	0.978
37	6-29-66	96	188	14.6	97			0.632	0.181	0.885	1.039
38	6-29-66	97	190	14.7	96			0.629	0.181	0.884	1.039
39	7-01-66	104, 105	143	8.5	87			0.848	0.237	0.574	0.975
40	7-01-66	106, 107	143	12.4	95			0.516	0.162	0.915	1.045

Table D-1. Cold Calibration Tests (Continued)

Test Point	Date	CADDE No.	Burner Inlet Conditions					Diffuser Inlet Mach Number	Duct Reference Mach No.	P_{S5}/P_{T5}	C_{d5}
			Airflow, W_a , lb/sec	Pressure, P_{T4} , psia	Temperature, T_{T4} , °F						
41	7-01-66	108, 109	299	18.5	74			0.835	0.225	0.575	0.962
42	7-01-66	110, 111	301	25.1	83			0.560	0.166	0.906	1.036
43	7-12-66	122, 123	150	9.4	92			0.848	0.225	0.577	0.955
44	7-12-66	124, 125	157	14.0	93			0.517	0.157	0.918	1.035
45	7-12-66	126, 127	283	17.6	77			0.829	0.225	0.601	0.956
46	7-12-66	128, 129	282	24.4	82			0.540	0.160	0.895	0.938
47	7-13-66	136, 137	281	23.7	82			0.566	0.164	0.887	0.946
48	7-13-66	138	281	18.0	75			0.825	0.218	0.684	0.926
49	7-13-66	139	281	18.0	76			0.827	0.218	0.632	0.939
50	7-13-66	140	280	17.9	76			0.828	0.219	0.576	0.942
51	7-13-66	141	281	17.9	74			0.828	0.219	0.575	0.940
52	7-13-66	142	280	17.9	78			0.831	0.219	0.574	0.943
53	7-13-66	149	111	12.7	337			0.462	0.147	0.933	1.047
54	7-14-66	150	256	28.8	95			0.555	0.170	0.907	1.058
55	7-14-66	151, 152	257	28.6	114			0.574	0.175	0.900	1.057
56	7-14-66	160	157	12.3	87			0.600	0.177	0.890	1.038
57	7-15-66	161, 162	265	29.5	597			0.571	0.175	0.898	1.057
58	7-15-66	163, 164	293	24.6	590			0.865	0.235	0.579	0.987
59	7-15-66	165	287	24.3	589			0.863	0.233	0.578	0.980

Table D-2. Combustion Tests

Test Point	Date	CADDE Number	Burner Inlet Conditions				Duct Reference Mach Number	Fuel/Air Ratio			Overall	Combustion Efficiency, %	Instability	Dominant Frequency, Hz
			Airflow*, W _a , lb/sec	Pressure, P _{T4} , psia	Temperature, T _{T4} , °F	Zone 1 Primary		Zone 2 Secondary	Zone 2					
Test Rig configuration as originally installed; inlet plenum contained vertical perforated pipe, flow distribution plate open area 380 in. ²														
60	7-26-66	173	152.4	24.8	396	0.106	--	--	--	--	--	No	--	
61	7-26-66	174	180.0	25.0	400	0.126	0.005	--	--	0.005	--	No	--	
62	7-26-66	175	220.0	23.7	335	0.156	--	--	--	--	--	No	--	
63	7-26-66	176	280.0	24.6	226	0.178	--	--	--	--	--	No	--	
64	7-26-66	177	280.0	24.6	230	0.179	0.004	--	--	0.004	--	No	--	
65	7-27-66	184	270.0	30.0	543	0.170	--	--	--	--	--	No	--	
66	7-27-66	185	270.4	30.0	537	0.171	0.005	--	--	0.005	--	No	--	
67	7-27-66	186	271.6	29.0	528	0.176	0.007	0.009	--	0.016	--	No	--	
68	7-29-66	192-193	273.7	29.5	618	0.182	--	--	--	--	--	No	--	
69	7-29-66	194-195	278.0	29.4	547	0.180	--	--	--	--	--	No	--	
70	7-29-66	196	277.7	29.3	552	0.181	--	--	--	--	--	No	--	
71	7-29-66	197-198	278.2	29.6	551	0.179	0.005	--	--	0.005	--	No	--	
72	7-29-66	199-200	277.0	29.4	552	0.180	0.007	0.013	--	0.020	--	No	--	
73	8-2-66	206-207	270.3	29.8	542	0.171	--	--	--	--	--	No	--	
74	8-2-66	208	254.0	29.9	584	0.164	0.007	0.023	--	0.030	--	No	--	
75	8-4-66	214	276.9	29.8	544	0.177	--	--	--	--	--	No	--	
76	8-4-66	215	275.8	29.8	548	0.176	0.007	--	--	0.007	--	No	--	
77	8-5-66	221	281.4	29.8	548	0.179	--	--	--	--	--	No	--	
78	8-5-66	222	281.3	30.0	549	0.179	0.006	0.013	--	0.019	--	No	--	
79	8-5-66	223-224	281.8	30.0	546	0.178	0.007	0.013	0.010	0.030	91.6	No	--	
80	8-5-66	225-226	282.2	30.0	549	0.178	0.007	0.013	0.010	0.030	90.7	No	--	
81	8-5-66	227-228	283.4	29.9	544	0.180	0.007	0.022	--	0.029	90.5	Yes	180	
82	8-6-66	234	276.8	30.1	549	0.175	--	--	--	--	--	No	--	
83	8-6-66	235-236	276.5	30.1	550	0.175	0.006	0.013	0.011	0.030	--	No	--	
84	8-6-66	237-238	276.8	30.0	548	0.176	0.006	0.013	0.011	0.030	91.9	No	--	
85	8-6-66	239	276.6	29.9	548	0.177	0.007	0.021	--	0.028	--	Yes	180	
86	8-6-66	240	276.0	29.9	549	0.176	0.007	0.003	0.019	0.029	--	Yes	--	
87	8-9-66	245	278.9	30.1	521	0.174	--	--	--	--	--	No	--	
88	8-9-66	246-247	275.8	30.2	521	0.170	0.007	0.016	--	0.023	90.9	Yes	180	
89	8-9-66	248-249	275.3	30.2	522	0.168	0.004	0.019	--	0.023	90.7	Yes	180	
90	8-9-66	250-251	277.8	30.2	505	0.170	0.007	0.003	0.016	0.026	81.7	No	--	

*Includes H₂O vapor present in combustion air

Table D-2. Combustion Tests (Continued)

Test Point	Date	CADDE Number	Burner Inlet Conditions			Duct Reference Mach Number	Fuel/Air Ratio			Overall	Combustion Efficiency, %	Instability	Dominant Frequency, Hz
			Airflow, W_a , lb/sec	Pressure, P_{T4} , psia	Temperature, T_{T4} , °F		Zone 1 Primary	Zone 1 Secondary	Zone 2				
91	8-18-66	258	278.0	30.5	534	0.172	--	--	--	--	No	--	
92	8-24-66	262	278.4	29.6	545	0.175	--	--	--	--	No	--	
93	8-24-66	263	277.5	29.5	552	0.179	0.007	0.018	--	0.025	Yes	--	
94	8-24-66	264-265	278.0	29.5	551	0.177	0.007	0.014	0.010	0.031	No	--	
95	8-24-66	266	277.4	29.5	548	0.180	--	--	--	--	No	--	
96	8-24-66	267-268	280.6	29.5	552	0.182	0.007	0.013	0.012	0.032	No	--	
97	8-24-66	269-270	280.2	29.5	553	0.182	0.007	0.013	0.014	0.034	No	--	
98	8-24-66	271-272	279.7	29.7	553	0.181	0.007	0.013	0.016	0.036	No	--	
99	8-25-66	277	277.7	29.3	547	0.180	--	--	--	--	No	--	
100	8-25-66	278-279	278.7	29.0	547	0.183	0.007	0.013	0.018	0.038	Yes	180	
101	8-25-66	280-281	278.5	29.2	543	0.181	0.007	0.011	0.018	0.036	Yes	180	
102	8-25-66	282-283	278.1	29.2	544	0.181	0.007	0.015	0.016	0.038	No	--	
103	8-25-66	284-285	278.6	29.2	542	0.181	0.007	0.015	0.018	0.040	Yes	180	
New burner* installed with diffuser bleed plates* and nose cone damping liners* installed.													
104	11-1-66	291-292	292.0	29.3	76	0.137	--	--	--	--	No	--	
105	11-1-66	293-294	328.8	29.2	75	0.154	--	--	--	--	No	--	
106	11-1-66	301-302	275.0	30.0	75	0.125	--	--	--	--	No	--	
107	11-2-66	303-304	275.0	30.0	535	0.173	--	--	--	--	No	--	
108	11-4-66	313-314	283.2	30.0	556	0.175	--	--	--	--	No	--	
109	11-4-66	315-316	281.5	29.7	550	0.175	0.007	0.011	--	0.018	No	--	
110	11-4-66	317-318	283.2	29.8	555	0.175	0.006	0.013	--	0.019	No	--	
111	11-9-66	325-326	277.0	30.4	533	0.172	--	--	--	--	No	--	
112	11-9-66	327	277.7	30.2	536	0.174	0.007	0.015	--	0.022	No	--	
113	11-9-66	328-329	277.0	30.7	551	0.172	0.007	0.013	--	0.020	No	--	
114	11-9-66	330-331	275.6	29.5	531	0.176	0.007	0.013	0.010	0.030	No	--	
115	11-9-66	332	275.7	29.2	529	0.178	0.007	0.013	0.015	0.035	Yes	450	
116	11-9-66	333	276.7	28.3	528	0.185	0.007	0.015	0.013	0.035	Yes	450	
117	11-9-66	334	276.0	29.1	530	0.179	0.007	0.011	0.014	0.032	Yes	--	
Installed acoustical boxes in the inlet plenum													
118	11-15-66	340-341	277.5	29.8	533	0.176	--	--	--	--	No	--	
Removed the blockage plates on the flow distribution plate so open area was 550 sq in.													
119	11-17-66	347-348	274.0	30.2	542	0.172	--	--	--	--	No	--	
120	11-17-66	349-350	274.6	30.4	546	0.172	0.007	0.013	--	0.020	No	--	
121	11-17-66	351-352	275.0	30.3	545	0.172	0.007	0.013	0.010	0.030	No	--	
122	11-17-66	353	275.0	29.2	544	0.179	0.007	0.013	0.015	0.035	Yes	450	

*This change was incorporated for the duration of the test program.

Table D-2. Combustion Tests (Continued)

Test Point	Date	CADDE Number	Burner Inlet Conditions			Duct Reference Mach Number	Fuel/Air Ratio			Overall	Combustion Efficiency, %	Instability	Dominant Frequency, Hz
			Airflow, W_a , lb/sec	Pressure, P_{T4} , psia	Temperature, T_{T4} , °F		Zone 1 Primary	Zone 1 Secondary	Zone 2				
123	11-17-66	354	276.4	29.2	542	0.180	0.007	0.013	0.015	0.035	--	Yes	450
124	11-17-66	355	235.2	29.4	542	0.151	0.008	0.012	0.013	0.033	--	Yes	--
125	11-17-66	356	137.9	14.8	534	0.176	--	--	--	--	--	No	--
126	11-17-66	357	137.9	15.2	539	0.172	0.014	0.006	0.010	0.030	--	No	--
127	11-17-66	358	136.7	15.1	540	0.171	0.013	0.006	0.016	0.035	--	Yes	450
128	11-17-66	359	137.4	15.2	541	0.171	0.014	0.006	0.020	0.040	--	Yes	450
129	11-29-66	366	272.2	29.8	540	0.173	--	--	--	--	--	No	--
130	11-29-66	367	272.7	29.8	542	0.174	0.007	--	--	0.007	--	No	--
131	11-29-66	368-369	272.4	30.0	541	0.172	0.007	0.014	0.010	0.031	--	No	--
Radial fins installed in the rig centerbody and added blockage so the flow distribution plate area was 480 sq. in.													
132	12-1-66	375-376	272.2	29.8	538	0.173	--	--	--	--	--	No	--
133	12-1-66	377-378	276.4	29.9	536	0.175	0.007	0.013	0.010	0.030	--	No	--
134	12-1-66	379	274.1	29.1	541	0.179	0.007	0.013	0.015	0.035	--	Yes	--
Removed flow distribution plates*, blocked diffuser bleed, cut hole in the inlet nose cone, and radial fins removed from the rig centerbody.													
135	12-8-66	385-386	275.4	29.5	535	0.176	--	--	--	--	--	No	--
136	12-8-66	387	280.6	29.6	537	0.180	0.007	0.013	--	0.020	--	No	--
137	12-8-66	388	280.5	29.7	538	0.179	0.007	0.013	0.010	0.030	--	No	--
138	12-8-66	389	280.2	30.0	538	0.177	0.006	0.018	0.010	0.034	--	No	--
139	12-8-66	390	281.2	29.3	537	0.182	0.007	0.013	0.015	0.035	--	Yes	--
140	12-8-66	391	282.3	29.4	537	0.182	0.007	0.018	0.013	0.038	--	Yes	--
Diffuser bleed and inlet nose cone restored to 1 November 1966 condition and vortex generators removed.													
141	12-16-66	398	282.1	30.1	539	0.178	--	--	--	--	--	No	--
142	12-16-66	399-400	282.1	30.0	544	0.178	0.007	0.013	0.010	0.030	--	No	--
143	12-16-66	401-402	281.8	30.1	557	0.175	0.007	0.013	0.015	0.035	--	No	--
144	12-16-66	404	281.4	30.5	554	0.175	0.007	0.013	0.020	0.040	--	No	--
145	12-16-66	405	214.8	22.8	555	0.176	0.009	0.011	0.010	0.030	--	No	--
146	12-16-66	406	215.4	23.3	557		0.009	0.011	0.020	0.040	--	No	--
147	12-16-66	407	215.6	24.1	546	0.170	0.009	0.011	0.024	0.044	96.9	No	--
148	12-16-66	408	215.7	24.1	549	0.170	0.008	0.011	0.030	0.049	96.8	No	--

*This change was incorporated for the duration of the test program.

Table D-2. Combustion Tests (Continued)

Test Point	Date	CADDE Number	Burner Inlet Conditions			Duct Reference Mach Number	Fuel/Air Ratio			Overall	Combustion Efficiency, %	Instability	Dominant Frequency, Hz
			Airflow, \dot{W}_a , lb/sec	Pressure, P_{t4} , psia	Temperature, T_{t4} , °F		Zone 1 Primary	Zone 1 Secondary	Zone 2				
Inner absorption liner installed* and 20 OD secondary scoops modified, vortex generators removed.													
149	2-8-67	415-416	270.9	29.2	522	0.174	--	--	--	--	No	--	
150	2-8-67	417-418	275.4	29.8	532	0.174	0.007	0.013	0.020	87.0	No	--	
151	2-8-67	419	274.2	29.4	537	0.176	0.007	0.012	0.019	87.8	No	--	
152	2-8-67	420	275.5	29.1	534	0.179	0.007	0.011	0.018	87.5	No	--	
153	2-8-67	421	276.0	28.8	533	0.181	0.007	0.010	0.017	87.0	No	--	
154	2-8-67	422	277.0	28.4	532	0.185	0.007	0.009	0.016	87.8	No	--	
155	2-8-67	423	275.3	28.0	532	0.186	0.007	0.008	0.015	87.7	No	--	
156	2-8-67	424	276.1	29.5	534	0.177	0.007	0.014	0.021	86.5	No	--	
157	2-8-67	425	276.3	29.8	532	0.175	0.007	0.015	0.022	86.5	No	--	
158	2-8-67	426	275.8	30.1	533	0.173	0.007	0.016	0.023	86.3	No	--	
159	2-9-67	432	295.9	14.8	285	0.153	--	--	--	--	No	--	
160	2-9-67	433	139.0	15.0	285	0.144	0.006	0.014	0.020	--	Yes	180	
161	2-9-67	434	137.7	15.3	286	0.146	0.014	--	0.036	86.3	Yes	98	
162	2-9-67	435	138.1	14.8	285	0.151	0.014	--	0.029	0.043	Yes	Unknown	
163	2-9-67	436	92.0	10.1	190	0.138	--	--	--	--	No	--	
164	2-9-67	437	76.5	10.2	459	0.135	--	--	--	--	No	--	
165	2-9-67	438	75.3	10.0	479	0.137	0.020	--	0.030	0.050	Yes	98	
166	2-9-67	439	88.4	11.1	233	0.124	--	--	--	--	No	--	
167	2-9-67	440	88.0	9.9	242	0.124	0.016	--	0.016	--	Yes	170	
168	2-9-67	441	272.5	28.8	538	0.175	--	--	--	--	No	--	
169	2-9-67	442	274.3	28.9	539	0.180	0.007	0.013	0.020	--	No	--	
170	2-9-67		139.0	15.0	285	0.144	0.007	0.013	0.020	--	Yes	Unknown	
171	2-9-67		139.0	15.0	285	0.144	0.013	0.005	0.002	0.020	Yes	Unknown	
172	2-9-67		134.0	15.0	285	0.144	0.010	--	0.022	0.032	Yes	--	
173	2-9-67		91.0	10.0	200	0.138	0.015	--	0.002	0.017	Yes	170	
174	2-10-67	447	226.8	24.2	539	0.178	--	--	--	--	No	--	
175	2-10-67	448	226.6	24.6	543	0.175	0.008	0.011	0.023	93.8	No	--	
176	2-10-67	449	226.9	24.7	541	0.174	0.008	0.011	0.023	94.0	No	--	
177	2-10-67	450	227.8	24.8	546	0.175	0.008	0.011	0.023	93.7	No	--	
178	2-10-67	451	217.9	24.9	556	0.167	0.009	0.011	0.030	94.2	No	--	
179	2-10-67	452	295.0	28.9	547	0.195	0.006	0.013	0.014	84.4	No	--	

* This change was incorporated for the duration of the test program.

Table D-2. Combustion Tests (Continued)

Test Point	Date	CADDE Number	Burner Inlet Conditions			Fuel/Air Ratio			Combustion Efficiency, %	Instability	Dominant Frequency, Hz
			Airflow, \dot{W}_a , lb/sec	Pressure, P_{T4} , psia	Temperature, T_{T4} , °F	Duct Reference Mach Number	Zone 1 Primary	Zone 2 Secondary			
180	2-10-67	453	296.3	29.3	543	0.193	0.006	0.012	0.015	0.033	--
181	2-10-67	454	296.2	30.0	543	0.188	0.006	0.012	0.017	0.035	--
182	2-10-67	455	296.9	30.7	540	0.184	0.006	0.013	0.018	0.037	--
183	2-10-67	456	296.5	33.1	540	0.170	0.006	0.012	0.027	0.045	--
184	2-10-67	457	296.2	32.3	540	0.174	0.006	0.013	0.023	0.042	--
185	2-10-67	458	295.2	32.9	540	0.170	0.006	0.013	0.026	0.045	--
Vortex generators installed and 20 OD secondary scoops were modified.											
186	2-15-67	464	274.9	28.6	542	0.183	--	--	--	--	--
187	2-15-67	465	279.9	28.4	545	0.188	0.007	0.018	--	0.025	300
188	2-15-67	466	279.7	26.9	545	0.199	0.007	0.008	0.014	0.029	315
189	2-15-67	469	135.8	14.7	280	0.150	--	--	--	--	--
190	2-15-67	470	135.7	14.7	280	0.149	0.014	0.005	--	0.019	185
191	2-15-67		276.0	29.0	550	0.181	0.007	0.013	--	0.020	Unknown
192	2-15-67		276.0	29.0	540	0.183	0.007	0.013	0.010	0.030	Unknown
193	2-15-67		276.0	29.0	550	0.181	0.007	0.013	0.005	0.025	310
Vortex generators removed, the outer burner case rotated 1 bolt hole, and 20 OD secondary scoops were modified.											
194	2-25-67	475	135.0	15.0	285	0.144	--	--	--	--	--
195	2-25-67		135.0	15.0	285	0.144	0.014	0.004	--	0.018	Unknown
196	2-27-67	480	90.3	9.6	198	0.143	--	--	--	--	--
197	2-27-67	481	88.6	9.9	211	0.137	0.015	--	--	0.015	Unknown
198	2-27-67	482	116.6	9.8	194	0.182	--	--	--	--	--
199	2-27-67	483	103.6	9.6	196	0.165	--	--	--	--	--
200	2-27-67	484	89.6	11.2	385	0.139	--	--	--	--	--
201	2-27-67	485	89.8	11.1	388	0.140	0.019	--	--	0.019	Unknown
202	2-27-67	486	102.6	11.3	388	0.158	--	--	--	--	--
203	2-27-67	487	102.2	11.2	394	0.160	0.015	0.005	--	0.020	Unknown
204	3-3-67	490 through 499	Test conducted to checkout combustion air orifice instrumentation								
205	3-6-67	500 through 508	Test conducted to checkout combustion air orifice instrumentation								

*This change was incorporated for the duration of the program.

Table D-2. Combustion Tests (Continued)

Test Point	Date	CADDE Number	Burner Inlet Conditions			Duct Reference Mach Number	Fuel/Air Ratio				Overall	Combustion Efficiency, %	Instability	Dominant Frequency, Hz
			Airflow, W _a , lb/sec	Pressure, P _{t4} , psia	Temperature, T _{t4} , °F		Zone 1 Primary	Zone 1 Secondary	Zone 2					
Vortex generators removed, installed burner annulus blockage plates, restored the outer burner case to the original geometric configuration, and modified the secondary scoops on the ID* and the remaining 20 secondary scoops on the OD*.														
206	3-23-67	511 through 513	130.9	15.1	278	0.138	--	--	--	--	--	No	--	--
207	3-23-67	514	130.4	15.3	283	0.138	0.011	--	--	0.011	--	Yes	150	--
208	3-23-67	515 through 517	90.1	10.0	215	0.137	--	--	--	--	--	No	--	--
209	3-23-67	518	93.7	10.7	212	0.135	0.009	--	--	0.009	--	Yes	130	--
210	3-23-67		91.0	10.0	200	0.138	0.011	--	--	0.011	--	Yes	140	--
Vortex generators removed, the fuel lines were capped off on every other Zone 1 secondary fuel nozzle, and the burner annulus blockage plates installed.														
211	3-24-67	524	129.0	14.9	285	0.140	--	--	--	--	--	No	--	--
212	3-24-67	525	129.8	15.0	284	0.140	0.006	--	--	0.006	--	No	--	--
213	3-24-67	526	130.1	15.1	283	0.140	0.006	0.005	--	0.011	--	No	--	--
214	3-24-67	527	130.0	15.1	284	0.139	0.006	0.009	--	0.015	--	No	--	--
215	3-24-67	528	129.7	15.0	284	0.140	0.006	0.010	--	0.016	--	Yes	260	--
216	3-24-67	529	130.0	15.1	283	0.139	0.010	--	--	0.010	--	No	--	--
217	3-24-67	530	130.3	14.9	283	0.141	0.010	0.004	--	0.014	--	Yes	270	--
218	3-24-67	531	130.3	15.0	282	0.140	0.012	--	--	0.012	--	No	--	--
219	3-24-67	532	130.2	15.0	285	0.140	0.012	0.005	--	0.017	--	Yes	270	--
220	3-24-67	533	130.0	15.0	283	0.140	0.004	--	--	0.004	--	No	--	--
221	3-24-67	534	130.1	15.0	282	0.140	0.004	0.006	--	0.010	--	No	--	--
222	3-24-67	535	129.6	15.2	282	0.138	0.004	0.014	--	0.018	--	Yes	260	--
223	3-24-67	536	130.1	15.0	282	0.140	--	0.006	--	0.006	--	No	--	--
224	3-24-67	537	130.0	15.0	283	0.140	--	0.016	--	0.016	--	No	--	--
225	3-24-67	538	130.0	15.1	284	0.139	--	0.021	--	0.021	--	No	--	--
226	3-24-67	539	130.0	15.1	284	0.139	--	0.021	0.010	0.031	--	No	--	--
227	3-24-67	540	129.1	15.2	284	0.137	--	0.021	0.020	0.041	--	No	--	--
228	3-24-67	541	129.2	15.3	284	0.136	--	0.021	0.026	0.047	--	Yes	95	--
229	3-24-67	542	128.8	15.2	283	0.137	--	0.021	0.023	0.044	--	No	--	--
230	3-24-67	543	141.9	20.5	279	0.111	--	0.016	--	0.016	--	No	--	--
231	3-24-67	544	141.9	20.1	280	0.113	--	0.016	--	0.016	--	No	--	--

*This change was incorporated for the duration of the test program.

Table D-2. Combustion Tests (Continued)

Test Point	Date	CADDE Number	Airflow, W_a , lb/sec	Pressure, P_{t4} , psia	Temperature, T_{t4} , °F	Duct Reference Mach Number	Zone 1 Primary Secondary	Zone 2	Overall	Combustion Efficiency, %	Instability	Dominant Frequency, Hz
Vortex generators removed, removed burner annulus blockage plates*, and the fuel lines capped off on every other Zone 1 secondary fuel nozzle.												
232	3-28-67	549	134.5	14.8	286	0.148	--	--	--	--	No	--
233	3-28-67	550	135.1	14.7	285	0.149	0.010	--	0.010	--	No	--
234	3-28-67	551	134.9	15.1	285	0.144	0.010	0.006	0.016	--	Yes	250
235	3-28-67	552	134.6	15.2	285	0.144	0.006	0.011	0.017	--	Yes	200
236	3-28-67	553	134.7	15.1	286	0.145	--	0.010	0.010	--	No	--
237	3-28-67	554	134.8	14.6	286	0.150	--	0.020	0.020	--	No	--
238	3-28-67	555	134.9	14.7	287	0.149	--	0.020	0.030	--	No	--
239	3-28-67	556	134.7	14.9	287	0.147	--	0.022	0.028	--	Yes	180
240	3-28-67	557	134.4	15.1	288	0.144	--	0.016	0.030	--	No	--
241	3-28-67	558	134.6	15.2	288	0.143	--	0.016	0.044	90.9	No	--
242	3-28-67	559	134.5	15.3	289	0.143	--	0.016	0.044	90.3	No	--
243	3-28-67	560	134.4	15.4	289	0.142	--	0.016	0.046	90.0	Yes	90
244	3-28-67		135.0	15.0	285	0.144	0.014	0.004	0.018	--	Yes	190
245	3-28-67		135.0	15.0	285	0.144	--	0.020	0.037	--	Yes	180
246	3-30-67	566	133.3	15.6	288	0.138	--	--	--	--	No	--
247	3-30-67	567	133.5	15.4	287	0.140	--	0.013	0.013	--	No	--
248	3-30-67	568	132.7	15.6	284	0.138	--	0.013	0.030	--	No	--
249	3-30-67	569	133.2	15.3	288	0.141	--	0.013	0.041	--	Yes	95
250	3-30-67	570	133.5	15.2	289	0.142	--	0.010	0.030	--	No	--
251	3-30-67	571	133.9	15.2	289	0.143	--	0.010	0.041	--	Yes	95
252	3-30-67	572	140.6	15.5	219	0.140	--	0.007	0.028	--	Yes	130
253	3-30-67	573	134.7	15.3	295	0.143	--	0.007	0.027	--	No	--
254	3-30-67	574	134.4	15.2	294	0.144	0.013	--	0.013	--	No	--
255	3-30-67	575	134.0	15.3	294	0.143	0.013	--	0.017	0.030	No	--
256	3-30-67	576	134.3	15.5	293	0.141	0.013	--	0.031	0.044	Yes	100
257	3-30-67	577	137.6	16.3	253	0.134	0.010	--	0.018	0.028	Yes	275
258	3-30-67	578	90.1	10.2	213	0.136	--	--	--	--	No	--
259	3-30-67	579	90.2	10.4	213	0.132	--	--	0.010	--	No	--
260	3-30-67	580	89.6	10.3	215	0.134	--	0.013	0.027	0.040	Yes	65
261	3-30-67	581	90.2	10.3	215	0.135	--	0.017	0.031	0.048	Yes	170
262	3-30-67	582	90.4	10.8	215	0.129	0.013	--	0.031	0.044	Yes	170
263	3-30-67		91.0	10.0	200	0.136	0.015	--	--	0.015	Yes	165
264	3-30-67		91.0	10.5	213	0.132	0.010	0.005	--	0.015	Yes	170
265	3-30-67		91.0	10.5	213	0.132	0.007	0.011	--	0.018	Yes	170
266	3-30-67		91.0	10.5	213	0.132	0.004	0.013	--	0.017	Yes	165
267	3-30-67		91.0	10.5	213	0.132	--	0.020	0.020	--	Yes	170

Table D-2. Combustion Tests (Continued)

Test Point	Date	CADDE Number	Burner Inlet Conditions			Duct Reference Mach Number	Fuel/Air Ratio			Overall Combustion Efficiency, %	Instability	Dominant Frequency, Hz
			Airflow, W_a , lb/sec	Pressure, P_{T4} , psia	Temperature, T_{T4} , °F		Zone 1 Primary	Zone 1 Secondary	Zone 2			
268	3-30-67		90.0	10.3	215	0.134	--	0.010	0.028	0.038	Yes	65
269	3-30-67		91.0	10.3	215	0.135	--	0.018	0.029	0.047	Yes	170
270	3-30-67		91.0	10.8	213	0.129	--	0.010	0.022	0.032	Yes	145
Vortex generators removed, diffuser vanes installed at 60 deg from rig centerline, and fuel lines capped off on every other Zone 1 secondary fuel nozzle.												
271	4-13-67	588-589	135.5	15.2	282	0.144	--	--	--	--	No	--
272	4-13-67	590	138.3	15.8	282	0.141	0.006	0.013	--	0.019	No	--
273	4-13-67	591	136.7	15.5	284	0.141	0.006	0.013	--	0.019	No	--
274	4-13-67	592	138.8	15.7	283	0.143	0.010	0.009	--	0.019	No	--
275	4-13-67	593	140.0	15.7	284	0.144	0.013	0.007	--	0.020	Yes	180
276	4-13-67	594	138.7	15.5	284	0.144	--	0.007	0.021	0.028	Yes	140
277	4-13-67	595	138.6	15.7	285	0.143	--	0.010	0.029	0.039	Yes	85
278	4-13-67	596	138.8	16.1	285	0.139	--	0.015	0.029	0.044	No	--
279	4-13-67	597	135.7	16.1	285	0.137	--	0.016	0.033	0.049	Yes	90
280	4-13-67	598	135.9	15.7	286	0.140	--	0.018	0.027	0.045	No	--
281	4-13-67	599	133.5	16.2	286	0.133	--	0.018	0.032	0.050	No	--
282	4-13-67	600	135.2	16.2	286	0.135	--	0.018	0.032	0.050	No	--
283	4-13-67	601	135.0	16.3	286	0.134	--	0.020	0.031	0.051	No	--
284	4-13-67	602	134.9	16.2	287	0.134	--	0.020	0.031	0.051	No	--
285	4-13-67	603	134.7	16.4	287	0.141	--	0.022	0.027	0.049	No	--
286	4-13-67	604	134.9	15.8	285	0.138	0.006	--	0.031	0.037	Yes	95
287	4-13-67	605	134.4	15.5	286	0.140	0.008	--	0.021	0.029	Yes	155
288	4-13-67	606	134.2	15.9	286	0.137	0.010	--	0.030	0.040	Yes	300
289	4-13-67	607	134.4	15.8	286	0.136	0.014	--	0.028	0.042	No	--
290	4-13-67	608-609	89.5	10.2	206	0.133	--	--	--	--	No	--
291	4-13-67	610	88.9	10.6	196	0.127	0.006	0.012	--	0.018	Yes	--
292	4-13-67	611	88.9	11.0	196	0.122	0.012	0.006	--	0.018	Yes	165
293	4-13-67	612	90.7	10.3	195	0.134	0.014	--	--	0.014	Yes	--
294	4-13-67	613	90.2	10.2	204	0.135	--	0.007	0.047	0.054	No	--
295	4-13-67	614	91.5	10.5	216	0.134	--	0.013	0.033	0.046	Yes	68
296	4-13-67	615	89.4	10.4	216	0.132	--	0.017	0.034	0.051	No	--
297	4-13-67	616	91.0	10.7	216	0.131	--	0.020	0.031	0.051	No	--
298	4-13-67	617	90.7	10.5	216	0.133	0.010	--	0.041	0.051	No	--

Table D-2. Combustion Tests (Continued)

Test Point	Date	CADE Number	Burner Inlet Conditions			Duct Reference Mach Number	Fuel/Air Ratio			Overall Combustion Efficiency, %	Instability	Dominant Frequency, Hz
			Airflow, W_a , lb/sec	Pressure, P_{T4} , psia	Temperature, T_{T4} , °F		Zone 1 Primary	Zone 1 Secondary	Zone 2			
299	4-13-67	618	91.0	10.5	216	0.134	0.014	--	0.019	0.033	Yes	170
Vortex generators removed, diffuser vanes set at 30 deg from rig centerline, and fuel lines capped off on every other Zone 1 secondary fuel nozzle.												
300	4-14-67	624	139.8	15.3	282	0.146	--	--	--	--	No	--
301	4-14-67	625	132.3	15.1	282	0.142	--	--	--	--	No	--
302	4-14-67	626	132.4	15.4	281	0.139	0.006	0.012	--	0.018	Yes	180
303	4-14-67	627	133.2	15.5	282	0.138	0.010	0.008	--	0.018	Yes	185
304	4-14-67	628	133.0	15.3	283	0.139	0.014	0.005	--	0.019	Yes	180
305	4-14-67	629	132.9	15.2	283	0.141	0.006	--	0.027	0.033	Yes	100
306	4-14-67	630	133.1	15.5	282	0.138	0.008	--	0.019	0.027	Yes	158
307	4-14-67	631	132.8	15.4	283	0.139	0.010	--	0.025	0.035	Yes	290
308	4-14-67	632	132.8	15.3	283	0.140	0.014	--	0.026	0.040	Yes	102
309	4-14-67	633	132.7	15.4	283	0.139	--	0.007	0.026	0.033	Yes	137
310	4-14-67	634	132.9	15.6	283	0.137	--	0.012	0.031	0.043	Yes	90
311	4-14-67	635	132.4	15.3	284	0.140	--	0.016	0.026	0.042	No	--
312	4-14-67	636	132.1	15.1	284	0.142	--	0.016	0.029	0.045	Yes	90
313	4-14-67	637	132.3	15.2	284	0.141	--	0.018	0.028	0.046	No	--
314	4-14-67	638	132.5	15.7	284	0.137	--	0.018	0.033	0.051	Yes	85
315	4-14-67	639-640	132.4	15.3	284	0.140	--	0.020	0.027	0.047	No	--
316	4-14-67	641-642	132.2	15.6	283	0.136	--	0.020	0.031	0.051	No	--
317	4-14-67	643	133.0	15.3	283	0.140	--	0.022	0.017	0.039	Yes	160
318	4-14-67	644	132.7	15.2	284	0.141	--	0.022	0.013	0.035	Yes	165
319	4-14-67	645	91.1	10.3	222	0.135	--	--	--	--	No	--
320	4-14-67	646	91.0	10.2	221	0.137	0.015	--	--	0.015	Yes	170
321	4-14-67	647	91.0	10.3	220	0.135	0.010	--	0.038	0.048	No	--
322	4-14-67	648-649	90.6	10.5	220	0.133	0.010	--	0.040	0.050	No	--
323	4-14-67	650-651	90.6	10.2	220	0.137	0.012	--	0.038	0.050	No	--
324	4-14-67	652-653	90.6	10.2	220	0.137	0.013	--	0.038	0.051	Yes	185
325	4-14-67	654	90.9	10.2	219	0.137	0.013	--	0.036	0.049	Yes	180
326	4-14-67	655	90.7	10.0	217	0.139	--	0.007	0.025	0.032	Yes	110
327	4-14-67	656	91.0	10.5	218	0.133	--	0.012	0.030	0.042	Yes	71

Table D-2. Combustion Tests (Continued)

Test Point	Date	CADDE Number	Burner Inlet Conditions			Duct Reference Mach Number	Fuel/Air Ratio			Overall Combustion Efficiency, %	Instability	Dominant Frequency, Hz	
			Airflow, W _a , lb/sec	Pressure, P ₀₄ , psia	Temperature, T ₀₄ , °F		Zone 1 Primary	Zone 1 Secondary	Zone 2				
328	4-14-67	657	90.8	10.5	218	0.133	--	0.012	0.039	0.051	76.5	Yes	65
329	4-14-67	658	90.5	10.5	217	0.133	--	0.016	0.035	0.051	--	No	--
330	4-14-67	659	90.5	10.4	217	0.134	--	0.016	0.035	0.051	--	No	--
331	4-14-67	660	90.2	10.4	215	0.133	--	0.020	0.028	0.048	--	Yes	170
332	4-14-67	661	90.8	10.2	217	0.137	--	0.022	0.010	0.032	--	Yes	170
Vortex generators removed, fuel lines capped off on every other Zone-1 secondary fuel nozzle, diffuser vanes installed at 30 deg from rig centerline, and 3-mesh screen installed in the rig inlet.													
333	4-19-67	667	135.1	15.4	328	0.144	--	--	--	--	--	No	--
334	4-19-67	668-669	134.2	15.5	282	0.140	--	--	--	--	--	No	--
335	4-19-67	670-671	134.4	16.2	280	0.133	--	--	--	--	--	No	--
336	4-19-67	672-673	134.6	13.1	280	0.167	--	--	--	--	--	No	--
337	4-20-67	678	135.4	15.2	288	0.145	--	--	--	--	--	No	--
338	4-20-67	679	135.7	15.4	290	0.143	0.006	0.012	--	0.018	--	Yes	215
339	4-20-67	680	135.9	15.1	290	0.147	0.010	0.008	--	0.018	--	Yes	215
340	4-20-67	681	135.6	15.2	290	0.144	0.013	0.006	--	0.019	--	Yes	180
341	4-20-67	682	135.8	15.9	290	0.139	0.006	--	0.029	0.035	--	Yes	95
342	4-20-67	683	136.1	15.6	283	0.141	0.008	--	0.029	0.037	--	Yes	285
343	4-20-67	684	135.3	15.3	290	0.144	0.010	--	0.028	0.038	--	Yes	300
344	4-20-67	685	135.1	15.4	291	0.142	0.013	--	0.027	0.040	91.3	Yes	100
345	4-20-67	686	135.3	15.3	291	0.144	--	0.007	0.020	0.027	--	Yes	135
346	4-20-67	687	135.0	15.3	291	0.143	--	0.012	0.026	0.038	--	Yes	90
347	4-20-67	688	135.0	15.3	291	0.143	--	0.012	0.029	0.041	--	Yes	90
348	4-20-67	689	135.4	15.4	291	0.143	--	0.016	0.024	0.040	91.0	No	--
349	4-20-67	690	135.1	15.1	290	0.145	--	0.016	0.026	0.042	90.1	No	--
350	4-20-67	691	135.2	15.4	290	0.143	--	0.018	0.026	0.044	91.4	No	--
351	4-20-67	692	135.2	16.0	290	0.138	--	0.018	0.032	0.050	90.0	No	--
352	4-20-67	693	135.1	15.4	290	0.143	--	0.020	0.024	0.044	90.3	No	--
353	4-20-67	694	135.4	16.0	290	0.138	--	0.020	0.030	0.050	89.5	No	--
354	4-20-67	695	135.1	15.3	290	0.143	--	0.022	0.006	0.028	--	Yes	160
355	4-20-67	696	91.0	10.1	223	0.140	--	--	--	--	--	No	--
356	4-20-67	697	91.0	10.2	218	0.137	0.010	--	0.038	0.048	77.4	No	--
357	4-20-67	698	91.1	10.4	218	0.135	0.012	--	0.035	0.047	--	No	--
358	4-20-67	699	91.3	10.3	218	0.137	--	0.012	0.027	0.039	--	Yes	66

Table D-2. Combustion Tests (Continued)

Test Point	Date	CADDE Number	Burner Inlet Conditions			Duct Reference Mach Number	Fuel/Air Ratio			Overall Combustion Efficiency, %	Instability	Dominant Frequency, Hz
			Airflow, W_a , lb/sec	Pressure, P_{t4} , psia	Temperature, T_{t4} , °F		Zone 1 Primary	Zone 1 Secondary	Zone 2			
359	4-20-67	700	91.1	10.4	217	0.135	--	0.016	0.032	0.048	No	--
360	4-20-67	701	91.1	10.4	216	0.135	--	0.020	0.028	0.048	No	--
361	4-20-67	702	91.2	9.9	217	0.142	--	0.021	--	0.021	Yes	168
Vortex generators removed, fuel lines capped off on every other Zone-1 secondary fuel nozzle, diffuser vanes installed at 30 deg from rig centerline, and 3-mesh screen installed in the rig inlet with 6 hoops - 1/4" tubing.												
362	4-21-67	708 thru 711	This data was not good due to a malfunction of the CADDE system. Vortex generators removed, fuel lines capped off on every other Zone-1 secondary fuel nozzle, diffuser vanes set at 30 deg from rig centerline, and installed 4-mesh screen in the rig inlet with O.D. ring (removed the 3-mesh screen).									
363	4-28-67	716	133.4	16.5	285	0.131	--	--	--	--	No	--
364	4-28-67	717	133.8	14.7	285	0.148	--	--	--	--	No	--
365	4-28-67	718	133.8	13.1	285	0.166	--	--	--	--	No	--
366	4-28-67	719	133.6	15.7	287	0.138	0.006	0.012	--	0.018	Yes	190
367	4-28-67	720	133.1	15.7	287	0.138	0.010	0.009	--	0.019	Yes	190
368	4-28-67	721	133.1	15.5	287	0.139	0.014	0.005	--	0.019	Yes	180
369	4-28-67	722	134.0	15.7	288	0.138	0.006	--	0.036	0.042	Yes	92
370	4-28-67	723	133.2	15.7	286	0.137	0.008	--	0.026	0.034	Yes	290
371	4-28-67	724	133.2	15.6	287	0.138	0.010	--	0.025	0.035	Yes	290
372	4-28-67	725	133.4	15.7	285	0.138	0.013	--	0.031	0.044	Yes	99
373	4-28-67	726	133.1	15.8	285	0.137	--	0.007	0.023	0.030	Yes	138
374	4-28-67	727	133.4	15.7	285	0.137	--	0.012	0.031	0.043	Yes	88
375	4-28-67	728	133.9	15.9	285	0.136	--	0.016	0.033	0.049	Yes	83
376	4-28-67	729	133.5	15.7	285	0.138	--	0.018	0.028	0.046	No	--
377	4-28-67	730	133.8	15.6	285	0.138	--	0.020	0.026	0.046	No	--
378	4-28-67	731	133.3	15.7	286	0.137	--	0.022	0.025	0.047	No	--
379	4-28-67	732	133.7	15.7	285	0.138	--	0.023	--	0.023	Yes	160
380	4-28-67	733	133.8	15.6	284	0.138	--	0.020	0.032	0.052	No	--
381	4-28-67	734	133.7	15.6	283	0.138	--	0.020	0.032	0.052	No	--
Vortex generators removed, Zone-1 secondary fuel nozzles restored to 40, diffuser vanes set at 30 deg from rig centerline, and 4-mesh screen in the rig inlet with the O.D. ring.												
382	5-03-67	743-744	87.1	10.6	204	0.125	--	--	--	--	No	--
383	5-03-67	745	87.8	10.8	204	0.122	0.005	0.015	--	0.020	Yes	125
384	5-03-67	746	88.0	11.0	204	0.122	0.010	0.007	--	0.017	Yes	153
385	5-03-67	747	87.9	12.3	204	0.109	0.005	--	0.041	0.046	Yes	92
386	5-03-67		88.0	11.4	204	0.117	0.014	--	--	0.014	Yes	180

Table D-2. Combustion Tests (Continued)

Test Point	Date	CADDE Number	Burner Inlet Conditions			Duct Reference Mach Number	Fuel/Air Ratio			Overall Combustion Efficiency, %	Instability	Dominant Frequency, Hz
			Airflow, W_a , lb/sec	Pressure, P_{T4} , psia	Temperature, T_{T4} , °F		Zone 1 Primary	Zone 1 Secondary	Zone 2			
387	5-03-67	748	87.4	10.9	203	0.122	0.010	--	0.041	0.051	No	--
388	5-03-67	749	88.1	11.1	203	0.120	0.015	--	0.020	0.035	Yes	168
389	5-03-67	750	87.9	11.2	202	0.119	--	0.007	0.030	0.037	Yes	41
390	5-03-67	751	87.6	10.9	202	0.122	--	0.013	0.038	0.051	No	--
391	5-03-67	752	87.8	10.9	202	0.122	--	0.017	0.008	0.025	Yes	150
392	5-03-67	753	87.8	11.3	202	0.118	--	0.019	--	0.019	Yes	148
393	5-03-67	754-755	134.0	15.1	286	0.143	--	--	--	--	No	--
394	5-03-67	756	134.2	15.3	286	0.142	0.005	0.014	--	0.019	Yes	177
395	5-03-67	757	134.3	15.5	287	0.140	0.010	0.008	--	0.018	Yes	200
396	5-03-67	758	133.9	15.3	287	0.142	0.014	0.007	--	0.021	Yes	182
397	5-03-67	759	133.9	14.8	288	0.147	0.006	--	0.034	0.040	Yes	92
398	5-03-67	760	134.1	15.2	289	0.143	0.010	--	0.027	0.037	Yes	295
399	5-03-67	761	133.3	16.1	289	0.134	0.014	--	0.036	0.050	No	--
400	5-03-67	762	133.7	16.2	290	0.134	0.014	--	0.037	0.051	Yes	95
401	5-03-67	763	133.5	16.6	289	0.131	--	0.007	0.041	0.048	Yes	70
402	5-03-67	764	134.1	16.4	290	0.132	--	0.010	0.040	0.050	No	--
403	5-03-67	765	133.6	15.4	290	0.141	--	0.017	0.005	0.022	Yes	180
404	5-03-67	766	133.4	16.9	290	0.128	--	0.018	--	0.018	Yes	183
405	5-03-67	767	90.4	10.8	198	0.127	--	--	--	--	No	--
406	5-03-67	768	88.7	10.7	198	0.125	0.010	--	0.055	0.065	No	--
407	5-03-67	769	89.2	10.6	195	0.127	--	0.013	0.047	0.060	No	--
Installed turbulators and capped the fuel lines on every other Zone 1 secondary fuel nozzle, diffuser vanes set at 30 deg from rig centerline, and 4-mesh screen in the rig inlet with the OD ring.												
408	5-03-67	777	90.0	10.7	195	0.127	--	--	--	--	No	--
409	5-03-67	778	98.1	12.3	200	0.120	0.006	0.009	--	0.015	Yes	150
410	5-03-67	779	90.4	11.2	200	0.122	0.010	0.005	--	0.015	Yes	166
411	5-03-67	780	90.1	11.4	198	0.120	0.016	--	--	0.016	Yes	168
412	5-03-67	781	90.8	11.6	199	0.118	0.006	--	0.029	0.035	Yes	122
413	5-03-67	782	90.1	10.8	199	0.127	0.008	--	0.022	0.030	Yes	143
414	5-03-67	783	89.1	10.7	200	0.128	0.010	--	0.020	0.030	Yes	150
415	5-03-67	784	89.7	10.1	201	0.136	0.014	--	0.017	0.031	Yes	173
416	5-03-67	785	89.3	10.4	200	0.132	--	0.007	0.027	0.034	Yes	111

Table D-2. Combustion Tests (Continued)

Test Point	Date	CADDE Number	Burner Inlet Conditions			Duct Reference Mach Number	Fuel/Air Ratio			Overall Combustion Efficiency, %	Instability	Dominant Frequency, Hz
			Airflow, \dot{W}_a , lb/sec	Pressure, P_{T4} , psia	Temperature, T_{T4} , °F		Zone 1 Primary	Zone 1 Secondary	Zone 2			
417	5-05-67	786	91.1	10.9	201	0.127	--	0.012	0.037	0.049	Yes	70
418	5-05-67	787	91.7	11.0	201	0.125	--	0.016	0.021	0.037	Yes	158
419	5-05-67	788-789	91.2	11.1	200	0.126	--	0.020	0.032	91.2	No	--
420	5-05-67	790	92.8	10.4	202	0.136	--	0.016	0.023	0.039	Yes	76
421	5-05-67	791	89.9	10.9	204	0.126	--	0.020	0.032	89.3	No	--
422	5-05-67	792	90.1	10.3	208	0.133	--	0.022	0.013	0.035	Yes	165
423	5-05-67	793	90.1	9.8	208	0.140	--	0.024	--	0.024	Yes	160
424	5-05-67	794	133.9	14.8	285	0.146	--	--	--	--	No	--
425	5-05-67	795	134.7	15.1	286	0.144	--	0.018	0.022	0.040	No	--
426	5-05-67	796	134.4	16.4	286	0.133	--	0.018	0.033	0.051	No	--
427	5-05-67	797	134.1	14.9	287	0.146	--	0.020	0.020	0.040	No	--
428	5-05-67	798	134.0	16.1	287	0.135	--	0.020	0.031	0.051	No	--
429	5-05-67	799	135.3	14.9	187	0.147	--	0.022	--	0.022	Yes	158
430	5-08-67	805-806	263.6	30.4	548	0.165	--	--	--	--	No	--
431	5-08-67	807	264.7	31.8	550	0.158	0.007	0.014	0.007	0.028	No	--
432	5-08-67	808	264.3	30.7	552	0.164	0.007	0.014	0.004	0.025	No	--
433	5-08-67	809	264.7	30.4	551	0.165	0.007	0.016	--	0.023	No	--
434	5-08-67	810	264.7	29.5	550	0.171	0.007	0.014	--	0.021	No	--
435	5-08-67	811	265.0	29.5	550	0.171	0.007	0.013	--	0.020	No	--
436	5-08-67	812	264.3	29.6	550	0.170	0.003	0.017	--	0.020	No	--
437	5-08-67	813	264.6	30.5	549	0.165	0.004	0.017	0.003	0.024	No	--
438	5-08-67	814	265.5	31.0	550	0.163	0.003	0.017	0.005	0.025	No	--
439	5-08-67	815	265.9	30.5	548	0.165	0.003	0.009	0.013	0.025	No	--
440	5-08-67	816	265.1	30.6	550	0.165	0.007	0.008	0.009	0.024	No	--
441	5-10-67	822	277.4	30.5	548	0.173	--	--	--	--	No	--
442	5-10-67	823	277.4	29.9	551	0.175	0.007	0.015	0.013	0.035	Yes	470
443	5-10-67	824	277.1	30.5	558	0.172	0.007	0.013	0.015	0.035	Yes	470
444	5-10-67	825	278.4	29.8	554	0.176	0.007	0.011	0.016	0.034	Yes	470
445	5-10-67	826	278.0	29.7	561	0.176	0.007	0.009	0.016	0.032	Yes	460
446	5-10-67	827	278.7	29.9	554	0.175	0.007	0.007	0.016	0.030	Yes	450
447	5-10-67	828	277.6	30.3	546	0.173	0.007	0.005	0.017	0.029	Yes	450
448	5-10-67	829	278.1	29.9	545	0.175	0.007	0.003	0.018	0.028	Yes	435

Table D-2. Combustion Tests (Continued)

Test Point	Date	CADDE Number	Burner Inlet Conditions			Fuel/Air Ratio			Overall Combustion Efficiency, %	Instability	Dominant Frequency, Hz
			Airflow, W_g , lb/sec	Pressure, P_{t4} , psia	Temperature, T_{t4} , °F	Duct Reference Mach Number	Zone 1 Primary	Zone 2 Secondary			
449	5-10-67	830	279.4	29.2	550	0.179	0.007	--	0.031	Yes	410
450	5-10-67	831	277.3	28.4	551	0.185	0.003	--	0.025	Yes	3.5
451	5-10-67	832	277.8	29.5	543	0.178	0.003	0.003	0.037	Yes	220
452	5-10-67	833	277.7	29.8	547	0.176	0.003	0.007	0.028	Yes	430
453	5-10-67	834	277.6	29.3	545	0.179	0.003	0.010	0.029	Yes	445
454	5-10-67	835	277.2	29.6	547	0.176	0.003	0.015	0.033	Yes	450
455	5-10-67	836	276.6	29.8	547	0.175	--	0.010	0.032	Yes	440
456	5-10-67	837	276.2	29.4	547	0.178	--	0.008	0.030	Yes	425
457	5-10-67	838	276.4	29.0	547	0.180	--	0.006	0.033	Yes	400
458	5-10-67	839	276.0	28.5	550	0.185	--	0.004	0.025	No	--
Turbulators installed, diffuser vanes removed, Zone 1 secondary fuel nozzles restored to 40, and 4-mesh screen in the rig inlet with OD ring.											
459	5-15-67	845	275.7	29.2	556	0.181	--	--	--	No	--
460	5-15-67	846	274.3	30.0	559	0.176	0.007	0.003	0.026	Yes	440
461	5-15-67	847	274.0	29.1	558	0.181	0.007	0.007	0.029	Yes	455
462	5-15-67	848	275.7	28.9	557	0.182	0.007	0.011	0.034	Yes	465
463	5-15-67	849	275.6	29.0	557	0.182	0.007	0.015	0.038	Yes	270
464	5-15-67	850	275.0	29.0	555	0.181	0.007	0.017	0.039	Yes	280
465	5-15-67	851	275.5	29.3	558	0.180	0.007	0.019	0.032	Yes	280
466	5-15-67	852	275.2	28.4	559	0.186	0.003	0.007	0.028	Yes	440
467	5-15-67	853	275.2	29.3	558	0.180	0.003	0.010	0.030	Yes	450
468	5-15-67	854	274.8	28.9	560	0.183	0.003	0.015	0.034	Yes	462
469	5-15-67	855	276.1	29.1	535	0.180	0.003	0.021	0.039	Yes	478
470	5-15-67	856	276.6	29.5	529	0.178	0.003	0.023	0.041	Yes	471
471	5-15-67	857	276.9	29.7	545	0.178	0.003	0.025	92.2	No	--
Every other turbulator removed on the OD and ID, Zone 1 secondary fuel nozzles restored to 40, diffuser vanes removed, and 4-mesh screen in the rig inlet with the OD ring.											
472	6-02-67	863	273.4	29.5	543	0.176	0.007	0.003	0.031	Yes	430
473	6-02-67	864	275.6	28.6	498	0.182	0.007	0.007	0.036	Yes	440
474	6-02-67	865	280.9	28.0	499	0.187	0.007	0.011	0.046	Yes	320
475	6-02-67	866	280.6	29.4	499	0.177	--	--	--	No	--
476	6-02-67	867	280.8	31.1	498	0.167	0.007	0.015	0.049	Yes	260
477	6-02-67	868	280.2	29.9	498	0.174	0.007	0.017	0.051	Yes	265

Table D-2. Combustion Tests (Continued)

Test Point	Date	CADDE Number	Burner Inlet Conditions				Duct Reference Mach Number	Fuel/Air Ratio			Overall Combustion Efficiency, %	Instability	Dominant Frequency, Hz
			Airflow, W_a , lb/sec	Pressure, P_{T4} , psia	Temperature, T_{T4} , °F	Zone 1 Primary		Zone 1 Secondary	Zone 2				
Every other turbulator installed, Zone 1 secondary fuel nozzles restored to 40, diffuser vanes removed, and 4-mesh screen in the rig inlet with OD ring.													
478	6-10-67	874-875	275.0	30.0	560	0.175	--	--	--	--	No	--	--
479	6-10-67	876	276.0	30.0	550	0.175	0.007	0.003	0.021	0.031	Yes	440	440
480	6-10-67	--	276.0	30.0	550	0.175	0.007	0.007	0.020	0.034	Yes	440	440
481	6-10-67	877	276.0	30.0	550	0.175	0.007	0.011	0.021	0.039	Yes	450	450
482	6-10-67	878	276.6	30.0	550	0.175	0.007	0.015	0.017	0.039	Yes	450	450
483	6-10-67	879	276.0	30.0	550	0.175	0.007	0.017	0.020	0.044	Yes	440	440
484	6-10-67	880	276.0	30.0	550	0.175	0.007	0.019	0.022	0.048	Yes	460	460
485	6-10-67	881	276.0	30.0	550	0.175	0.007	0.021	0.022	0.050	Yes	440	440
486	6-10-67	882	277.7	31.0	560	0.172	0.007	0.021	0.019	0.047	No	--	--
487	6-10-67	883	278.1	31.4	558	0.169	0.007	0.023	0.020	0.050	No	--	--
488	6-10-67	884	276.0	30.0	550	0.175	0.007	0.013	--	0.020	No	--	--
Every other turbulator installed, Zone 1 secondary fuel nozzles restored to 40, diffuser vanes removed, 4-mesh screen in the rig inlet with OD ring, and Zone 2 ID spraybars capped off.													
489	6-10-67	885-886	277.3	30.0	559	0.177	--	--	--	--	No	--	--
490	6-10-67	887	277.0	30.3	560	0.175	0.007	0.003	0.024	0.034	No	--	--
491	6-10-67	888	276.0	30.0	550	0.175	0.007	0.019	0.014	0.040	Yes	280	280
492	6-10-67	889	276.0	30.0	550	0.175	0.007	0.015	0.016	0.038	Yes	320	320
493	6-10-67	890	276.0	30.0	550	0.175	0.007	0.011	0.019	0.037	Yes	230	230
494	6-10-67	891	276.7	30.4	561	0.175	0.007	0.007	0.024	0.038	No	--	--
495	6-10-67	892	276.0	30.0	550	0.175	0.007	0.023	0.020	0.050	Yes	260	260
All turbulators installed, 6 low flow Zone 2 OD spraybars installed, 4-mesh screen in the rig inlet with OD ring, and 40 Zone 1 secondary nozzles.													
496	6-16-67	898	276.0	30.2	551	0.174	--	--	--	--	No	--	--
497	6-16-67	899-900	279.6	30.4	545	0.175	0.007	0.029	0.008	0.044	No	--	--
498	6-16-67	901	279.5	31.5	546	0.169	0.007	0.029	0.014	0.050	No	--	--
499	6-16-67	902	278.1	31.3	549	0.169	0.007	0.027	0.015	0.049	No	--	--
500	6-16-67	903	277.7	30.8	550	0.171	0.007	0.025	0.014	0.046	No	--	--
501	6-16-67	904	278.0	31.5	550	0.168	0.007	0.025	0.018	0.050	No	--	--
502	6-16-67	905	278.0	30.0	550	0.176	0.007	0.003	0.019	0.029	Yes	435	435
503	6-16-67	906	278.4	30.1	541	0.176	0.007	0.007	0.016	0.030	Yes	455	455
504	6-16-67	907	278.0	39.9	541	0.176	0.007	0.011	0.016	0.034	Yes	460	460
505	6-16-67	908	278.2	29.8	542	0.177	0.007	0.013	0.017	0.037	Yes	460	460
506	6-16-67	909	278.3	29.9	541	0.176	0.007	0.017	0.015	0.039	Yes	280	280
507	6-16-67	910	277.8	30.1	541	0.175	0.007	0.021	0.015	0.043	Yes	465	465

Table D-2. Combustion Tests (Continued)

Test Point	Date	CADDE Number	Burner Inlet Conditions			Duct Reference Mach Number	Fuel/Air Ratio			Overall Combustion Efficiency, %	Instability	Dominant Frequency, Hz
			Airflow, W_a , lb/sec	Pressure, P_{t4} , psia	Temperature, T_{t4} , °F		Zone 1 Primary	Zone 1 Secondary	Zone 2			
508	6-16-67	911	277.0	30.1	541	0.175	0.007	0.013	0.017	0.047	No	--
509	6-16-67	912	277.0	30.1	541	0.175	0.007	0.013	0.020	0.050	Yes	440
510	6-16-67	913	276.0	30.0	550	0.175	0.007	0.025	0.020	0.050	No	--
All turbulators installed, Zone 1 secondary fuel nozzles restored to 40, diffuser vanes removed, 4-mesh screen in the rig inlet with OD ring.												
511	6-20-67	920-921	275.6	29.4	555	0.179	--	--	--	--	No	--
512	6-20-67	922-923	275.4	29.0	557	0.182	0.007	0.009	--	0.016	No	--
513	6-20-67	924	275.4	29.4	557	0.180	0.007	0.010	--	0.017	No	--
514	6-20-67	925	274.9	29.8	557	0.177	0.007	0.011	--	0.018	No	--
515	6-20-67	926	275.7	29.8	557	0.177	0.007	0.012	--	0.019	No	--
516	6-20-67	927	275.3	29.8	557	0.177	0.007	0.013	--	0.020	No	--
517	6-20-67	928	275.3	29.7	558	0.177	0.007	0.014	--	0.021	No	--
518	6-20-67	929	275.4	30.1	558	0.175	0.007	0.015	--	0.022	No	--
519	6-20-67	930	275.0	30.3	558	0.173	0.007	0.016	--	0.023	No	--
520	6-20-67	931	275.5	30.8	558	0.171	0.007	0.017	--	0.024	No	--
521	6-20-67	932	275.0	31.0	557	0.169	0.007	0.018	--	0.025	No	--
522	6-20-67	933	275.7	31.4	558	0.168	0.007	0.019	--	0.026	No	--
523	6-20-67	934	275.6	31.6	557	0.167	0.007	0.020	--	0.027	No	--
524	6-20-67	935	275.5	32.0	557	0.164	0.007	0.021	--	0.028	No	--
525	6-20-67	936	274.9	31.7	556	0.165	0.007	0.013	0.008	0.028	No	--
526	6-20-67	937	276.0	30.0	557	0.175	0.007	0.009	--	0.018	No	--
Turbulators installed, every other Zone 1 secondary fuel nozzle capped off, and 4-mesh screen in the rig inlet with OD ring.												
527	6-22-67	947	91.0	10.0	200	0.138	--	--	--	--	No	--
528	6-22-67	948	91.0	10.0	200	0.138	0.010	--	0.020	0.030	Yes	160
529	6-22-67	949	91.0	10.0	200	0.138	--	0.013	0.033	0.046	Yes	70
530	6-22-67	950	91.0	10.0	200	0.138	--	0.016	0.020	0.036	Yes	150
531	6-22-67	951	91.0	10.0	200	0.138	--	0.018	0.015	0.033	Yes	160
532	6-22-67	952	91.0	10.0	200	0.138	--	0.020	0.013	0.033	Yes	160
533	6-22-67	953	91.0	10.0	200	0.138	--	0.022	0.001	0.023	Yes	160
534	6-22-67	954	91.0	10.0	200	0.138	--	0.007	0.043	0.050	No	--
535	6-22-67	955	91.0	10.0	200	0.138	0.019	--	--	0.019	Yes	158
536	6-22-67	956	91.0	10.0	200	0.138	--	0.007	0.043	0.050	No	--

Table D-2. Combustion Tests (Continued)

Test Point	Date	CADDE Number	Burner Inlet Conditions			Duct Reference Mach Number	Fuel/Air Ratio			Overall Combustion Efficiency, %	Instability	Dominant Frequency, Hz
			Airflow, \dot{W}_a , lb/sec	Pressure, P_{T4} , psia	Temperature, T_{T4} , °F		Zone 1 Primary	Zone 1 Secondary	Zone 2			
Turbulators installed, Zone 1 secondary fuel nozzles restored to 40, and 4-mesh screen in the rig inlet with OD ring.												
537	6-23-67	967	280.1	30.1	516	0.174	--	--	--	--	No	--
538	6-23-67	968	280.8	30.3	512	0.173	0.006	0.023	0.012	0.041	No	--
539	6-23-67	969	280.8	30.6	512	0.171	0.007	0.023	0.014	0.044	No	--
540	6-23-67	970	280.0	31.0	513	0.168	0.007	0.023	0.016	0.046	No	--
541	6-23-67	971	280.5	31.0	512	0.169	0.007	0.023	0.016	0.046	Yes	460
542	6-23-67	972	280.5	30.6	516	0.172	0.007	0.025	0.012	0.044	No	--
543	6-23-67	973	280.9	30.9	511	0.169	0.007	0.025	0.014	0.046	No	--
544	6-23-67	974	281.3	31.4	510	0.167	0.007	0.025	0.016	0.048	No	--
545	6-23-67	975	281.2	31.7	509	0.165	0.007	0.025	0.018	0.050	No	--
546	6-23-67	976	281.1	30.8	508	0.170	0.007	0.025	0.018	0.050	No	--
547	6-23-67	977	281.1	30.4	507	0.172	0.007	0.027	0.010	0.044	No	--
548	6-23-67	978	281.5	30.6	506	0.170	0.007	0.027	0.012	0.046	No	--
549	6-23-67	979	281.6	31.2	508	0.168	0.007	0.027	0.014	0.048	No	--
550	6-23-67	980	280.8	30.7	508	0.170	0.007	0.027	0.016	0.050	No	--
551	6-23-67	981	281.7	30.3	511	0.173	0.006	0.030	0.008	0.044	No	--
552	6-23-67	982	281.0	30.7	510	0.171	0.007	0.029	0.010	0.046	No	--
553	6-23-67	983	280.8	31.0	511	0.169	0.007	0.029	0.012	0.048	No	--
554	6-23-67	984	281.0	30.6	512	0.172	0.007	0.029	0.014	0.050	No	--
555	6-23-67	985	280.4	31.3	510	0.167	0.007	0.029	0.014	0.050	No	--
Turbulators installed, every other Zone 1 secondary fuel nozzle capped off, and 4-mesh screen in the rig inlet with OD ring and 3 additional rings spaced evenly.												
556	6-26-67	992	89.9	9.7	208	0.142	--	--	--	--	No	--
557	6-26-67	993	89.3	10.2	209	0.134	--	0.018	0.016	0.034	Yes	160
558	6-26-67	994	89.9	10.3	208	0.133	--	0.020	0.013	0.033	Yes	170
559	6-26-67	995	89.7	10.2	208	0.134	--	0.022	--	0.022	Yes	160
560	6-26-67	996	89.4	10.5	209	0.130	--	0.014	0.030	0.044	Yes	75
561	6-26-67	997	89.7	10.9	211	0.126	--	0.014	0.035	0.049	Yes	75
562	6-26-67	998	89.7	10.5	209	0.131	--	0.014	0.035	0.049	Yes	--
563	6-26-67	999	91.7	10.2	208	0.138	--	0.016	0.021	0.037	No	--
564	6-26-67	1000	91.8	10.4	209	0.135	--	0.016	0.024	0.040	No	--
565	6-26-67	1001	91.8	10.2	208	0.137	--	0.016	0.024	0.040	--	--
566	6-26-67	1002	92.0	10.4	207	0.136	--	0.016	0.025	0.041	No	--
567	6-26-67	1003	91.6	10.5	207	0.133	--	0.016	0.028	0.044	No	--

Table D-2. Combustion Tests (Continued)

Test Point	Date	CADDE Number	Burner Inlet Conditions			Duct Reference Mach Number	Fuel/Air Ratio			Overall Combustion Efficiency, %	Instability	Dominant Frequency, Hz
			Airflow, W_a , lb/sec	Pressure, P_{T4} , psia	Temperature, T_{T4} , °F		Zone 1 Primary	Zone 1 Secondary	Zone 2			
568	6-26-67	1004	92.0	10.7	207	0.132	--	0.016	0.029	0.045	No	--
569	6-26-67	1005	91.6	10.5	207	0.134	--	0.016	0.030	0.046	No	--
570	6-26-67	1006	92.0	10.6	207	0.132	--	0.016	0.031	0.047	No	--
571	6-26-67	1007	92.1	10.7	207	0.131	--	0.016	0.033	0.049	No	--
572	6-26-67	1008	92.2	10.8	207	0.130	--	0.018	0.031	0.049	No	--
573	6-26-67	1009	92.1	10.9	207	0.129	--	0.020	0.030	0.050	No	--
574	6-26-67	1010	91.8	10.8	206	0.129	--	0.022	0.027	0.049	No	--
575	6-26-67	1011	91.9	11.0	206	0.128	--	0.024	0.028	0.052	Yes	160
576	6-26-67	1012	91.9	10.1	207	0.140	--	0.018	0.022	0.040	Yes	160
577	6-26-67	1013	91.8	11.1	208	0.126	--	0.012	0.037	0.049	Yes	65
578	6-26-67	1014	91.0	10.0	210	0.138	--	0.016	0.034	0.050	No	--
579	6-27-67	1020	133.9	15.2	291	0.144	--	--	--	--	No	--
580	6-27-67	1021	134.0	15.2	292	0.143	--	0.012	0.024	0.036	No	--
581	6-27-67	1022	134.1	15.5	295	0.141	--	0.012	0.026	0.038	No	--
582	6-27-67	1023	133.8	15.8	293	0.138	--	0.012	0.028	0.040	No	--
583	6-27-67	1024	133.9	15.2	293	0.144	--	0.012	0.028	0.040	No	--
584	6-27-67	1025	133.6	15.4	294	0.142	--	0.012	0.030	0.042	No	--
585	6-27-67	1026	133.9	15.6	293	0.139	--	0.012	0.032	0.044	No	--
586	6-27-67	1027	133.7	15.9	293	0.137	--	0.012	0.034	0.046	No	--
587	6-27-67	1028	133.9	16.1	293	0.136	--	0.012	0.036	0.048	Yes	90
588	6-27-67	1029	134.0	16.2	290	0.134	--	0.012	0.038	0.050	Yes	90
589	6-27-67	1030	134.5	15.0	286	0.146	--	0.012	0.022	0.034	No	--
590	6-27-67	1031	134.2	15.5	285	0.140	--	0.014	0.024	0.038	No	--
591	6-27-67	1032	134.2	15.8	285	0.137	--	0.014	0.026	0.040	No	--
592	6-27-67	1033	134.3	15.2	284	0.143	--	0.014	0.026	0.040	No	--
593	6-27-67	1034	134.1	15.2	285	0.143	--	0.014	0.026	0.040	Yes	175
594	6-27-67	1035	134.1	15.4	285	0.141	--	0.016	0.019	0.035	Yes	180
595	6-27-67	1036	134.0	15.0	285	0.144	--	0.018	0.016	0.034	Yes	180
596	6-27-67	1037	134.1	15.5	285	0.140	--	0.020	--	0.020	Yes	160
597	6-27-67	1038	134.1	15.0	286	0.145	--	0.010	0.022	0.032	Yes	160
598	6-27-67	1039	134.0	16.2	285	0.134	--	0.012	0.038	0.050	Yes	90
599	6-27-67	1040	134.1	15.3	284	0.142	0.010	--	0.018	0.028	Yes	280

Table D-2. Combustion Tests (Continued)

Test Point	Date	CADDE Number	Burner Inlet Conditions			Duct Reference Mach Number	Fuel/Air Ratio			Overall	Combustion Efficiency, %	Instability	Dominant Frequency, Hz
			Airflow, W_a , lb/sec	Pressure, P_{T4} , psia	Temperature, T_{T4} , °F		Zone 1 Primary	Zone 1 Secondary	Zone 2				
600	6-27-67	1041	133.6	15.2	284	0.142	0.012	--	0.026	0.038	93.8	No	--
601	6-27-67	1042	134.0	15.2	284	0.142	0.012	--	0.028	0.040	93.5	No	--
602	6-27-67	1043	133.9	15.5	285	0.140	0.012	--	0.030	0.042	93.5	No	--
603	6-27-67	1044	133.8	15.7	285	0.138	0.012	--	0.032	0.044	93.7	No	--
604	6-27-67	1045	133.5	15.9	285	0.136	0.012	--	0.034	0.046	93.2	No	--
605	6-27-67	1046	133.9	16.0	285	0.135	0.012	--	0.036	0.048	92.5	No	--
606	6-27-67	1047	133.5	16.2	286	0.133	0.012	--	0.038	0.050	91.4	No	--
607	6-27-67	1048	133.5	15.0	288	0.146	0.012	--	0.038	0.050	--	No	--
608	6-27-67	1049	133.5	14.9	288	0.146	0.014	--	0.024	0.038	94.5	No	--
609	6-27-67	1050	133.4	15.1	287	0.143	0.014	--	0.026	0.040	94.6	No	--
610	6-27-67	1051	133.6	15.4	287	0.141	0.014	--	0.028	0.042	94.5	No	--
611	6-27-67	1052	133.7	15.6	287	0.139	0.014	--	0.030	0.044	94.3	No	--
612	6-27-67	1053	133.6	15.8	286	0.137	0.014	--	0.032	0.046	93.7	No	--
613	6-27-67	1054	133.6	16.0	286	0.135	0.014	--	0.034	0.048	92.9	No	--
614	6-27-67	1055	133.7	16.1	287	0.135	0.014	--	0.035	0.049	--	Yes	320

APPENDIX E
FUEL SYSTEM

The fuel system provided three zones of operation (see figure E-1) with each zone operating in an identical manner and with each zone consisting of identical components. Common to each fuel zone were a main supply valve, heat exchanger, and a 10-micron filter. Each fuel zone had identical pumps and motors, which delivered a maximum flow rate of 120 gpm, at a discharge pressure of 1000 psig. A bypass system controlled the pump discharge pressure in each zone. For control of fuel into the rig, each zone had a main control valve for approximate fuel flow settings and a vernier control valve for accurate fuel flow settings. To determine the fuel flow rate through each fuel zone, turbine flowmeters were provided, two with a flow range of 1200 lb/hr to 50,000 lb/hr and one with a flow range of 550 lb/hr to 10,000 lb/hr. Each fuel zone had a shutoff valve connected to the ignition control panel.

A safety abort system monitored five parameters that would initiate a shutdown:

1. If ignition failed to occur during some preset time interval
2. If a flame blowout occurred at any time during continuous operation
3. If the fuel flow rate on any one of the three turbine flowmeters increased beyond a preset value
4. If the water flow rate on any one of the three turbine flowmeters decreased below a preset value
5. If the fuel pressure to the pressure switch on the pump inlet supply line decreased below a preset value.

Also, a manually operated abort button was supplied on the pump control panel.

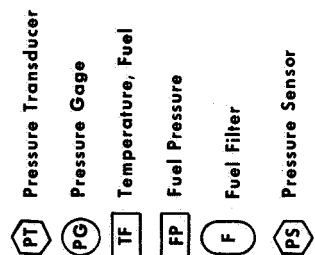
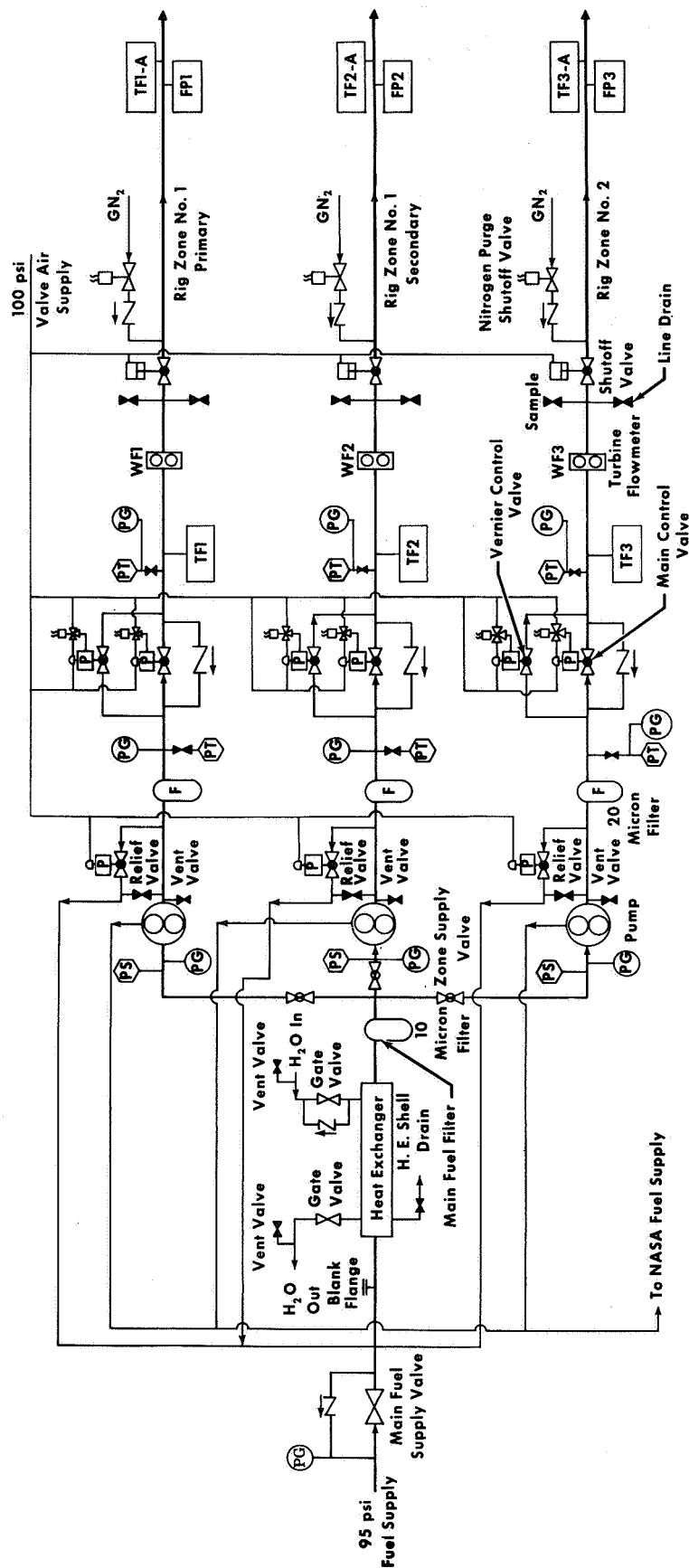


Figure E-1. Fuel System Schematic

FD 23721

The ignition and the flame blowout abort parameters utilized the following components:

1. A variable ignition timer with a range of 0-60 seconds
2. A SW-24 facility duct purge timer with a variable range of 0-10 minutes
3. An ignition detector that measured the temperature difference between the burner inlet and the burner exit.

In operation, the ignition detector abort limit was preset at a low temperature differential. A preselected time interval was set on the 0-60 second ignition timer. Also, a preselected time interval of 0-10 minutes was set on the SW-24 facility duct purge timer. When the igniter button was depressed, power was supplied to the two rig igniters and the fuel shutoff valve was opened simultaneously to light the duct burner. This situation existed until the ignition timer completed its cycle. If at that time burner ignition was obtained, the ignition detectors indicated a temperature differential higher than the abort limit, a green light came on, the igniters were de-energized and continuous rig testing could be maintained. If, at that time, burner ignition was not obtained, the ignition detector indicated a temperature differential lower than the abort limit, a red light came on, the igniters were de-energized and the fuel shutoff valves became inoperable during the SW-24 facility duct purge timer cycle. If a burner blowout occurred at any time while testing, the same operating sequence occurred as when initial ignition was not obtained. A manual purge button allowed the same operating sequence to be initiated at any time.

For an abort due to an excessive flow rate of fuel, two major components were used:

1. Turbine flowmeters (one for each fuel zone)
2. Optical meter relays (one for each turbine flowmeter).

In operation, the optical meter relay abort limits were set at a predetermined maximum fuel flow rate. A signal from the turbine flowmeter was sent to the optical meter relay, which indicated actual fuel

flow. If the fuel flow rate increased beyond the preset value, an abort occurred. The shutoff valves closed, the control valves closed, and the pumps shut down. (The optical meter relays were equipped with an abort reset button that had to be depressed before operation could be continued.) Since fuel flow to the burner had been shut off, the ignition detector sensed a flame blowout and the SW-24 facility duct purge timer cycle was initiated.

Two major components were used for an abort caused by inadequate flow rate of cooling water:

1. Turbine flowmeters (one for the water-cooled pressure probes, one for the inner nozzle, and one for the outer nozzle and nozzle plugs)
2. Optical meter relays (one for each turbine flowmeter).

In operation, the optical meter relay abort limits were set at a predetermined minimum cooling water flow rate. A signal from the turbine flowmeter was sent to the optical meter relay, which indicated actual cooling water flow rate. An abort occurred if the cooling water flow rate decreased below the preset value. The abort sequence was identical to the previously described sequence for excessive fuel flow.

An abort occurred if the fuel supply pressure to the pump inlet became less than a preset value. The system consisted basically of one adjustable pressure switch for each fuel zone. Prior to running, the pressure switch abort limit was set at a selected level. An abort occurred if the fuel supply pressure became less than the preset level. The shutoff valves closed and the pumps shut down. Since fuel flow to the burner had been shut off, the ignition detector sensed a flame blowout and the SW-24 facility duct purge timer cycle was initiated.

Another abort parameter consisted of a manual abort button. When the abort button was depressed, the shutoff valves and the control valves closed. The pumps also shut down and the SW-24 facility duct purge timer cycle was initiated.

APPENDIX F
DISTRIBUTION LIST OF FINAL REPORT
FOR CONTRACT NAS3-7907

NASA Lewis Research Center 21000 Brookpark Road Cleveland, Ohio 44135 Attention: Report Control Office, MS 5-5	(1)	NASA Lewis Research Center 21000 Brookpark Road Cleveland, Ohio 44135 Attention: W. H. Roudebush MS 60-6	(1)
NASA Lewis Research Center 21000 Brookpark Road Cleveland, Ohio 44135 Attention: Technology Utilization Office MS 3-19	(1)	NASA Lewis Research Center 21000 Brookpark Road Cleveland, Ohio 44135 Attention: John H. DeFord MS 60-5	(1)
NASA Lewis Research Center 21000 Brookpark Road Cleveland, Ohio 44135 Attention: Library MS 60-3	(2)	NASA Lewis Research Center 21000 Brookpark Road Cleveland, Ohio 44135 Attention: J. B. Esgar MS 60-4	(1)
NASA Lewis Research Center 21000 Brookpark Road Cleveland, Ohio 44135 Attention: Fluid Systems Com- ponents Division MS 5-3	(1)	NASA Lewis Research Center 21000 Brookpark Road Cleveland, Ohio 44135 Attention: H. H. Ellerbrock MS 60-4	(1)
NASA Lewis Research Center 21000 Brookpark Road Cleveland, Ohio 44135 Attention: I. I. Pinkel MS 5-3	(1)	NASA Lewis Research Center 21000 Brookpark Road Cleveland, Ohio 44135 Attention: L. Macioce MS 60-6	(1)
NASA Lewis Research Center 21000 Brookpark Road Cleveland, Ohio 44135 Attention: W. L. Stewart MS 77-2	(1)	NASA Lewis Research Center 21000 Brookpark Road Cleveland, Ohio 44135 Attention: W. T. Olson MS 3-16	(1)
NASA Lewis Research Center 21000 Brookpark Road Cleveland, Ohio 44135 Attention: P. Hacker MS 5-3	(1)	NASA Lewis Research Center 21000 Brookpark Road Cleveland, Ohio 44135 Attention: Robert R. Hibbard MS 302-1	(1)
NASA Lewis Research Center 21000 Brookpark Road Cleveland, Ohio 44135 Attention: J. Howard Childs MS 60-4	(1)	NASA Lewis Research Center 21000 Brookpark Road Cleveland, Ohio 44135 Attention: J. F. Dugan, Jr. MS 501-2	(1)

Pratt & Whitney Aircraft

PWA FR-2542

NASA Lewis Research Center
21000 Brookpark Road
Cleveland, Ohio 44135
Attention: Seymour Lieblein
MS 7-1

NASA Lewis Research Center
21000 Brookpark Road
Cleveland, Ohio 44135
Attention: R. E. Jones
MS 60-6

NASA Lewis Research Center
21000 Brookpark Road
Cleveland, Ohio 44135
Attention: Jack Grobman
MS 60-6

NASA Lewis Research Center
21000 Brookpark Road
Cleveland, Ohio 44135
Attention: J. Robert Branstetter
MS 60-6

NASA Scientific & Technical
Information Facility
P.O. Box 33
College Park, Maryland 20740
Attention: NASA Representative
RQT-2448

FAA Headquarters
800 Independence Avenue, S.W.
Washington, D. C. 20553
Attention: Brigadier General
J. C. Maxwell

FAA Headquarters
800 Independence Avenue, S.W.
Washington, D. C. 20553
Attention: F. B. Howard/SS120

NASA Headquarters
600 Independence Avenue, S.W.
Washington, D. C. 20546
Attention: N. F. Rekos (RAP)

Department of the Army
U.S. Army Aviation Material
Laboratory
Fort Eustis, Virginia 23604
Attention: John White

(1) Headquarters (2)
Wright-Patterson AFB, Ohio 45433
Attention: J. L. Wilkins, SESOS

AFAPL (APTC) (1)
Wright-Patterson AFB, Ohio 45433
(1) Attention: Lt. D. H. Quick

Air Force Office of Scientific (1)
Research, Propulsion Research Div
USAF Washington, D. C. 20025

(1) Defense Documentation Center (1)
(DDC)
Cameron Station
5010 Duke Street
Alexandria, Virginia 22314

(25) Department of the Navy (1)
Bureau of Naval Weapons
Washington, D. C. 20025
Attention: Robert Brown RAP14

Department of the Navy (1)
(6) Bureau of Ships
Washington, D. C. 20360
Attention: G. L. Graves

NASA-Langley Research Center (1)
Langley Station
Technical Library
(1) Hampton, Virginia 23365
Attention: Mark R. Nichols

NASA-Langley Research Center (1)
Langley Station
Technical Library
(1) Hampton, Virginia 23365
Attention: John V. Becker

United States Air Force (1)
Aero Propulsion Laboratory
(1) Building 18D, Room 119
Wright-Patterson AFB, Ohio 45433
Attention: Robert E. Henderson

United Aircraft Corporation (2)
(1) Pratt & Whitney Aircraft Division
400 Main Street
East Hartford, Connecticut 06108
Attention: G. Andreini

Pratt & Whitney Aircraft

PWA FR-2542

United Aircraft Corporation Pratt & Whitney Aircraft Division 400 Main Street East Hartford, Connecticut 06108 Attention: Library	(1)	General Electric Company Flight Propulsion Division Cincinnati, Ohio 45215 Attention: Technical Information Center N-32	(1)
United Aircraft Research East Hartford, Connecticut 06108 Attention: Library	(1)	General Electric Company 1000 Western Avenue West Lynn, Massachusetts 01905 Attention: Dr. C. W. Smith Library Bldg. 2-40M	(1)
Allison Division of GMC Department 8894, Plant 8 P.O. Box 894 Indianapolis, Indiana 46206 Attention: J. N. Barney	(1)	General Electric Company 1000 Western Avenue West Lynn, Massachusetts 01905 Attention: Paul C. Setze	(1)
Allison Division of GMC Department 8894, Plant 8 P.O. Box 894 Indianapolis, Indiana 46206 Attention: G. E. Holbrook	(1)	Curtiss-Wright Corporation Wright Aeronautical Division Wood-Ridge, New Jersey 07075 Attention: S. Lombardo	(1)
Allison Division of GMC Department 8894, Plant 8 P.O. Box 894 Indianapolis, Indiana 46206 Attention: Library	(1)	Curtiss-Wright Corporation Wright Aeronautical Division Wood-Ridge, New Jersey 07075 Attention: G. Provenzale	(1)
Northern Research & Engineering Corporation 219 Vassar Street Cambridge, Massachusetts 02139 Attention: K. Ginwala	(1)	Air Research Manufacturing Co. 402 South 36th Street Phoenix, Arizona 85034 Attention: Robert O. Bullock	(1)
General Electric Company Flight Propulsion Division Cincinnati, Ohio 45215 Attention: J. W. McBride	(1)	Air Research Manufacturing Co. 9851 Sepulveda Boulevard Los Angeles, California 90009 Attention: Dr. H. Van Le	(1)
General Electric Company Flight Propulsion Division Cincinnati, Ohio 45215 Attention: F. Burggraf	(1)	AVCO Corporation Lycoming Division 550 South Main Street Stratford, Connecticut 06497 Attention: Claus W. Bolton	(1)
General Electric Company Flight Propulsion Division Cincinnati, Ohio 45215 Attention: S. N. Suci	(1)	AVCO Corporation Lycoming Division 550 South Main Street Stratford, Connecticut 06497 Attention: Charles Kuintzle	(1)
General Electric Company Flight Propulsion Division Cincinnati, Ohio 45215 Attention: C. Danforth	(1)		

Pratt & Whitney Aircraft

PWA FR-2542

Continental Aviation & Engineering Corporation 12700 Kercheval Detroit, Michigan 48215 Attention: Eli W. Bernstein	(1)	Aerojet-General Corporation Sacramento, California 95809 Attention: M. S. Nylin	(1)
Continental Aviation & Engineering Corporation 12700 Kercheval Detroit, Michigan 48215 Attention: Howard C. Walch	(1)	Aerojet-General Corporation Sacramento, California 95809 Attention: Library	(1)
International Harvester Company Solar Division 2200 Pacific Highway San Diego, California 92112 Attention: P. A. Pitt	(1)	New England Materials Laboratory, Inc. 35 Commercial Street Medford, Massachusetts 02155 Attention: Allan S. Bufferd	(1)
International Harvester Company Solar Division 2200 Pacific Highway San Diego, California 92112 Attention: Mrs. L. Walper	(1)	Cornell Aeronautical Laboratory 4455 Genessee Street Buffalo 21, New York	(1)
Goodyear Atomic Corporation Box 628 Piketon, Ohio Attention: C. O. Langebrake	(1)	Marquardt Corporation 16555 Saticoy Street Van Nuys, California	(1)
George Derderian AIR 53622 B Department of the Navy Bureau of Navy Washington, D. C. 20360	(1)	Thompson Ramo Wooldridge 7209 Platt Avenue Cleveland, Ohio 44117	(1)
The Boeing Company Commerical Airplane Division P.O. Box 3991 Seattle, Washington 98124 Attention: G. J. Schott MS 80-66	(1)	Aro, Inc. Arnold Air Force Station, Tennessee	(1)
The Boeing Company Missile and Information Systems Division 224 N. Wilkinson Street Dayton, Ohio 45402 Attention: Warren K. Thorson	(1)	A.E.L. Naval Air Center Philadelphia, Pennsylvania Attention: S. Fiorello	(1)
Wall Colmonoy Corporation 19345 John R. Street Detroit 3, Michigan Attention: R. L. Peaslee	(1)	Director Government Research Laboratory Esso Research & Engineering Company P.O. Box 8 Linden, New Jersey 07036	(1)
	(1)	Douglas Aircraft Company 3855 Lakewood Blvd. Long Beach, California 90801 Attention: Technical Informa- tion Center C1-250 For J. E. Merriman	(1)
	(1)	Air Research Manufacturing Company 9851 Sepulveda Boulevard Los Angeles, California 90009 Attention: George Sotter	(1)